MICROWAVE INTEGRATED CIRCUITS

Preparation of and Measurement Techniques for Metal and Dielectric Films

- by -

R. S. Butlin B.Sc.(Eng.)

A thesis submitted for the degree of Doctor of Philosophy at the University of Warwick, England.

September, 1973.

ABSTRACT

The work reported in this thesis is concerned with evaluating the properties of materials used for lumped element microwave circuits. The investigation included surface roughness measurements of commercially available alumina and glass substrates, measurement of the surface resistance of evaporated, electroplated and bulk conductors, and measurement of the dielectric properties of alumina and silicon dioxide films. Factorially designed experiments were used to study the effects of the processing parameters for electroplating and RF sputtering on the quality of the metal and dielectric films obtained.

The surface resistance measurements were performed using a cylindrical H_{011} cavity. The design of the cavity allowed a calibration curve to be drawn such that measurement of the return loss at resonance alone allowed the sample surface resistance to be read directly from a graph with an accuracy of $\pm$ 0.0013Ω. The simplicity of the method is a significant advance on former methods. The effects of various surface finishing processes on the surface resistance of bulk conductors of copper and brass have been studied together with an investigation of the effects of the electroplating parameters on the surface resistance of copper films deposited from two acid solutions. The surface resistance of the metal films formed from these solutions was found to be dependent upon the current density, stirring rate, temperature and chemical composition of the solution. Results are also given for gold, silver and copper films deposited from commercially available plating solutions. The effect of film thickness on the surface resistance of evaporated

copper films was also studied, the results being in good agreement with the theoretical values.

The investigation of dielectric film properties required the construction of an RF sputtering unit. This is described in detail. The dielectric film properties were measured using a co-axial cavity. The effects of three sputtering parameters on the quality of the films obtained were studied. The application of a longitudinal magnetic field during sputtering was found to be particularly beneficial.

A new technique has also been developed for the deposition of films onto selected areas of a substrate without the need for etching. This work was performed with a fellow research student and is covered by a UK Patent application. This method was required for the fabrication of microwave planar capacitors where the substrate and the capacitor dielectric were made of the same material.

ACKNOWLEDGEMENTS

I am grateful to Professor J.A. Shercliff, Chairman of the Department of Engineering of the University of Warwick, for providing the facilities used for conducting this research and the UK Science Research Council for the financial support.

The work was supervised by Mr. M.K. McPhun and I am grateful for the guidance he has given me during the past three years.

I wish to thank the following people in the Department of Engineering: Mr. P.J. Smith for his skilled mechanical construction work, Mr. L. Baker for his electronic assistance and Mr. J. Darmon for Talysurf and Talystep measurements. I take this opportunity of thanking the following people for many useful discussions: Dr. H.V. Shurmer, Dr. K. Mehmet, Dr. K. Bowen, Messrs. D. Michie, E.F. Da Silva and B.G. Marchent.

I am also grateful to the following organizations: the Electrical Research Association for information provided on the subject of sputtering, the General Electric Company (Stoke Works, Coventry) for providing the copper pyrophosphate plating solution, Hockley Chemicals (Birmingham) for providing additives for an acid copper plating solution, Microwave Associates for providing samples of gold plating and Shell Thornton Research Centre for the annealing of copper samples.

I dedicate this thesis to my wife for her moral and financial support over the last three years and for the typing of the thesis from a difficult handwritten document.

CONTENTS

Chapter 1
INTRODUCTION

1-1 General

The term microwave integrated circuit (MIC) is applied to both monolithic and hybrid circuits.[1] The monolithic circuit may have active devices grown in situ in or on a semiconducting substrate, while the hybrid circuit is manufactured on a single planar substrate. For the hybrid integrated circuit, passive elements may be formed by partial metalization of the substrate while active devices are inserted by bonding to metal conductors. The most popular form of hybrid MIC is that of the microstrip transmission line[2] shown in figure 1-1. The line consists of a conducting strip separated from the ground plane by a dielectric layer (the substrate). The electrical properties of the line are characterized by its impedance, attenuation and guide wavelength. More recently, greater interest has been shown in the lumped element (LE) approach to hybrid MICs.[3,4,5] This approach requires the fabrication of passive components e.g. capacitors, inductors and resistors, on the substrate. These components are usually formed by the vacuum deposition of metal and dielectric films. The guide wavelength in a microstrip transmission line is a function of the permittivity of the substrate. For example, the guide wavelength for an alumina substrate is approximately 1 cm. at 10GHz. For a component to be truly "lumped" there must be no phase change across it and therefore the physical size of the component must be much

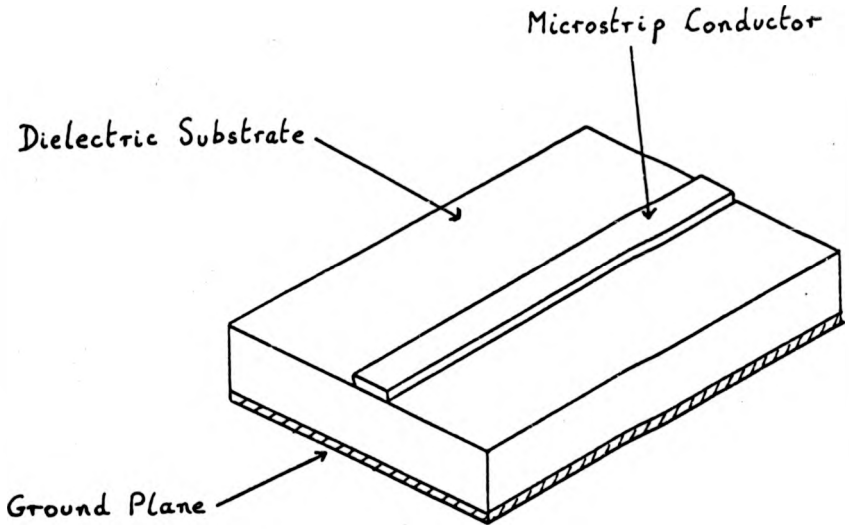

FIGURE 1-1 : MICROSTRIP TRANSMISSION LINE

smaller than the guide wavelength. It is for this reason that the development of LE circuits has followed closely on the advances in photoresist technology [6]. The advantages of the LE circuit over the distributed (microstrip) circuit are those of reduced size and low cost.

The microwave group at the University of Warwick has been concerned with the measurement and fabrication of LE components suitable for operation at 10 GHz (X-band). Topics investigated include:

a. The development of a cavity technique for the measurement of the permittivity and loss tangent of thin dielectric films. [7]
b. Measurement of capacitor properties. [8]
c. Measurement of inductor properties. [9]
d. The evaluation of material properties.

The work reported in this thesis is chiefly concerned with the effects of processing parameters on the electrical properties of thin metal and dielectric films, although a great deal of overlap with the other research topics exists. I will therefore review each topic separately in the relevent chapter.

1-2 Materials Research for Lumped Element MICs

Metal and dielectric films are nearly always deposited by vacuum processing techniques e.g. evaporation [10] and sputtering (Chapter 3)

The electrical and physical properties of a thin film in general differ from those of the initial bulk material. For this reason alone, the film properties of interest must be measured and it is shown here that the deposition parameters must be closely controlled if reproducible film quality is to be obtained. Industrial organizations have preferred the indirect measurement of the microwave properties of thin metal and dielectric films. For example, Caulton [4] of the Radio Corporation of America (RCA) performed measurements on thin film planar capacitors (figure 1-2). From his measurements he estimated the electrode and dielectric losses contributing to the total loss of the capacitor. He found that the predicted and measured values of the electrode loss differed by an order of magnitude. Aitchison [11] of Mullards, (England) on the other hand, has restricted his work to interdigital capacitors (figure 1-3), thus eliminating the need for a dielectric. This type of capacitor is however restricted to values below 1pF.

Most workers in this field have paid great attention to the use of silicon dioxide films as a capacitor dielectric owing to its ease of evaporation and to the low dielectric loss of the bulk material. However, the lowest loss tangent at 10 GHz recorded by Mehmet [7] for electron beam evaporated silicon dioxide films was 10^{-2}, which was much higher than the bulk value of 10^{-4}. The high loss of dielectric films is usually attributed to their highly disordered structure and to contamination of the film. Silicon dioxide is also hygroscopic i.e. water vapour is adsorbed and may result in an increased leakage current through the dielectric. Dielectric loss mechanisms have not been investigated at microwave

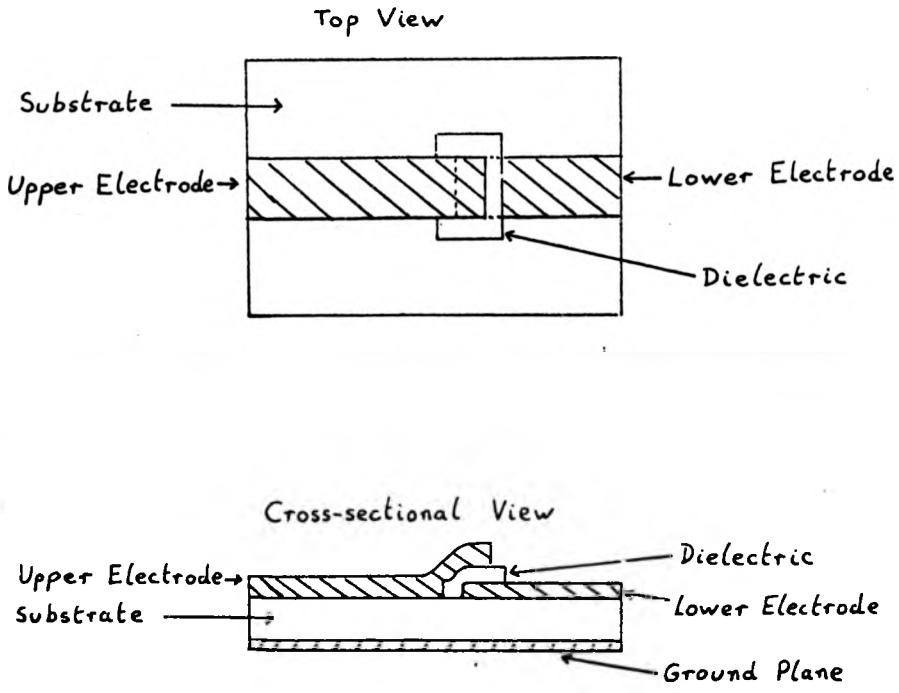

FIGURE 1-2 : THIN FILM PLANAR CAPACITOR

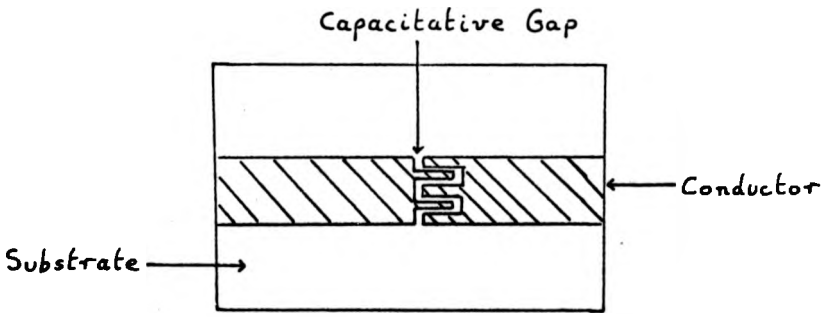

FIGURE 1-3 : INTERDIGITAL CAPACITOR

frequencies. Argoll and Jonscher [12] however, have studied the loss of evaporated "silicon oxide" films in the frequency range 10^{-2} to 10^{7} Hz. They concluded that high frequency losses were probably due to a two-centred electronic hopping mechanism, the natural frequency of which might lie in the microwave or near infra red regions. Mehmet and McPhun [13] have observed a relaxation phenonemon at 3 GHz in electron beam evaporated silicon monoxide (SiO) films. They attribute this loss peak to "local torsional vibration of Si -O chains" as predicted by Hirose and Wada [14]. The discussion in this section demonstrates clearly the need for further investigation of material properties at microwave frequencies.

1-3 Outline of Research

The surface finish of the substrate can greatly affect the reliability and performance of MICs. The surface finish of alumina and glass substrates was investigated in order to choose substrates suitable for the work of the microwave group.

Mehmet's investigation of the microwave dielectric loss of evaporated silicon dioxide (mentioned in the previous section) prompted an investigation of the properties of silicon dioxide films deposited by radio frequency (RF) sputtering. The lack of suitable commercial RF sputtering equipment at the commencement of the project made it necessary to construct one for this purpose. The research was initially directed towards the study of the electrical properties of silicon dioxide films deposited under different conditions.

Owing to the large number of sputtering parameters that may be varied, an experimental approach known as factorial design (Chapter 4 and Appendix 2) was used in order to extract the maximum amount of information from these experiments. The permittivity and loss tangents of the films were measured using the cavity technique developed by Mehmet [7]. An outstanding difficulty of this method was that of obtaining an accurate measurement of the thickness of the film. As will be explained later, it was thought that evaluation of the film properties by capacitor measurements would improve the accuracy of the results. Some time was spent in developing the process necessary to make the capacitors. This work was performed with a fellow research student who was developing a capacitor measurement technique using a microstrip resonator.

If the dielectric loss is to be determined from capacitor measurements, the electrode loss must be accurately known. A cavity measurement method was developed for this purpose to evaluate the surface resistance of metal films. Surface resistance measurements have been performed on films deposited from commercially available electroplating solutions and factorial design has allowed the effects of the plating bath parameters to be studied.

Unfortunately, the capacitor measurement technique being developed by Michie [8] was not available by the end of this project. The dielectric film measurements were therefore performed using the cavity technique mentioned earlier but with more accurate measurement of the film thickness.

Chapter 2

EVALUATION OF SUBSTRATE SURFACE FINISH

2-1 Introduction

The choice of substrate for thin film work depends greatly upon the application. However, several general conditions must be fulfilled.[15,16] These include chemical inertness, good surface finish, low dielectric loss and low cost. Substrates must also be compatible with processing procedures e.g. porosity and vacuum degassing must be considered together with thermal and mechanical strength. In microwave circuits, the substrate not only supports the circuit but also forms the transmission medium. For this reason alone, a low-loss substrate is essential. The dielectric constant of a substrate will also determine the guide wavelength and therefore the physical size of the circuit - the higher the substrate permittivity the smaller the guide wavelength. The use of a substrate of high dielectric constant reduces radiation losses and therefore a high-permittivity, low-loss substrate is required for microwave circuits. For lumped element (LE) circuits, however, the component must be small compared to a wavelength in order for it to be truly lumped; if a substrate of very high dielectric constant were used, this requirement might be difficult to meet by present photolithographic techniques. Typical substrates used for thin film microwave circuits are listed in table 2-1.

Table 2-1

Substrates Suitable for Microwave Circuits

Distributed Circuits		L.E. Circuits	
Material	Permittivity	Material	Permittivity
Alumina (Al_2O_3)	10	Sapphire	9-11
Sapphire (Al_2O_3)	9-11	Quartz (SiO_2)	4
Rutile (TiO_2)	100		

The substrate surface finish affects the circuit losses for both distributed and LE circuits, but where lumped elements are involved more stringent requirements on substrate roughness must be met. Schilling [17] investigated the losses of mircostrip line attributable to surface roughess and has shown as might be expected, that smoother surfaces result in lower losses. More recently Bosnell[18] has shown that substrates having a centre line average (CLA) of less than 0.25 μm are perfectly suitable for distributed circuits. Lumped element circuits, however, require an atomically smooth surface. If a capacitor were formed on an area where a surface defect existed (e.g. pit or peak), a direct short or a region of low dielectric strength might result. Schwartz and Brown [19] showed that the yield and life of Ta - Ta_2O_5 - Au capacitors were greatly reduced on rough substrates.

A further substrate requirement for all thin film circuits is that of flatness, since the photographic mask must be in intimate contact with the substrate to ensure good definition. This requirement is probably more important in microwave work in order to obtain

constant impedance lines. Substrate manufacturers' data includes such information as the CLA as a measure of the surface characteristics. Interpretation of the surface finish from such a measurement is difficult as it is affected by the roughness and waviness or flatness of the substrate. For this reason, it was decided to examine the surface profiles of various substrates using a Talysurf No. 1 made by Rank, Talor Hobson, and to compare the results with surface photographs taken on a Scanning Electron Microscope (SEM).

2-2 Interpretation of Talysurf Measurements (20)

The Talysurf is basically a device which draws a diamond stylus, connected to a displacement transducer, across the surface under examination. Clearly, the radius of the stylus tip limits the accuracy of measurements of the substrate topology. In the present work, a tip of radius 2.5 μm was used. The Talysurf can be used in two modes;

1. To determine CLA values which are displayed on a meter. This is done by integrating the displacement readings over small sample lengths and outputting an average displacement for the length involved.
2. To obtain a representation of the surface profile by the continuous display of the transducer output on a strip chart recorder.

The instrument operates in three ranges and for any given traverse length there is a fixed sample length, otherwise known as the meter cut-off length. Consequently, the number of displacement readings contributing to the final CLA value obtained is fixed for each range,

constant impedence lines. Substrate manufacturers' data includes such information as the CLA as a measure of the surface characteristics. Interpretation of the surface finish from such a measurement is difficult as it is affected by the roughness and waviness or flatness of the substrate. For this reason, it was decided to examine the surface profiles of various substrates using a Talysurf No. 1 made by Rank, Talor Hobson, and to compare the results with surface photographs taken on a Scanning Electron Microscope (SEM).

2-2 Interpretation of Talysurf Measurements (20)

The Talysurf is basically a device which draws a diamond stylus, connected to a displacement transducer, across the surface under examination. Clearly, the radius of the stylus tip limits the accuracy of measurements of the substrate topology. In the present work, a tip of radius 2.5 μm was used. The Talysurf can be used in two modes;

1. To determine CLA values which are displayed on a meter. This is done by integrating the displacement readings over small sample lengths and outputting an average displacement for the length involved.
2. To obtain a representation of the surface profile by the continuous display of the transducer output on a strip chart recorder.

The instrument operates in three ranges and for any given traverse length there is a fixed sample length, otherwise known as the meter cut-off length. Consequently, the number of displacement readings contributing to the final CLA value obtained is fixed for each range,

as will be seen from the table following.

CLA Measurements by Talysurf

Range	Traverse length mm	Metor cut-off length mm	Number of sample intervals
L	7.6	2.5	3
K	3.8	0.75	5
J	1.9	0.25	7

It is useful in the examination of surface profiles to distinguish between a roughness component (of relatively high frequency) and a waviness component (of much lower frequency) and upon which the former is superimposed.

Hence, in using the Talysurf to include the effects of low-frequency waviness on the CLA, Rangle L would be selected; if roughness only was to be considered, Range J would be chosen. Since waviness was considered to have equal importance with roughness for the evaluation of substrates, all substrates were tested using Range L. In contrast, for measurements on the roughness of metal films (reported in Chapter 9), Range J was used, in order to minimize the effects of any substrate undulations.

Owing to the short traverse lengths available with the Talysurf, flatness over the whole area of the substrate could not be evaluated. The substrates could therefore be compared only in terms of roughness and waviness. The number of traces obtained was too great for inclusion of them all in this Thesis. In order to compare the measurements on different samples, result are quoted for typical

peak-to-peak roughness together with a quantitative assessment of waviness. A typical waviness trace is shown below. The waviness [19] shall be defined as the ratio x/y, where the amount of waviness depends on the maximum deviation from the mean level (x) divided by the distance (y) between two adjacent points at which the trace crosses the mean level.

The waviness trace is recorded using low horizontal and vertical magnifications while the roughness may be seen only on high magnifications. Table 2-2 lists the results obtained for the substrates investigated, and figures 2-1 and 2-2 are typical examples of waviness and roughness profiles.

2-3 S.E.M. Observation of Surface Features

All samples were coated with a 200Å chromium film to prevent charge build-up occurring from the electron beam. No surface features were visible for the sapphire, glazed alumina and glass samples. Figures 2-3 and 2-4 show SEM photographs of "as-fired" and polished alumina substrates.

2-4 Discussion of Results of Substrate Examination

Samples 4 and 5 demomstrate how CLA measurements could be misinterpreted. Both substrates have indentical CLA values but for

TABLE 2-2 : MEASUREMENTS OF ROUGHNESS AND WAVINESS ON 13 SUBSTRATE SAMPLES

Sample No. and Manufacturer	Material	CLA μm	Typical pk/pk roughness μm	Waviness factor $x/y \times 10^{-3}$	Comments
	Quartz Flat	0.02	-	-	
1 - M.R.C.	Alumina 99.5%	0.35	0.2	1.07	Small grain size 0.5 - 1.5 μm
2 - Pilkington	Alumina (99.5%)	0.38	0.2 - 0.3	1.00	Small grains 1 - 3 μm
3 - Coors	Alumina ADS995	0.45	0.6	1.00	Large grains 4 - 10 μm
4 - Coors	Alumina ADS965	0.55	0.8 - 1.0	0.5	Large grains 4 - 10 μm
5 - Coors	Alumina ADS965	0.55	-	1.25	Glazed
6 - Lucolox	Alumina	0.06	-	-	Polished pits up to 1.5 μm depth
7 - Deranox	Alumina 97.5%	0.02	-	-	Polished pits of 0.5 μm depth
8 - American Lava	Alumina Al 300	0.15	-	-	Polished pits up to 2.5 μm depth
9 - Insaco	Sapphire	0.05	-	-	
10 - Gooch and Hausego	Quartz (SiO_2)	0.04	-	-	
11 - Corning	7059 Glass	0.07	-	-	
12 - Corning	0211 Glass	0.03	-	-	
13 - Kodak	Photographic glass plate	0.03	-	-	

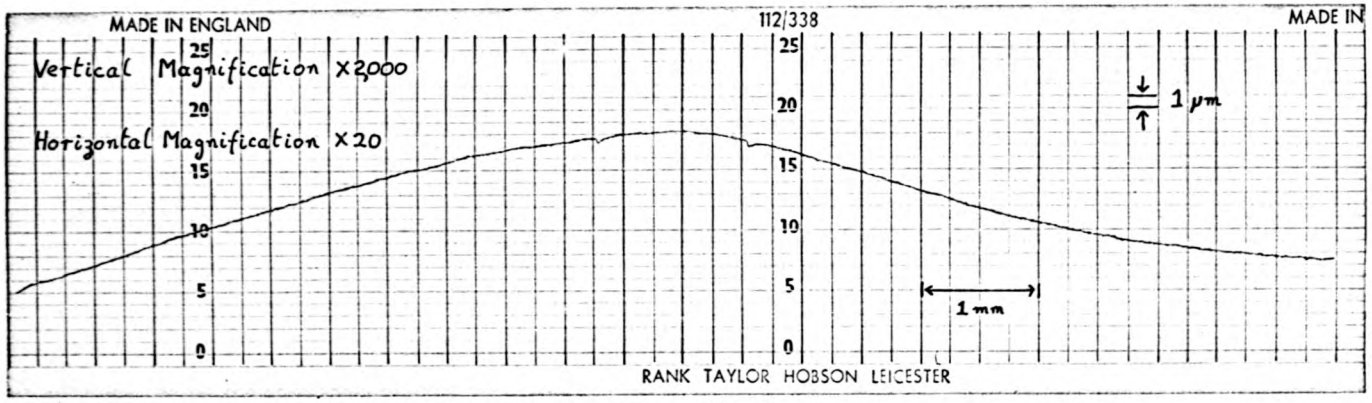

(a) Materials Research Co. (MRC) Alumina

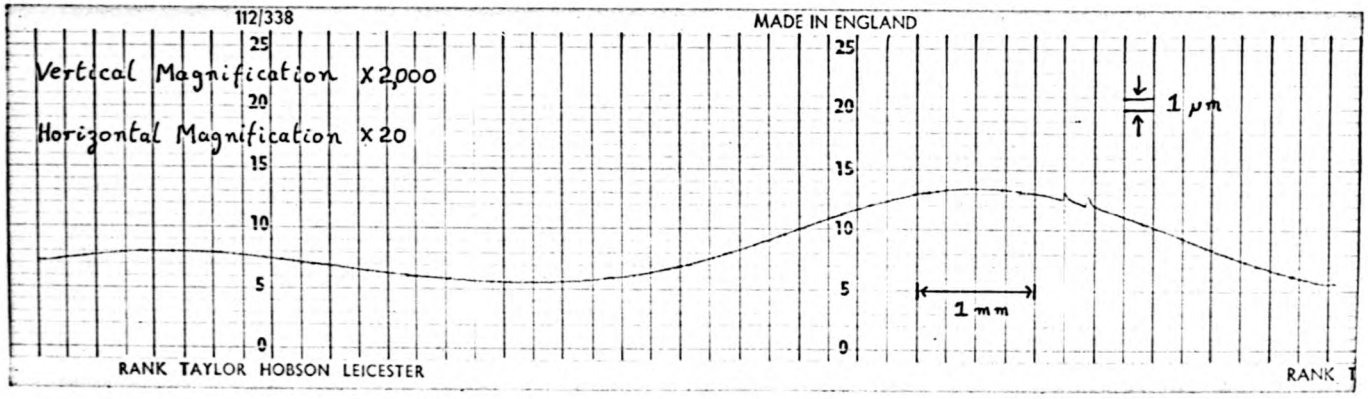

(b) Coors ADS 965 Glazed Alumina

FIGURE 2-1 : TALYSURF TRACES ON TWO SUBSTRATES

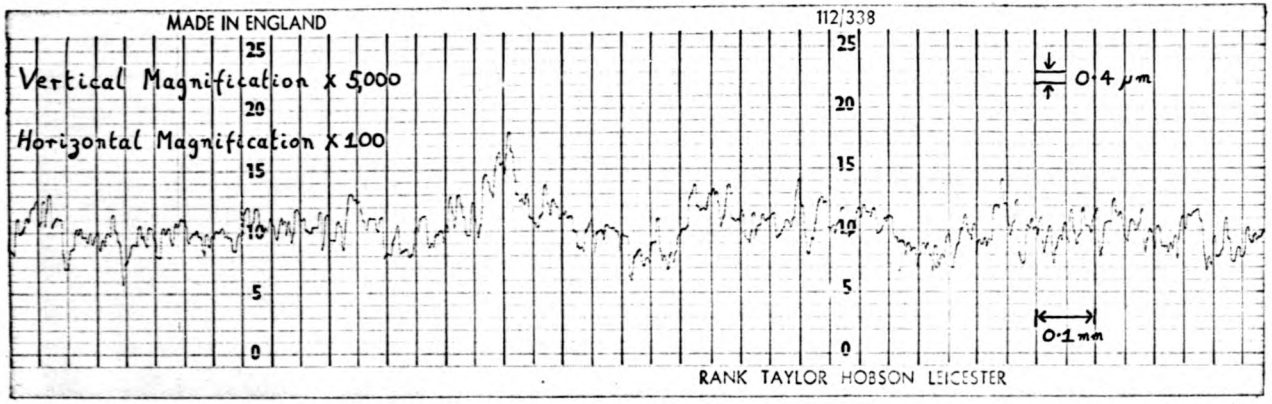

(a) Coors ADS 965 As-fired Alumina

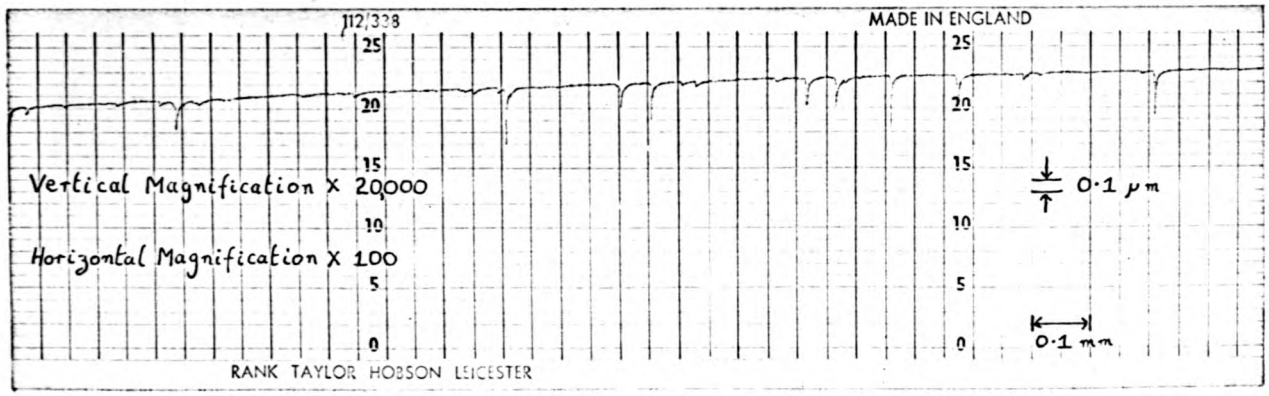

(b) Deranox 975 Polished Alumina

FIGURE 2-2 : TYPICAL ROUGHNESS TRACES

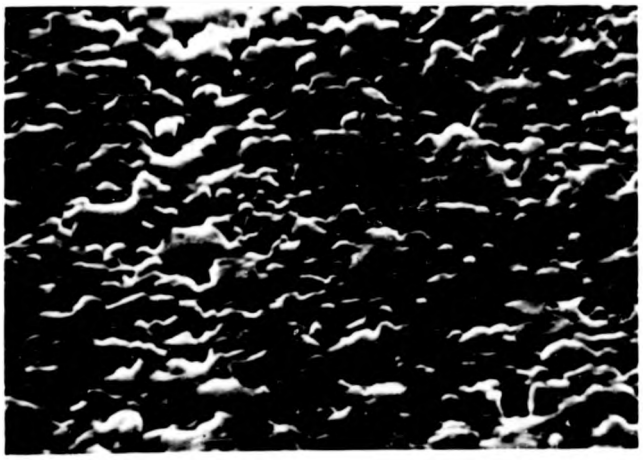

Sample No. 1
MRC

Magnification x 5,000

2 μm

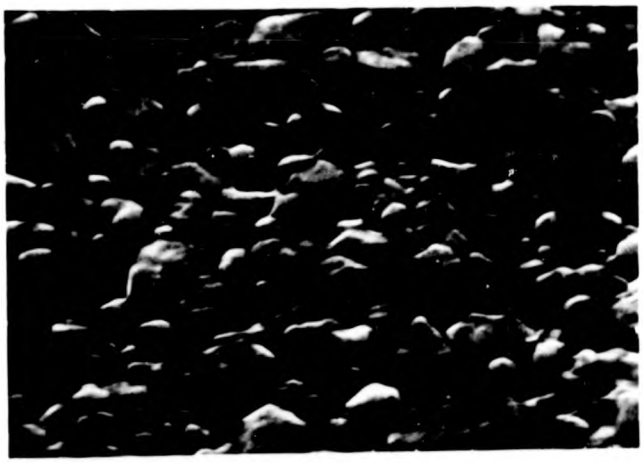

Sample No. 2
Pilkington

Magnification x 5,000

2 μm

Sample No. 4
Coors

Magnification x 5,000

2 μm

FIGURE 2-3 : SEM PHOTOGRAPHS OF AS-FIRED ALUMINA SUBSTRATES

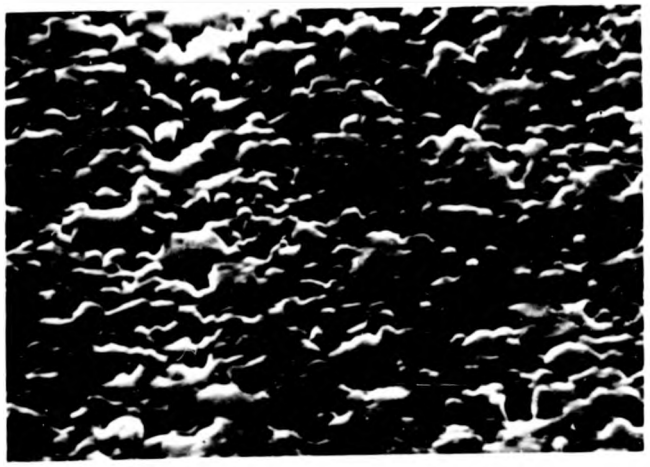

Sample No. 1
MRC
Magnification x 5,000

2 μm

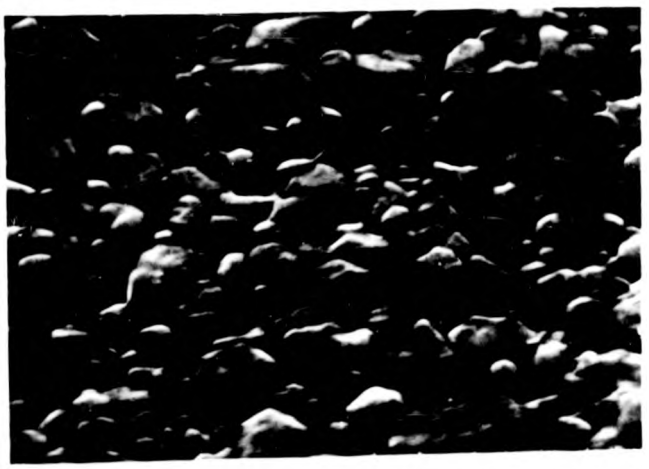

Sample No. 2
Pilkington
Magnification x 5,000

2 μm

Sample No. 4
Coors
Magnification x 5,000

2 μm

FIGURE 2-3 : SEM PHOTOGRAPHS OF AS-FIRED ALUMINA SUBSTRATES

Sample No. 6
Lucalox

Magnification X 500

20 μm

Sample No. 7
Deranox

Magnification X500

20 μm

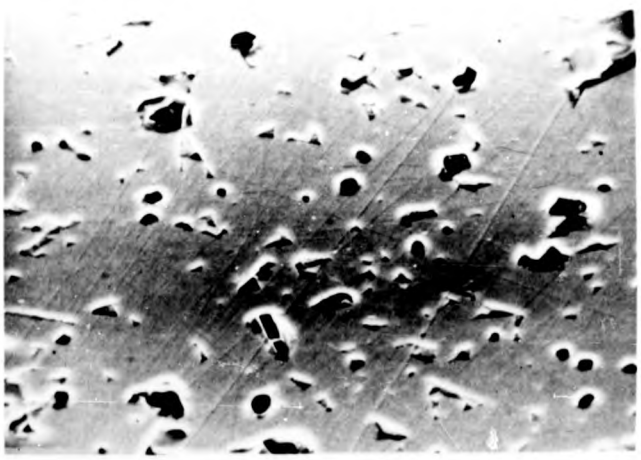

Sample No. 8
American Lava

Magnification X 500

20 μm

FIGURE 2-4 : SEM PHOTOGRAPHS OF POLISHED ALUMINA SUBSTRATES

Sample No. 6
Lucalox

Magnification X 500

20 μm

Sample No. 7
Deranox

Magnification X500

20 μm

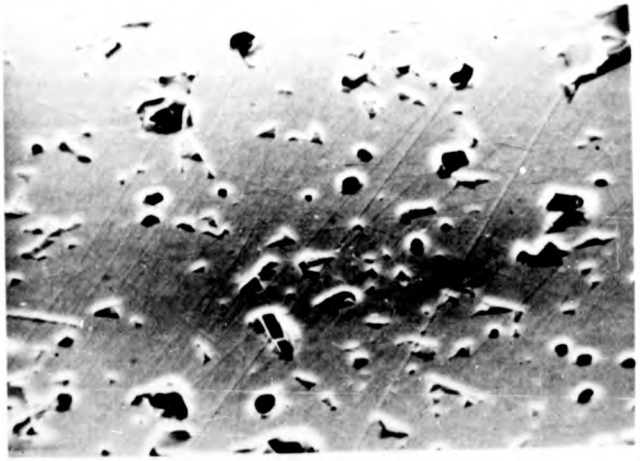

Sample No. 8
American Lava

Magnification X 500

20 μm

FIGURE 2-4 : SEM PHOTOGRAPHS OF POLISHED ALUMINA SUBSTRATES

different reasons, The glazed alumina sample had no visible surface roughness but showed a high degree of waviness, while the "as-fired" sample had a very rough surface with only a small amount of waviness. Neither of these substrates would be suitable for microwave applications.

Comparision of the roughness of the "as-fired" alumina substrate with the corresponding SEM photographs shows that for large-grained substrates a high degree of surface roughness is obtained. The MRC substrate is claimed to be suitable for polishing owing to its fine grained structure. The MRC and Pilkington substrates would both be suitable for microstrip circuits but unacceptable for lumped components.

It is difficult to assess the polished substrates. SEM observations show that these substrates exhibit pits, (figure 2-4) presumably caused by grains being dragged out during grinding and polishing. If the width of the pits approached the diameter of the Talysurf stylus, then pit depth measurements would be inaccurate. From examination of figure 2-4 it can be seen that Deranox 975 has pits of small diameter and this probably explains the low measurements obtained for pit depth and CLA. The presence of pits is likely to cause discontinuities in microstrip and component failure in lumped element circuits.

The remaining substrates all show immeasurable waviness and roughness and would, therefore, be suitable for the present application. The final choice must therefore be based on their electrical properties. Corning 0211 has an alkali content in its chemical composition and

would therefore be unsuitable for electronic applications because adsorbed moisture would form an electrolyte with the hydroxyl ions which would move rapidly in an electric field, thus increasing the surface conductivity. Quartz and sapphire were finally chosen for their low loss at 10 GHz ($\tan\delta \approx 10^{-4}$).

2-5 Comments

The majority of samples used for this investigation were obtained in 1969/70. The MRC and Pilkington substrates became available only recently and were obtained in 1972. It would appear that manufacturers are attempting to reduce grain size in order to improve the surface finish. Talysurf measurements alone are suitable for substrate evaluation but CLA measurements are meaningless unless information on roughness and waviness is also available.

would therefore be unsuitable for electronic applications because adsorbed moisture would form an electrolyte with the hydroxyl ions which would move rapidly in an electric field, thus increasing the surface conductivity. Quartz and sapphire were finally chosen for their low loss at 10 GHz ($\tan\delta \simeq 10^{-4}$).

2-5 Comments

The majority of samples used for this investigation were obtained in 1969/70. The MRC and Pilkington substrates became available only recently and were obtained in 1972. It would appear that manufacturers are attempting to reduce grain size in order to improve the surface finish. Talysurf measurements alone are suitable for substrate evaluation but CLA measurements are meaningless unless information on roughness and waviness is also available.

Chapter 3

DEPOSITION OF THIN FILMS BY SPUTTERING

3-1 Introduction

The phenomenon of sputtering has been known for over a century but only in the last decade has it become a widely applied technique for the deposition of metal and dielectric films for the microelectronic industry. Some reviews of this subject were extant when this work was begun [21,22,23,24] and others have appeared more recently [25,26,27,28] so that only general principles will be described here.

Sputtering is the term applied to the ejection of material from a target by ion bombardment. When the kinetic energy of the bombarding ions exceeds that of the lattice binding energy of the target material, neutral target atoms may be ejected. This momentum transfer process is the underlying principle of all sputtering systems. There are three main methods of sputtering: direct current (DC) sputtering may be used for the deposition of conducting materials, radio frequency (RF) sputtering for deposition of dielectric or conducting materials and reactive sputtering for depositing compounds formed during deposition in the presence of a reactive gas. A brief account of these three methods is given in the following sections together with a detailed account of the design and construction of an RF sputtering unit used for the present research. Further details of the effect of sputtering parameters on dielectric properties and deposition rates are given in Chapter 10.

3-2 DC Sputtering

Ions of sufficient energy for sputtering may be generated in a diode glow discharge tube which is represented in figure 3-1. The target material forms the cathode; upon application of a sufficiently high voltage, breakdown of the gas occurs and a self maintaining glow discharge appears. Figure 3-2 illustrates the main features of the discharge. Argon is the gas mainly used (see section 3-4) for sputtering for the following reasons. Sputtering is a momentum transfer process so that for a given energy dissipation, "heavy" ions have greater momentum and therefore give a higher sputtering yield. In order to prevent chemical reaction between the gas and target material an inert gas is usually chosen. Argon fulfils these technical requirements and is easily available at low cost.

The greatest potential gradient between the electrodes occurs in the Crooke's dark space (CDS) so that this region is of particular interest in sputtering work. Ions from the region of negative glow (NG) are accelerated across the CDS and impinge on the target giving rise to sputtering and secondary electron emission. The secondary electrons are then accelerated across the CDS and cause further ionization of the gas. It is this process which renders the glow self-maintaining. As the mean free path of an electron is inversely propertional to the pressure, a decrease in pressure will require the electrons to travel further before sufficient ionizing collisions have taken place to sustain the discharge. This results in an increase in the width of the CDS. When the CDS extends as far as the anode, the discharge can no longer be maintained and the glow is extinguished.

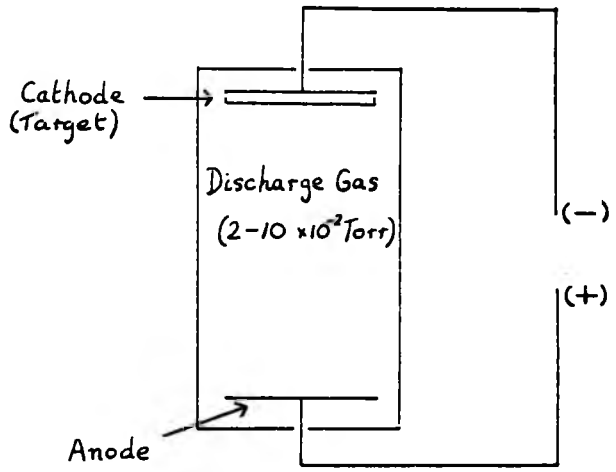

FIGURE 3-1 : DIODE GLOW DISCHARGE TUBE

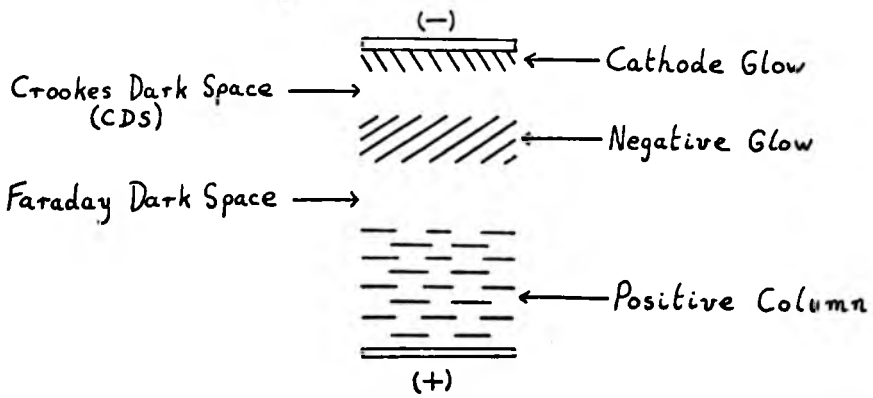

FIGURE 3-2 : MAIN FEATURES OF A DC DISCHARGE

The product of the width of the CDS and gas pressure for argon is about 0.3 Torr cm. thus restricting the working pressure to the range 20 - 100 milli torr. [23] Lower pressures may be used by employing a triode system [26] with a heated filament to provide electrons for the discharge and thus reduce the need for secondary electron emission. Application of a longitudinal magnetic field [26] is another method which permits the use of lower pressures; in this case, the electrons move in a spiral along the magnetic field, thus increasing the ionization efficiency in the region of the negative glow.

In a DC sputtering system the anode is usually earthed and also forms the work table. To prevent discharge occuring between other grounded parts of the vacuum chamber, an earthed shield is placed around the target so that the separation between the two is less than the width of the CDS.

3-3 RF Sputtering

Dielectrics cannot be sputtered by the above process because the target would quickly aquire positive charge which would extinquish the glow. Anderson et. al. [29] first applied the technique of RF sputtering to the cleaning of glass. The principle of RF sputtering stems from the fact that ions and electrons have different mobilities. The applications of an RF potential to a dielectric surface causes more electrons to be attracted in the positive half-cycle than positive ions in the negative half-cycle. This would give rise to an excess electron current to the insulator. As the net DC current to the dielectric must be zero, the dielectric surface must

become negatively biassed creating a positive ion sheath in the region of the dielectric surface. This is illustrated graphically in figure 3-3. The positive ion sheath is the counterpart of the CDS in a dc system. At sufficiently high fields across the ion sheath, sputtering can occur. Davidse and Maissel [30] used RF sputtering as a practical method for depositing thin insulating films and Anderson [29] showed that typical frequencies required were about 10 MHz.

Three basic types of electrode structures are used for RF sputtering and are shown in figure 3-4. The diode system of figure 3-4a. is the most simple one. If, however, this system is used when the substrate electrode is grounded all other earthed parts of the vacuum system will also act as electrodes and unwanted sputtering of these components will occur. Re-sputtering of the film is possible under these conditions. The use of an RF system with two non-grounded electrodes (figures 3-4b and 3-4c) minimizes these effects.

As in the case of the DC apparatus, an earthed shield is placed around the target electrode to prevent unwanted discharge to earthed parts of the system. The separation distance, however, is more critical than for the DC case because a separation which is too small will result in loss of RF power owing to the low impedance to ground. Davidse [31] found a spacing of 0.5 cm to be satisfactory.

A typical working pressure for RF sputtering is 5×10^{-3} Torr. Increasing the ionization efficiency by application of a longitudinal magnetic field allows sputtering pressures of about 10^{-3} Torr to be used.

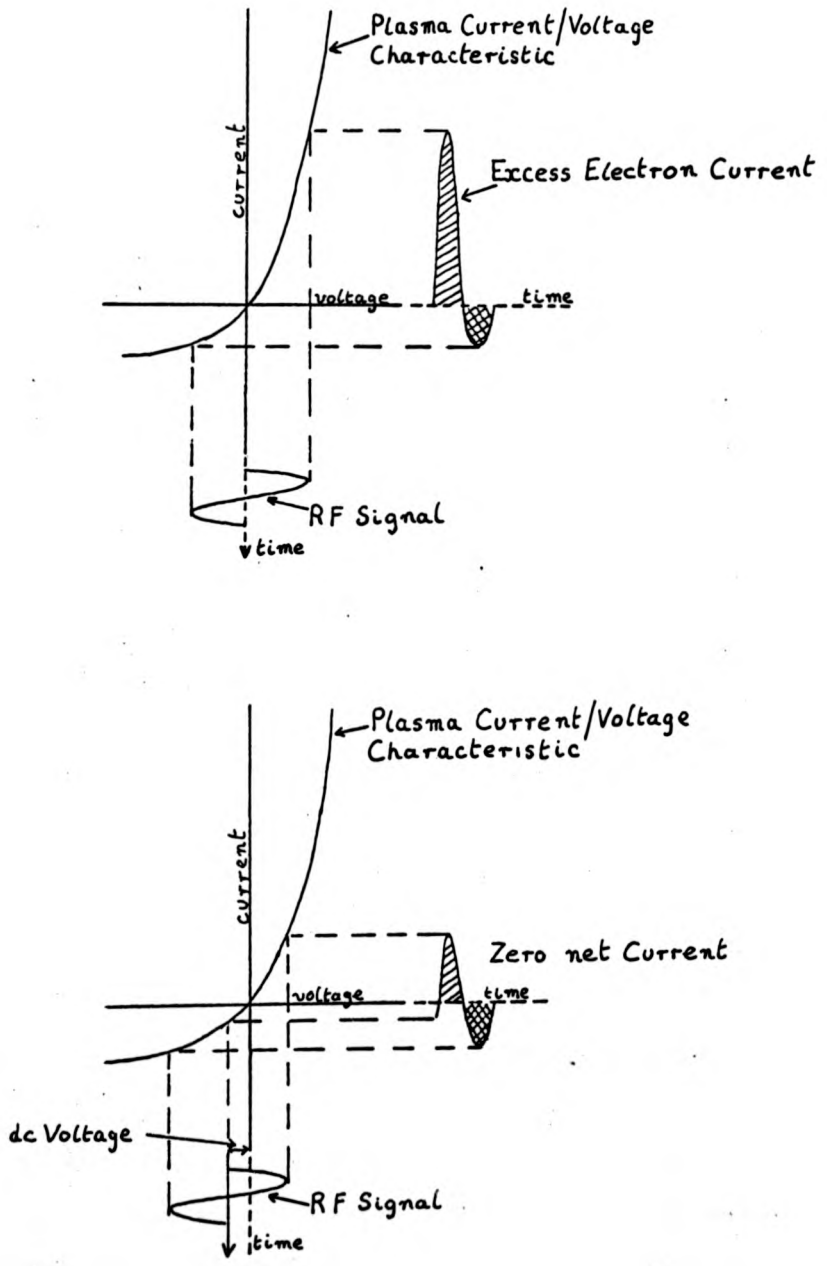

FIGURE 3-3 : MECHANISM OF RF SPUTTERING (24)

Although RF sputtering was primarily developed for the deposition of dielectrics, it is also applicable to the deposition of metals. It is merely necessary to introduce a blocking capacitor between the target electrode and the RF oscillator. The equivalent effect may be produced by placing the metal target on top of a dielectric target.

3-4 Reactive Sputtering

As mentioned earlier, argon gas is normally used for sputtering. However, if this gas is partially or wholly replaced by a reactive gas (e.g. oxygen, nitrogen) which will react with the target material during sputtering, compound films may be deposited. Janus and Shirm [32] successfully deposited silicon nitride ($Si_3 N_4$) films using a silicon cathode and a gas mixture of argon and nitrogen.

3-5 Comparision of Sputtering and Evaporation Methods

Before the development of sputtering, thermal evaporation, using resistive or electron beam heating, was probably the most common method used for depositing films. The two methods are compared below.

a) Deposition Rate

Sputtering rates are usually slower than evaporation rates although high sputtering rates have been obtained by Grantham et. al. [33] using very high RF powers. The sputtering rate is dependent upon the input power to the discharge, the sputtering pressure, the source/substrate distance and the strength of the magnetic field.

b) Compounds

Compounds deposited by thermal evaporation undergo thermal dissociation yielding non-stoichiometric films. Silicon dioxide films deposited by RF sputtering, however, have been shown [34] to resemble closely the bulk material in chemical composition.

c) Adhesion

Sputtered films are in general more adherent than evaporated films. This is usually attributed to the higher arrival energy of sputtered atoms.

A particular advantage of sputtering is its capability of depositing high melting point materials which are difficult to deposit by evaporation. Perhaps the main disadvantage of sputtering is contamination of the film by the sputtering gas. Schwartz and Jones [35], however, have shown that the presence of argon in silicon dioxide films does not appear to have any adverse effect on film quality.

3-6 Design Considerations for an RF Sputtering Unit

Although sputtering systems were commercially available when this work was begun, they were mainly intended for batch production; no small systems were available for research purposes. It was, therefore, decided that an RF sputtering unit should be built utilizing a vacuum system that had already been obtained.

The basic equipment required for an RF sputtering unit is shown in figure 3-5. The pumping unit should be capable of evacuating the chamber to a very low pressure in order to avoid contamination of the sputtering gas with atmospheric gases. It has been shown [31] that a slight amount of oxygen present in the sputtering gas during the deposition of silicon dioxide causes a decrease in the deposition rate. For this reason alone, a high purity sputtering gas should be used. Precise control of the sputtering pressure is also required. Introduction of the argon through a needle valve with fine control by adjustment of the baffle valve is satisfactory.

Typical oscillators used for sputtering have a power output of 1 - 6 KW and operate in the Megahertz frequency range. A matching network allows maximum power transfer to the discharge and is essential if a remote RF generator is used. It may also help to ignite the discharge. Application of a longitudinal magnetic field is not essential but is useful in striking the discharge, increasing the deposition rate and allows the use of lower sputtering pressures. Other techniques for striking a plasma include "spark-plug" ignition and high pressure starting, the pressure being subsequently reduced to the working pressure.

Although sputtering is essentially a cold deposition technique, a great deal of heat is produced both at the target and substrate through bombardment by energetic particles. For this reason it is necessary to cool both the target electrodes and the work table. When atoms bombard a substrate, some will be deposited while others

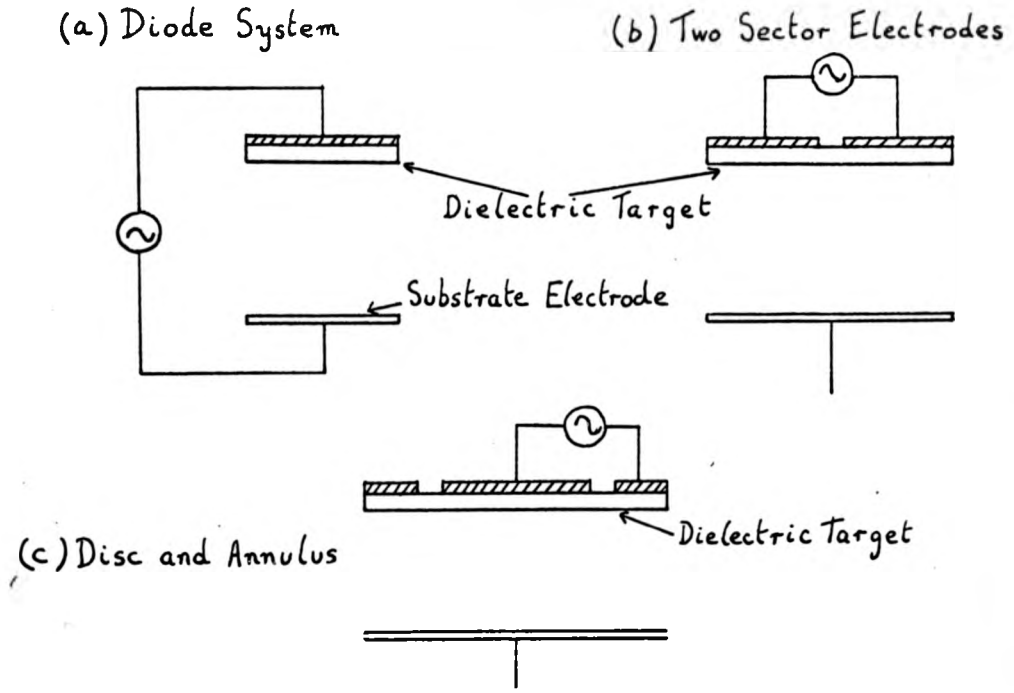

FIGURE 3-4 : ELECTRODE STRUCTURES FOR RF SPUTTERING

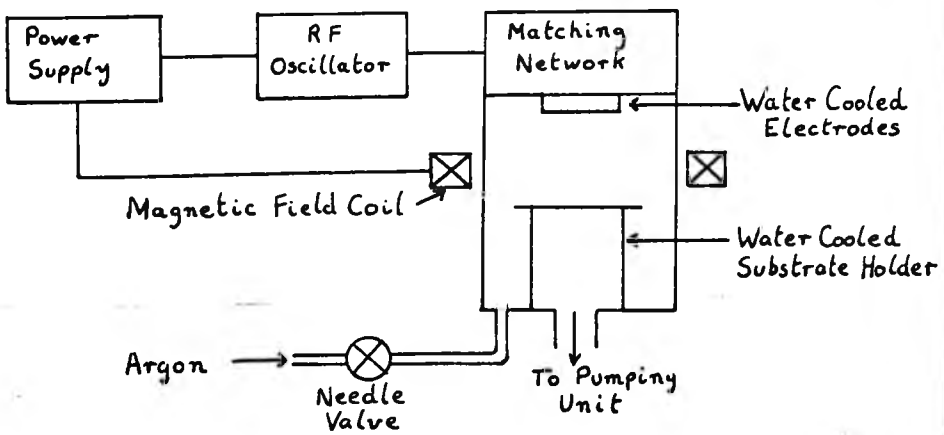

FIGURE 3-5 : EQUIPMENT FOR RF SPUTTERING

may have sufficient energy to be re-emitted. The ratio of the number of deposited atoms to the number of incident atoms is known as the "sticking coefficient". An increased substrate temperature decreases the sticking coefficient. Deposition rates in sputtering are low and the use of a cooled work table will allow the maximum deposition rate to be obtained. Cooling of these parts of the system is also essential to minimize outgassing which may contaminate the sputtering gas and cause the sputtering pressure to vary. It is also useful, for experimental purposes, to have a variable target/substrate distance as this affects uniformity (36) and deposition rate (see section 3-11).

As mentioned earlier, correct spacing of the target electrodes and ground shield is of great importance if unwanted discharges in these regions is to be avoided. Attachment of the target to the electrodes depends on the target material and on whether sputtering is upwards or downwards. There are available various bonding techniques for making good thermal contact between the target and the electrode. (37)

A useful addition to a sputtering unit is a shutter which may be used for pre-sputtering of the target. This allows cleaning of the target by removal of surface contaminants, and operating conditions may be stabilized before the start of the actual deposition.

The above requirements fall into two categories, namely essential requirements and useful additions. These are summarized overleaf.

may have sufficient energy to be re-emitted. The ratio of the number of deposited atoms to the number of incident atoms is known as the "sticking coefficient". An increased substrate temperature decreases the sticking coefficient. Deposition rates in sputtering are low and the use of a cooled work table will allow the maximum deposition rate to be obtained. Cooling of these parts of the system is also essential to minimize outgassing which may contaminate the sputtering gas and cause the sputtering pressure to vary. It is also useful, for experimental purposes, to have a variable target/substrate distance as this affects uniformity (36) and deposition rate (see section 3-11).

As mentioned earlier, correct spacing of the target electrodes and ground shield is of great importance if unwanted discharges in these regions is to be avoided. Attachment of the target to the electrodes depends on the target material and on whether sputtering is upwards or downwards. There are available various bonding techniques for making good thermal contact between the target and the electrode. (37)

A useful addition to a sputtering unit is a shutter which may be used for pre-sputtering of the target. This allows cleaning of the target by removal of surface contaminants, and operating conditions may be stabilized before the start of the actual deposition.

The above requirements fall into two categories, namely essential requirements and useful additions. These are summarised overleaf.

a) Essential Requirements

1. A high-vacuum pumping unit capable of 10^{-6} Torr.
2. An RF oscillator operating in the Megahertz range with a power output of 1 KW or more.
3. Efficient cooling of target electrodes and substrate holder.
4. Shielding of target electrodes with correct spacing.
5. Precise control of the sputtering pressure.

b) Useful Additions

1. Method of striking a plasma (other than high pressure starting).
2. Shutter for pre-sputtering.
3. Work table of adjustable height.
4. Matching network for maximum power transfer.

3-7 Construction

The sputtering unit built was of the non-grounded double electrode type. The oscillator circuit and electrode configuration were based on a design by Probyn (38) of the Electrical Research Association (ERA). A schematic diagram of the system is shown in figure 3-6. The vacuum chamber consists of a 12" diameter glass cylinder seated on a convential base plate. The system is sealed by a top plate on which the RF oscillator is accommodated. The electrodes are fed directly from the oscillator, through the top plate to the vacuum chamber, thus eliminating the need for a matching network. The electrode structure shown in more detail in figures 3-7 and 3-8, consists of two semicircular water-cooled discs separated by a 4 mm. gap to prevent discharge in this region. A similar gap exists between the

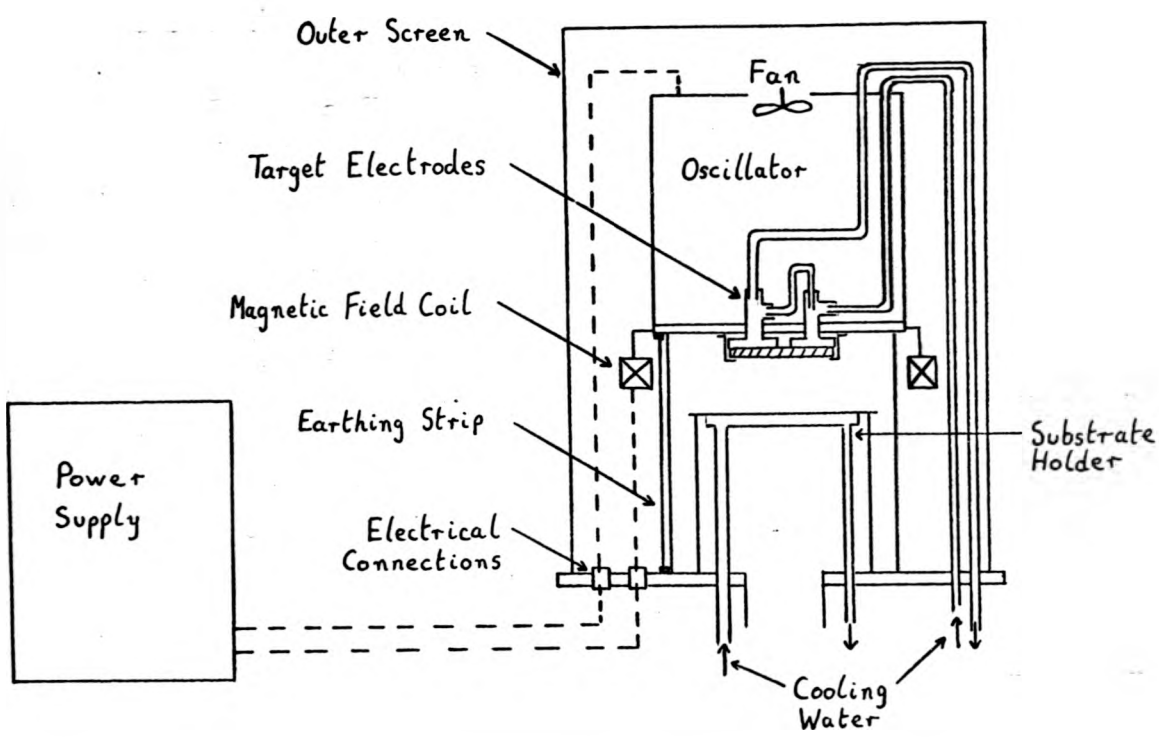

FIGURE 3-6 : A SCHEMATIC DIAGRAM OF THE RF SPUTTERING UNIT

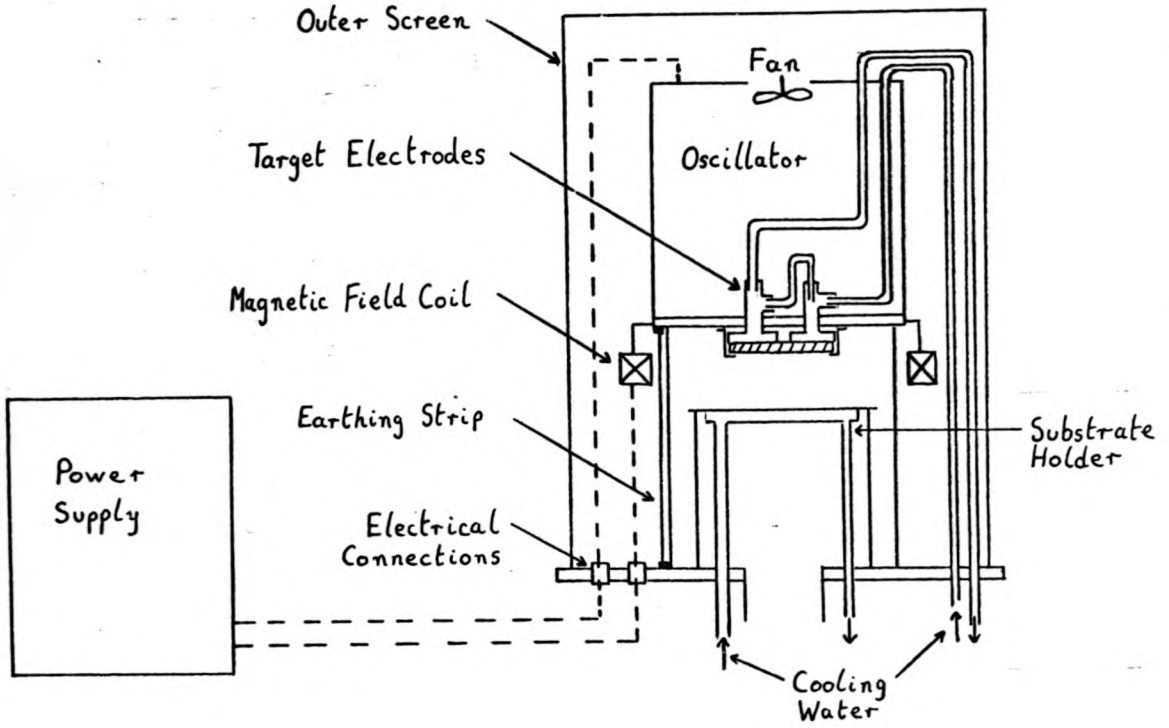

FIGURE 3-6 : A SCHEMATIC DIAGRAM OF THE RF SPUTTERING UNIT

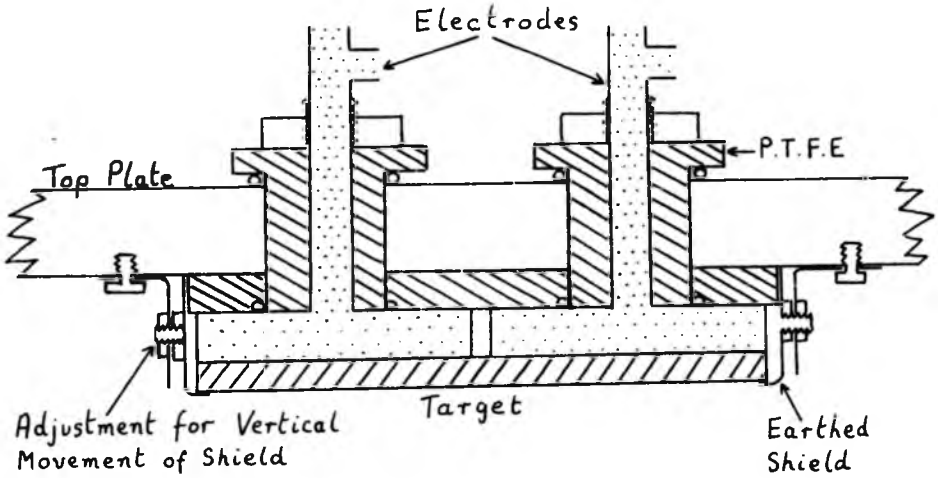

FIGURE 3-7 : SCHEMATIC DIAGRAM OF THE TARGET AND ELECTRODE ASSEMBLY

FIGURE 3-8 : PHOTOGRAPH OF THE TARGET AND MAGNETIC FIELD COIL

electrode and the ground shield which is also used to support the target as shown. The ground shield also has vertical adjustment to cater for varying thickness of target. The insulating feed-throughs were made of polytetraflourethylene (PTFE) and the whole structure formed the top plate of the vacuum chamber. The top plate formed the chassis for the oscillator thus eliminating the need for a matching network and considerably reducing RF interference with other electronic equipment.

Figure 3-9 shows the circuit diagram of the oscillator which is capable of a maximum power output of 1 KW. It uses a conventional Hartley push pull circuit operating in class C. At high powers, removal of heat from the anodes of the triode valves is essential. This is achieved by using anodized chimneys on the valves and a cooling fan in the perforated screen surrounding the oscillator. All electrical connections to the power supply were taken through the top of the screen to sockets in the base plate (figure 3-6) while water connections were taken through the base plate directly to the water supply. Only one water supply was used for cooling both electrodes, the outlet from the first electrode being taken to the inlet of the second. To minimize leakage current through the cooling water, a 21 ft. length of $\frac{1}{4}$in. ID polythene tubing was used between the electrodes. This corresponded to a resistance path of approximately 1 MΩ. Some initial problems with the sputtering unit were traced to poor earthing of the vacuum chamber top plate. Further details of this fault are given in Appendix 1 and experience has shown that a good earth connection is essential for correct operation. The top plate also supports a magnetic field coil used for striking the discharge and

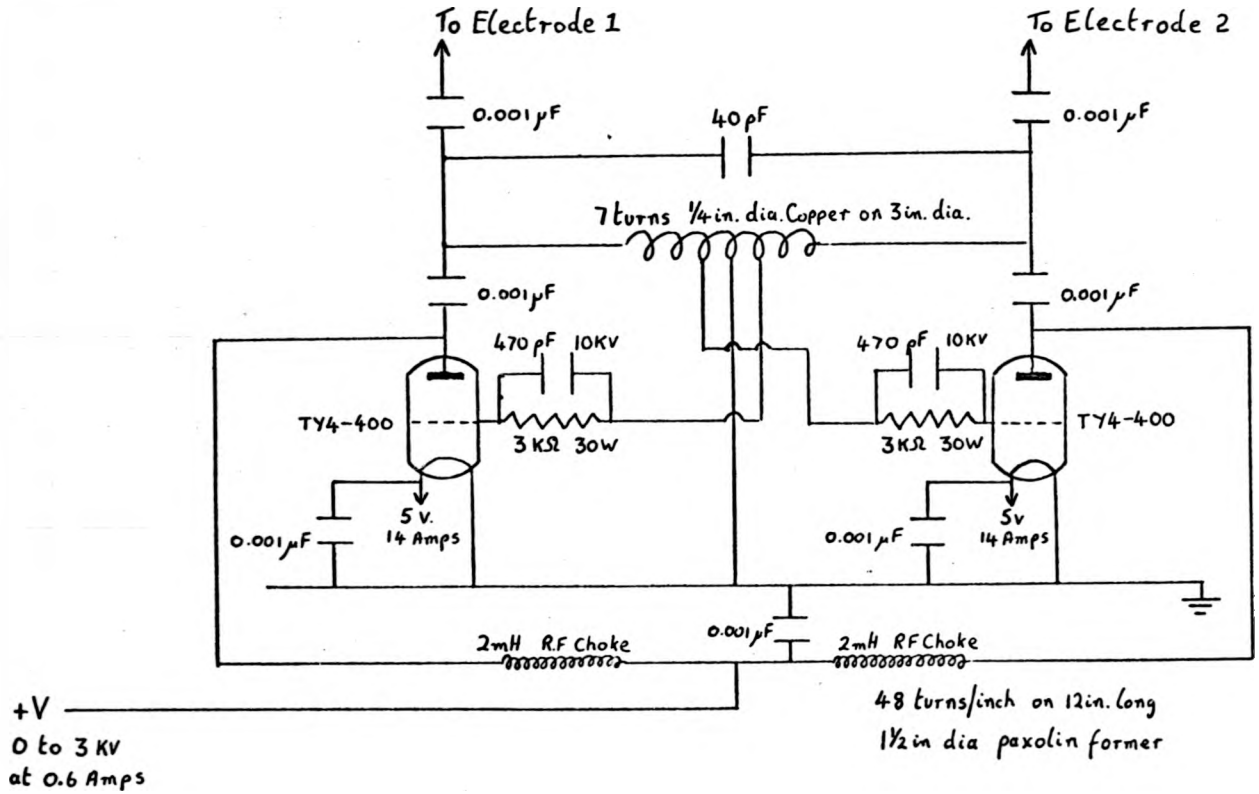

FIGURE 3-9 : CIRCUIT DIAGRAM OF R F OSCILLATOR

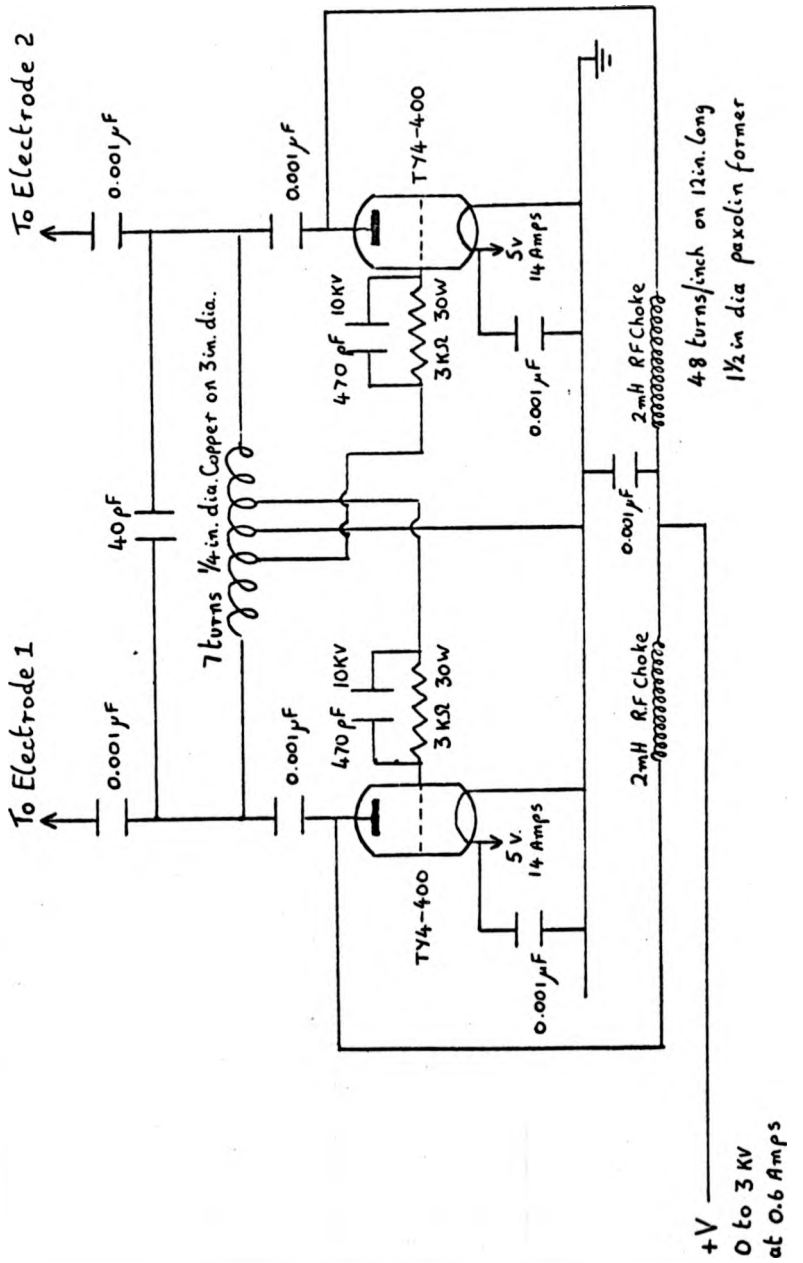

FIGURE 3-9 : CIRCUIT DIAGRAM OF R F OSCILLATOR

increasing deposition rates. These supports were designed to allow for vertical movement of the magnet to suit any source/substrate distance.

Access to the interior of the chamber requires removal of the top plate assembly. The total weight of the oscillator and magnet is 80 lb. Lifting is achieved by constant-force springs suspended from a gantry which is fixed to the frame supporting the vacuum pumping unit. This mechanism can be seen in the photograph of the completed system in figure 3-10. Two lifting rods were taken from the top plate through the top of the oscillator screen to connections for two constant force springs. Each spring supplies 36 lb. force thus requiring a further 8 lb. force to be exerted by the operator for lifting. Catches at the top of the gantry may be brought down under the lifting handles for full support of the oscillator assembly. In the fully up position there is also access to the target, which may be changed quickly and easily (see figure 3-8).

A circuit diagram of the power supply is given in figure 3-11. Four safety circuits are incorporated to protect the power supply and oscillator. A vacuum switch, relay 1, prevents activation of the supply when the chamber is at atmospheric pressure. Relay 2 ensures that the valve filament current is on before the high tension supply can be applied, and relay 3 requires the HT variac to be at zero before HT can be applied thus preventing the sudden application of high voltage. Relay 4 is an overload cut-out which was found to be necessary, particularly at high pressure operation. This relay is normally closed. The voltage across a 5Ω resistor in the earth return

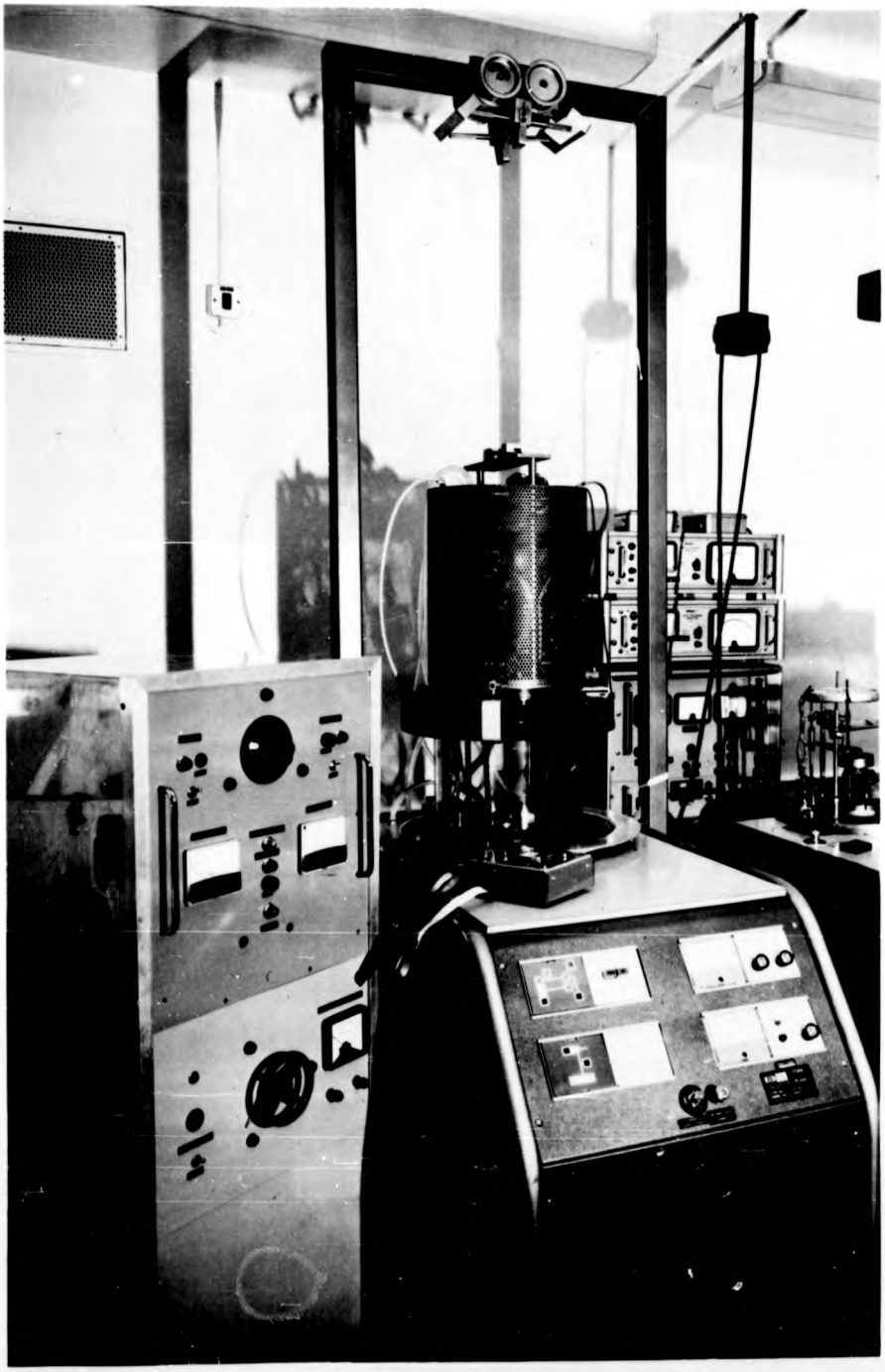

FIGURE 3-10 : PHOTOGRAPH OF RF SPUTTERING UNIT

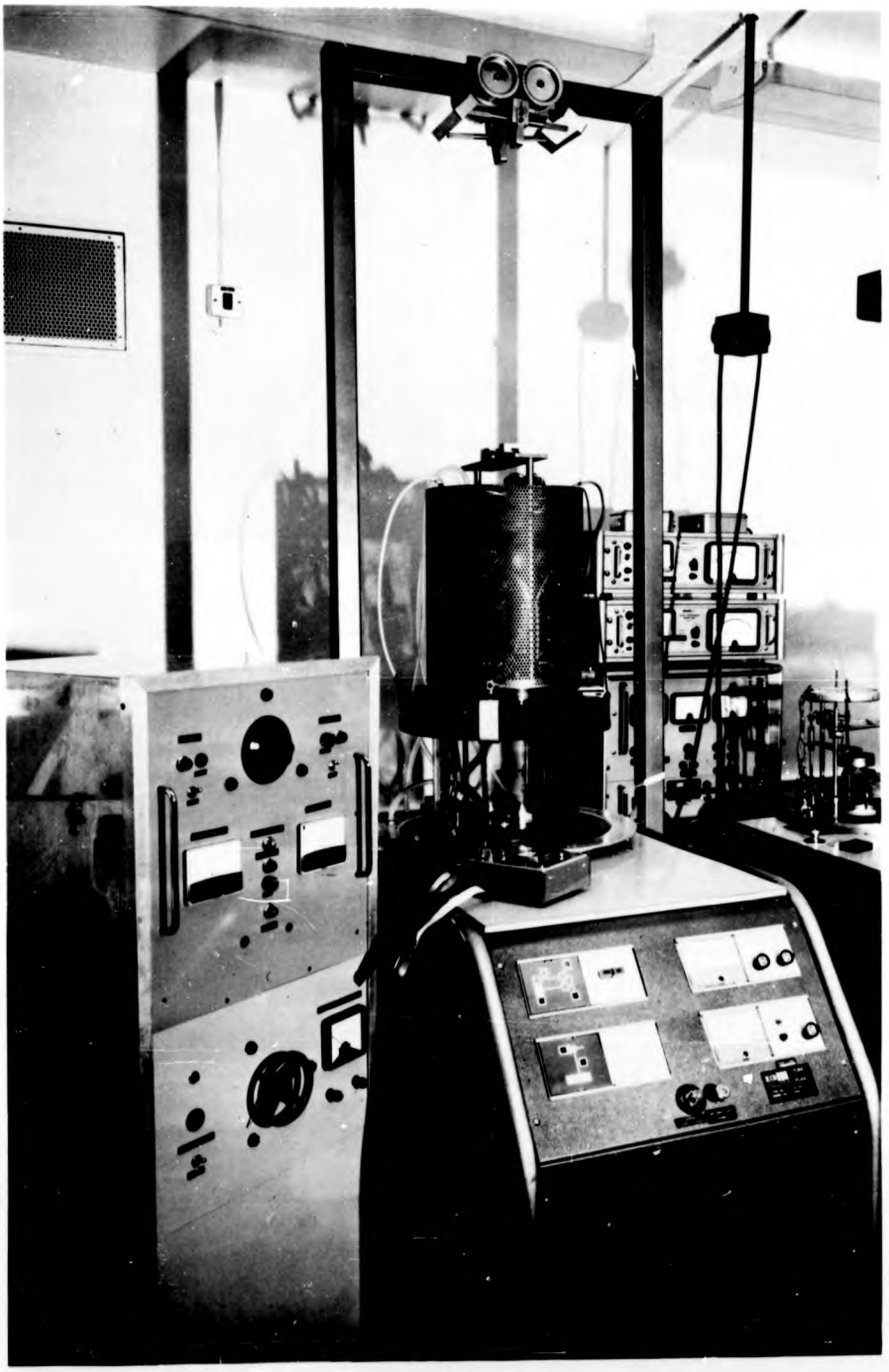

FIGURE 3-10 : PHOTOGRAPH OF RF SPUTTERING UNIT

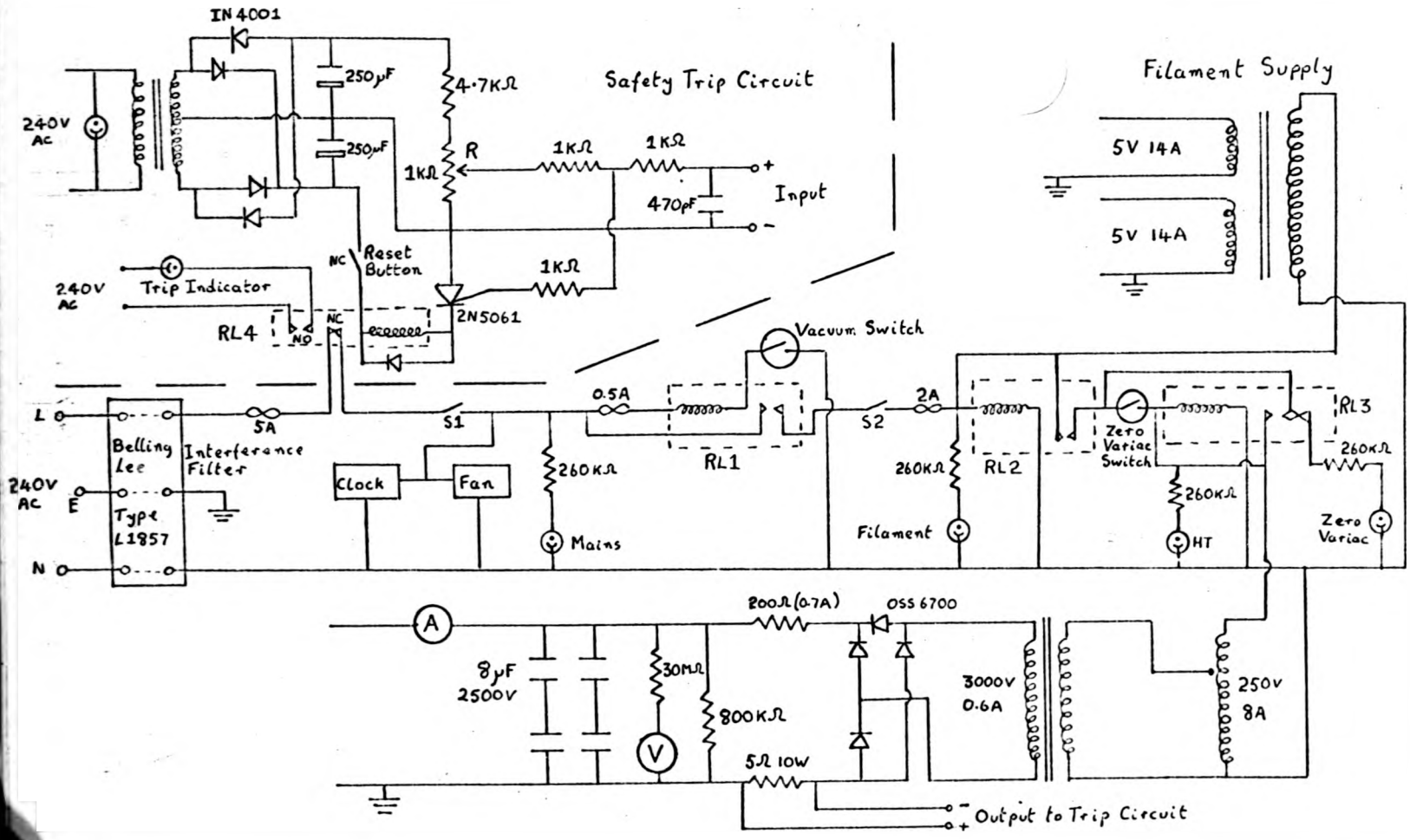

FIGURE 3-11 : CIRCUIT DIAGRAM OF POWER SUPPLY FOR RF OSCILLATOR

line of the HT supply is used to monitor the HT current and is applied to the gate of a Silicon controlled rectifier (SCR). When this voltage exceeds a preset limit determined by the variable bias resistor R, the SCR fires and relay 4 opens. The relay open circuits the mains input to the power supply and remains open until the reset is operated.

Also included in the power supply circuit is an electric clock requiring a manual start. The clock is started when the film deposition is commenced. If, for any reason, the overload cut-out should operate the clock is stopped and the film deposition time is accurately known.

The substrate work table is made of copper with copper cooling coils soldered to its base. Feedthroughs were designed to allow vertical movement of the work table while also insulating the work table from earth, allowing bias sputtering to be performed if required (39, 40) . A diagram of the feedthroughs is shown in figures 3-12. A shutter, used for pre-sputtering is also fitted into the vacuum chamber. A five leaf shutter of the Schmitter shape as used by Priestland (36) was made for this purpose(see figure 3-13).

During operation, the oscillator and vacuum chamber are surrounded by a perforated aluminium screen clamped to the base plate. This provides RF screening and also serves as a protective screen for the vacuum system.

The pumping unit is a commercially available apparatus made by

line of the HT supply is used to monitor the HT current and is applied to the gate of a Silicon controlled rectifier (SCR). When this voltage exceeds a preset limit determined by the variable bias resistor R, the SCR fires and relay 4 opens. The relay open circuits the mains input to the power supply and remains open until the reset is operated.

Also included in the power supply circuit is an electric clock requiring a manual start. The clock is started when the film deposition is commenced. If, for any reason, the overload cut-out should operate the clock is stopped and the film deposition time is accurately known.

The substrate work table is made of copper with copper cooling coils soldered to its base. Feedthroughs were designed to allow vertical movement of the work table while also insulating the work table from earth, allowing bias sputtering to be performed if required (39, 40) . A diagram of the feedthroughs is shown in figures 3-12. A shutter, used for pre-sputtering is also fitted into the vacuum chamber. A five leaf shutter of the Schmitter shape as used by Priestland (36) was made for this purpose(see figure 3-13).

During operation, the oscillator and vacuum chamber are surrounded by a perforated aluminium screen clamped to the base plate. This provides RF screening and also serves as a protective screen for the vacuum system.

The pumping unit is a commercially available apparatus made by

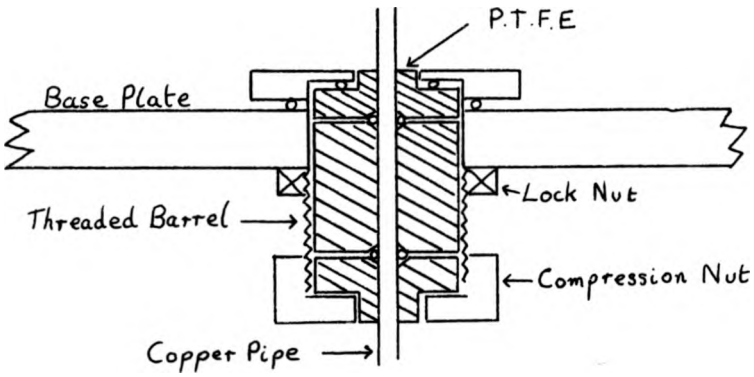

FIGURE 3-12 : COOLING WATER FEEDTHROUGH FOR SUBSTRATE HOLDER

FIGURE 3-13 : PHOTOGRAPH OF SHUTTER

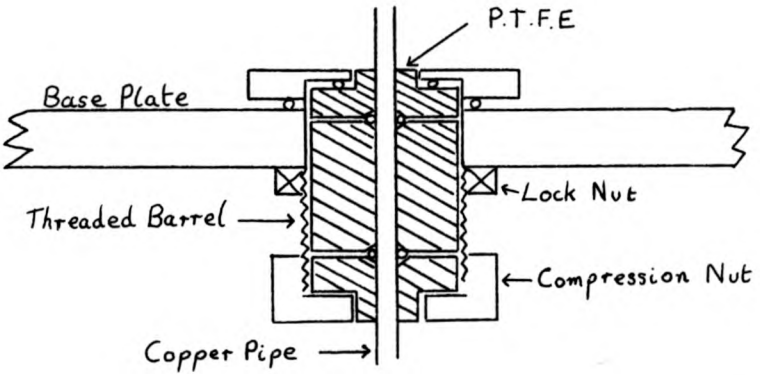

FIGURE 3-12: COOLING WATER FEEDTHROUGH FOR SUBSTRATE HOLDER

FIGURE 3-13 : PHOTOGRAPH OF SHUTTER

Birvac. This utilizes an Edwards E04 diffusion pump with a pumping speed of 600 litres/min. and an Edwards ES150 rotary pump having a capacity of 150 litres/min. A Birvac H1001 Pirani gauge is used for measuring the backing line pressure and a Birvac H101 Penning gauge was initially used for measuring the chamber pressure. The Penning gauge however was found to be inaccurate for measuring sputtering pressures (see Appendix 1) and it was later found that these gauges are useless for measuring pressures above 10^{-3} Torr. For this reason an Edwards Pirani gauge is now used for measurement of pressures in the 10^{-2} to 10^{-3} Torr range.

3-8 Balancing of the Oscillator

This is performed in a simple but effective manner. Incorrect balancing was first detected during measurements of the uniformity of the thickness profile of some early work pieces. It was found that one side of the substrate received a thicker coating than the other. Furthermore, on application of high DC input powers it was noticed that one of the anodes of the oscillator would glow. Balancing was achieved by adjustment of the centre tap of the tank coil with corresponding adjustment of the grid bias tappings until both anodes began to glow at the same high input power. A further check on uniformity of deposition gave a symmetrical deposition around the centre of the work table.

3-9 Operation of the Sputtering Unit

Routine operating instructions have been prepared as follows.

a) Rough pump chamber to 0.1 Torr. Admit argon to flush out connecting pipes and re-pump to 0.1 Torr.

b) Evacuate chamber on diffusion pump to below 10^{-5} Torr.

c) Admit argon to required sputtering pressure.

d) Ensure cooling water is flowing in electrodes and work table.

e) Switch on power supply, filament current, and magnetic field coil current set to 4 Amps. (1.25×10^{-2} Wb/m^2)

f) With shutter closed apply HT slowly until plasma shows. Allow ten minutes for initial outgassing before setting HT to required power.

g) Pre-sputter for about 15 minutes at operating conditions.

h) Open shutter and start clock.

If for any reason the HT trip circuit should operate, the power supply should be switched off and the reset button operated. Possible reasons for excessive current drain on the power supply are:

1) Discharge occuring in the interelectrode spacing. This may result from failing in the cooling water system. Excessive heating of electrodes or target will produce outgassing with consequent local rises in chamber pressure.

2) An increase in the sputtering pressure owing to insufficient flow of cooling water in both target electrodes or work table causing excessive outgassing.

In either case, the fault should be corrected before re-starting the cycle at operation (e) although pre-sputtering may be omitted.

3-10 Effect of Deposition Parameters on Deposition Rate

Experiments were performed to determine the effect of DC input power, magnetic field strength and pressure on the deposition rate for fused quartz ($Si\ O_2$). This information was needed for later experiments.

A glass substrate was placed at the centre of the work table with silicone vacuum grease between the two. This was found to be essential for reproducible results and acceptable deposition rates to be obtained (see chapter 5). The silicone grease is a good thermal conductor. An out-of-contact stainless steel mask was placed over the substrate to provide an edge between the deposited film and the substrate so that thickness measurements could be made with a Talystep.

It can be seen from figure 3-14 that the depsotion rate increases linearly with DC input power. This type of variation was reported by Probyn [38] using a disc and annulus electrode structure, although deposition rates reported by him for a given input power are considerably less than those shown in figure 3-14. It is probable that the use of silicone grease in these experiments maintained the substrate at a low temperature thus increasing the "sticking coefficient" and hence the deposition rate. Probyn also used an out-of-contact target which he has shown to decrease the deposition rate.

The effect of pressure on the deposition rate is shown in figure 3-15. Only three pressures were used because the pressure gauge was calibrated only at these points. However, it can be seen that the deposition rate remains approximately constant between 10^{-3} and

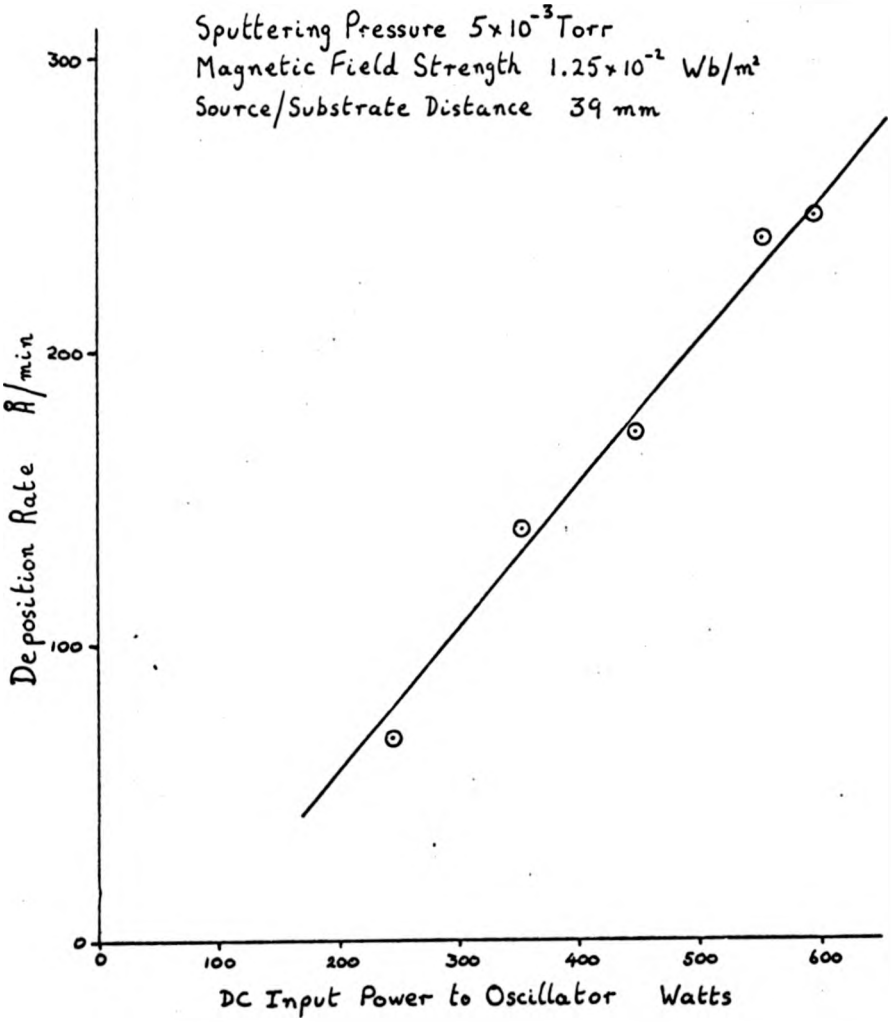

FIGURE 3-14 : THE EFFECT OF DC INPUT POWER ON THE DEPOSITION RATE OF SILICON DIOXIDE

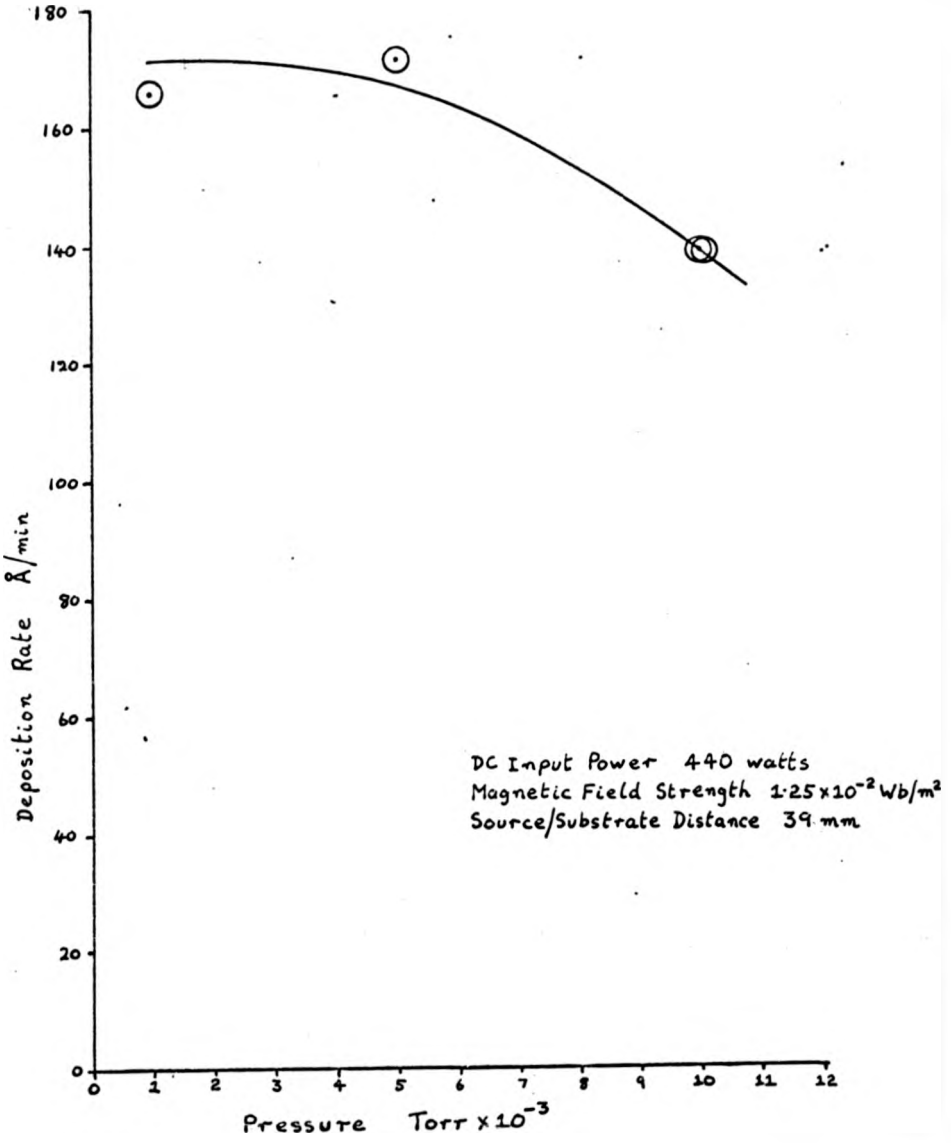

FIGURE 3-15 . THE EFFECT OF SPUTTERING PRESSURE ON THE DEPOSITION RATE OF SILICON DIOXIDE

5×10^{-3} Torr; at pressures greater than 5×10^{-3} Torr, there is a definite fall in deposition rate. This can be explained by the decrease in the mean free path of the sputtered material causing more atoms to be back scattered to the target, fewer atoms being able to reach the substrate. Vossen and O'Neil [24] found a constant deposition rate between pressures of 2×10^{-3} and 1.5×10^{-2} Torr; above this latter pressure, a decrease occurred. The results of Vossen and O'Neil cannot be compared directly because their actual deposition conditions are not described. It is shown in Chapter 10 that the effect of pressure on the deposition rate at a given point on the substrate is dependent on the magnetic field strength used and the DC input power to the oscillator.

Figure 3-16 shows the variation of deposition rate with magnetic flux density. It can be seen that twice the "no field" deposition rate can be obtained by using a field of 1.25×10^{-2} Wb/m^2. As reported by Davidse [31] there is a tendency for a saturation level in the deposition rate to occur at high magnetic field strengths, probably corresponding to a saturation in the ion density.

3-11 Uniformity Measurements

These measurements were performed by depositing nine strips of silicon dioxide through an out-of-contact mask onto 7.5 cm x 2.5 cm (3 in. x 1 in.) microscope slides positioned on a line through the centre of the work table. Unlike the disc and annulus electrode structures, which produce thickness profiles radially symmetrical about the centre, the two sector electrode structure produces different

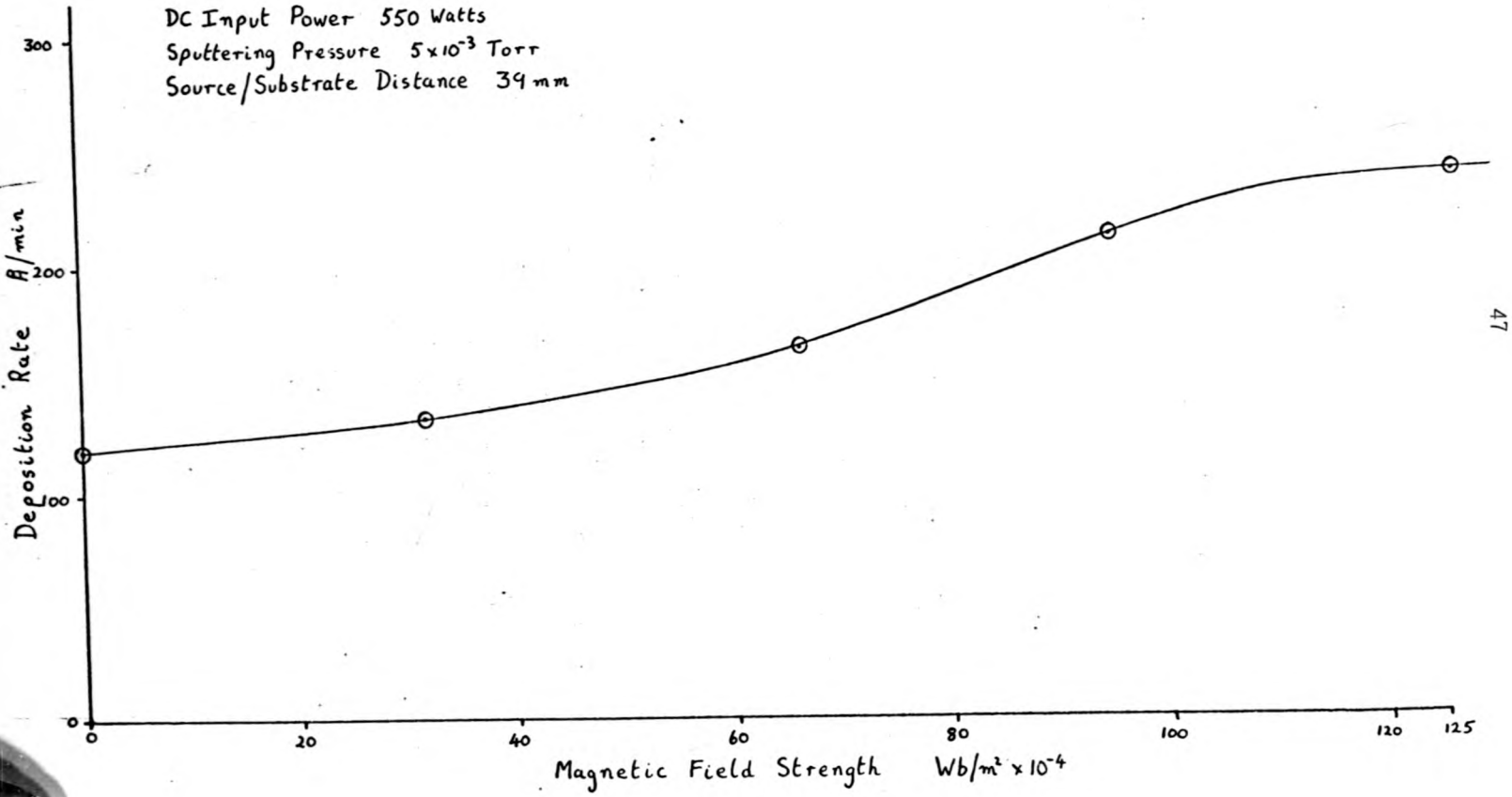

FIGURE 3-16 : THE EFFECT OF A MAGNETIC FIELD ON THE DEPOSITION RATE OF SILICON DIOXIDE

profiles in directions perpendicular and parallel to the electrode gap. This can be seen in figure 3-17. It was also observed that maximum etching of the target occured at the perimeter and on a line corresponding to the electrode gap.

The effects of magnetic field strength and source/substrate distance have also been investigated. Figure 3-18 shows the thickness profile obtained across substrates placed perpendicularly to the electrode gap. Curves I and II were obtained from films deposited with magnetic fields of 1.25×10^{-2} Wb/m^2 and 0 Wb/m^2 respectively. It can be seen that the use of a magnetic field greatly improves uniformity. This is probably caused by the increased ion density causing sputtered atoms to undergo more collisions and therefore giving a more random direction to atoms arriving at the substrate. Curves I and III were obtained with source/substrate distances of 3.9 and 6.0 cm respectively. Again uniformity is improved (at the expense of deposition rate) for the larger seperation distance. This may again be explained in terms of collisions; as the distance a sputtered atom must travel to reach the substrate is increased, it will naturally undergo more collisions with both gas ions and atoms and lose most of its initial sputtered kinetic energy, and reach the substrate by diffusion.

3-12 Comments

The system described worked well for the purpose of this research. Two design features that could be improved, although not detrimental to the sputtering process, are as follows:-

profiles in directions perpendicular and parallel to the electrode gap. This can be seen in figure 3-17. It was also observed that maximum etching of the target occured at the perimeter and on a line corresponding to the electrode gap.

The effects of magnetic field strength and source/substrate distance have also been investigated. Figure 3-18 shows the thickness profile obtained across substrates placed perpendicularly to the electrode gap. Curves I and II were obtained from films deposited with magnetic fields of 1.25×10^{-2} Wb/m^2 and 0 Wb/m^2 respectively. It can be seen that the use of a magnetic field greatly improves uniformity. This is probably caused by the increased ion density causing sputtered atoms to undergo more collisions and therefore giving a more random direction to atoms arriving at the substrate. Curves I and III were obtained with source/substrate distances of 3.9 and 6.0 cm respectively. Again uniformity is improved (at the expense of deposition rate) for the larger seperation distance. This may again be explained in terms of collisions; as the distance a sputtered atom must travel to reach the substrate is increased, it will naturally undergo more collisions with both gas ions and atoms and lose most of its initial sputtered kinetic energy, and reach the substrate by diffusion.

3-12 Comments

The system described worked well for the purpose of this research. Two design features that could be improved, although not detrimental to the sputtering process, are as follows:-

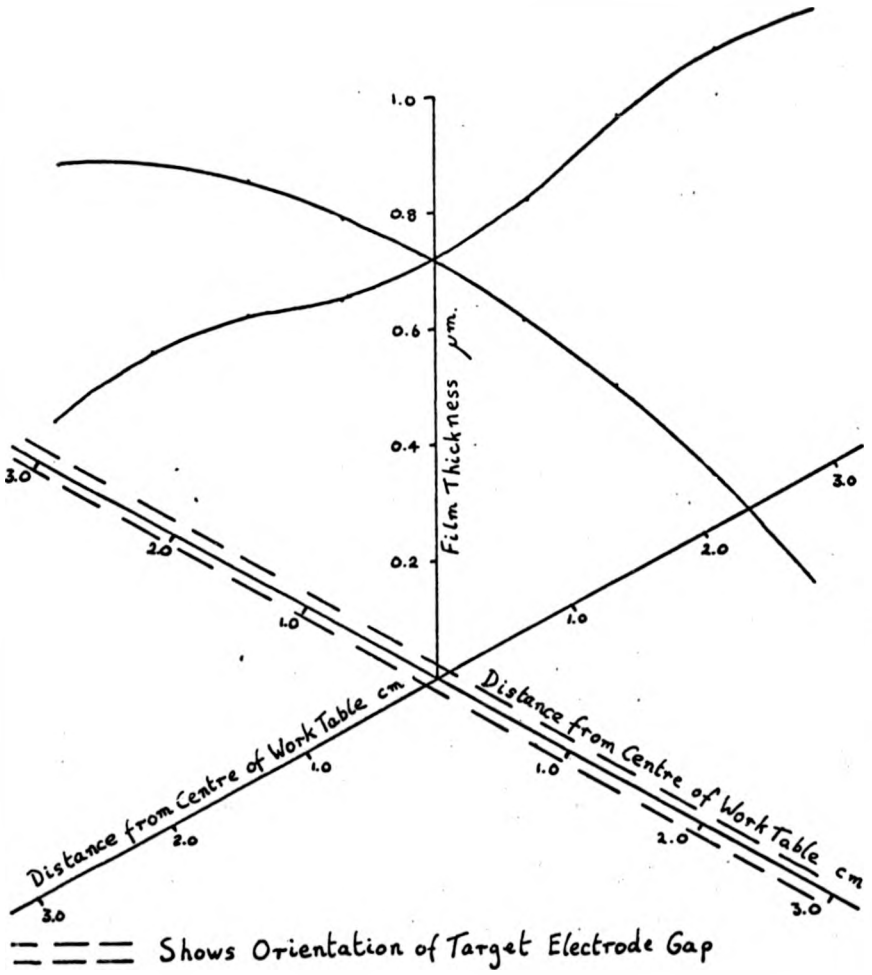

FIGURE 3-17 : THICKNESS PROFILES RELATIVE TO THE ELECTRODE GAP

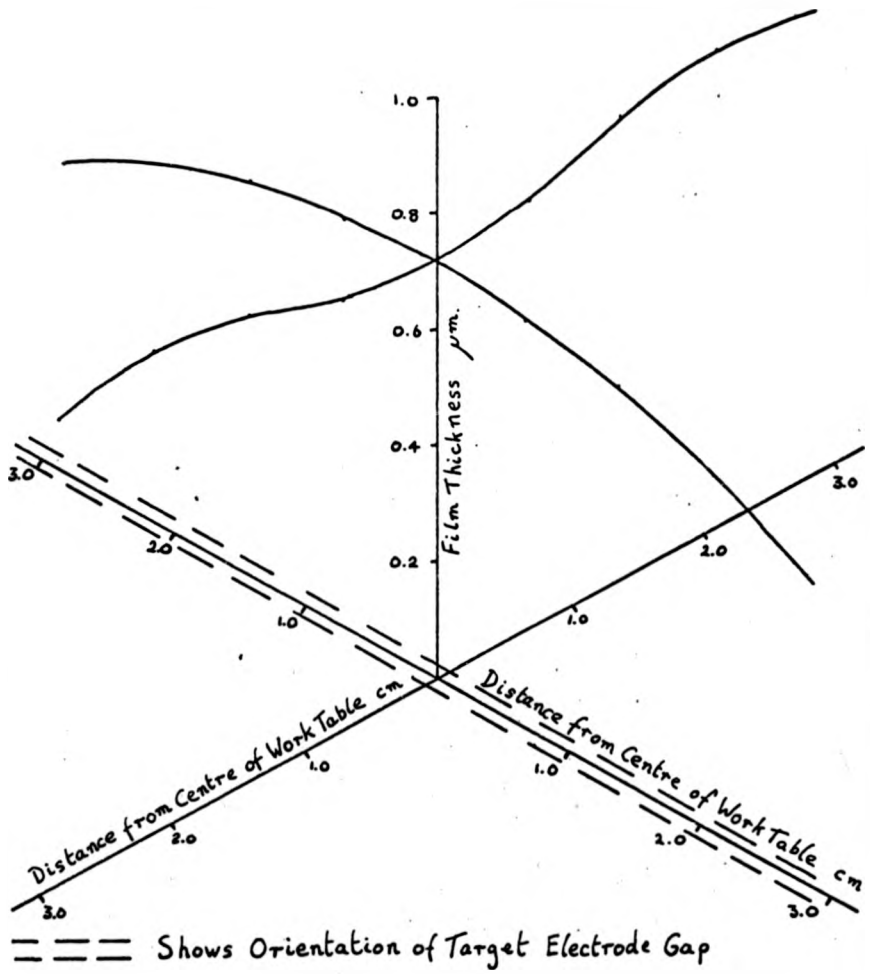

FIGURE 3-17 : THICKNESS PROFILES RELATIVE TO THE ELECTRODE GAP

Graph	Magnetic field strength Wb/m^2	Source to Substrate Distance cm
I	1.25×10^{-2}	3.9
II	0	3.9
III	1.25×10^{-2}	6.0

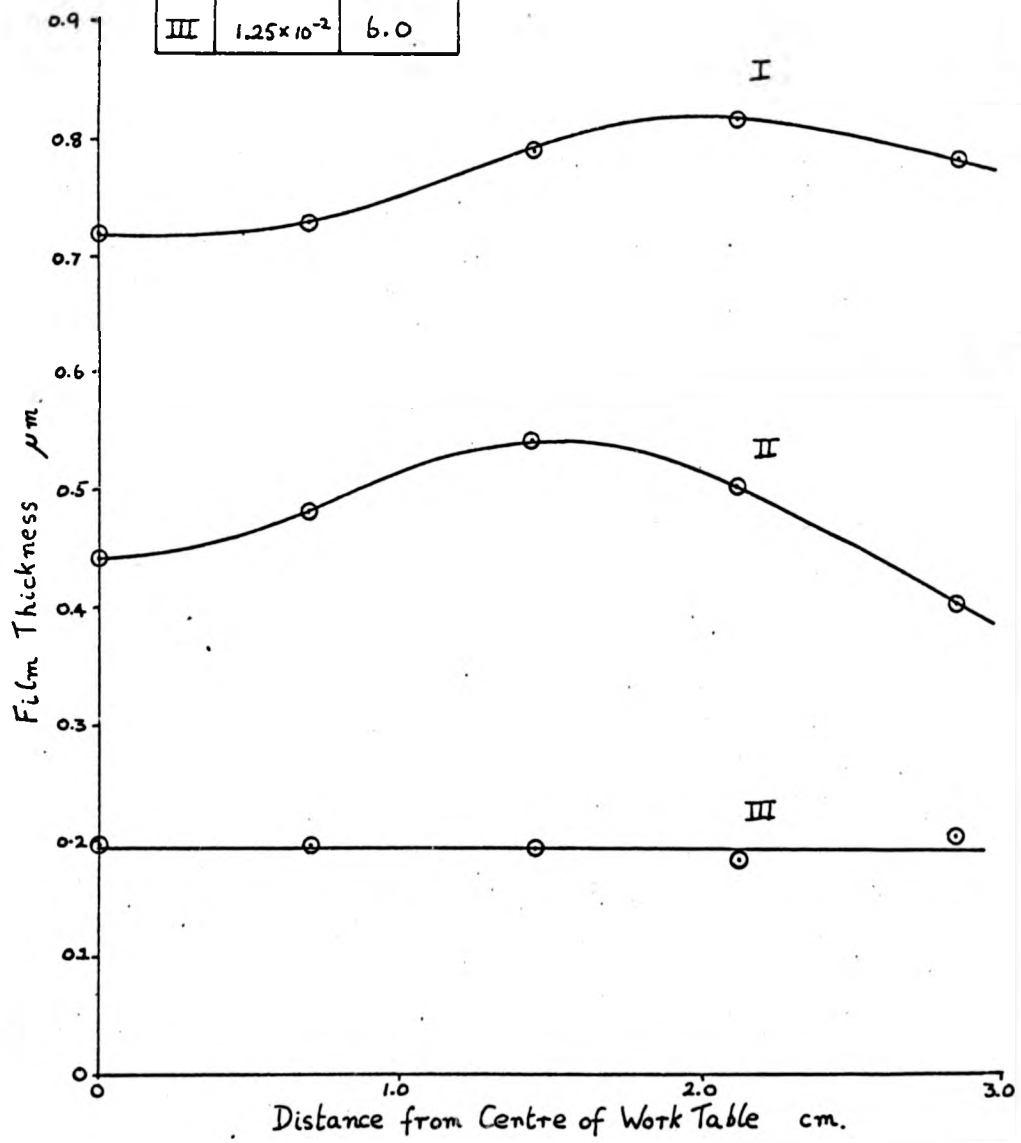

FIGURE 3-18 : THICKNESS PROFILES PERPENDICULAR TO THE ELECTRODE GAP

a) The rotary pump used was an Edwards ES150 having a pumping speed of 150 litres/min. Admitting argon to 10^{-3} to 10^{-2} Torr appeared to overload the pump causing the backing pressure to rise quite considerably. In the present system this was counteracted by baffling the diffusion pump at the expense of a much lower pumping speed. The use of a bigger pump would eliminate the need for this.

b) As mentioned above, the thickness profile is not radially symmetrical. If a large number of substrates are to be processed during one run it is only possible to give two substrates the same thickness if they lie on the same diameter at the same radial distance. The use of a disc and annulus structure would allow all substrates on a given radius to receive the same deposit thickness.

Chapter 4

FACTORIAL DESIGN AND ANALYSIS OF EXPERIMENTS

4-1 Introduction

As mentioned in Chapter 1, it was proposed to investigate the effects of the deposition parameters on the electrical properties of RF sputtered silicon dioxide films at 10GHz. Factorially designed experiments not only enable the effects of the parameters to be determined but also indicate the extent, if any, of interactions that may occur between the parameters. The purpose of this chapter is to give a brief description of the technique, but more detailed information may be found in references (41,42,43,44) . A copy of an internal report written by the author on the subject is given in Appendix 2.

4-2 Terminology

In order to simplify explanation of the technique, some terms in common use in factorial design will be defined.

1) Factor:- This denotes any parameter of an experiment that may be varied.
2) Level of a Factor:- The level of a factor is the value of a parameter used in a particular experiment.
3) Treatment:- The set of levels of all factors used for a given trial is called the treatment or treatment combination.
4) Response:- The numerical result of a trial is termed the response.
5) Effect of a Factor:- The effect of a factor is the change in response produced by changing the level of the factor.

Chapter 4

FACTORIAL DESIGN AND ANALYSIS OF EXPERIMENTS

4-1 Introduction

As mentioned in Chapter 1, it was proposed to investigate the effects of the deposition parameters on the electrical properties of RF sputtered silicon dioxide films at 10GHz. Factorially designed experiments not only enable the effects of the parameters to be determined but also indicate the extent, if any, of interactions that may occur between the parameters. The purpose of this chapter is to give a brief description of the technique, but more detailed information may be found in references (41,42,43,44) . A copy of an internal report written by the author on the subject is given in Appendix 2 .

4-2 Terminology

In order to simplify explanation of the technique, some terms in common use in factorial design will be defined.

1) Factor:- This denotes any parameter of an experiment that may be varied.
2) Level of a Factor:- The level of a factor is the value of a parameter used in a particular experiment.
3) Treatment:- The set of levels of all factors used for a given trial is called the treatment or treatment combination.
4) Response:- The numerical result of a trial is termed the response.
5) Effect of a Factor:- The effect of a factor is the change in response produced by changing the level of the factor.

6) Main Effect (Mean Difference) and Interactions:- The main effect (mean difference) is defined as the effect of a factor averaged over all levels of the other factors. If the effect of one factor is different over the different levels of another, then the two factors are said to interact.

4-3 Contrast Between Classical Method and Factorial Design Method

In a two-factor experiment, the classical approach to determine the effects of the factors is to vary each parameter separately until the conditions yielding the "best" result are obtained. If the two factors interact, then this best result will not be the optimum. Factorial design overcomes this by considering the combinations of all levels of all factors. The simplified design is one in which each factor is allocated two levels. Assessment of the response of all treatment combinations in a two-factor two level experiment therefor requires $2^2 = 4$ trials to be performed. The main effect of each factor is the average of the calculated effects at the different levels of the other, and will be zero if no interaction exists. Because of experimental error, even if these effects do not exist, it is still likely that some numerical value will be obtained. For this reason it is necessary to apply statistical analysis to the results in order to determine the significance of the effects.

4-4 Statistical Analysis of the Results

To obtain the significance of a result, the calculated effect must be compared with the experimental error. An estimate of the error may be found by duplicating each trial. For each treatment,

the variance of the mean response can be calculated. Although the means of each response will be different, the variance will only differ because of sampling fluctuations. Thus, all samples of all means are assumed to have the same variance. It is therefore possible to use the variance of all treatments to give a reliable estimate of the variance of a single result. The error in calculating the main effects and interactions may then be obtained. It is shown in Appendix 2 that the error of all effects and interactions are the same for a fully replicated design. For this reason it is termed the standard error and is given by

$$\text{standard error} = s\sqrt{\frac{1}{n_1} + \frac{1}{n_2}}$$

where s = standard deviation of a single result

n_1, n_2 = number of treatments in each mean

As the main effect is the difference of two means, the t-test may be applied to determine the probability that the two means are merely samples drawn from the same population, a low value indicating a highly significant effect. Another statistical test which may be used is the F-test. Both methods are discussed in Appendix 2. If some previous knowledge of the effects does exist and it is known that some of the interactions are not present, then these interactions may themselves be used to estimate the experimental error. This is particularly useful for large designs where higher order interactions can be assumed not to exist.

4-5 Comments

Information gained from factorial experiments can also be used to optimize processes. The approach is one of determining the "path of steepest ascent". Time has not allowed optimization of the process investigated and the reader should consult references 41 and 42 for further information. For large designs, the calculations become laborious. A computor programme (see Appendix 2) has been written to perform the analysis of two level designs. The programme can handle up to four factor experiments, single or duplicated, and the analysis is performed by the F-test.

Chapter 5

INITIAL MEASURMENTS OF THE PROPERTIES OF RF SPUTTERED SILICON DIOXIDE

5-1 Introduction

Before commencing the factorially designed experiments, it was thought advisable to perform some low frequency measurements on silicon dioxide in order to compare the quality of the films obtained with those described by other workers. It was during this work that the use of silicone vacuum grease, mentioned in Chapter 3, was found to be particularly beneficial.

Unknown to the author at this stage of the work, there were two faults on the sputtering system. These were faulty earthing of the vacuum chamber top plate upon which the oscillator stood and incorrect operation of the Penning gauge used for measuring the sputtering pressure. The evidence for, and correction of, these faults is outlined in Appendix 1. The results given in this chapter are for films deposited at 10^{-3} Torr as indicated by the Penning gauge. It is believed that the actual pressure was of the order of 5×10^{-4} Torr or less.

5-2 Low Frequency Measurements on Silicon Dioxide

The dielectric loss of silicon dioxide at a frequency of 1KHz was investigated by measuring the properties of thin film capacitors. A 3 in. x 1 in. microscope slide was first coated with copper (the bottom electrode) and the dielectric was deposited upon this. Twelve capacitors were formed on one substrate, the top electrode being

fabricated using standard photolithographic techniques. The capacitor properties were measured on a Marconi Universal Bridge. Measurements on capacitors for which the dielectric was deposited without a vacuum grease interface between the substrate and water cooled substrate holder typically gave loss factors between 0.01 and 0.001. The use of silicone grease for more efficient cooling of the substrate resulted in the production of capacitors having reproducible low loss factors. The loss factors of these capacitors approached the sensitivity limit of the bridge but were measured to be 0.0005 ± 0.0005. The vacuum grease also doubled the deposition rate to a value of approximately 65 Å/min. These results are in good agreement with those reported by Franklin [45] who achieved loss factors of 0.001 at 1.6 KHz. These results alone show the superiority of sputtered silicon dioxide films to evaporated films; comparisons have been made with a number of published results. For example, Siddal [46] reported permittivity and loss tangents measured at 1KHz of 4 and 0.04 respectively for silicon oxide films deposited at rates in excess of 1200 Å/min, and 2.5 and 0.01 respectively for rates of 120 Å/min. Hirose and Wada [14] investigated silicon oxide films and found that the purity of their initial silicon monoxide material had a much smaller effect on the dielectric loss than had the rate of deposition. The low loss of the sputtered films may therefore be partially attributed to the low deposition rate ($\sim$70 Å/min) which may be controlled far more accurately than evaporation rates. Measurements of the permittivity at 1KHz were also performed on films that had previously been measured at 10GHz. These results are given in the following section.

5-3 Microwave Measurements of Silicon Dioxide

The cavity technique developed by Mehmet [7] was used for the microwave evaluation of the dielectric films. Figure 5-1 shows a cross-sectional view of the co-axial cavity. The centre conductor of the bottom half of the cavity is recessed by approximately 25 μm forming a capacitative gap in the centre conductor. The cavity Q factor, resonant frequency and voltage standing were ratio (VSWR) at resonance were measured. The dielectric film was then deposited onto the centre conductor of the top half of the cavity. This resulted in a change in the properties of the cavity which were measured again. Use of equations 5-1 and 5-2 allow the permittivity (E') and loss tangent ($\tan\delta$) of the dielectric to be measured.

$$E' = x\left[\left(\frac{(m+1)\, f_1 \tan\frac{\pi}{v} f_1 L}{f_2 \tan\frac{\pi}{v} f_2 L} - m\right)^{-1} + x - 1\right]^{-1} \qquad \ldots\ldots 5\text{-}1$$

$$\text{where } m = \frac{4Go}{\pi Di} \ln\frac{(Do - Di)}{Go}$$

where L = length of cavity = 32 mm

v = velocity of light

Do = outer diameter of cavity = 15 mm

Di = diameter of centre conductor = 3 mm

Go = width of capacitive gap before deposition

x = Filling factor = film thickness/Go

f_1 = resonant frequency without film

f_2 = resonant frequency with film

$$\text{and } \tan\delta = \frac{\left[\frac{s_2}{s_1} - \left(\frac{f_1}{f_2}\right)^{\frac{3}{2}}\right]\left[1 + m\left(1 + \frac{x}{E'} - x\right)\right]^2}{\frac{x}{E'}(1+m)\,Q_o\,K} \qquad \ldots\ldots\ldots 5\text{-}2$$

where s_1 and s_2 are the VSWRs at resonance without and with the film

Q_o is the cavity Q factor without the film

$$\text{and } K = 1 - 2\pi\left(\frac{2\pi f_1 L}{v} + \sin\frac{2\pi f_1 L}{v}\right)^{-1}$$

The apparatus used for measuring the cavity parameters was the swept frequency waveguide reflectometer system described in Chapter 8. Mehmet claimed an accuracy of $\pm$ 7.5% for permittivity and $\pm$ 10% for $\tan\delta$. The masking arrangement used for the deposition is shown in figure 5-2. A PTFE sleeve surrounds the centre conductor of the cavity and a microscope cover slide with a hole above the centre conductor is placed on top. The cavity is then surrounded by a copper block and mounted on the cooled copper substrate holder. The thickness of the film on the microscope cover slide was measured using the Talystep and was assumed to be equal to the thickness on the cavity.

Using this method, two experiments were performed with identical deposition conditions. Each film was deposited upon the centre conductor of the cavity and its microwave properties measured. A top copper electrode was then evaporated onto the film to form a capacitor and the properties of the capacitor were measured at 1KHz. Table 5-1 outlines the results obtained. There appears to be remarkable agreement between the low and high frequency permittivities. The increased loss at 10 GHz is expected because various relaxation processes will occur throughout the frequency band covered. Harrop and Campbell [47] made the interesting observation that the dielectric loss appeared to be a factor of the forbidden band width which is a

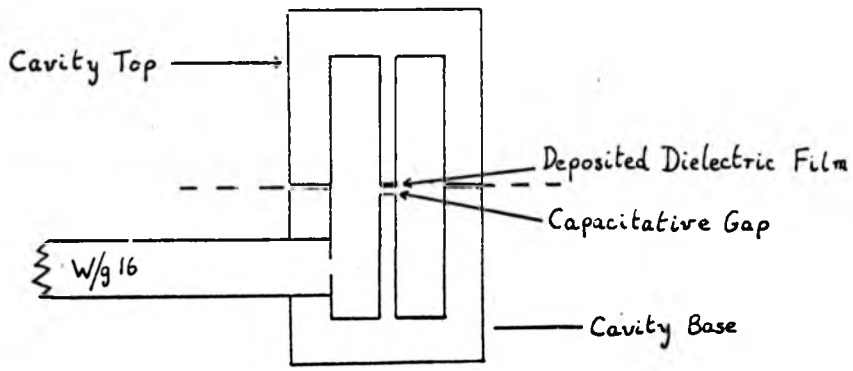

FIGURE 5-1 : CO-AXIAL CAVITY FOR THIN FILM DIELECTRIC MEASUREMENTS[7]

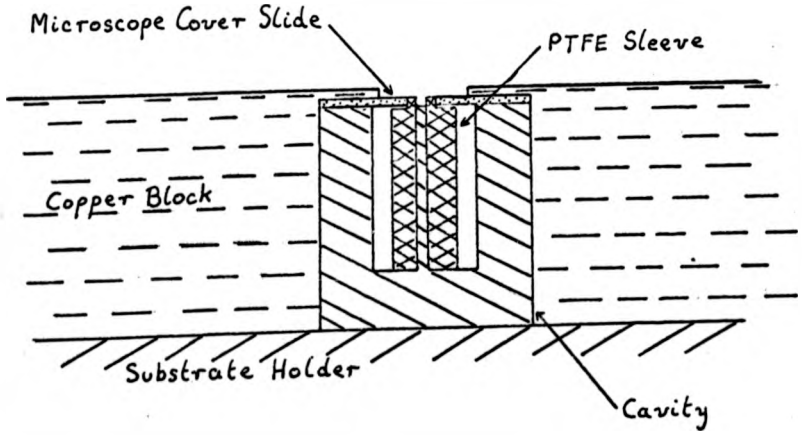

FIGURE 5-2 : MASKING ARRANGEMENT FOR FILM DEPOSITION

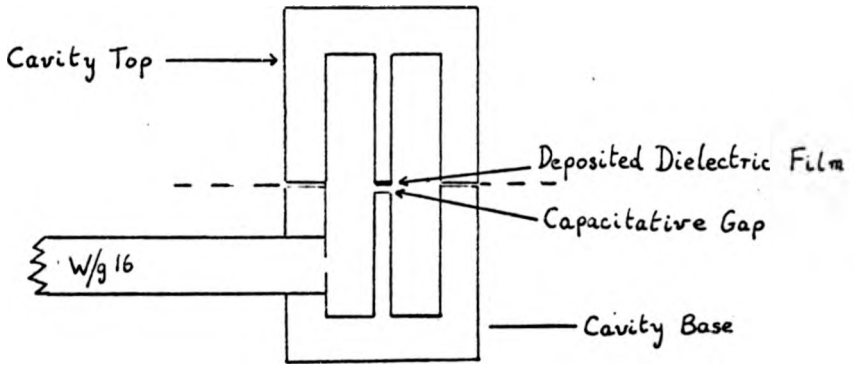

FIGURE 5-1 : CO-AXIAL CAVITY FOR THIN FILM DIELECTRIC MEASUREMENTS[7]

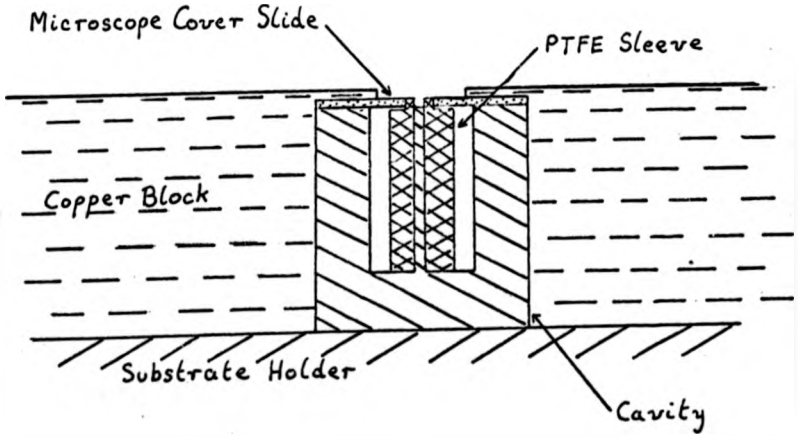

FIGURE 5-2 : MASKING ARRANGEMENT FOR FILM DEPOSITION

Table 5-1

Dielectric Properties of Silicon Dioxide at 10GHz and 1KHz

Run No.	Deposition Rate (Å/min)	Permittivity at 10GHz	Tan δ at 10GHz	Permittivity at 1KHz	Tan δ at 1KHz
1	76	3.72	0.0049	3.72	0.0005
2	73	3.91	0.0043	3.94	0.0005

characteristic of a material: the larger the energy gap the lower is the loss. Jonscher and Wally[48] using Harrop's results, suggested loss mechanisms that might occur at various frequencies. They suggested that high frequency losses might be covered by an electronic hopping mechanism, the activation energy decreasing with increasing frequency.

More recently, Lynch[49] has obtained an equation to describe the variation of permittivity with frequency (equation 5-3).

$$\frac{\Delta E'}{E'} \approx 1.5 \tan\delta \log_{10}\left(\frac{f_2}{f_1}\right) \qquad \ldots. 5\text{-}3$$

where $\Delta E'$ is the change in permittivity

E' is the permittivity at frequency f_2 (the lower frequency)

$\tan\delta$ is the loss tangent at f_2

f_1 is the higher frequency for which the permittivity is required.

Using the results of run 2, this equation predicts a decrease of 0.02 in E' at 10GHz compared to the 1KHz measurement. This change, however, is far smaller than the accuracy with which the measurements

were made. The results, therefore, cannot be used to verify this relationship.

At this point, factorially designed experiments were started but very soon abandonded for the following reasons. The accuracy of the Talystep for measuring film thickness is ± 4% of full scale. Although this error is included in the accuracy figure quoted for the permittivity measurements it was found that the measured dielectric constant was very dependent on thickness. For example, a thickness of 3.4 μm gave $E' = 4.5$ while a thickness of 3.5 μm gave $E' = 4.1$. It was thought that this type of error might conceal any changes that occur from varying the deposition parameters. A large number of replicated treatments therefore would have been necessary if any reliable information was to be obtained from the experiments. The measurement of the thickness on the microscope cover slide was not always found to be reliable. This was observed from quite large changes in the permittivity occuring for films deposited under identical conditions. This was attributed to differences in the surface temperatures of the slide and the cavity, for it is known that an increased substrate temperature decreases the sticking coefficient (see section 3-6). If the temperature of the masking slide was higher than that of the cavity, then the deposit thickness on the slide would be less than that on the cavity. This would result in the calculation of high values of dielectric constant.

5-4 Comments

For the reasons given above, it was decided to abandon the use of the cavity for the dielectric measurements. A separate project being

studied within the microwave group was that of thin film capacitor measurements using stripline techniques. It was thought that capacitor measurements might well give more accurate permittivity measurements because the dielectric thickness could then be measured in situ. If the dielectric loss is to be determined from these measurements, then the electrode loss must be accurately known. It was therefore decided to direct the research effort towards these measurements.

Chapter 6

MICROWAVE CAPACITOR FABRICATION

6-1 Introduction

Up to this time, no capacitors had actually been made. It was therefore agreed that the author, in conjunction with Mr. D. Michie (a fellow research student), should attempt the manufacture of capacitors, as several processing difficulties had already been forseen. On completion of this work Mr. D. Michie would develop the capacitor measurement technique while the author concentrated on the evaluation of surface resistance of evaporated and plated metal films in order to distinguish between the electrode and dielectric losses. In this way it was hoped that the dielectric properties could be determined accurately.

Typical values of capacitors required for microwave work are:-

1) By-pass capacitor : 7-120pF
2) Coupling capacitor : 0.1-3.0pF
3) Tuning capacitor : 0.58pF at 10GHz for a typical inductance of 500pH

Small values of capacitors (< 1pF) are usually obtained using interdigital capacitors (figure 1-3), larger values being obtained from the parallel plate configuration (figure 1-2). For this work, a 1pF capacitor was chosen in order to suit a proposed measurement technique (8). For a component to be truly "lumped", its physical size must be smaller than a guide wavelength. The substrate used was quartz.

The guide wavelength in quartz at 10GHz is ~1.7cms. For a test capacitor of 1pF with a 1 μm thick silicon dioxide dielectric, the physical dimensions chosen were 100 μm x 300 μm. If however, a silicon dioxide dielectric is to be used on a quartz substrate, then from figure 1-2 it can be clearly seen that conventional photolithographic techniques cannot be used to define the dielectric area, because etching of the dielectric would also result in etching of the substrate. In low frequency circuits this can be overcome by depositing the dielectric through an out-of-contact mask. However, the restriction on the physical dimensions of microwave components does not allow this method to be applied. The only alternative is to use negative relief masks [6,50]. The masks commonly used in the technique were found to have severe disadvantages, but by suitable modification, a new process has been developed to allow well-defined small areas of film to be deposited without the need for etching. The process described is covered by a UK patent application [51], a copy of which will be found in Appendix 3.

6-2 Negative Relief Mask Technology

A negative relief mask is one which forms a thick coating which is the complement of the required deposition pattern. For example, a thick coating of photoresist may be applied to a substrate, and the required pattern exposed and developed. The film (metal or dielectric) is then deposited all over the substrate area, (see figure 6-1). The photoresist and unwanted areas of the film are then removed leaving the required film pattern. This method was attemped in order to form the dielectric area, but it was found that the adhesion of the film

was poor and a number of pin holes were also present in the film. It is generally accepted that where resist has once existed, film adhesion is weak. The cause of the pin-holes was traced to under-developed spots of resist remaining in the dielectric area. The existence of pin-holes is a problem commonly encountered in capacitor fabrication. An alternative to the photoresist is a metal mask. In this application, however, metal masks could not be used for the following reasons. The relief mask must be much thicker than the deposited film in order to achieve a discontinuity in the film at the boundary of the substrate and mask. If a thick metal film is used, etching of the required pattern will result in severe undercutting yielding poorly defined areas. If a thin metal film is used, then etched and plated up, this would overcome the undercutting problem. However, in the present application any plating up of the mask after defining the dielectric area would also result in plating up of the lower electrode. These problems were finally overcome by using a compound photoresist/metal mask retaining the principle of relief mask technology.

6-3 Process for the Deposition onto Selected Areas Without the Need of Etching

When the metal bottom electrode has been formed, the substrate is covered with a thin protective coating of a different metal. Thick photoresist is then applied and the required pattern exposed and developed. The protective coating is then etched away in the area on which the dielectric is required. The protective film serves two purposes. It protects the dielectric area from the photoresist and thus allows the dielectrid to adhere well to the bottom electrode and

the substrate. Any remaining particles of resist within the defined area are also removed during the etching of the protective layer, thus preventing the risk of pin-holes occuring within the dielectric film. The dielectric is then deposited (see figure 6-2). The compound mask is removed and the top electrode formed using conventional photolithography. Microwave capacitors have been successfully made in this way.

6-4 Application of a Thick Photoresist Coating

It was found difficult to apply a thick even coating of photoresist. Slowly spinning the substrate during application of the resist appeared to give an evenly thick layer. However, during the drying period, the resist was found to be drawn to the edges of the substrate, as shown by the dark areas in figure 6-3a. Placement of the substrate on a larger glass plate and the application of photoresist all over the substrate and edges result in an even film being obtained (see figure 6-3b). After drying, the substrate is gently eased from the plate.

6-5 Advantages and Application of the New Process

The advantages of the method may be listed as follows:-

1) Depositing in selected areas without etching.
2) Good adhesion. Adhesion is not impaired as is the case using a photoresist relief mask.

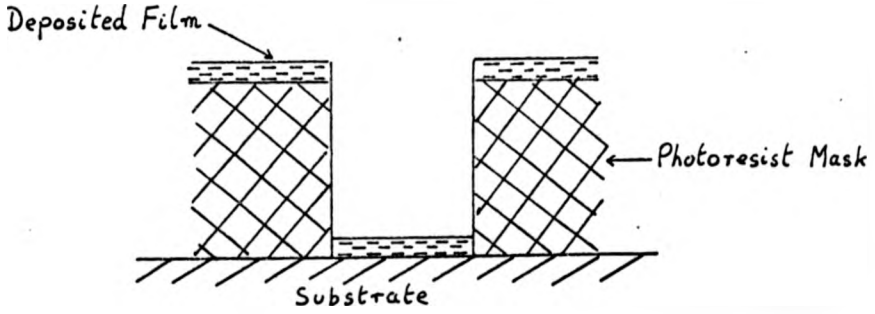

FIGURE 6-1 : CONVENTIONAL PHOTORESIST NEGATIVE RELIEF MASK

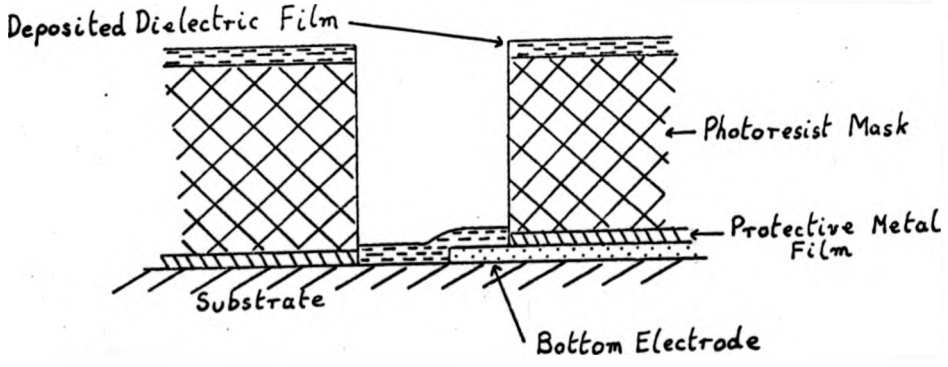

FIGURE 6-2 : NEW METAL/PHOTORESIST NEGATIVE RELIEF MASK

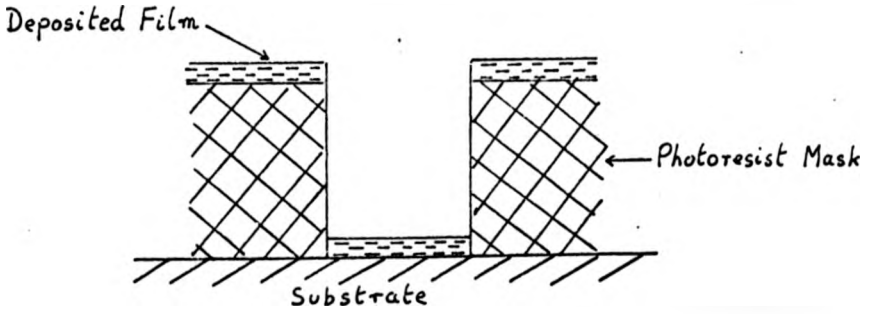

FIGURE 6-1 : CONVENTIONAL PHOTORESIST NEGATIVE RELIEF MASK

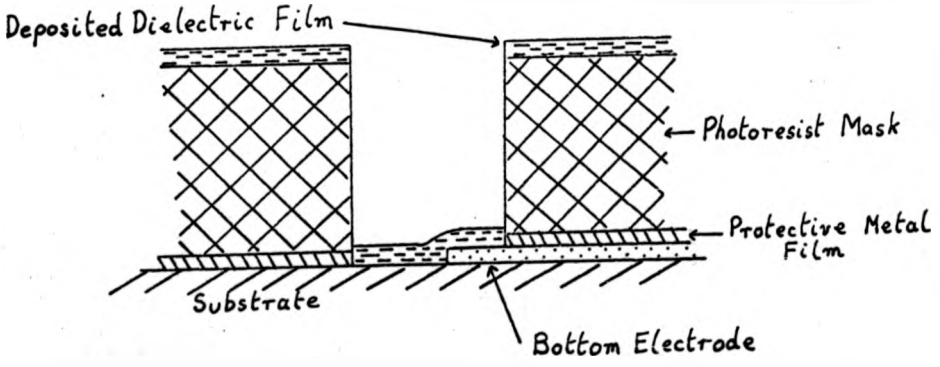

FIGURE 6-2 : NEW METAL/PHOTORESIST NEGATIVE RELIEF MASK

3) No undercutting of the film. The edge profile can in fact be tailored to suit the application. This is achieved by varying the thickness and etching times of the protective layer (see Appendix 3).
4) Pin-hole free films.
5) All advantages of conventional photolithography (e.g. good definition).

This process is not restricted to microwave applications. Other areas where this technique could be useful are:-

1) Where the film and substrate are of the same material.
2) When photoresist masks have to withstand strong alkali or acid etchants.
3) Where out-of-contact masks do not have the required definition.
4) Where the control of edge profile is mandatory.
5) When no suitable etchant can be used.

A common etchant for silicon dioxide is P-etch (15 parts hydrofluoric acid, 10 parts nitric acid, 300 parts water). This etch has also been found to attack alumina (Al_2O_3). Similar problems would therefore have occured if alumina dielectric or substrate had been used.

6-6 Definition of Capacitor Area

One of the claims of the above process is that of good definition. This can be seen in figure 6-4 which shows the definition of the dielectric area after exposure and development of the photoresist.

FIGURE 6-3 : PHOTOGRAPH OF TWO THICK PHOTORESIST COATINGS APPLIED BY DIFFERENT METHODS

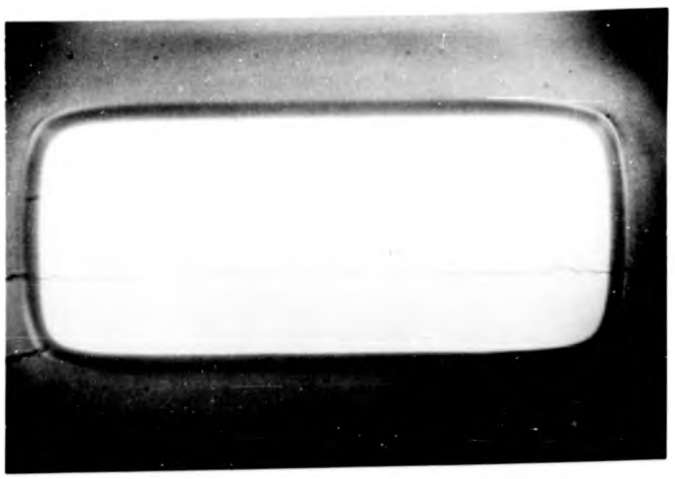

FIGURE 6-4 : PHOTOGRAPH OF DEFINED DIELECTRIC AREA AFTER DEVELOPMENT OF PHOTORESIST

Figure 6-5 shows the deposited dielectric after removal of the resist. The rounded corners are a common result of photolithography but are probably exaggerated owing to the thickness of the photoresist coating. Figure 6-6 is a scanning microscope photograph of a 1pF capacitor made using this technique.

6-7 Comments

The procedure of the process is given in Appendix 3 together with information on the actual materials used. It is thought that this technique is a valuable addition to the methods available for fabrication of thin film circuits generally, but it is particularly useful for microwave work where good definition is essential.

FIGURE 6-5 · PHOTOGRAPH OF DEPOSITED DIELECTRIC AFTER REMOVAL OF THE METAL/PHOTORESIST RELIEF MASK

FIGURE 6-6 : PHOTOGRAPH OF A 1 pF CAPACITOR

Chapter 7

CAVITY DESIGN FOR SURFACE RESISTANCE MEASUREMENTS OF THIN FILMS

7-1 Introduction

The loss of a capacitor is determined by the electrode loss and the dielectric loss. The loss tangent of a dielectric could be found from capacitor measurements, provided that the electrode loss can be accurately known. For this reason the surface resistances of evaporated and plated metal films were investigated.

At high frequencies, current penetrates only to a limited depth into the surface of a conductor. This phenomenon is known as "skin effect". For this reason, the impedance of a conductor to high frequency currents becomes a surface characteristic. The "surface impedance" Z_s, may be expressed as

$$Z_s = R_s + j X_s \qquad \ldots\ldots 7\text{-}1$$

where R_s is the surface resistance

and X_s is the surface reactance

It can be shown [52] that for an infinitely thick conductor

$$Z_s = \frac{1}{\delta \sigma} (1 + j) \qquad \ldots\ldots 7\text{-}2$$

where σ is the conductivity of the material

and δ is the skin depth

$$\delta = \sqrt{2/\omega \mu \sigma}$$

where ω is the angular frequency

and μ is the permeability of the material

From equations 7-1 and 2 it can be seen that

$$R_s = X_s = 1/\delta \sigma \qquad \ldots\ldots 7\text{-}3$$

The skin depth is defined as that depth at which the current falls to 1/e of the surface value. The phase of the current at this depth lags the surface current by 1 radian. This is shown in figure 9-7 which includes a polar plot showing the variation of the current amplitude and phase with depth into an infinitely thick conductor. From equation 7-3 R_s has the dimensions of ohms, or more strictly ohms per square and is equal to the direct current resistance of a unit square of a conductor of thickness δ. It is shown in section 9-3 that equation 7-3 may be applied, provided the thickness of the conductor is greater than three skin depths.

Several techniques have been used by other workers to determine the surface resistance, skin depth and conductivity of bulk and thin film materials. These include

(a) Measurement of the Q factor of an open-circuited half wavelength co-axial line, the inner conductor of which is the material under test [53,54].

(b) Measurement of the transmission and reflection coefficients of a film supported on a glass substrate mounted in a waveguide [55].

(c) Resonant cavity techniques[56,57,58,59].

Films are usually deposited on a flat substrate. It is therefore convenient to choose a measurement method which can accept a flat specimen. Methods b and c would therefore be suitable. For method b, however, the surface resistance of the sample must be much lower than the surface resistance of the waveguide if accurate results are to be obtained. As it was intended to measure materials of good conductivity e.g. copper, silver and gold, method b would be unsuitable. A resonant cavity technique was the final choice.

Maxwell [58] suggested several types of cavity suitable for surface resistance measurements at 24 GHz. Although he was only interested in bulk samples, two of the suggested methods may be used for thin film investigations and they are outlined below.

(i) Cylindrical H_{011} Resonator

The sample under test forms one end-plate of a cylindrical H_{011} cavity. The field configuration for the H_{01} mode is shown in figure 7-1. It will be noticed that all current paths are circumferential. There are therefore no current paths between the bore of the cavity and the end plates. For this reason the H_{011} cavity is particularly useful for surface resistance measurements as the contact resistance between the bore of the cavity and the sample end plate will have no effect on the Q of the cavity. Unfortunately, associated with the H_{01} mode is the degenerate E_{11} mode i.e. both modes have the same cut off frequency [60]. If this mode is excited (see figure 7-2) current will flow across the bore/end plate boundary and thus

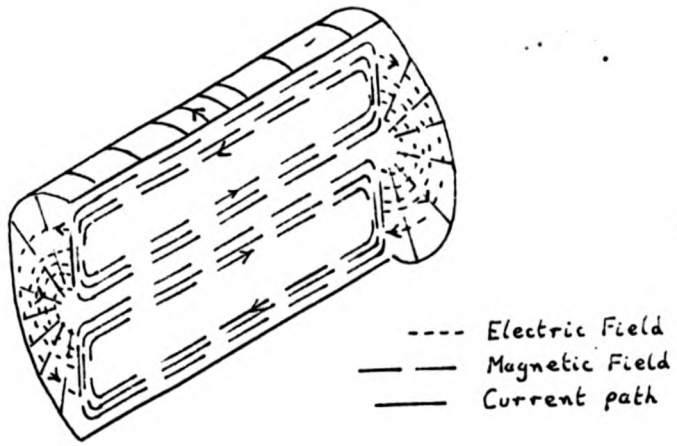

FIGURE 7-1 : FIELD CONFIGURATION FOR H_{01} MODE

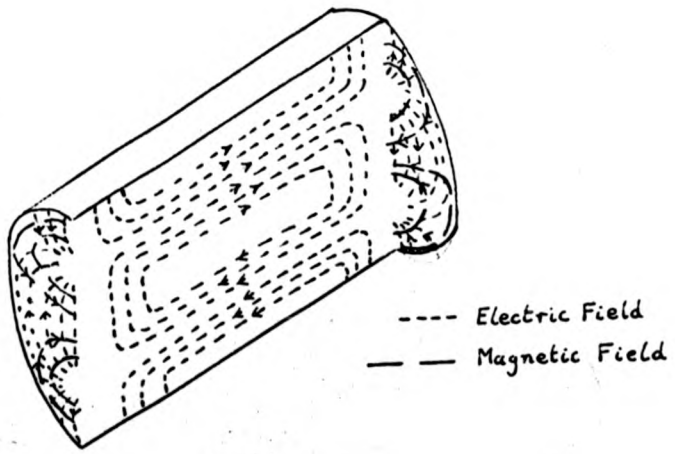

FIGURE 7-2 : FIELD CONFIGURATION FOR E_{11} MODE

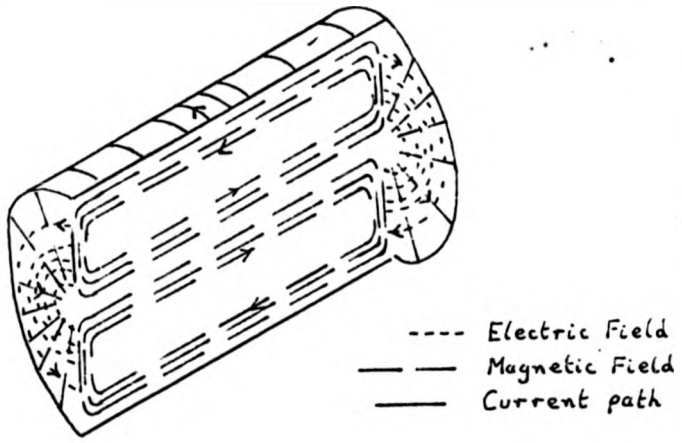

FIGURE 7-1 : FIELD CONFIGURATION FOR H_{01} MODE

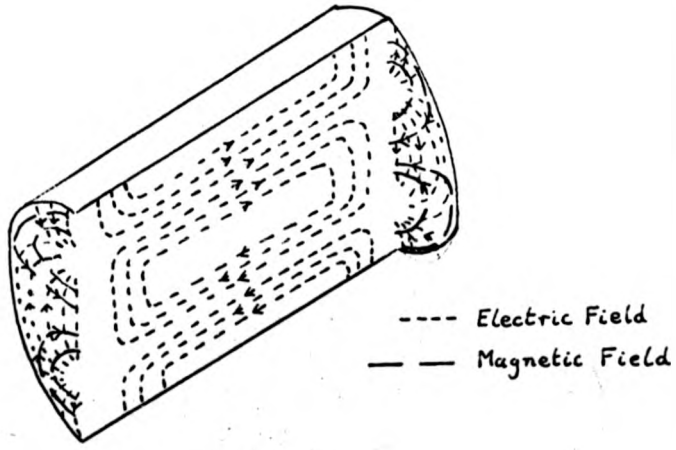

FIGURE 7-2 : FIELD CONFIGURATION FOR E_{11} MODE

contact resistance may affect the measurements.

(ii) Rectangular H_{10n} Cavity

This resonator is shown in figure 7-3. The sample forms part of the cavity as shown, with contact points situated at current nodes thus minimizing the effect of contact resistance. Use of this cavity for bulk samples is feasible since the sample can be accurately machined to give a flush fit with the interior face of the cavity. For thin film samples supported on glass substrates, mounting of the sample would be difficult if discontinuities at the cavity sample boundary are to be avoided.

The H_{011} cylindrical cavity technique has been used successfully by other workers [56,57,59] for measurement of bulk materials. Surface resistance measurements were made by this method, since sample attachment presents few problems and several techniques exist for removing the effects of the E_{111} degeneracy. The suppression of this mode is discussed in section 7-3.

7-2 Design of H_{011} Cavity for Surface Resistance Measurements

By definition, the Q of a cavity may be expressed as

$$\frac{1}{Q} = \frac{\text{Energy lost per radian } (W^1)}{\text{Total energy stored } (W)}$$

The total loss of the cavity includes a contribution from the bore (W_1) and losses at both end plates (W_2).

$$\therefore \frac{1}{Q} = \frac{W_1}{W} + \frac{W_2}{W}$$

This may be expressed as $$\frac{1}{Q} = \frac{1}{Q_{\text{bore}}} + \frac{1}{Q_{\text{end plates}}}$$

The Q of an H_{011} cavity is given by [61] (for a full derivation see Appendix 4)

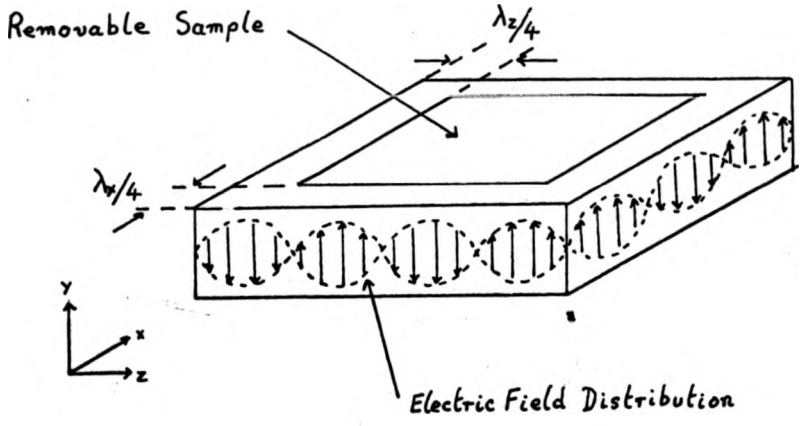

FIGURE 7-3 : RECTANGULAR H_{10n} RESONATOR

$$\frac{1}{Q} = \frac{\alpha \lambda^2}{\pi \lambda_g} + \frac{4 \lambda^3}{\pi \lambda_g^3 \eta \delta_e \sigma_e} \quad \ldots\ldots 7\text{-}4$$

where λ is the free space wavelength at resonant frequency

λ_g is the guide wavelength at resonant frequency

η is the intrinsic impedance of free space = 377 ohms

σ_e is the conductivity of the end plate material

δ_e is the skin depth in end plate material

α is the attenuation constant of H_{01} circular waveguide mode.

The attenuation constant, α , is given by

$$\alpha = \frac{1}{\delta_b \sigma_b \eta r} \left(\frac{\lambda}{\lambda_c}\right)^2 \left[1 - \left(\frac{\lambda}{\lambda_c}\right)^2\right]^{\frac{-1}{2}} \quad \ldots\ldots 7\text{-}5$$

where r is the radius of the cavity

λ_c is the cut off wavelength for circular H_{01} waveguide

σ_b is the conductivity of the bore material

δ_b is the skin depth in the bore material

Let $\alpha = K/\delta_b \sigma_b$ 7-6

where $K = \frac{1}{\eta r} \left(\frac{\lambda}{\lambda_c}\right)^2 \left[1 - \left(\frac{\lambda}{\lambda_c}\right)^2\right]^{\frac{-1}{2}}$

Substituting equation 7-6 into equation 7-4,

$$\frac{1}{Q} = \frac{K \lambda^2}{\pi \lambda_g \delta_b \sigma_b} + \frac{4 \lambda^3}{\pi \lambda_g^3 \eta \delta_e \sigma_e} \quad \ldots\ldots 7\text{-}7$$

For the present application, it is required that a change in the conductivity of one of the end plates should cause a large change in the cavity Q factor. This requires the losses of the cavity to be

concentrated in the end plates. This may be achieved by the correct choice of the length, L , and diameter, D, of the cavity.

The free space wavelength, λ , at resonance is given by

$$\frac{1}{\lambda^2} = \frac{1}{\lambda_g^2} + \frac{1}{\lambda_o^2} \qquad \ldots\ldots 7\text{-}8$$

For an H_{011} mode $\lambda_g = 2L$

$\lambda_o = 0.82D$

Substituting for λ_g and λ_o in equation 7-8 gives the dimensionless equation

$$\frac{L^2}{\lambda^2} = \frac{1}{(0.82)^2}\left(\frac{L}{D}\right)^2 + \frac{1}{4} \qquad \ldots\ldots 7\text{-}9$$

Equation 7-9 allows the length and diameter of the cavity to be determined for a given resonant frequency and length/diameter ratio. Values for λ_g and λ_c may then be obtained. Equations 7-7 and 9 may be used to observe the variation of the cavity Q factor with the length/diameter ratio. Figure 7-4 shows the variation in Q with L/D when the bore and end plates have the same conductivity. Maximum Q is obtained when L/D = 1. As mentioned earlier, it is necessary to make the end plate loss as large as possible. Assuming the conductivity of the bore is equal to that of the end plates, it is shown in Appendix 4 that the ratio of total end plate loss, W_2, to the loss of the bore, W_1 is given by

$$\frac{W_2}{W_1} = \frac{4\lambda}{\lambda_g^2 \eta K} \qquad \ldots\ldots 7\text{-}10$$

Again, using equations 7-9 and 10, this ratio may be plotted against L/D (see figure 7-5). It can be seen that for a large end plate loss a short cavity is required, corresponding to a low Q cavity (see

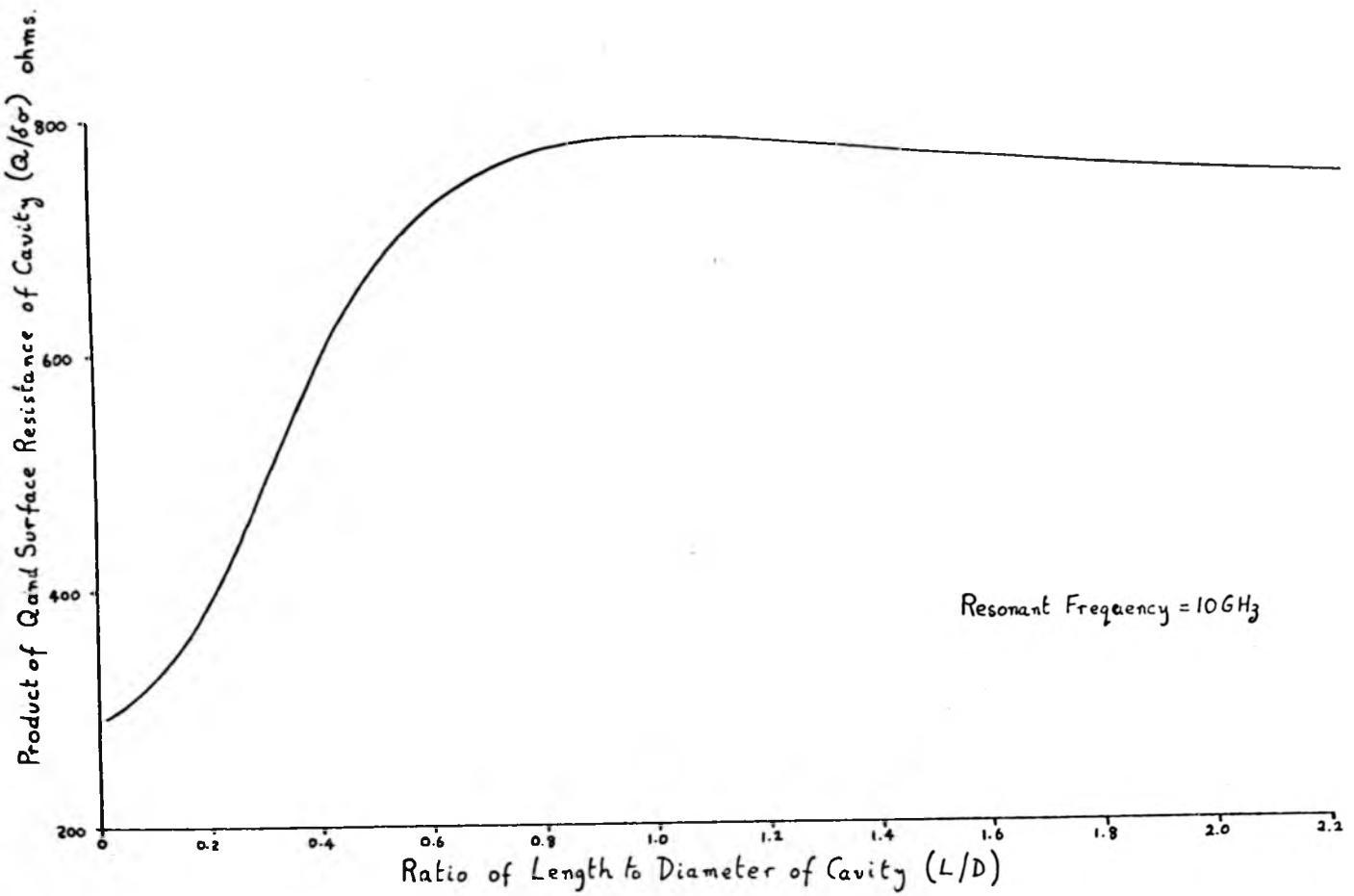

FIGURE 7-4 · VARIATION OF Q WITH LENGTH TO DIAMETER RATIO FOR H_{011} CYLINDRICAL CAVITY

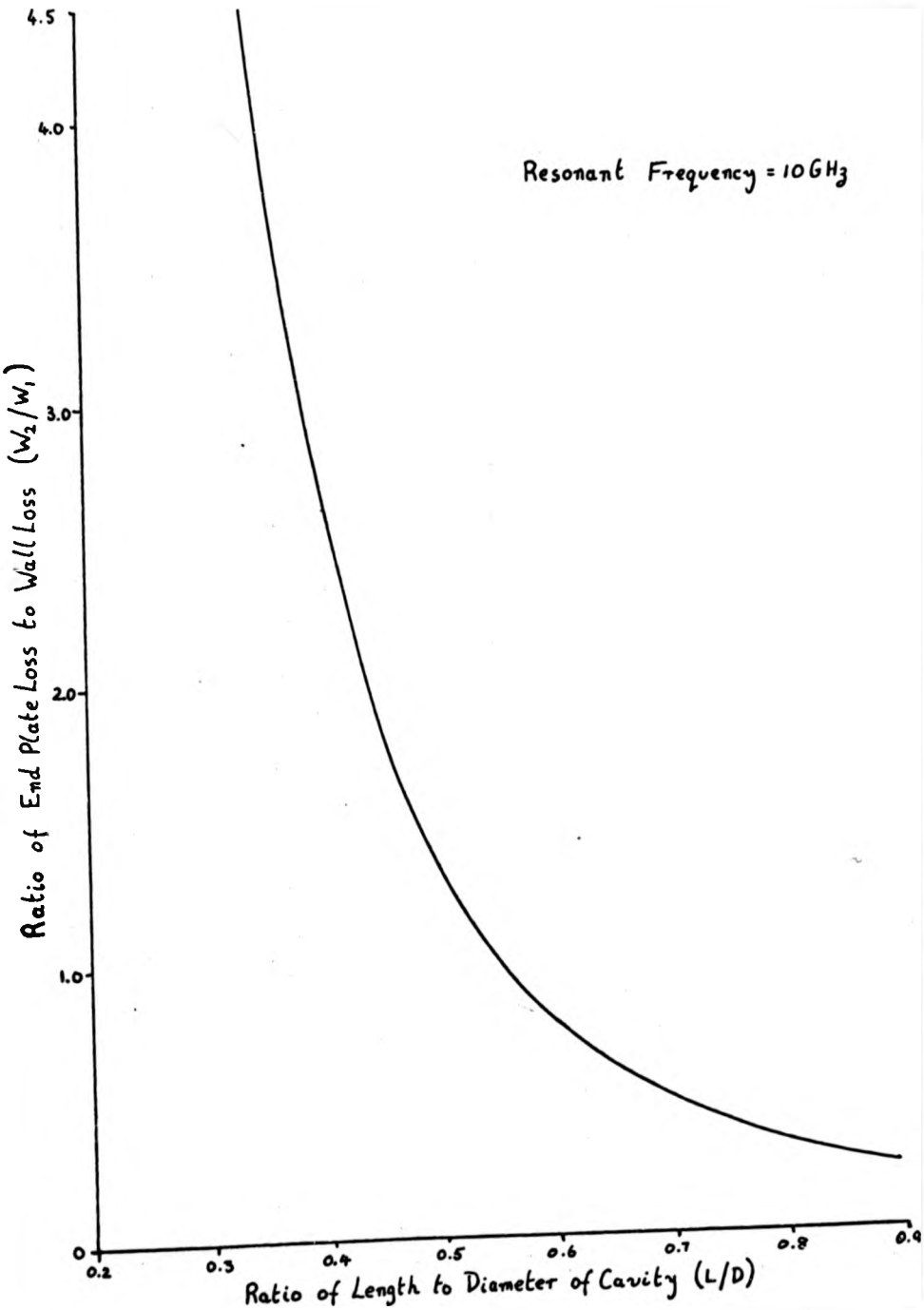

FIGURE 7-5 : DISTRIBUTION OF LOSSES WITH LENGTH TO DIAMETER RATIO FOR H_{011} CYLINDRICAL CAVITY

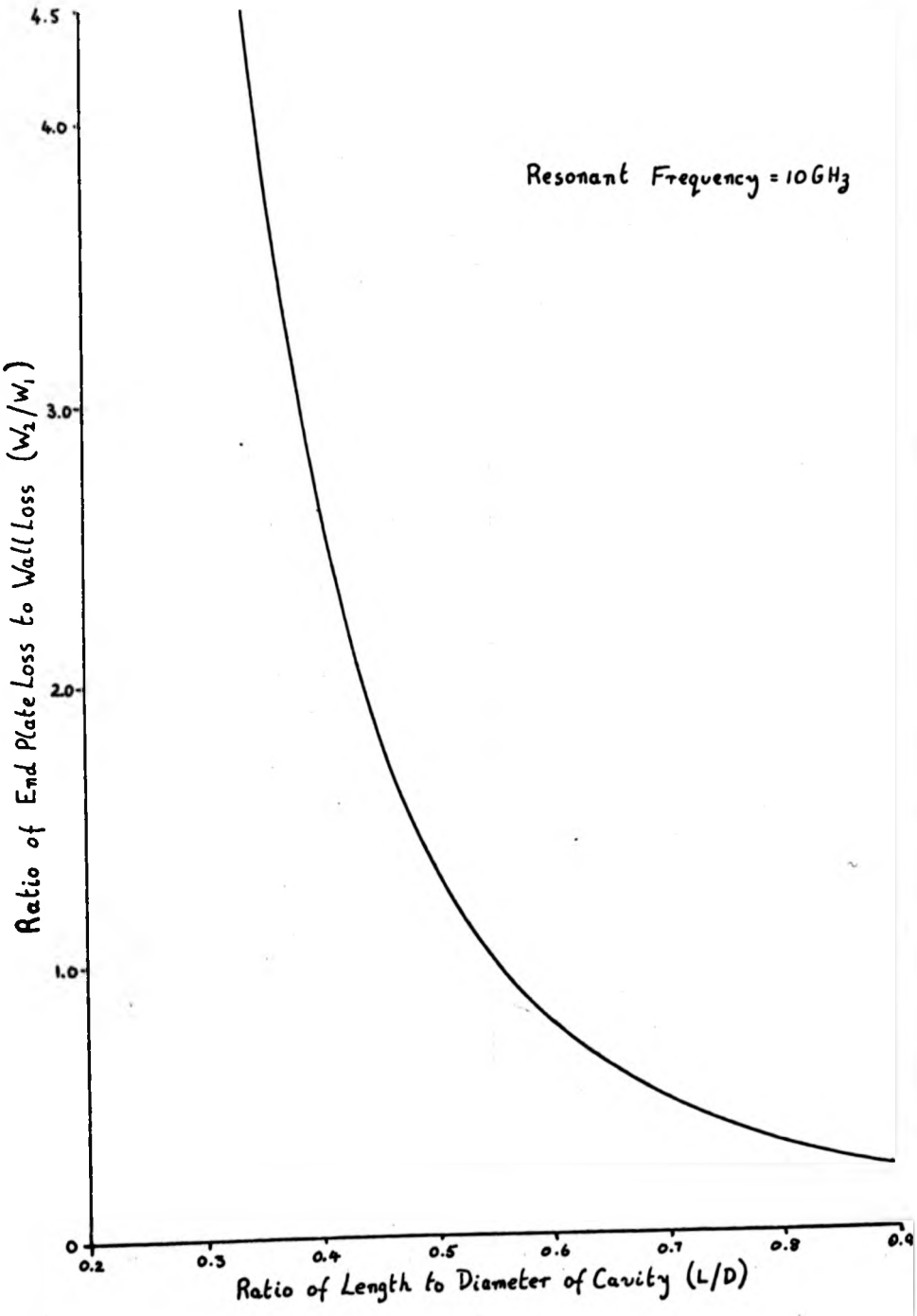

FIGURE 7-5 : DISTRIBUTION OF LOSSES WITH LENGTH TO DIAMETER RATIO FOR H_{011} CYLINDRICAL CAVITY

figure 7-4). The only limitations on the L/D ratio for practical purposes are the actual dimensions of the cavity at the operating frequency. For example, at 10 GHz, for L/D = 0.3, the diameter must be 61.95 mm and the length 18.58 mm. Thus a rather large substrate would be required to cover one end of the cavity. The actual L/D ratio chosen for this work was 0.5 as this gave D = 47.31mm and L = 23.66 mm at 10 GHz. Thus the films were deposited on a 50 mm square substrate (i.e. 2 in. x 2 in.).

Before the surface resistance of a sample end plate can be determined, the surface resistance of the cavity parts must be known. If the bore and end plates are made from the same material and have the same surface finish then these parts will also have the same surface resistance (i.e. $1/\delta_b\sigma_b = 1/\delta_e\sigma_e$). Measurement of the Q, resonant frequency and dimensions of the cavity enable the surface resistance of the cavity parts to be evaluated from equation 7-7. Changing one end plate for the material under test gives

$$\frac{1}{Q_s} = \underbrace{\frac{K\lambda^2}{\pi\lambda_g\delta\sigma}}_{\text{(bore)}} + \underbrace{\frac{2\lambda^3}{\pi\lambda_g^3\eta\delta\sigma}}_{\text{(end plate)}} + \underbrace{\frac{2\lambda^3}{\pi\lambda_g^3\eta\delta_s\sigma_s}}_{\text{(sample end plate)}} \qquad \ldots\ldots 7\text{-}11$$

where Q_s is the cavity Q with the sample end plate

δ is the skin depth in cavity material

σ is the conductivity of cavity material

σ_s is the conductivity of the sample

δ_s is the skin depth in sample material

figure 7-4). The only limitations on the L/D ratio for practical purposes are the actual dimensions of the cavity at the operating frequency. For example, at 10 GHz, for L/D = 0.3, the diameter must be 61.95 mm and the length 18.58 mm. Thus a rather large substrate would be required to cover one end of the cavity. The actual L/D ratio chosen for this work was 0.5 as this gave D = 47.31mm and L = 23.66 mm at 10 GHz. Thus the films were deposited on a 50 mm square substrate (i.e. 2 in. x 2 in.).

Before the surface resistance of a sample end plate can be determined, the surface resistance of the cavity parts must be known. If the bore and end plates are made from the same material and have the same surface finish then these parts will also have the same surface resistance (i.e. $1/\delta_b\sigma_b = 1/\delta_e\sigma_e$). Measurement of the Q, resonant frequency and dimensions of the cavity enable the surface resistance of the cavity parts to be evaluated from equation 7-7. Changing one end plate for the material under test gives

$$\frac{1}{Q_s} = \underbrace{\frac{K\lambda^2}{\pi\lambda_g\delta\sigma}}_{\text{(bore)}} + \underbrace{\frac{2\lambda^3}{\pi\lambda_g^3\eta\delta\sigma}}_{\text{(end plate)}} + \underbrace{\frac{2\lambda^3}{\pi\lambda_g^3\eta\delta_s\sigma_s}}_{\text{(sample end plate)}} \quad \ldots\ldots 7\text{-}11$$

where Q_s is the cavity Q with the sample end plate

δ is the skin depth in cavity material

σ is the conductivity of cavity material

σ_s is the conductivity of the sample

δ_s is the skin depth in sample material

Measurement of Q_s and the resonant frequency allows the sample surface resistance to be determined.

In practice, it was found necessary to remove the degenerate E_{111} mode mentioned in section 7-1. This degeneracy and its effect on the above theory are discussed in the following section.

7-3 Removal of the Degenerate E_{111} Mode

Initial measurements on the cavity (see section 7-5) indicated that the end plate contact resistance did affect the cavity Q. This was attributed to the degenerate E_{111} mode. Techniques used to shift the resonant frequency of this mode include; corrugating the bore [62], the corrugations affecting longitudinal currents more than circumferential currents; the use of a corrugated non-contacting end plate [63] preventing the excitation of the E_{111} mode; and a centred post perturbation method [57] where a post one quarter the length of the cavity is positioned at the centre of one end plate.

Any modification to the cavity to remove the degeneracy will also affect the H_{011} mode and hence the cavity Q. It is therefore necessary to be able to calculate or measure this effect. The method used for this cavity was to place annular grooves in one end plate as shown in figure 7-6 as it was believed that the effect of the grooves could be measured and taken into account for the surface resistance measurements. Provided the width and depth of the grooves are small compared to half a guide wavelength then there should be little field penetration into the grooves. If this is the case the

current is concentrated on the inner surface of the end plate. This plate, which formed an integral part of the cavity may then be considered to have some unknown conductivity, σ_g , which will be called the "effective conductivity". The losses of the cavity now depend upon the conductivity of the bore, σ_b , the conductivity of the sample, σ_s , and the effective conductivity, σ_g , of the grooved end. The Q of the cavity is now given by

$$\frac{1}{Q_s} = \underbrace{\frac{K\lambda^2}{\pi\lambda_g\delta_b\sigma_b}}_{\text{(bore)}} + \underbrace{\frac{2\lambda^3}{\pi\lambda_g^3\eta\,\delta_g\sigma_g}}_{\text{(grooved end)}} + \underbrace{\frac{2\lambda^3}{\pi\lambda_g^3\eta\,\delta_s\sigma_s}}_{\text{(sample end)}} \qquad \ldots\ldots \text{7-12}$$

It is therefore necessary to evaluate σ_b and σ_g before the sample surface resistance can be measured.

7-4 Standerdization of the Cavity Parts

Figure 7-7 shows the cavity together with the standard end plates. To evaluate σ_b and σ_g , the cavity Q factor is first measured with a plane detachable end plate of conductivity σ_b . The Q, Q_b, is given by

$$\frac{1}{Q_b} = \frac{K\lambda_b^2}{\pi\lambda_g\delta_b\sigma_b} + \frac{2\lambda_b^3}{\pi\lambda_g^3\eta\,\delta_g\sigma_g} + \frac{2\lambda_b^3}{\pi\lambda_g^3\eta\,\delta_b\sigma_b}$$

where suffix "b" indicates the cavity parameters for end plate σ_b .

Let $A_b = \dfrac{K\lambda_b^2}{\pi\lambda_g}$

and $B_b = \dfrac{2\lambda_b^3}{\pi\lambda_g^3\eta}$

current is concentrated on the inner surface of the end plate. This plate, which formed an integral part of the cavity may then be considered to have some unknown conductivity, σ_g , which will be called the "effective conductivity". The losses of the cavity now depend upon the conductivity of the bore, σ_b , the conductivity of the sample, σ_s , and the effective conductivity, σ_g , of the grooved end. The Q of the cavity is now given by

$$\frac{1}{Q_s} = \frac{K\lambda^2}{\pi\lambda_g\delta_b\sigma_b} + \frac{2\lambda^3}{\pi\lambda_g^3\eta\delta_g\sigma_g} + \frac{2\lambda^3}{\pi\lambda_g^3\eta\delta_s\sigma_s} \quad \ldots\ldots 7\text{-}12$$

(bore) (grooved end) (sample end)

It is therefore necessary to evaluate σ_b and σ_g before the sample surface resistance can be measured.

7-4 Standardization of the Cavity Parts

Figure 7-7 shows the cavity together with the standard end plates. To evaluate σ_b and σ_g , the cavity Q factor is first measured with a plane detachable end plate of conductivity σ_b . The Q, Q_b, is given by

$$\frac{1}{Q_b} = \frac{K\lambda_b^2}{\pi\lambda_g\delta_b\sigma_b} + \frac{2\lambda_b^3}{\pi\lambda_g^3\eta\delta_g\sigma_g} + \frac{2\lambda_b^3}{\pi\lambda_g^3\eta\delta_b\sigma_b}$$

where suffix "b" indicates the cavity parameters for end plate σ_b .

Let $A_b = \frac{K\lambda_b^2}{\pi\lambda_g}$

and $B_b = \frac{2\lambda_b^3}{\pi\lambda_g^3\eta}$

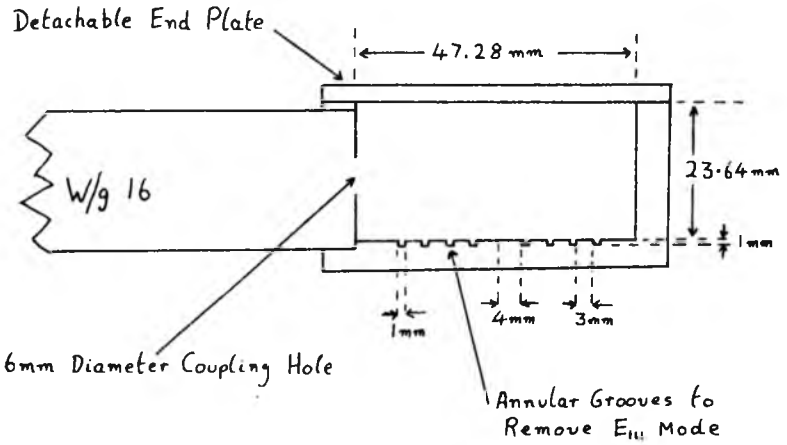

FIGURE 7-6 : SCHEMATIC DIAGRAM OF THE H_{011} MODE CAVITY

FIGURE 7-7 : PHOTOGRAPH OF CAVITY, STANDARD END PLATES AND THIN FILM SAMPLE FOR SURFACE RESISTANCE MEASUREMENTS

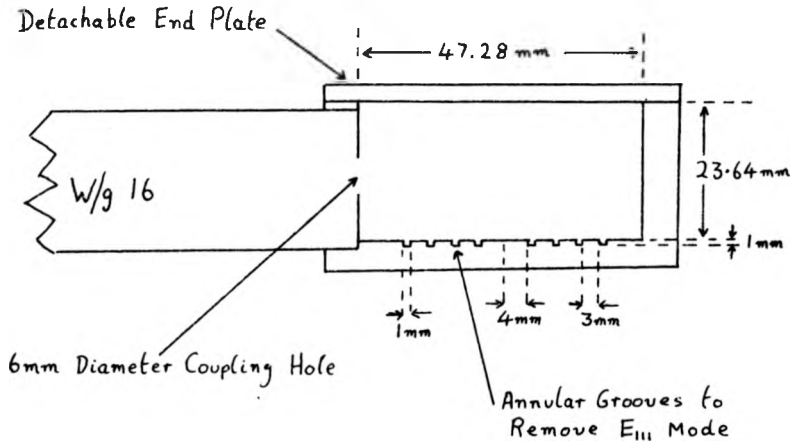

FIGURE 7-6 : SCHEMATIC DIAGRAM OF THE H_{011} MODE CAVITY

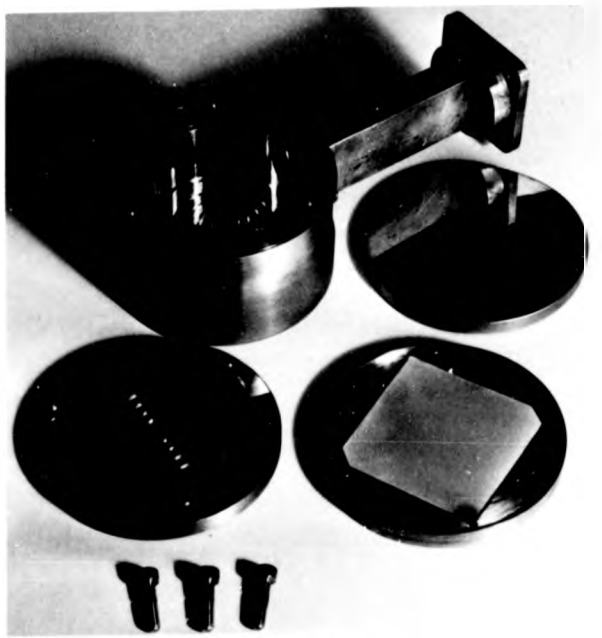

FIGURE 7-7 : PHOTOGRAPH OF CAVITY, STANDARD END PLATES AND THIN FILM SAMPLE FOR SURFACE RESISTANCE MEASUREMENTS

$$\therefore \frac{1}{Q_b} = \frac{A_b}{\delta_b \sigma_b} + \frac{B_b}{\delta_g \sigma_g} + \frac{B_b}{\delta_b \sigma_b} \qquad \ldots\ldots 7\text{-}13$$

The detachable end plate is then replaced by one having an effective conductivity σ_g , i.e. of the same material, surface finish and identical grooves as the grooved end. The Q, Q_g, under these conditions using similar notation as above is given by

$$\frac{1}{Q_g} = \frac{A_g}{\delta_b \sigma_b} + \frac{2B_g}{\delta_g \sigma_g} \qquad \ldots\ldots 7\text{-}14$$

From equations 7-13 and 14, the surface resistance of the bore ($1/\delta_b \sigma_b$) and grooved end ($1/\delta_g \sigma_g$) can be determined.

Replacing the detachable end plate with the sample gives a cavity Q, Q_s, of

$$\frac{1}{Q_s} = \frac{A_s}{\delta_b \sigma_b} + \frac{B_s}{\delta_g \sigma_g} + \frac{B_s}{\delta_s \sigma_s} \qquad \ldots\ldots 7\text{-}15$$

Measurement of Q_s allows the sample surface resistance to be determined.

In practice $A_s = A_b$ and $B_s = B_b$ as there is no significant change in the resonant frequency when measuring samples of good conductivity. With a detachable end plate of conductivity σ_g , however, the resonant frequency decreased by 9 MHz (i.e.$\sim$ 0.1%). This is taken into account by evaluating the coefficients A_b, A_g, B_b, and B_g for equations 7-13 and 14. This frequency shift corresponded to an increase in the effective length of the cavity of 0.05 mm. As a rough approximation, the effect of the grooves on the cavity Q can be predicted by considering the decrease in total surface area caused by the presence

of the grooves. The grooves decreased the total surface area by 3.7% while a 3.8% decrease in Q was observed when measuring the grooved standard end plate. It would therefore appear that field penetration into the grooves is indeed negligible.

7-5 Cavity Construction

It was intended to measure the surface resistance of high conductivity metals such as copper, silver and gold. It was advantageous to make the cavity of a lower conductivity material thus giving a large change in Q when measuring test samples. The material used was brass (BS 249). All parts were machined from the same bar to eliminate any possible variations in the electrical properties of the cavity parts. The cavity was made in two sections, namely, the bore with waveguide feed and integral end plate, and a detachable end plate. All parts were highly polished to give a CLA value of 0.02 μm.

The cavity was magnetically coupled to a waveguide system by means of a hole in the bore of the cavity. The size of the coupling hole was found by experiment. The cavity resonance was observed on a Hewlett Packard network analyzer Smith chart display using a co-axial reflectometer unit. Using a high conductivity copper end plate to give maximum coupling the hole was enlarged until the cavity was just less than critically coupled. The diameter of the coupling hole was 6.5 mm.

At this stage no attempt had been made to remove the degenerate

E_{111} mode i.e. a grooved end plate was not used. Tests were performed on the cavity to study the effect, if any, of variation in the contact pressure of the detachable end plate. This was done by applying different torques to the three fixing screws holding the end plate in position. The cavity Q was measured using the waveguide reflectometer system shown in figure 8-3 . Using a swept frequency oscillator the accuracy of the Q measurements was $\pm$ 1.5%. This was later improved by the use of a Gunn diode source (see section 8-3). With a brass end plate the Q of the cavity was measured to be 11,720 with no measurable change occuring for different contact pressures. However, with a copper end plate large changes were noticeable as can be seen from Table 7-1. These changes were attributed to the presence of the E_{111} mode. Experiments were then performed with a grooved copper end plate to remove the E_{111} mode. Four grooves were found to be necessary. Identical grooves were then machined into the integral end plate of the cavity, (see figure 7-7). The experiments with the copper end plate were then repeated and as can be seen from Table 7-1 the variation in Q with contact pressure was greatly reduced. The dimensions and positions of the grooves are given in figure 7-6. The details of the final design of the cavity together with the standardization end plates and a thin film sample are shown in the photograph in figure 7-7.

Several problems arose in the attachment of the thin film sample to the cavity. First attempts were made by placing the substrate in a 50 mm. square recess machined into a brass end plate. However, it was found that with this arrangement the substrate could be easily distorted if not cracked when fitting to the cavity. Also, there

E_{111} mode i.e. a grooved end plate was not used. Tests were performed on the cavity to study the effect, if any, of variation in the contact pressure of the detachable end plate. This was done by applying different torques to the three fixing screws holding the end plate in position. The cavity Q was measured using the waveguide reflectometer system shown in figure 8-3 . Using a swept frequency oscillator the accuracy of the Q measurements was $\pm$ 1.5%. This was later improved by the use of a Gunn diode source (see section 8-3). With a brass end plate the Q of the cavity was measured to be 11,720 with no measurable change occuring for different contact pressures. However, with a copper end plate large changes were noticeable as can be seen from Table 7-1. These changes were attributed to the presence of the E_{111} mode. Experiments were then performed with a grooved copper end plate to remove the E_{111} mode. Four grooves were found to be necessary. Identical grooves were then machined into the integral end plate of the cavity, (see figure 7-7). The experiments with the copper end plate were then repeated and as can be seen from Table 7-1 the variation in Q with contact pressure was greatly reduced. The dimensions and positions of the grooves are given in figure 7-6. The details of the final design of the cavity together with the standerdization end plates and a thin film sample are shown in the photograph in figure 7-7.

Several problems arose in the attachment of the thin film sample to the cavity. First attempts were made by placing the substrate in a 50 mm. square recess machined into a brass end plate. However, it was found that with this arrangement the substrate could be easily distorted if not cracked when fitting to the cavity. Also, there

was a risk that reflections caused by the metal backing would lead to difficulties when measuring very thin films. For this reason, a hole having the same diameter as the bore was machined in the centre of the recess. This would minimize any reflections and would support the substrate at the corners and edges only. However, distortion of the substrate still occurred. This was finally overcome by supporting the substrate on a narrow rim, the internal diameter of which was the same as the bore, machined into the end plate. This arrangement is shown in figure 7-8.

7-6 Comments

If the cavity components are accurately standardized the theory described in this chapter permits the calculation of the surface resistance of a sample from measurement of the cavity Q. Satisfactory removal of the E_{111} mode was obtained by use of a grooved end plate. Field penetration into the grooves appeared to be negligible although the concept of calculating an "effective conductivity" for a grooved end plate does not require the assumption of negligible field penetration.

It was realized that the measurement procedure could be greatly simplified by calibrating the cavity. This calibration is possible provided that no frequency shift occurs when measuring the sample. This is discussed in the following chapter.

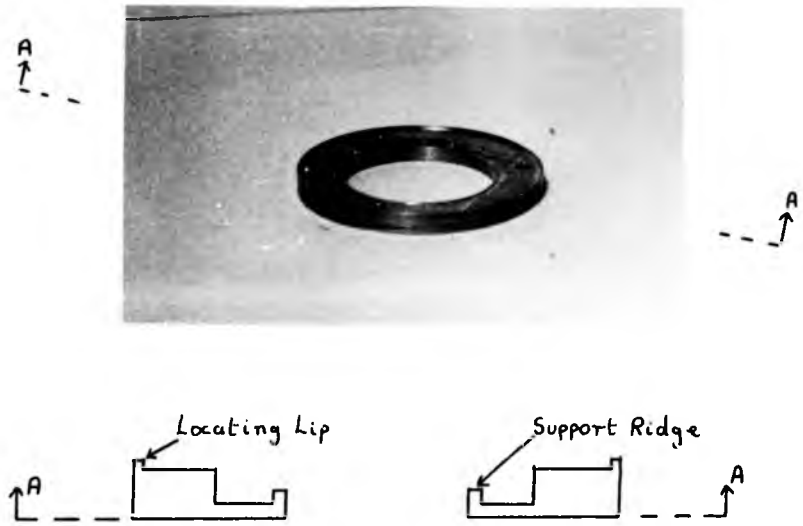

FIGURE 7-8 : PHOTOGRAPH AND CROSS-SECTIONAL DRAWING OF SUBSTRATE SUPPORTIING END PLATE

TABLE 7-1 EFFECT OF CONTACT PRESSURE OF DETACHABLE COPPER END PLATE ON THE Q AND RESONANT FREQUENCY OF H_{011} CAVITY

Torque inch/lbs.	Plain cavity		Cavity with grooved integral end plate	
	Q	Resonant frequency MHz.	Q	Resonant frequency MHz.
Finger tight	13774	9978.6	13243	9970.6
3	13176	9979.1	13479	9971.1
10	12130	9978.9	13403	9970.4

Chapter 8

A SIMPLIFIED AND ACCURATE SURFACE RESISTANCE MEASUREMENT TECHNIQUE

8-1 Introduction

From the cavity theory explained in the preceeding chapter, three Q measurements are required to determine the surface resistance of a given sample. However, once the standardization procedure (section 7-4) has been performed, it is possible to calibrate the cavity so that a single measurement of the return loss at resonance allows the sample conductivity or surface resistance to be obtained directly from a graph. This technique greatly reduces the number of measurements that have to be made in order to achieve an accurate result and is considered to be a major development in this field.

8-2 Measurement of the Unloaded Q of the Cavity

The cavity may be regarded as a series-tuned circuit coupled through a mutual inductance M [64] as shown in figure 8-1. The loaded Q, Q_L, of the cavity is given by

$$Q_L = \frac{Qu}{1+\beta} \qquad \ldots\ldots \quad 8\text{-}1$$

where Qu = unloaded cavity Q = $\omega L/R$

and β = cavity coupling coefficient = $\frac{(\omega M)^2}{RZ_o}$

where R is the resistive component of the equivalent circuit

Z_o is the characteristic impedance of measuring system

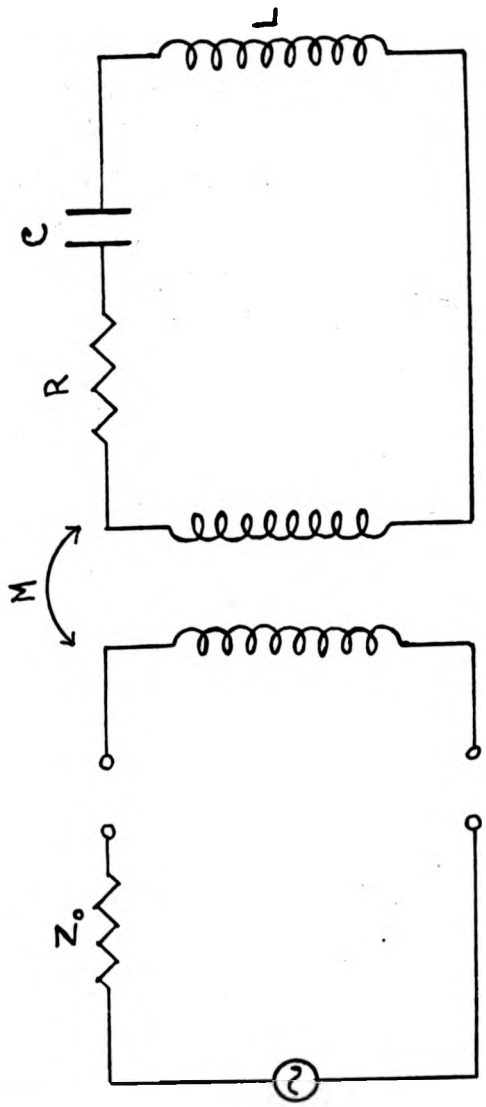

FIGURE 8-1 : EQUIVALENT CIRCUIT OF CAVITY AND COUPLING HOLE

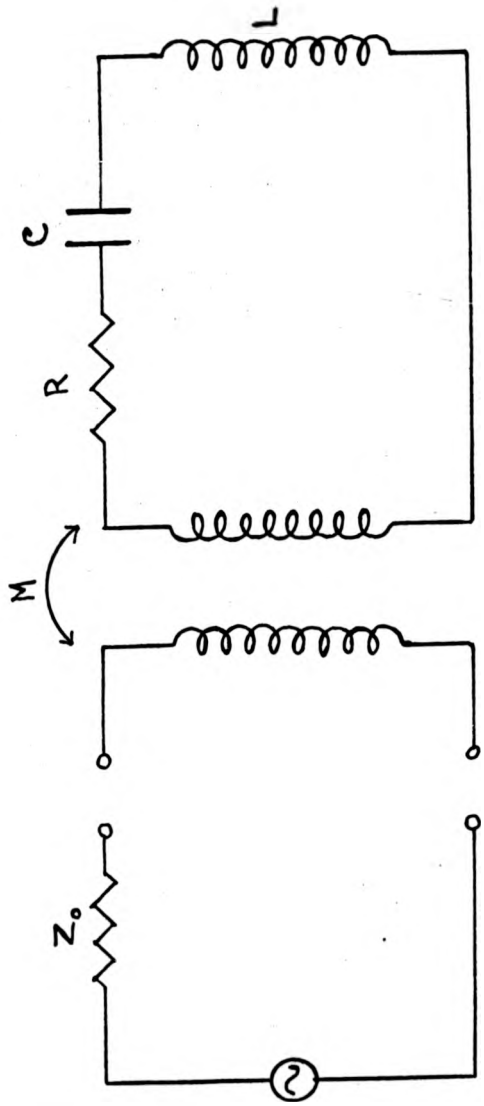

FIGURE 8-1: EQUIVALENT CIRCUIT OF CAVITY AND COUPLING HOLE

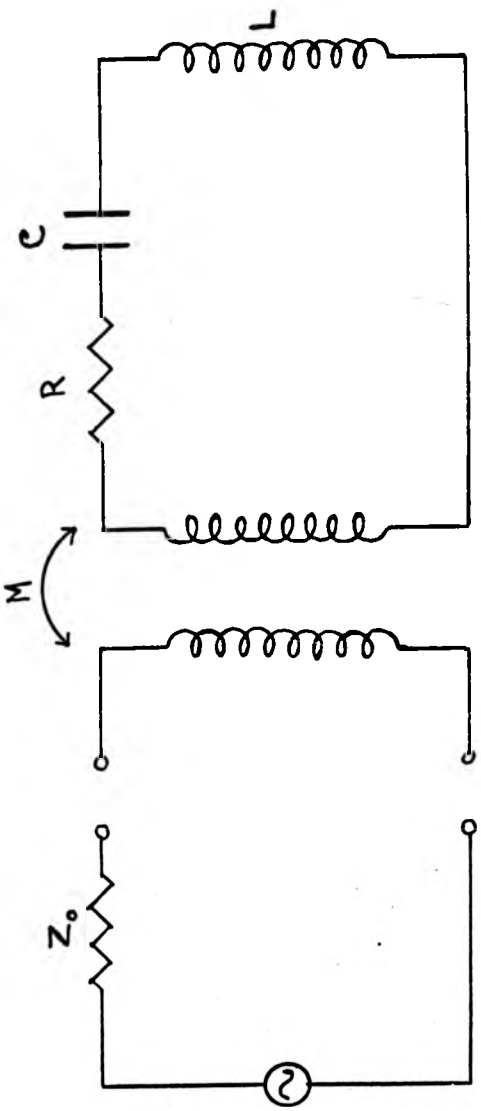

FIGURE 8-1 : EQUIVALENT CIRCUIT OF CAVITY AND COUPLING HOLE

where ω is the angular resonant frequency

In the present application, it is required to measure changes in the resistive component of the cavity equivalent circuit. To do this, the unloaded Q must therefore be evaluated. As has been shown (7), measurement of the reflection coefficient at resonance, Γ_o, allowed the coupling coefficient to be calculated by the equation

$$|\Gamma_o|^2 = \frac{(\beta - 1)^2}{(\beta + 1)^2} \qquad \ldots\ldots 8\text{–}2$$

The calculated value of β was then used to determine the reflection coefficient of two points on the resonance curve corresponding to the band width points of the unloaded cavity. The reflection coefficient, Γ_B, at these points is given by

$$|\Gamma_B|^2 = \frac{(\beta - 1)^2 + 1}{(\beta + 1)^2 + 1} \qquad \ldots\ldots 8\text{–}3$$

Derivation of equations 8–2 and 8–3 is given in reference 7. In practice, return loss measurements were made, the return loss, R_L, being related to the reflection coefficient, Γ, by the equation

$$R_L = 20 \log_{10} |\Gamma| \quad \text{dB} \qquad \ldots\ldots 8\text{–}4$$

In summary, the measurement of the unloaded Q is as follows.

1) Measure return loss at resonance. From equations 8–4, 8–2 and 8–3, calculate the return loss corresponding to the bandwidth points of the unloaded cavity.

2) Measure the frequencies f_{2B} and f_{1B} corresponding to the upper and lower bandwidth points.

The unloaded Q is then given by

$$Q_u = \frac{2\,(f_{2B} - f_{1B})}{(f_{2B} + f_{1B})} \qquad \ldots\ldots \quad 8\text{-}5$$

From equations 8-2, 8-3 and 8-4 it is possible to draw a graph of return loss at the bandwidth points versus return loss at resonance. This is shown in figure 8-2.

8-3 Precision Measurement of the Unloaded Q of the Cavity

All cavity measurements were performed using the waveguide reflectometer apparatus shown in figures 8-3 and 8-4. With a Hewlett Packard 8694B sweep oscillator source, the maximum error obtained in ten Q measurements was $\pm$ 1.5% in measuring Q factors of the order of 12,000. The maximum error E max is defined as

$$E_{max} = \frac{3\,s}{\sqrt{n}}$$

where s = best estimate of the standard deviation of a single result

n = the number of observation

and $\frac{s}{\sqrt{n}}$ = standard error (see Appendix 2)

The coefficient of 3 allows for a 99.7% confidence limit, i.e. there is a 99.7% chance that the mean Q value falls within $\pm$ E max of the true value. Mehmet [7], using an identical system, obtained a maximum error of $\pm$ 0.5% when measuring Q values of the order of 4,000.

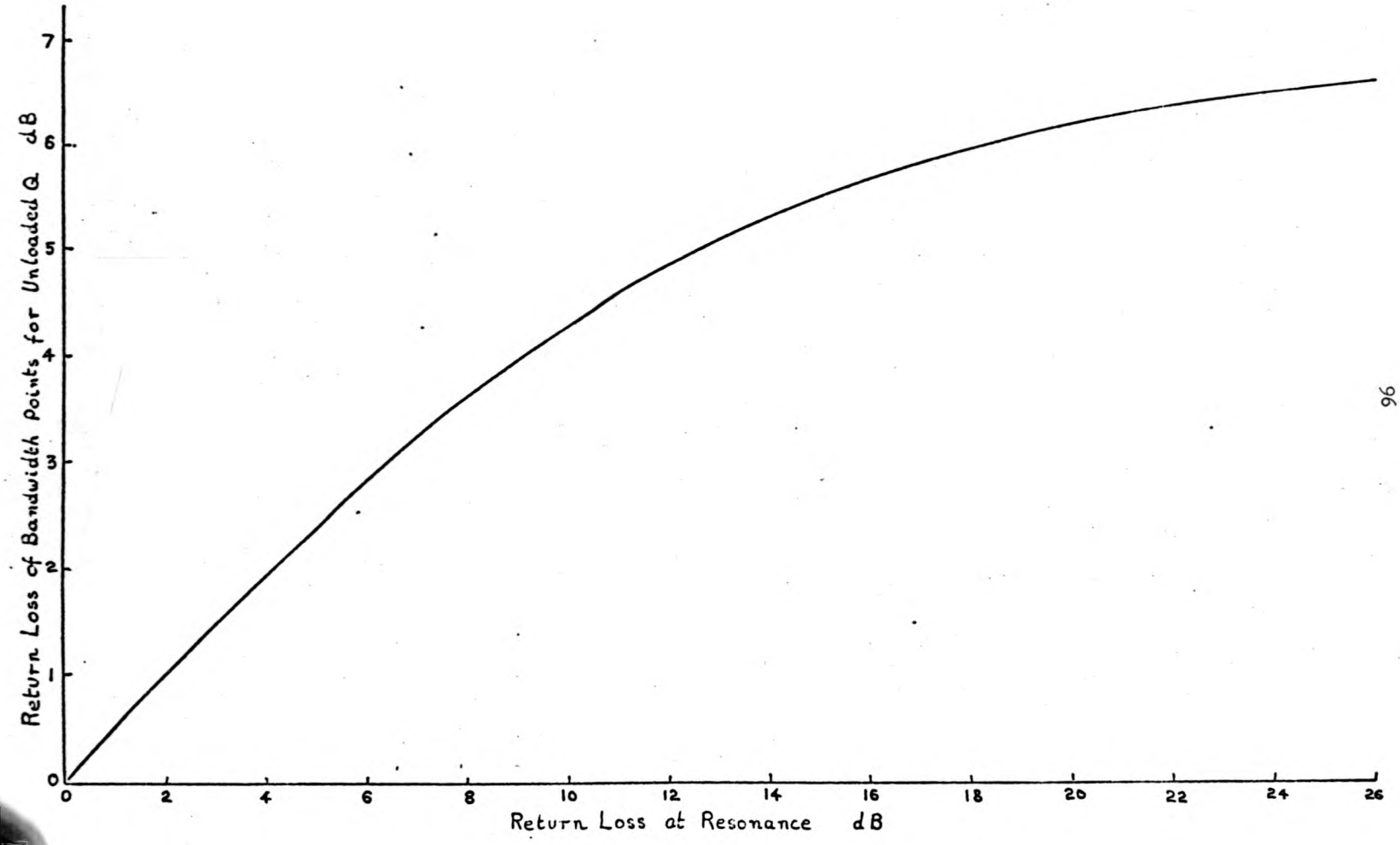

FIGURE 8-2 : RETURN LOSS OF BANDWIDTH POINTS VERSUS RETURN LOSS AT RESONANCE FOR UNLOADED Q MEASUREMENTS

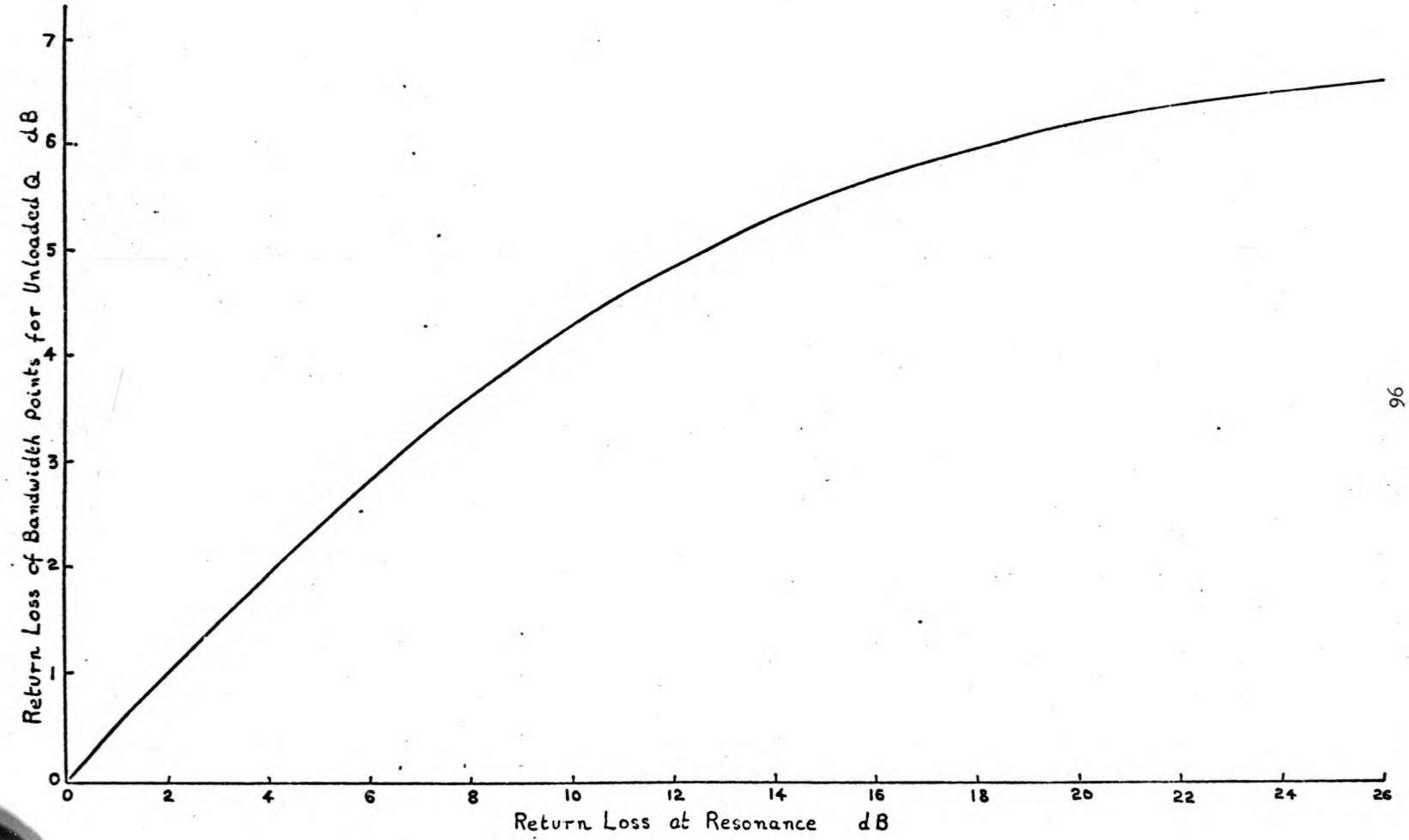

FIGURE 8-2 : RETURN LOSS OF BANDWIDTH POINTS VERSUS RETURN LOSS AT RESONANCE FOR UNLOADED Q MEASUREMENTS

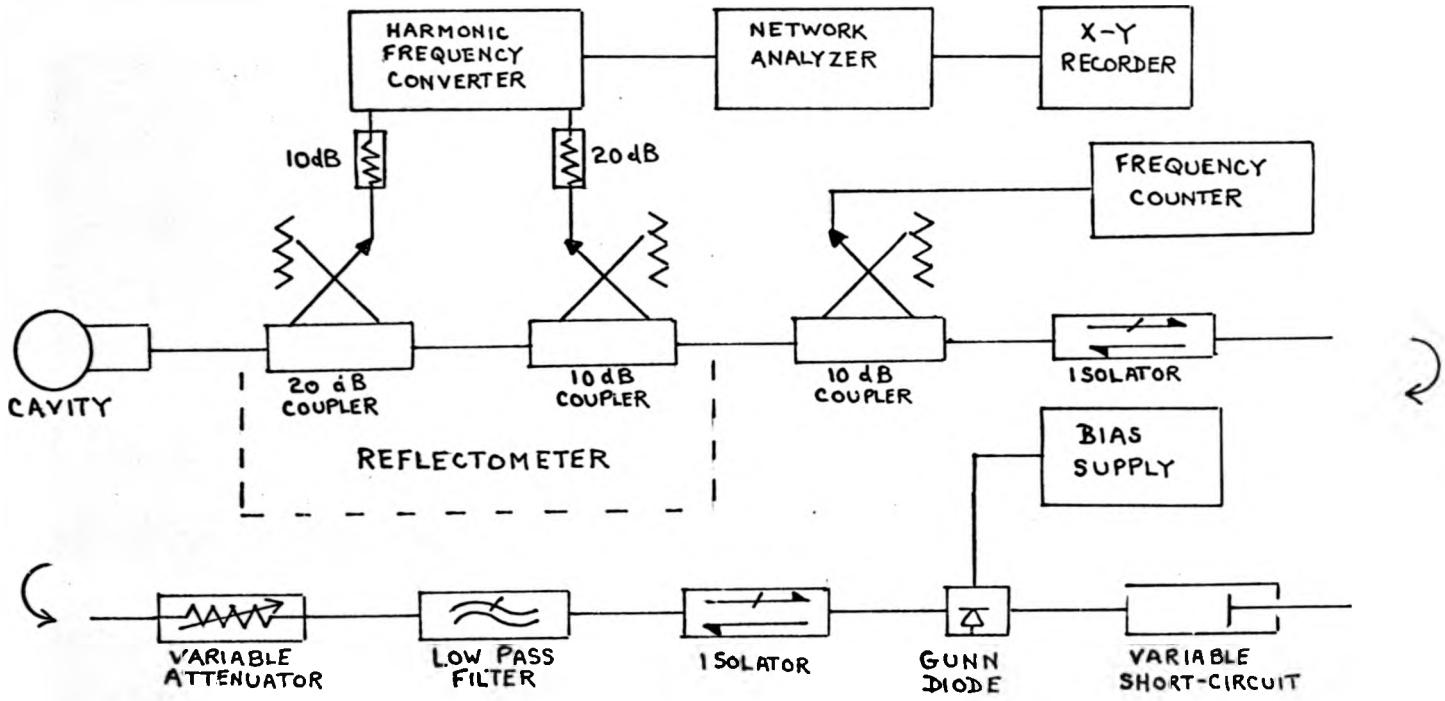

FIGURE 8-3 : SCHEMATIC DIAGRAM OF WAVEGUIDE REFLECTOMETER MEASUREMENT SYSTEM

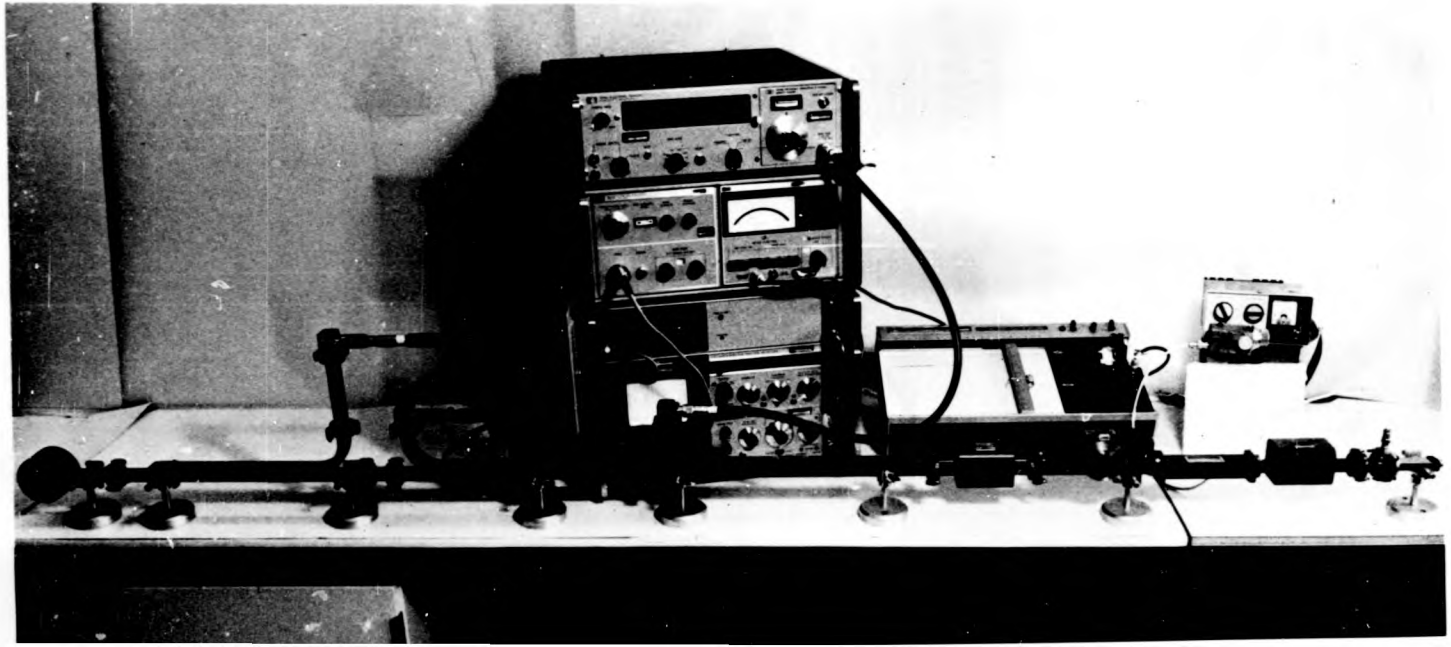

FIGURE 8-4 : PHOTOGRAPH OF WAVEGUIDE REFLECTOMETER APPARATUS

The loss of accuracy for high Q measurements is due entirely to lack of frequency stability of the oscillator. This was overcome by the use of a Gunn diode source. The diode was mounted centrally in a waveguide with a conical base for improved matching [65] and backed by an adjustable short circuit for coarse frequency tuning. Fine tuning was obtained by varying the applied bias voltage. For this purpose, a "minireg" stabalized power supply was used in conjunction with the fine voltage adjustment circuit shown in figure 8-5. A ten-turn potentiometer, A, was used for fine voltage control while potentiometer, B, varied the sensitivity of A. This arrangement allowed the system to be used for low or high Q measurements. Zener diode protection of the Gunn diode was also included. Figure 8-6 shows spectrum analyser photographs of the Gunn diode and sweep oscillator outputs. It can be seen that a purer and more stable signal was obtained from the diode. The maximum error obtained from ten Q measurements using the Gunn diode source was $\pm$ 0.4%. It should be emphasized that this error figure also includes any effect from removal and replacement of the cavity end-plate for each measurement.

8-4 Calibration of the Cavity for Surface Resistance Measurements

Consideration of the series tuned equivalent circuit of the cavity shown in figure 8-1 shows that a change in the conductivity of one end-plate will result only in a change of the resistive component R, of the equivalent circuit. The unloaded Q of this circuit and the voltage standing wave ratio (VSWR) at resonance are therefore given by

The loss of accuracy for high Q measurements is due entirely to lack of frequency stability of the oscillator. This was overcome by the use of a Gunn diode source. The diode was mounted centrally in a waveguide with a conical base for improved matching [65] and backed by an adjustable short circuit for coarse frequency tuning. Fine tuning was obtained by varying the applied bias voltage. For this purpose, a "minireg" stabalized power supply was used in conjunction with the fine voltage adjustment circuit shown in figure 8-5. A ten-turn potentiometer, A, was used for fine voltage control while potentiometer, B, varied the sensitivity of A. This arrangement allowed the system to be used for low or high Q measurements. Zener diode protection of the Gunn diode was also included. Figure 8-6 shows spectrum analyser photographs of the Gunn diode and sweep oscillator outputs. It can be seen that a purer and more stable signal was obtained from the diode. The maximum error obtained from ten Q measurements using the Gunn diode source was $\pm$ 0.4%. It should be emphasized that this error figure also includes any effect from removal and replacement of the cavity end-plate for each measurement.

8-4 Calibration of the Cavity for Surface Resistance Measurements

Consideration of the series tuned equivalent circuit of the cavity shown in figure 8-1 shows that a change in the conductivity of one end-plate will result only in a change of the resistive component R, of the equivalent circuit. The unloaded Q of this circuit and the voltage standing wave ratio (VSWR) at resonance are therefore given by

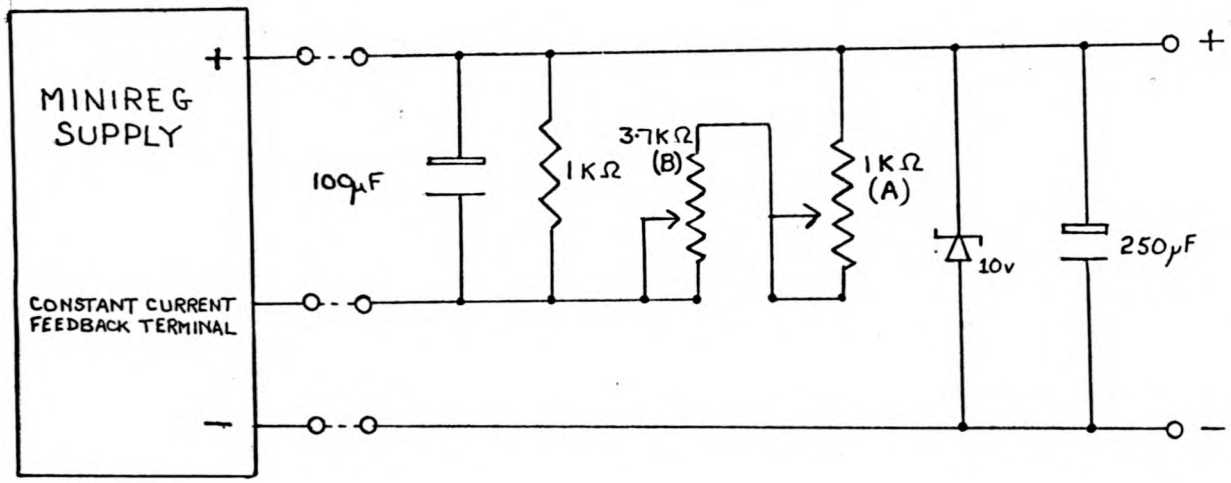

A – 10-TURN POTENTIOMETER FOR FINE VOLTAGE CONTROL
B – SENSITIVITY ADJUSTMENT

FIGURE 8-5: POWER SUPPLY FOR GUNN DIODE BIAS

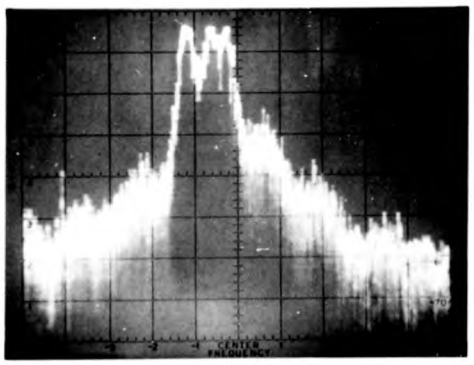

Frequency 9·5GHz
Sweep 20KHz/div
Bandwidth 10KHz
Log Scale

Hewlett Packard Sweep Oscillator Model No. 8694B

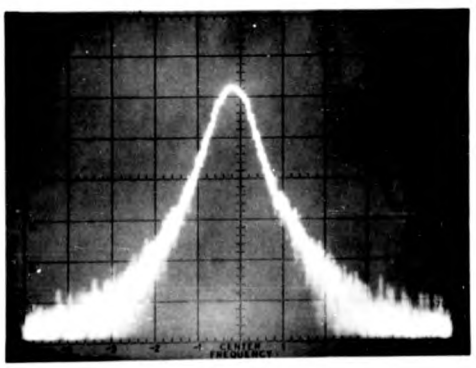

Frequency 9·5GHz
Sweep 20KHz/div
Bandwidth 10KHz
Log Scale

Gunn Diode

FIGURE 8-6 : SPECTRUM ANALYSER PHOTOGRAPHS OF GUNN DIODE AND SWEEP OSCILLATOR OUTPUTS

$$Q_1 = \frac{\omega L}{R_1}$$

and $$S_1 = \frac{Z_o R_1}{(\omega M)^2}$$

where Q_1 and S_1 are the unloaded Q and VSWR for resistive component R_1.

For samples which are good conductors, their introduction will have a negligible effect on the resonant frequency. A change in the conductivity of the end plate will therefore give a new unloaded Q, Q_2 and VSWR, S_2, given by

$$Q_2 = \frac{\omega L}{R_2}$$

and $$S_2 = \frac{Z_o R_2}{(\omega M)^2}$$

where R_2 is the new resistance component of the cavity equivalent circuit.

From the above equations it is easily shown that

$$\frac{Q_1}{Q_2} = \frac{R_2}{R_1} = \frac{S_2}{S_1} \qquad \text{..... 8-6}$$

similarly $$\frac{Q_1}{Q_2} = \frac{\beta_1}{\beta_2}$$

Thus, measurement of Q_1 and both VSWRs allows Q_2 to be calculated.

The theory assumes that no change occurs in the resonant frequency and therefore that there is no change in the mutual inductance of the

coupling hole. These conditions were satisfied by the cavity used when measuring samples of good conductivity. In practice, small changes in the resonant frequency did occur ($\sim$ 1MHz). On the assumption that M remained constant, small frequency shifts could be taken into account. Extension of the above theory for variable ω gives

$$\frac{Q_1}{Q_2} = \frac{S_2}{S_1} \left(\frac{\omega_2}{\omega_1}\right)^2 \qquad \text{..... (8-7)}$$

In practice these small frequency shifts had a negligible effect on the results and were therefore ignored. To check the validity of equation 8-6, measurements of Q and return loss were made with end plates of different conductivity. The return loss is related to the VSWR by

$$\text{Return loss} = 20 \log_{10} \left(\frac{s - 1}{s + 1}\right) \qquad \text{..... (8-8)}$$

When the Q and return loss for a given end plate have been measured, a theoretical curve of Q versus return loss can be drawn using equation 8-6. Figure 8-7 shows the theoretical curve together with the actual measured value of Q. As can be seen, the theoretical and practical results are in excellent agreement.

Returning to equation 7-13, the sample surface resistance is given by

$$\frac{1}{\delta_s \sigma_s} = \left(\frac{1}{Q_s} - \frac{A_s}{\delta_b \sigma_b} - \frac{B_s}{\delta_g \sigma_g}\right) \Big/ B_s$$

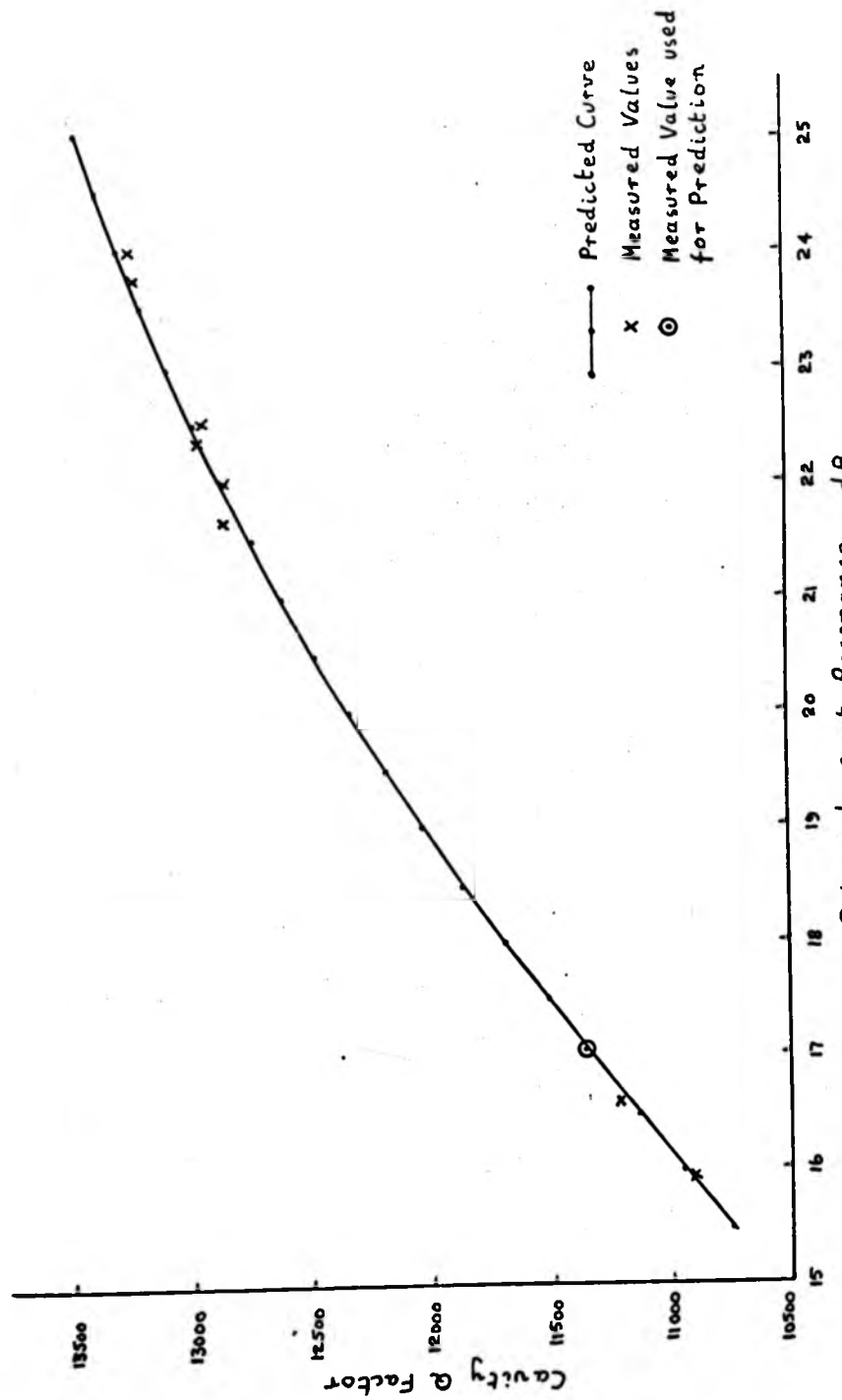

FIGURE 8-7 : VARIATION OF CAVITY Q WITH RETURN LOSS AT RESONANCE

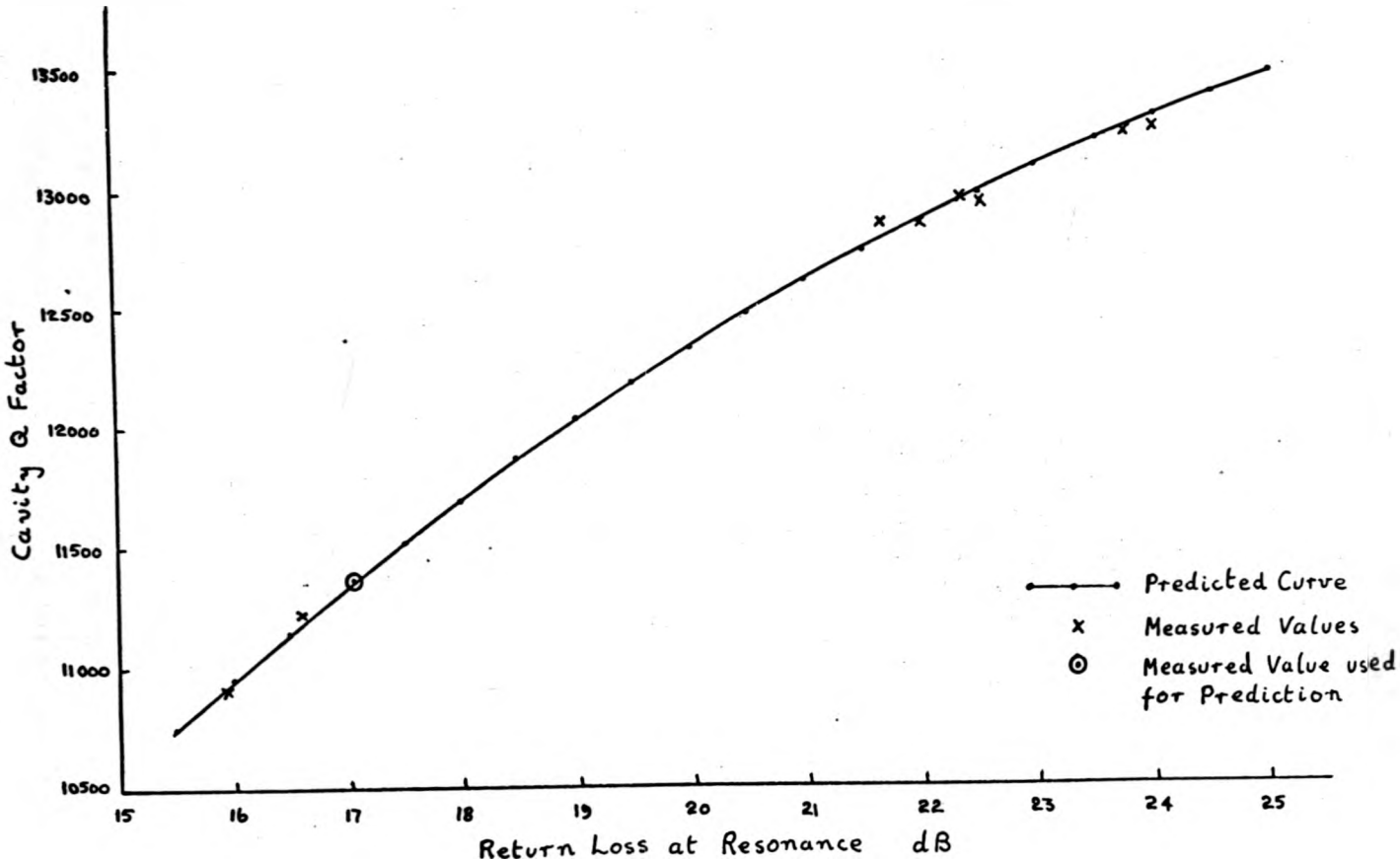

FIGURE 8-7 : VARIATION OF CAVITY Q WITH RETURN LOSS AT RESONANCE

Provided there is no significant frequency change when measuring the sample this may be re-written as

$$\frac{1}{\delta_s \sigma_s} = \left(\frac{1}{Q_s} - \frac{A_b}{\delta_b \sigma_b} - \frac{B_b}{\delta_g \sigma_g} \right) \Big/ B_b$$

Applying equation 8–6 gives

$$Q_s = Q_b \frac{S_b}{S_s}$$

where suffix s denotes measurements with sample end plate

and " b " " " end plate of conductivity σ_b

$$\frac{1}{\delta_s \sigma_s} = \left(\frac{S_s}{Q_b S_b} - \frac{A_b}{\delta_b \sigma_b} - \frac{B_b}{\delta_g \sigma_g} \right) \Big/ B_b \quad \ldots\ldots 8\text{–}9$$

When the cavity standards have been measured as described in section 7–4, and S_b has been measured, a graph of $1/\delta_s \sigma_s$ versus S_s may be drawn. With the information on the cavity properties given in Table 8–1, the calibration curve shown in figure 8–8 was drawn for the cavity used.

8–5 Summary of Measurement Procedure

1) With a detachable end plate of conductivity σ_b (i.e. the same conductivity as the bore material) the cavity Q (Q_b), resonant frequency, f_{ob}, and return loss, R_{Lb}, are measured.

2) With a detachable end plate having an effective conductivity σ_g (i.e. identical grooves and surface finish to the grooved end) the Q (Q_g), resonant frequency, f_{og}, and return loss, R_{Lg}, are

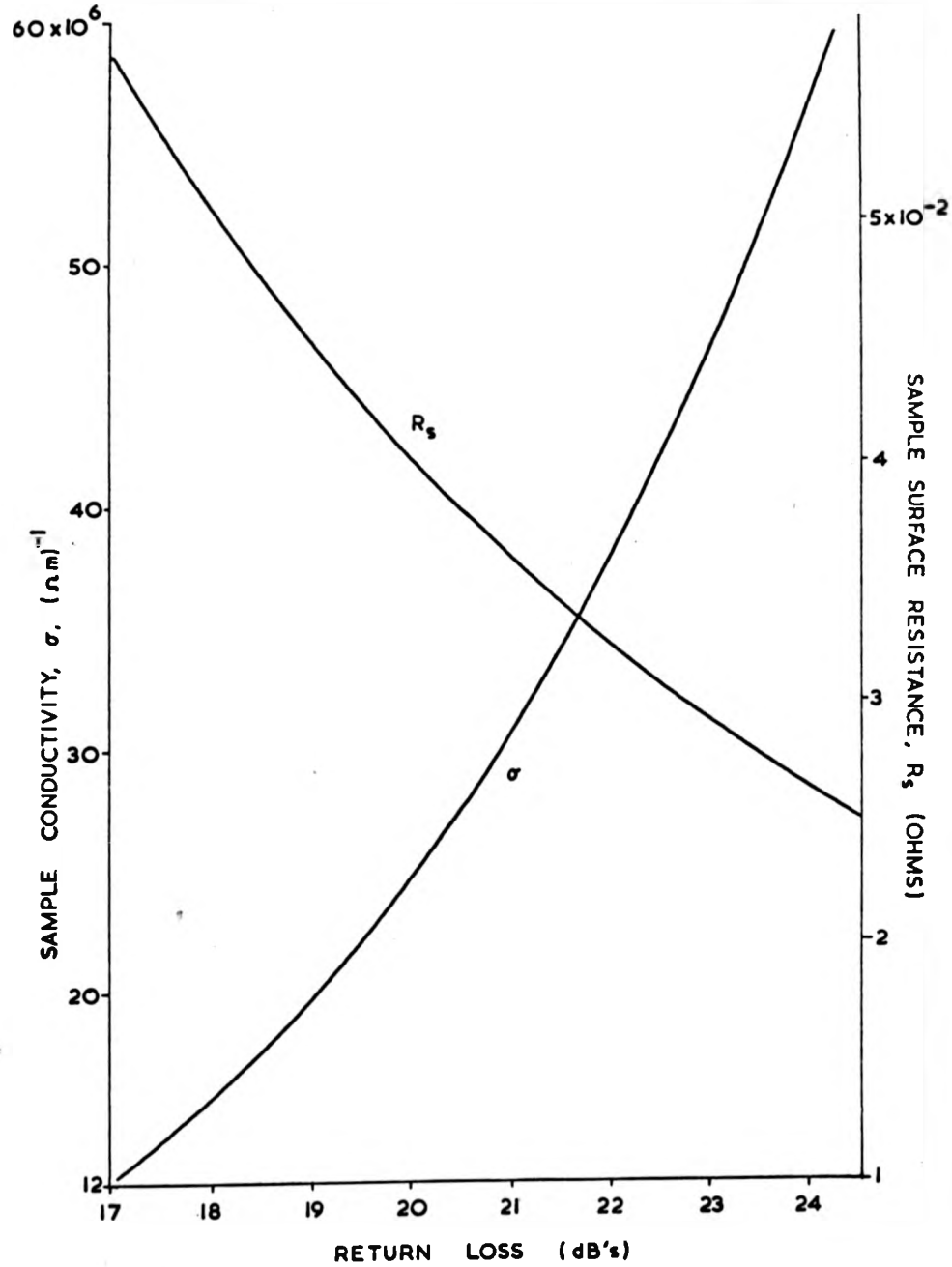

FIGURE 8-8: CALIBRATION CURVE SHOWING VARIATION OF SAMPLE SURFACE RESISTANCE AND CONDUCTIVITY WITH RETURN LOSS

measured. As mentioned earlier, a decrease of 9MHz. occurs in the resonant frequency. Assuming that the mutual inductance of the coupling hole remains constant, it is possible to predict Q_g from equation 8-6. The theoretical and practical values were found to be well within the experimental error.

3) Knowing Q_b and Q_g, equations 7-8 and 7-9 may be used to calculate $1/\delta_g\sigma_g$ and $1/\delta_b\sigma_b$. Using equation 8-9, the calibration curve may now be drawn.

4) Test samples are then attached and the return loss measured. The conductivity or surface resistance may then be obtained from the calibration curve.

After calibration of the cavity, it was found unnecessary to re-calibrate from day to day, although before each set of measurements was made, the calibration was checked. The resonant frequency with the test sample was also checked to ensure that no significant change in the resonant frequency occurred.

8-6 Analysis of Errors

The measured parameters together with their maximum errors are given in Table 8-1. Equations 7-11, 7-12 and 7-13, may be rewritten as

$$\frac{1}{\delta_b\sigma_b} = \left[\frac{1}{Q_b} - \frac{B_b}{2B_gQ_g}\right]\left[A_b + B_b - \frac{B_gA_g}{2B_g}\right]^{-1} \quad \ldots\ldots \text{8-10a}$$

$$\frac{1}{\delta_g\sigma_g} = \left[\frac{1}{Q_g} - \frac{A_g}{\delta_b\sigma_b}\right] \Big/ 2B_g \quad \ldots\ldots \text{8-10b}$$

measured. As mentioned earlier, a decrease of 9MHz. occurs in the resonant frequency. Assuming that the mutual inductance of the coupling hole remains constant, it is possible to predict Q_g from equation 8-6. The theoretical and practical values were found to be well within the experimental error.

3) Knowing Q_b and Q_g, equations 7-8 and 7-9 may be used to calculate $1/\delta_g\sigma_g$ and $1/\delta_b\sigma_b$. Using equation 8-9, the calibration curve may now be drawn.

4) Test samples are then attached and the return loss measured. The conductivity or surface resistance may then be obtained from the calibration curve.

After calibration of the cavity, it was found unnecessary to re-calibrate from day to day, although before each set of measurements was made, the calibration was checked. The resonant frequency with the test sample was also checked to ensure that no significant change in the resonant frequency occurred.

8-6 Analysis of Errors

The measured parameters together with their maximum errors are given in Table 8-1. Equations 7-11, 7-12 and 7-13, may be rewritten as

$$\frac{1}{\delta_b\sigma_b} = \left[\frac{1}{Q_b} - \frac{B_b}{2B_g Q_g}\right]\left[A_b + B_b - \frac{B_g A_g}{2B_g}\right]^{-1} \quad \ldots\ldots 8\text{-}10a$$

$$\frac{1}{\delta_g\sigma_g} = \left[\frac{1}{Q_g} - \frac{A_g}{\delta_b\sigma_b}\right] \Big/ 2B_g \quad \ldots\ldots 8\text{-}10b$$

$$\frac{1}{\delta_s \sigma_s} = \left[\frac{S_s}{Q_b S_b} - \frac{A_b}{\delta_b \sigma_b} - \frac{B_b}{\delta_g \sigma_g} \right] \Big/ B_b \qquad \ldots\ldots \text{8-10c}$$

For the purpose of error calculations the coefficients A and B may be regarded as constant for all measurements. Typical values are

$$A_b = A_g = 6.4711 \times 10^{-4} \pm 1.27 \times 10^{-6}$$

$$B_b = B_g = 4.2364 \times 10^{-4} \pm 8.75 \times 10^{-7}$$

For any function

$$z = f(x,y)$$

it can be shown [66] that the variance of z, V(z), is given by

$$V(z) = \left(\frac{dz}{dx}\right)^2 V(x) + \left(\frac{dz}{dy}\right)^2 V(y) + \text{covariance term} \qquad \ldots\ldots \text{8-11}$$

where V(x) is the variance of parameter x

V(y) is the variance of parameter y

If x and y are independent variables, then the covariance term is zero. Equation 8-11 can be extended to any number of variables. Applying this method to equations 8-10a, b, c and substituting the information given in Table 8-1 yields

$$1/\delta_b \sigma_b = 0.05649 \pm 0.00053 \quad (\pm 0.93\%)\ \Omega$$

$$1/\delta_g \sigma_g = 0.06499 \pm 0.00057 \quad (\pm 0.88\%)\ \Omega$$

and for $R_{Ls} = 24.00$, $1/\delta_s \sigma_s = 0.02642 \pm 0.00128 \quad (\pm 4.8\%)\ \Omega$

The maximum error in measuring the sample surface resistance is therefore $\pm 0.0013\,\Omega$ (i.e. $\pm 4.8\%$ for high purity bulk copper).

$$\frac{1}{\delta_s \sigma_s} = \left[\frac{S_s}{Q_b S_b} - \frac{A_b}{\delta_b \sigma_b} - \frac{B_b}{\delta_g \sigma_g} \right] \Big/ B_b \qquad \ldots\ldots \text{8-10c}$$

For the purpose of error calculations the coefficients A and B may be regarded as constant for all measurements. Typical values are

$$A_b = A_g = 6.4711 \times 10^{-4} \pm 1.27 \times 10^{-6}$$

$$B_b = B_g = 4.2364 \times 10^{-4} \pm 8.75 \times 10^{-7}$$

For any function

$$z = f(x,y)$$

it can be shown [66] that the variance of z, V(z), is given by

$$V(z) = \left(\frac{dz}{dx}\right)^2 V(x) + \left(\frac{dz}{dy}\right)^2 V(y) + \text{covariance term} \qquad \ldots\ldots \text{8-11}$$

where V(x) is the variance of parameter x

V(y) is the variance of parameter y

If x and y are independent variables, then the covariance term is zero. Equation 8-11 can be extended to any number of variables. Applying this method to equations 8-10a, b, c and substituting the information given in Table 8-1 yields

$$1/\delta_b \sigma_b = 0.05649 \pm 0.00053 \quad (\pm 0.93\%)\ \Omega$$

$$1/\delta_g \sigma_g = 0.06499 \pm 0.00057 \quad (\pm 0.88\%)\ \Omega$$

and for $R_{Ls} = 24.00$, $1/\delta_s \sigma_s = 0.02642 \pm 0.00128 \quad (\pm 4.8\%)\ \Omega$

The maximum error in measuring the sample surface resistance is therefore $\pm 0.0013\,\Omega$ (i.e. $\pm 4.8\%$ for high purity bulk copper).

$$\frac{1}{\delta_s \sigma_s} = \left[\frac{S_s}{Q_b S_b} - \frac{A_b}{\delta_b \sigma_b} - \frac{B_b}{\delta_g \sigma_g} \right] \Big/ B_b \qquad \ldots\ldots \text{8-10c}$$

For the purpose of error calculations the coefficients A and B may be regarded as constant for all measurements. Typical values are

$$A_b = A_g = 6.4711 \times 10^{-4} \pm 1.27 \times 10^{-6}$$
$$B_b = B_g = 4.2364 \times 10^{-4} \pm 8.75 \times 10^{-7}$$

For any function

$$z = f(x,y)$$

it can be shown [66] that the variance of z, V(z), is given by

$$V(z) = \left(\frac{dz}{dx}\right)^2 V(x) + \left(\frac{dz}{dy}\right)^2 V(y) + \text{covariance term} \qquad \ldots\ldots \text{8-11}$$

where V(x) is the variance of parameter x

V(y) is the variance of parameter y

If x and y are independent variables, then the covariance term is zero. Equation 8-11 can be extended to any number of variables. Applying this method to equations 8-10a, b, c and substituting the information given in Table 8-1 yields

$$1/\delta_b \sigma_b = 0.05649 \pm 0.00053 \quad (\pm 0.93\%)\ \Omega$$
$$1/\delta_g \sigma_g = 0.06499 \pm 0.00057 \quad (\pm 0.88\%)\ \Omega$$

and for $R_{Ls} = 24.00$, $1/\delta_s \sigma_s = 0.02642 \pm 0.00128 \quad (\pm 4.8\%)\ \Omega$

The maximum error in measuring the sample surface resistance is therefore $\pm 0.0013\,\Omega$ (i.e. $\pm 4.8\%$ for high purity bulk copper).

TABLE 8-1 : MEASURED PROPERTIES OF H_{011} CAVITY

Parameter	Measured Value	Maximum Error
Cavity Diameter	47.288 mm	$\pm$ 2 x 10^{-4} mm
For detachable end plate of conductivity σ_b		
Q (Q_b)	11,360	$\pm$ 45
Return Loss (R_{Lb})	17.05 dB	$\pm$ 0.05 dB
Resonant Frequency (f_{ob})	9969.67 MHz.	$\pm$ 0.03 MHz.
For detachable end plate of conductivity σ_g		
Q (Q_g)	10,928	$\pm$ 43
Return Loss (R_{Lg})	15.90 dB	$\pm$ 0.05
Resonant Frequency (f_{og})	9961.25 MHz.	$\pm$ 0.03 MHz.
For typical thin film sample of conductivity σ_s		
Resonant Frequency (f_{os})	9970.31 MHz.	$\pm$ 0.03 MHz.
Return Loss (R_{Ls})	24.00 dB	$\pm$ 0.05 dB
VSWR Ratio (S_s/S_b)	0.8552	$\pm$ 0.0017

8-7 Comments

Application of the theory described above greatly simplified the surface resistance measurements. Use of the calibration curve allows the conductivity or surface resistance of a sample to be obtained quickly and accurately. The only assumption made in order to calibrate the cavity is that of constant resonant frequency such that no change in the mutual inductance of the coupling hole occurs. This is justified for the present cavity by the excellent agreement between the measured and predicted Q values shown in figure 8-7.

Chapter 9

SURFACE RESISTANCE MEASUREMENTS OF BULK AND THIN FILM SAMPLES

9-1 Introduction

It is well known that microwave losses in a conductor are always greater than that predicted from dc conductivity measurements. Morgan (67) made a theoretical investigation of the effect of surface roughness on eddy current losses at microwave frequencies. He concluded that the presence of scratches on a conducting surface can increase the loss by as much as 100% and is dependent on the ratio of rms surface roughness to skin depth, and whether the scratches are transverse or parallel to the current flow. His treatment, however, was restricted to scratches of specific shape and therefore represents a somewhat idealized case. Expressions have been derived by Allison and Benson (68) for the calculation of the attenuation in rectangular waveguide so as to take into account the surface roughness of the guide. Their investigation of electropolished copper waveguide demonstrated that the surface roughness of the precision-drawn guide contributed an increase of only 2% to the attenuation and they therefore concluded that electropolishing was not a worthwhile process for most applications. As many of the measurements performed by the University microwave group involve the use of cavities, it was decided to investigate the effects of surface finishing processes on the surface resistance of high purity copper and 60-40 (BS 249) brass. The samples were subjected to machining, mechanical polishing, electrolytic polishing and annealing.

As was mentioned earlier, the surface resistance measurements were started in order to evaluate the electrode loss of thin film capacitors. Results will be reported for both evaporated films and films deposited from various commercially available electroplating solutions. The work was extended to cover an investigation of the effects of the plating conditions on the surface resistance, surface finish and dc conductivity of copper films. The results were evaluated using factorial analysis.

9-2 Measurements on Bulk Samples

The surface resistance of an infinitely thick conductor was given in section 7-1 as

$$R_s = X_s = \frac{1}{\delta \sigma}$$

It will be shown in section 9-3-1 that the above relationship holds for thickness greater than three skin depths. The results obtained for high purity copper and 60-40 brass samples are given in Table 9-1. Surface features of each sample were examined on a Vickers 55 microscope and surface profiles were obtained from a Talysurf No. 1. Centre line average (CLA) values were also determined to give a quantitative assessment of the surface roughness. The results are discussed in the following sections, together with some observations on annealed samples.

9-2-1 Machined Surfaces

Brass and copper plates were turned with both steel and diamond

TABLE 9-1 : SURFACE RESISTANCE OF BULK MATERIALS

Material	Finishing Process	Centre Line Average (CLA) μm	Surface Resistance (OHMS)	RF Conductivity $(\Omega m)^{-1} \times 10^6$	Conductivity of bulk material * $(\Omega m)^{-1} \times 10^6$
High Purity Copper	Steel Tool Turned	0.18	0.0306	42.03	
	Diamond Tool Turned	0.03	0.0303	42.86	
	Steel Tool Flycut	0.3	0.0334	35.23	
	Diamond Tool Flycut	0.2	0.0310	40.92	
	Mechanically Polished	0.018	0.323	37.72	58.00
	Electro-polished	0.07	0.0271	53.56	
Annealed High Purity Copper	Electro-polished (1)	0.07	0.0262	57.31	
	Steel Tool Turned (2)	0.18	0.0281	49.71	
	Diamond Tool Turned (2)	0.03	0.0275	52.04	
Brass (BS249)	Steel Tool Turned	0.11	0.0592	11.23	14.68
	Diamond Tool Turned	0.035	0.0600	10.88	

* Values obtained from reference 82.

(1) Annealed at 850°C for 1 hour.

(2) " " 650°C for 2.5 hours.

tools. Figures 9-1 and 9-2 show typical surface finishes obtained. It can be clearly seen that use of a diamond tool removes a great deal of the roughness, although some turning marks are still formed. Although the surface profiles are very different there is a negligible difference in the measured values of surface resistance (Table 9-1). The turning marks are circumferential about the centre of the plate and therefore lie in the direction of current flow in the plate. It is therefore unlikely that they will affect the surface resistance to any great extent. Cold-working of a metal decreases the conductivity by increasing the dislocation density in the material [69,70]. The high surface resistance of the samples can be explained as a result of work-hardening of the metals, both the steel and diamond tools giving the same degree of work-hardening.

The effect of surface finish is more noticeable for the "fly-cut" samples, where the machining marks are not circumferential. In this case, the diamond tool gives a lower surface resistance owing to the slightly better surface finish.

9-2-2 Polished Samples

Mechanical polishing of a steel tool machined copper sample caused yet a further increase in the surface resistance. The sample was polished first on 600 grit and finally lapped on a 0.25 μm wheel. A smooth flat surface was obtained (see figure 9-3) although

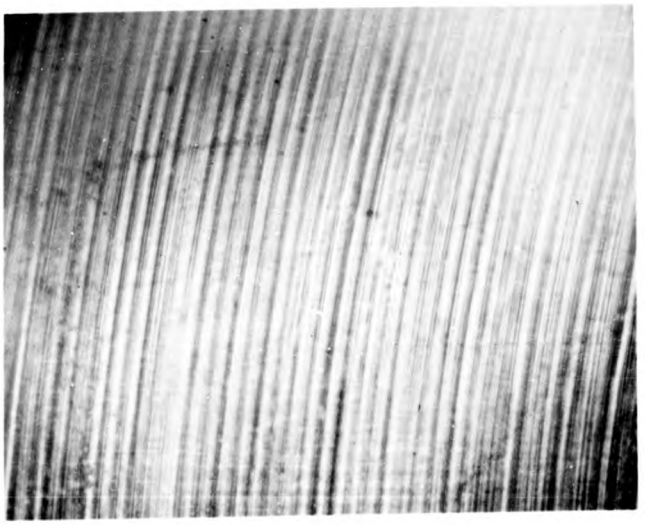

Magnification
x 100

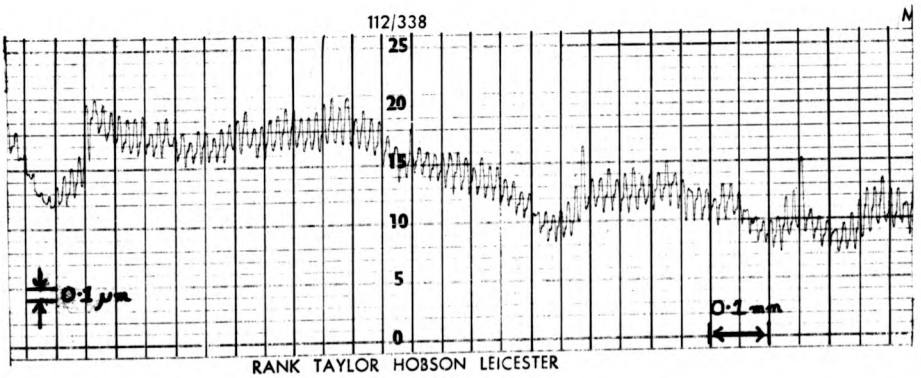

Horizontal Magnification x100
Vertical Magnification x 20,000

FIGURE 9-1: PHOTOGRAPH AND TALYSURF TRACE OF STEEL TOOL FINISH ON COPPER

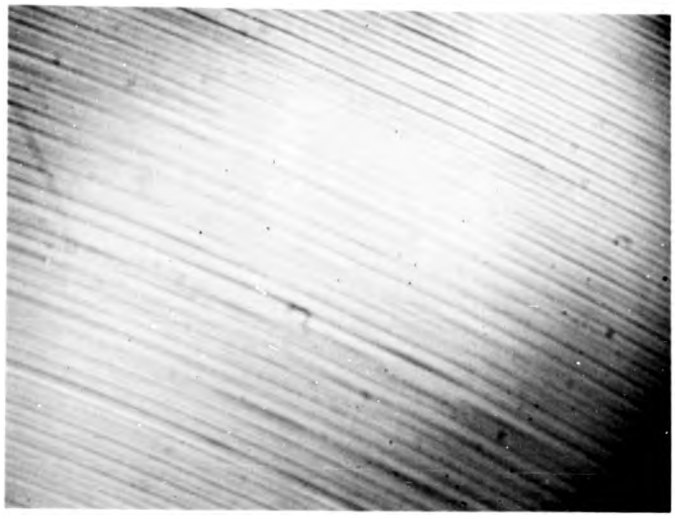

Magnification
X 100

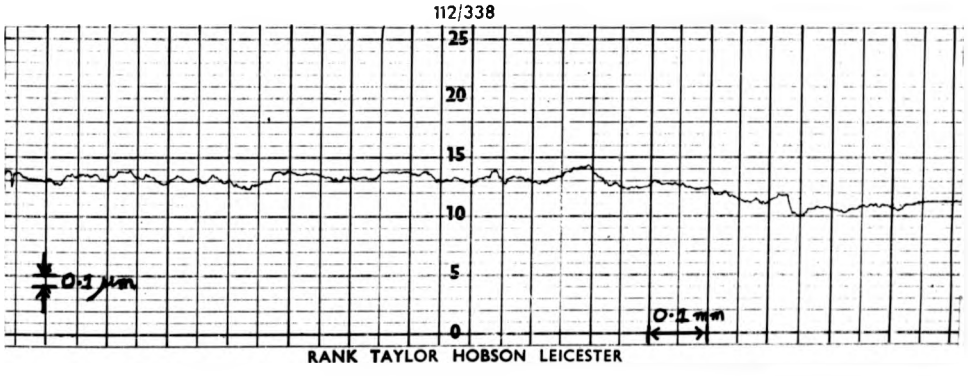

Horizontal Magnification X 100
Vertical Magnification X 20,000

FIGURE 9-2 : PHOTOGRAPH AND TALYSURF TRACE OF DIAMOND TOOL FINISH ON COPPER

Magnification
x 100

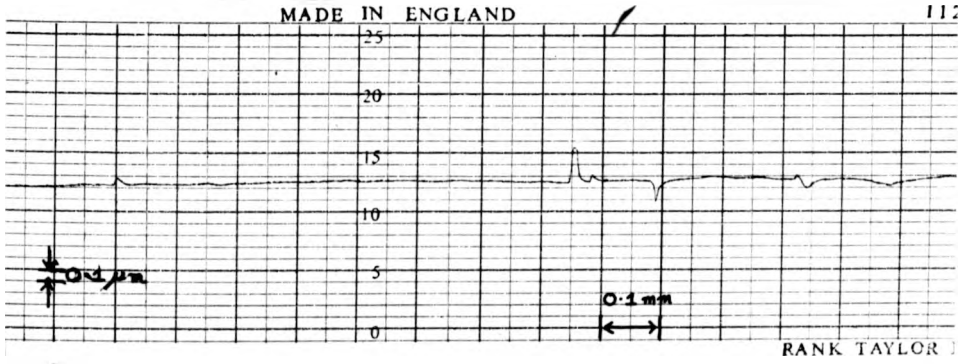

Horizontal Magnification x 100
Vertical Magnification x 20,000

FIGURE 9-3: PHOTOGRAPH AND TALYSURF TRACE OF MECHANICALLY POLISHED COPPER

some polishing marks were visible. The increase in surface resistance could only be attributed to further work-hardening of the surface from polishing. For this reason, an attempt was made to polish a machined surface by electropolishing methods in order to smooth the surface and remove the work-hardened layers.

Electropolishing [71,72,73] is the continued dissolution of a metal in an electrolyte in such a way that surface irregularities are removed. The metal to be polished forms the anode in an electrolytic cell and polishing occurs by the action of chemically complex layers which form on the surface of the anode at certain cell voltages. The composition of the solution used was

Syrupy Orthophosphoric Acid	700 ml
Distilled water	350 ml

The current-voltage characteristics of the cell are shown in figure 9-4. Polishing occurs on the current plateau, most efficient polishing taking place at point B (i.e. cell voltage $\sim$ 2.0 v.). It was found necessary to polish the sample for about 12 hours. Prolonged polishing caused the formation of etch pits, examples of which can be seen in figure 9-5. This process removed the surface roughness but the waviness of the surface was still present (compare figures 9-1 and 9-5). This technique greatly reduced the surface resistance by removing the surface roughness and some of the work-hardened layers.

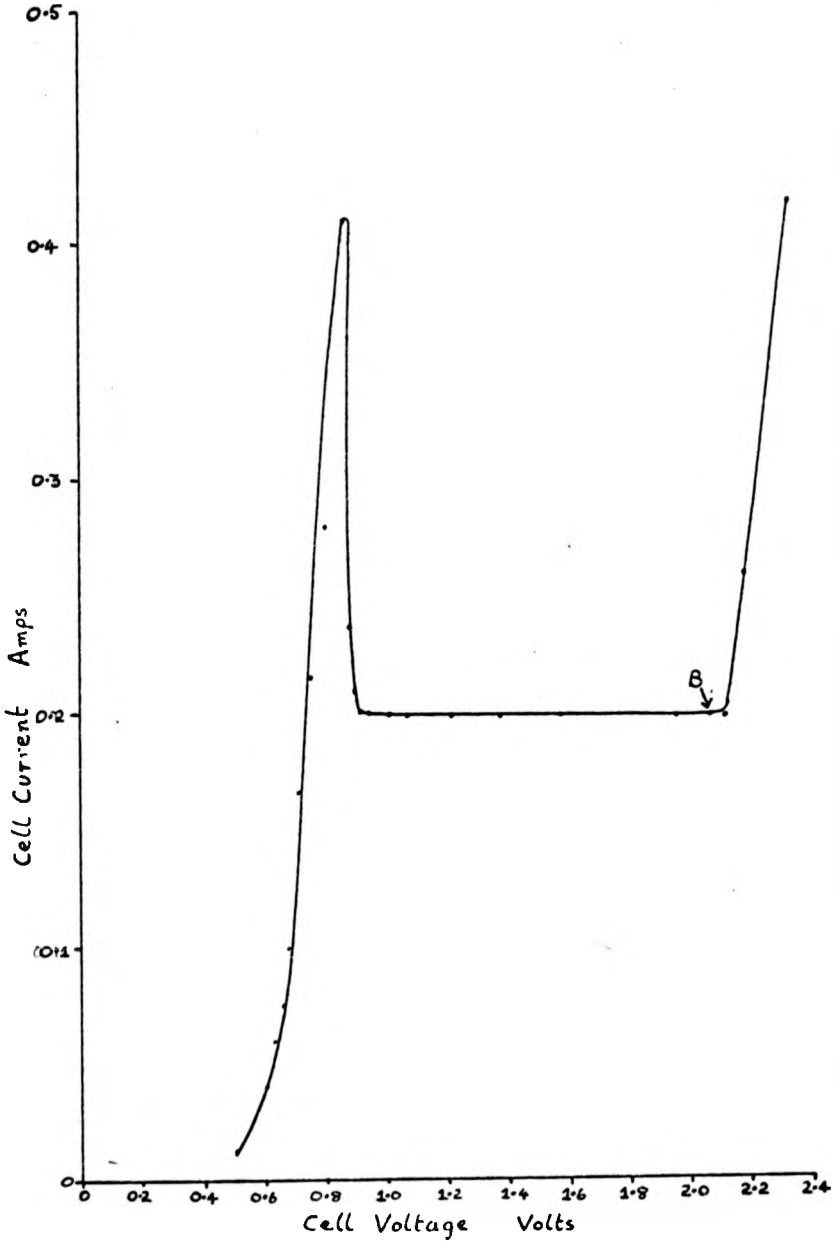

FIGURE 9-4 : CURRENT/VOLTAGE CHARACTERISTIC OF ELECTROPOLISHING CELL

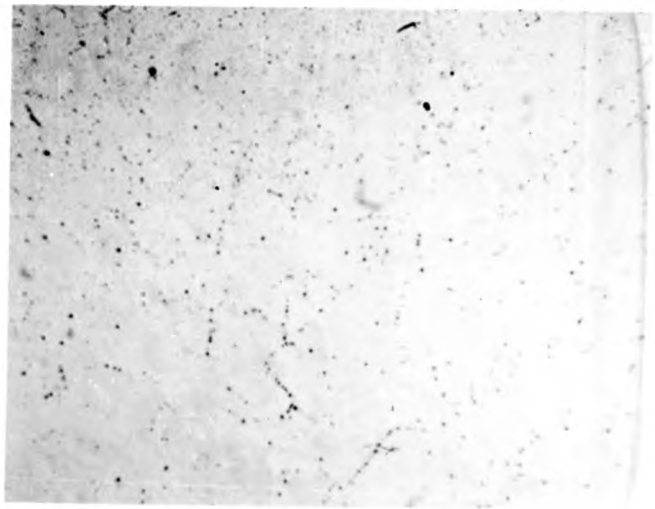

Magnification
X100

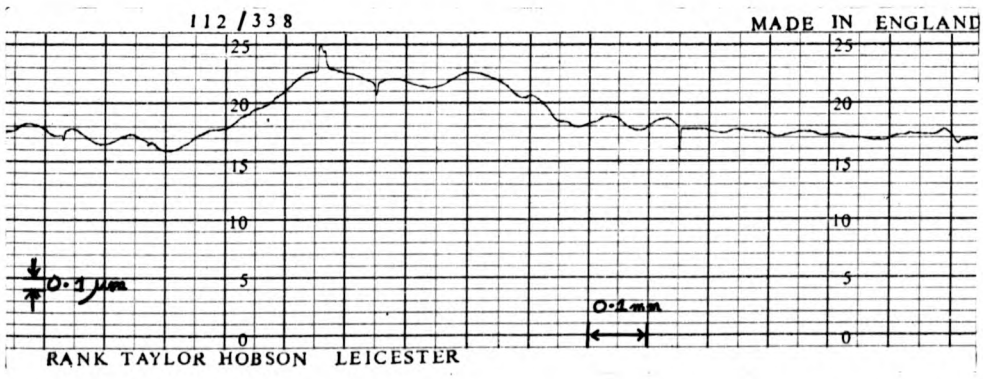

Horizontal Magnification X100
Vertical Magnification X 20,000

FIGURE 9-5 : PHOTOGRAPH AND TALYSURF TRACE OF ELECTROPOLISHED COPPER

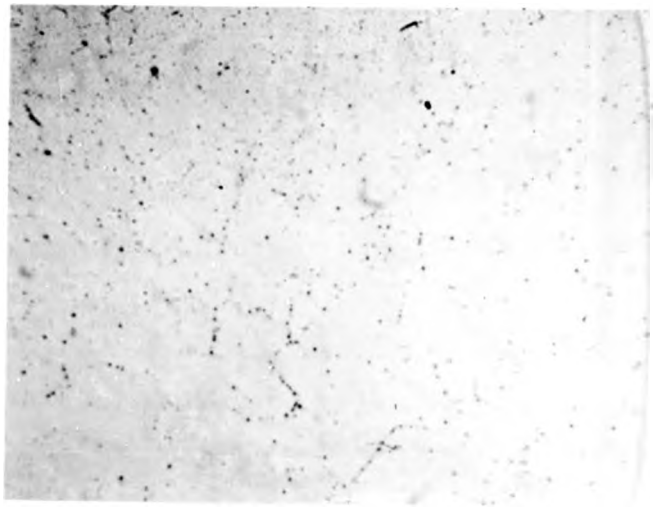

Magnification
×100

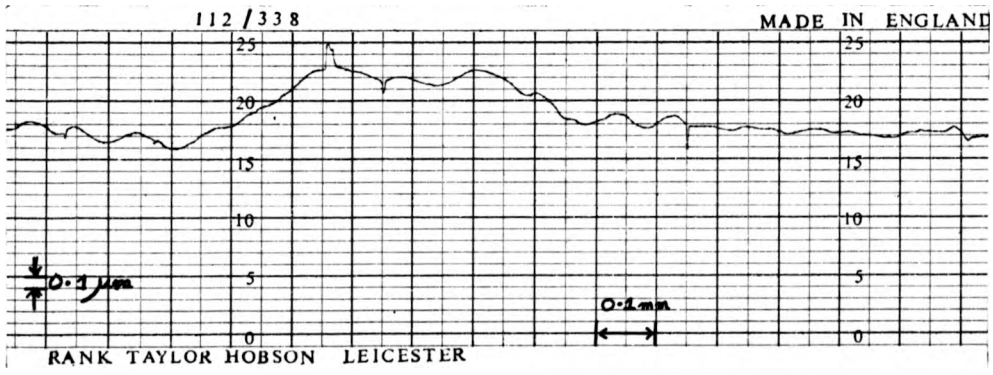

Horizontal Magnification ×100
Vertical Magnification × 20,000

FIGURE 9-5 : PHOTOGRAPH AND TALYSURF TRACE OF ELECTROPOLISHED COPPER

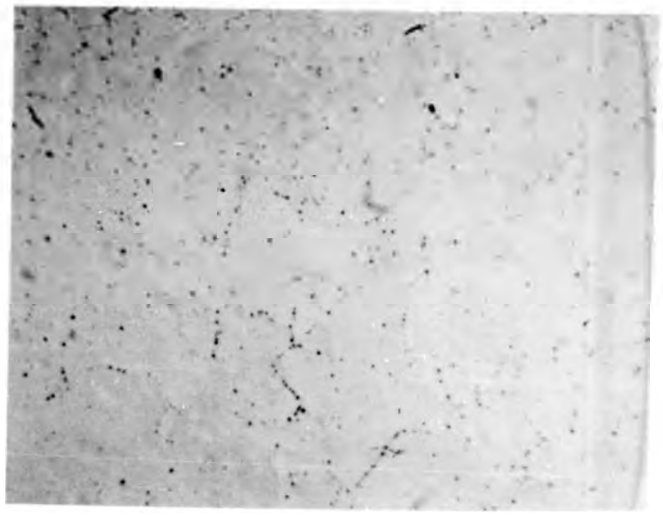

Magnification
x 100

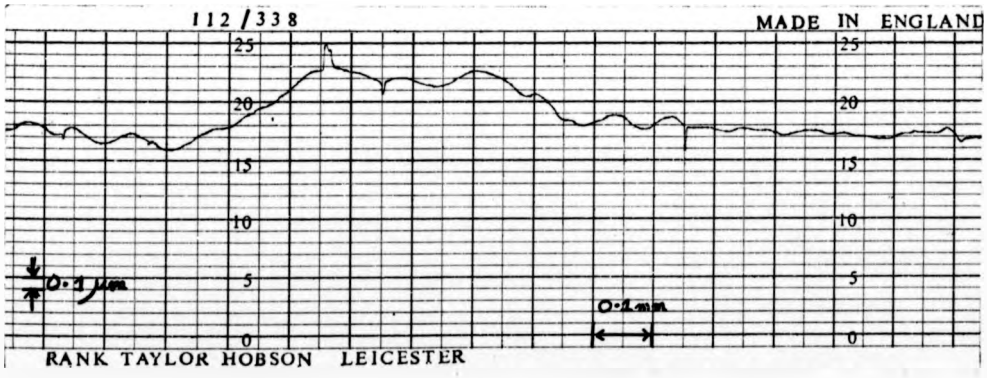

Horizontal Magnification x 100
Vertical Magnification x 20,000

FIGURE 9-5 : PHOTOGRAPH AND TALYSURF TRACE OF ELECTROPOLISHED COPPER

Magnification
×100

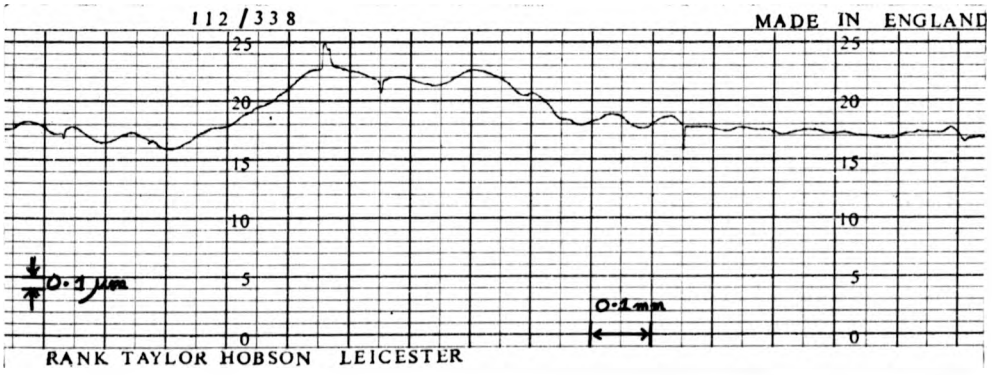

Horizontal Magnification ×100
Vertical Magnification × 20,000

FIGURE 9-5 : PHOTOGRAPH AND TALYSURF TRACE OF ELECTROPOLISHED COPPER

9-2-3 Annealing

No annealing facilities were available for this work. I am therefore grateful to Shell Thornton Research Centre for annealing the samples. The removal of the cold-worked conditions occurs by three successive processes, [69,70] namely recovery, recrystallization and grain growth. Recovery is the re-arrangement of the dislocations introduced by cold-working of the metal to reduce the lattice strain energy. Recrystallization is a nucleation and growth process whereby stress-free grains grow from nuclei in the deformed matrix. Structure-sensitive properties of the material change significantly during this stage. The final stage, grain growth, occurs with extensive annealing when larger grains grow at the expense of small grains.

Annealing was performed at pressures below 10^{-4} Torr. The rf conductivity of the electropolished sample, annealed at 850°C for one hour increased to a value approaching that of the dc standard. The rf conductivity of the machined samples, annealed at 650°C for $2\frac{1}{2}$ hours increased but was significantly lower than that for the electropolished sample. The only explanation for the difference in the results can be the occurrence of varying amounts of grain growth as both sets of annealing conditions should have been sufficient for complete recrystallization of the samples.

Bussey [57], using a similar cavity, measured the conductivity of copper at 10 GHz to be 55.6×10^6 $(\Omega\ m)^{-1}$. His sample was annealed before being subjected to a diamond tool cut and a certain

amount of work-hardening would therefore be present. There would, however, seem to be some agreement between this result and those shown in Table 9-1 for the annealed samples.

9-3 Measurements on Thin Film Samples

The actual surface resistance, R, of a conductor of finite thickness is complicated by the presence of reflections from the back surface of the sample. It can be shown [52] that the surface resistance of such a conductor is given by

$$R = R_s \left[\frac{\sinh (2t/\delta) + \sin (2t/\delta)}{\cosh (2t/\delta) - \cos (2t/\delta)} \right] \quad \ldots\ldots 9\text{-}1$$

where R_s is the surface resistance of an infinitely thick sample

t is the thickness

δ is the skin depth

A full derivation of equation 9-1 may be found in Appendix 5. A plot of R/R_s versus t/δ is given in figure 9-6. It can be seen that for thicknesses greater than three skin depths the surface resistance approaches that for the infinite case. However, it can also be seen that a minimum occurs when $t/\delta = \pi/2$ (~ 1.57). This can be explained by considering the relationship between the current, I_F, on the front surface and the back surface current I_B. If the intrinsic impedance of the film is much less than that of the propagating media on either side, then these quantities are related by (see Appendix 5)

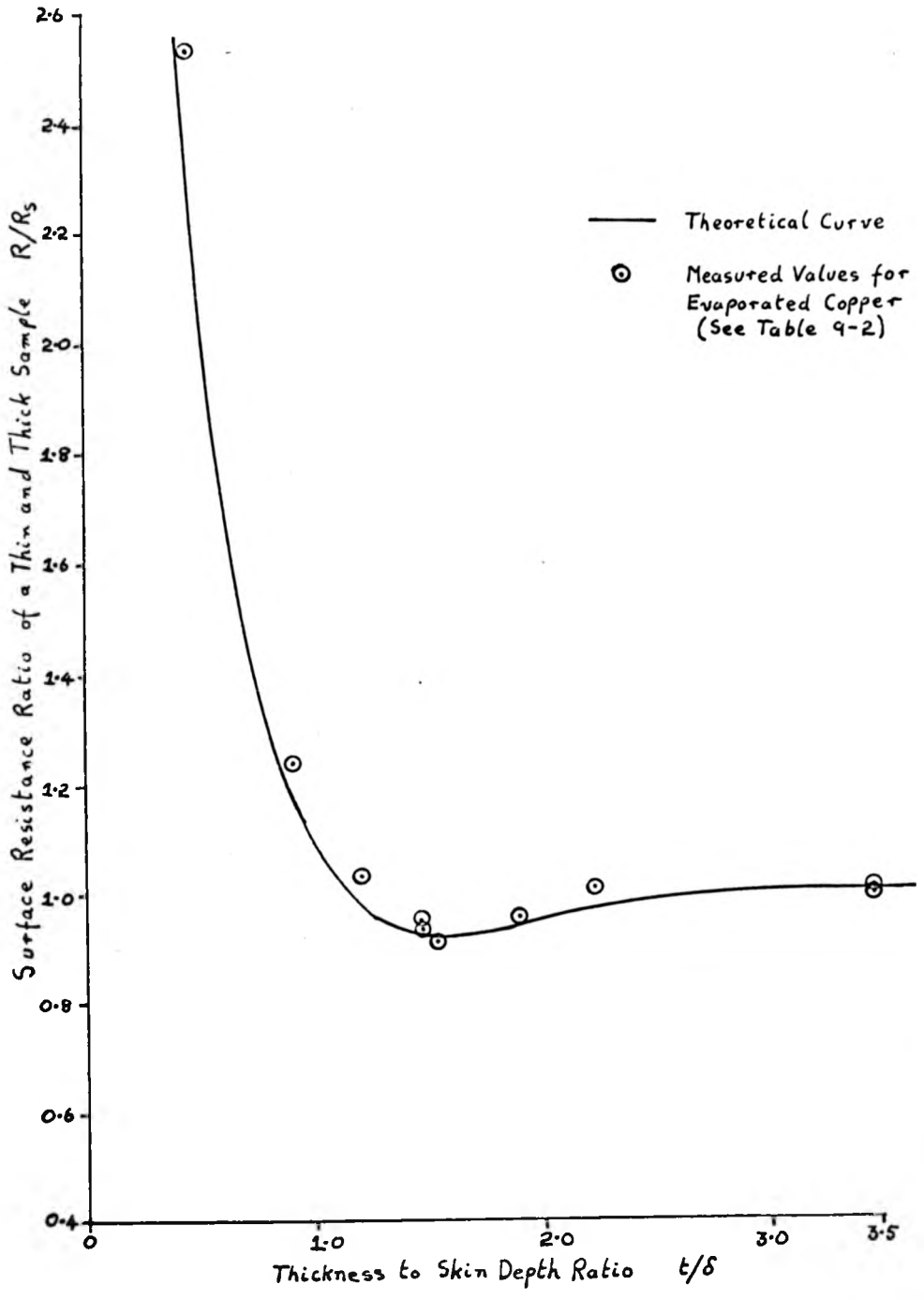

FIGURE 9-6 : GRAPH SHOWING VARIATION OF SURFACE RESISTANCE WITH SAMPLE THICKNESS

$$\frac{I_B}{I_F} = 2\left[e^{(1+j)\frac{t}{\delta}} + e^{-(1+j)\frac{t}{\delta}}\right]^{-1} \quad \ldots\ldots 9\text{-}2$$

This equation approximates to Wheeler's [74] formula for $t \gg \delta$
A polar plot of I_B/I_F versus t/δ is shown in figure 9-7. At $t/\delta = \pi/2$ the current on the back surface lags by 90°. The current produced on the front surface by the reflected wave is therefore 180° out of phase and thus causes a decrease in I_F and the electric field at this surface. The total current, however, must remain constant as the magnetic field at the surface is constant. The surface impedance is by definition

$$Z_z = \frac{E_F}{J_z}$$

where E_F is the electric field at the front surface

J_z is the total current density

As J_z remains constant then a decrease in E_F will cause a reduction in the surface resistance.

9-3-1 Effect of Thickness on the Surface Resistance of Evaporated Copper

As mentioned earlier, the surface resistance measurements were started in order to evaluate the electrode loss of a parallel plate capacitor. For such a capacitor, the bottom electrode must be thin compared to the dielectric thickness in order to prevent breakdown of the capacitor at the edge of the electrode. A similar argument also requires the electrode to be smooth. For

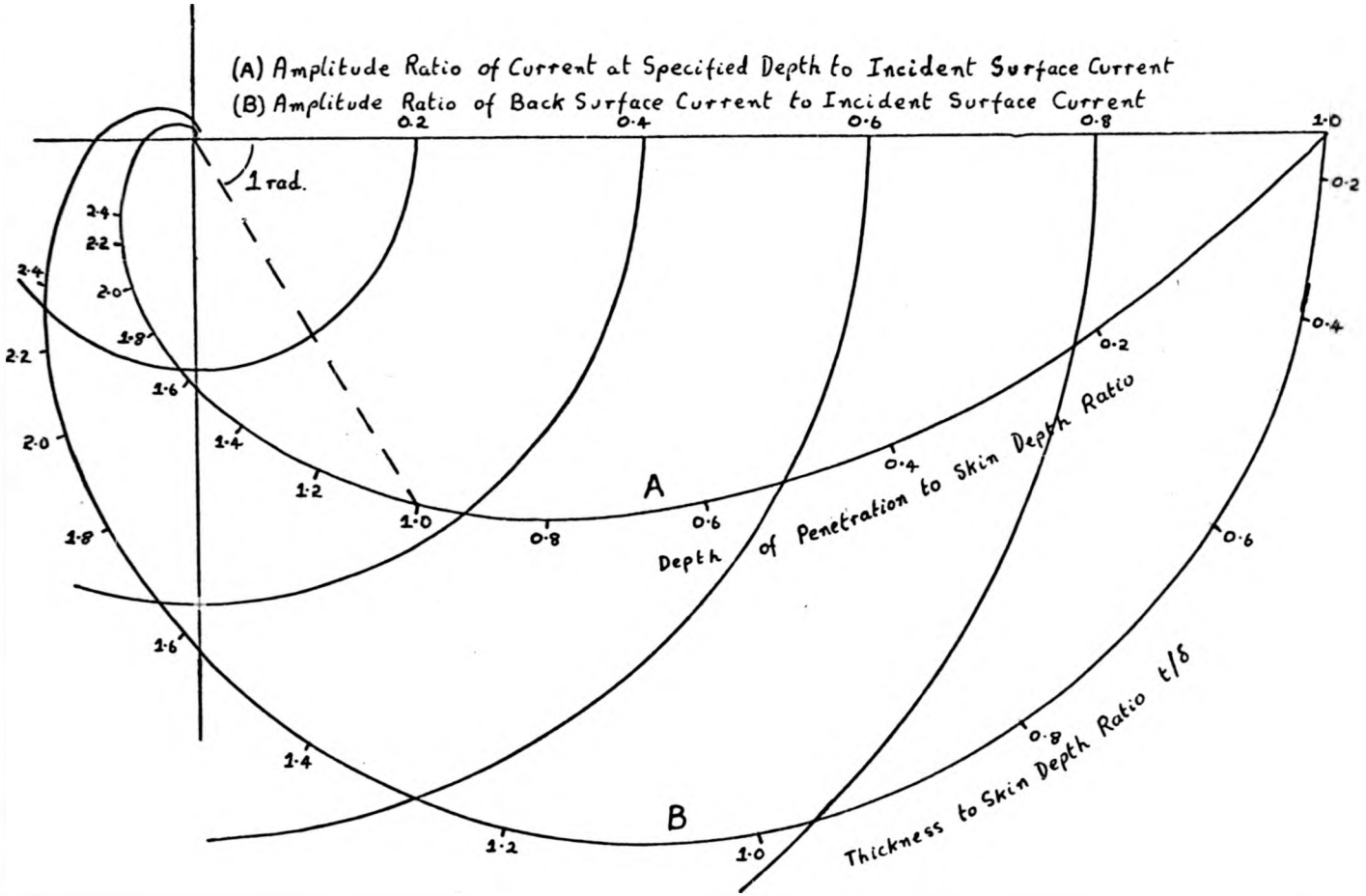

FIGURE 9-7 : (A) POLAR PLOT SHOWING CURRENT VARIATION WITH DEPTH OF PENETRATION IN A CONDUCTOR OF INFINITE THICKNESS

(B) POLAR PLOT SHOWING VARIATION OF BACK SURFACE CURRENT WITH THICKNESS OF A CONDUCTOR

these reasons, evaporated films are usually used for the base electrode . Surface resistance measurements were therefore made on various thicknesses of evaporated copper and the results are shown in Table 9-2. All samples were deposited onto 2in. x 2in. glass photographic plates, as these were readily available, smooth and flat. The dielectric properties of these substrates were unknown, but it was assumed that the intrinsic impedance in the plates was much greater than that in the deposited film. There would thus be negligible wave propagation in the substrate. A 200 Å chromium film was deposited on the substrate before deposition of the copper films. These were deposited under the following conditions.

Initial pump down pressure	=	4×10^{-6} Torr
Deposition pressure	=	2×10^{-5} Torr
Filament current	=	26A
HT Voltage	=	2.7KV
HT Current	=	60 mA
Deposition rate	=	1,980 Å/min.

In order to check that no change in the physical properties of the films occurred dc conductivity and surface finish measurements were made on each sample. The film was etched to give five lines each 3 mm wide. Solder contacts were then made to each line and two probes, placed 4.775 mm apart, used to detect the potential drop along the line, the voltage being measured on a sensitive Hewlett

TABLE 9-2 : SURFACE RESISTANCE OF VARIOUS THICKNESSES OF EVAPORATED COPPER

Thickness (t) (μm)	Centre Line Average (CLA) (μm)	Surface (R) Resistance (OHMS)	RF Conductivity $(\Omega m)^{-1} \times 10^6$	DC Conductivity $(\Omega m)^{-1} \times 10^6$	t/δ	R/R_s
0.32	0.015	0.0724	7.51	48.55	0.44	2.53
0.65	0.012	0.0356	31.06	49.76	0.89	1.24
0.87	0.012	0.0297	44.63	49.23	1.19	1.03
1.07	0.0125	0.0273	52.82	48.04	1.47	0.95
1.07	0.012	0.0267	55.10	49.54	1.47	0.93
1.11	0.013	0.0262	57.35	51.03	1.52	0.92
1.38	0.013	0.0275	52.06	49.63	1.89	0.96
1.62	0.0125	0.0292	46.17	50.18	2.22	1.02
2.52	0.0125	0.0288	47.46	52.37	3.46	1.01
2.52	0.014	0.0286	48.13	51.85	3.46	1.00
3.1 (1)	0.013	0.0286	48.09	51.32	4.26	1.00

(1) This sample used to calculate skin depth, δ , = 0.727 μm.

Packard voltmeter type 3420A. The calculation is given by

$$\sigma_{dc} = \frac{4.775 \times 10^{-3} \times I}{W \; t \; V} \qquad \ldots\ldots 9\text{-}3$$

where I is the current

W is the width of the line

t is the film thickness

V is the voltage between the probes

σ_{dc} is the DC conductivity of the sample

3 mm. wide lines were used in order to eliminate any effect from undercutting. The errors in the measurements are listed below.

Avo current reading	= ± 1% of full scale
Hewlett Packard Voltmeter reading	= ± 3% of full scale
Line width	= ± 0.01 mm. i.e. ~ 0.3%
Thickness	= ± 4% of full scale

Five measurements made on each sample yielded a typical standard deviation of the mean of ± 3%. The dc conductivity and CLA values given in Table 9-2 indicate that any variation in the measured surface resistance is unlikely to be caused by variation of these parameters.

The surface resitance of the 3.1 μm thick sample was taken to represent the "bulk" value (i.e. R_s in equation 9-1) and the

corresponding skin depth was calculated. A plot of the ratio of the measured surface resistance to R_s versus the thickness to skin depth ratio was made, the points being shown in figure 9-6. It can be seen that the measured and theoretical results are in good agreement.

9-3-2 Factorial Experiments on Acid Copper Plating Solutions

The microwave group at the University has for some time used acid copper plating solutions. It was therefore decided to investigate the effect of the plating conditions and the composition of the plating solution on the surface resistance of the films obtained. Factorially designed experiments (Chapter 4) were performed to study the effect of current density (J), temperature (T), stirring rate (S) and chemical composition (C). Suggested composition and operating conditions for an acid solution are (75)

Copper sulphate ($CuSO_4\ 5H_2O$)	162 - 206 g./litre
Sulphuric Acid (84%)	25 - 62 g./litre
Current Density	20 - 100 mA/cm^2
Temperature ^oC	21 - 48
Agitation -	Cathode and/or air-blowing

For the present investigation, two solutions, C_1 and C_2 were used with the following composition

	C_1	C_2
Copper Sulphate g.	200	165
Sulphuric Acid (84%) g.	30	62
Deionized Water	to 1 litre	to 1 litre

The plating conditions used were

	Low Value	High Value
Current Density	$20mA/cm^2$	$40mA/cm^2$
Temperature	20^oC	40^oC
Stirring rate (5cm magnetic stirrer)	60 rpm	130 rpm

Sixteen experiments are required to investigate the four parameters. Table 9-3 outlines the experiments with the usual notation of lower case letters corresponding to the treatment combination the letter "c" indicating composition C_2. Duplicate measurements were made of eight treatments in order to obtain an estimate of the error involved. After calculation of the main effects and interactions, each effect was analysed by use of the t-test (see Appendix 2). Again, dc conductivity and CLA measurements were made, the results of which were examined in relation to the surface resistance measurements.

The results of surface resistance, dc conductivity and CLA measurements are given in Table 9-4, 9-5 and 9-6. The most outstanding effect on surface resistance is that of chemical composition, solution C_2 giving deposits of a lower surface resistance than did C_1. This parameter also has a significant effect on the surface finish (Table 9-5), C_2 giving a smoother surface. Another highly

TABLE 9-3 : EXPERIMENTAL DESIGN FOR PLATING EXPERIMENTS

			COMPOSITION (C)			
			C_1		C_2	
			Stirring Rate (S) rpm			
			60	130	60	130
TEMPERATURE (T) °C	20	Current Density (J) mA/cm^2 20	x	s	c (1)	sc
		40	j	js	jc	jsc
	40	20	t	st	tc	stc
		40	jt	jst	jtc	jstc

(1) "c" Denotes composition C_2.

TABLE 9-4 : EFFECT OF PLATING PARAMETERS ON SURFACE RESISTANCE

Treatment	Surface Resistance (OHMS)		Mean (OHMS)	Main Effect	t	Significance	Effect Symbol
x	0.0313	0.0315	0.0314				
j	0.0309	0.0312	0.03105	-4.687×10^{-4}	4.64	0.2%	J
s	0.0323	0.0326	0.03245	3.125×10^{-5}	0.31		S
js	0.0311	0.0313	0.0312	1.563×10^{-4}	1.55		JS
t	0.0333	0.0338	0.03355	7.813×10^{-4}	7.74	< 0.1%	T
jt	0.0318	0.0322	0.0320	-4.375×10^{-5}	0.43		JT
st	0.0325	0.0329	0.0327	-2.437×10^{-4}	2.41	4%	ST
jst	0.0323	0.0327	0.0325	1.563×10^{-4}	1.55		JST
c	0.0311		0.0311	-1.081×10^{-3}	10.10	< 0.1%	C
jc	0.0306		0.0306	3.687×10^{-4}	3.65	0.4%	JC
sc	0.0306		0.0306	-1.813×10^{-4}	1.79		SC
jsc	0.0310		0.0310	4.375×10^{-5}	0.43		JSC
tc	0.0314		0.0314	-3.813×10^{-4}	3.77	0.4%	TC
jtc	0.0313		0.0313	-6.25×10^{-6}	0.06		JTC
stc	0.0312		0.0312	1.438×10^{-4}	1.42		STC
jstc	0.0310		0.0310	-4.063×10^{-4}	4.02		JSTC

Standard deviation of a single result = 2.48×10^{-4} OHMS

Standard error for all effects except C = 1.01×10^{-4}

Standard error for effect C = 1.07×10^{-4}

No. of degrees of freedom of standard error = 8

$t = \frac{\text{Main effect}}{\text{Standard Error}}$ (see Appendix 2)

TABLE 9-5 : EFFECT OF PLATING PARAMETERS ON DC CONDUCTIVITY

Treatment	DC Conductivity $(\Omega_m)^{-1} \times 10^6$		Mean $(\Omega_m)^{-1} \times 10^6$	Main Effect $\times 10^6$	t	Significance	Effect Symbol
x	49.58	49.54	49.56	.	.		
j	50.27	50.99	50.63	0.412	1.32		J
s	47.36	47.42	47.39	-0.582	1.87	10%	S
js	49.02	50.22	49.62	0.44	1.42		JS
t	49.88	49.90	49.89	-0.769	2.48	4%	T
jt	49.12	47.06	48.09	0.552	1.81		JT
st	48.82	47.15	47.985	0.0731	0.24		ST
jst	47.36	48.06	47.71	0.6695	2.16	6%	JST
c	49.11		49.11	-0.393	1.18		C
jc	48.21		48.21	0.101	0.32		JC
sc	50.42		50.42	0.779	2.52	4%	SC
jsc	47.44		47.44	-0.232	0.74		JSC
tc	47.33		47.33	0.116	0.39		TC
jtc	48.83		48.83	1.90	6.13	< 0.1%	JTC
stc	45.99		45.99	-0.145	0.48		STC
jstc	50.42		50.42	-0.583	1.87	10%	JSTC

Standard deviation of a single result = 0.77×10^6 $(\Omega_m)^{-1}$ Degrees of freedom = 8

Standard error for all effects except C = 0.31×10^6

Standard error for effect C = 0.33×10^6

TABLE 9-6 : EFFECT OF PLATING PARAMETERS ON SURFACE FINISH

Treatment	Centre Line Average (μm)		Mean (μm)	Main Effect	t	Significance	Effect Symbol
x	0.275	0.250	0.2625				
j	0.220	0.200	0.2100	-1.781×10^{-2}	2.58	4%	J
s	0.190	0.200	0.1950	9.375×10^{-4}	0.14		S
js	0.250	0.250	0.2500	2.031×10^{-2}	2.94	2%	JS
t	0.300	0.310	0.3050	7.468×10^{-2}	10.82	< 0.1%	T
jt	0.250	0.280	0.2650	-5.093×10^{-2}	7.38	< 0.1%	JT
st	0.480	0.440	0.4600	7.812×10^{-3}	1.13		ST
jst	0.350	0.320	0.3350	-1.406×10^{-2}	2.04	6%	JST
c	0.225		0.225	-1.656×10^{-2}	2.27	5%	C
jc	0.275		0.275	2.281×10^{-2}	3.31	0.5%	JC
sc	0.210		0.210	-4.843×10^{-2}	7.02	< 0.1%	SC
jsc	0.290		0.290	1.468×10^{-2}	2.13	6%	JSC
tc	0.390		0.390	-3.718×10^{-2}	5.38	0.1%	TC
jtc	0.280		0.280	-9.062×10^{-3}	1.31		JTC
stc	0.240		0.240	-5.531×10^{-2}	8.02	< 0.1%	STC
jstc	0.240		0.240	3.406×10^{-2}	4.93	0.1%	JSTC

Standard deviation of a single result = 1.7×10^{-2} μm

Standard error for all effects except C = 0.69×10^{-2} μm

Standard error for effect C = 0.73×10^{-2}

Number of degrees of freedom = 8

significant parameter is temperature, an increase in temperature always causing an increase in the surface resistance. This can be explained in terms of the dc conductivity and CLA results; from Tables 9-5 and 9-6 it can be seen that an increase in temperature results in an increase in the surface roughness and a decrease in the conductivity. The significance of the first order interaction TC, however, does indicate that the effect of temperature is not the same for both solutions. Calculation of the main effect, T, for the individual solutions shows that the effect for solution C_2 is only one third of that for solution C_1. This interaction is also present in the CLA results, the effect of temperature on solution C_2 being approximately half that for solution C_1. Increasing the current density in general decreases the surface resistance and the surface roughness. Again, this parameter interacts with the solution composition as indicated by interaction JC. Examination of the effect of current density on each solution shows that current density has a negligible effect on the surface resistance and CLA for solution C_2, but for solution C_1, increasing the current density decreases the CLA and surface resistance. It can also be seen that interaction JSTC is also significant in the surface resistance and CLA results. As there are many significant effects and interactions for the surface roughness measurements, it is likely that this interaction is significant and is not caused by accumulation of errors. This interaction signifies that all the experimental parameters do interact with each other, which is not a surprising result for electroplating.

significant parameter is temperature, an increase in temperature always causing an increase in the surface resistance. This can be explained in terms of the dc conductivity and CLA results; from Tables 9-5 and 9-6 it can be seen that an increase in temperature results in an increase in the surface roughness and a decrease in the conductivity. The significance of the first order interaction TC, however, does indicate that the effect of temperature is not the same for both solutions. Calculation of the main effect, T, for the individual solutions shows that the effect for solution C_2 is only one third of that for solution C_1. This interaction is also present in the CLA results, the effect of temperature on solution C_2 being approximately half that for solution C_1. Increasing the current density in general decreases the surface resistance and the surface roughness. Again, this parameter interacts with the solution composition as indicated by interaction JC. Examination of the effect of current density on each solution shows that current density has a negligible effect on the surface resistance and CLA for solution C_2, but for solution C_1, increasing the current density decreases the CLA and surface resistance. It can also be seen that interaction JSTC is also significant in the surface resistance and CLA results. As there are many significant effects and interactions for the surface roughness measurements, it is likely that this interaction is significant and is not caused by accumulation of errors. This interaction signifies that all the experimental parameters do interact with each other, which is not a surprising result for electroplating.

It is possible to predict the best treatment to give the lowest surface resistance by considering the CLA and dc conductivity results only. For example, for solution C_1 the best conductivity is obtained for treatment j, which also gives a good surface finish. Treatment S gives a slightly better surface but a much worse conductivity. It is therefore likely that treatment j would give the best surface resistance result for this solution. This in fact is the case. Similarly for solution C_2, combination so would give the best result.

It is obvious from the results that the most sensitive charactor-istic of the film is surface finish. No further work to determine the optimum solution and operating parameters was done as it was thought that commercially available solutions might well give better results.

9-3-3 Surface Resistance Measurements of Commercial Plating Solutions

The plating solutions tested are given below:

Solution	Supplier
Gold Transtherm	P.M.D. Chemicals Ltd., Coventry
Argonant Bright Silver	P.M.D. Chemicals Ltd., Coventry
Bright acid copper	Hockley Chemicals Ltd., Birmingham
Copper Pyrophosphate	G.E.C.
Engelhardt E56	Samples provided by Microwave Associates Ltd.

The recommended conditions for use of those mixtures together with the actual conditions of use are given in Table 9-7. For the bright acid solution, the cell voltage was found to have a greater effect on the brightness than the current density, a cell voltage of 1 to 2 volts yielding a bright deposit. It was also found that at room temperature the solution gave a brighter film than that obtained from a heated solution. The concentrations of copper sulphate and sulphuric acid were the same as for solution C_2 given in section 9-3-2. The conditions for the pyrophosphate solution are extremely critical [76] the pH of the solution having to be continually monitored and controlled. Initial films deposited from this solution had good brightness and conductivity but the solution was soon found to deteriorate. Moderate air agitation provided by a peristaltic pump was used for all solutions except silver where re-circulation was used because air agitation caused vigorous frothing.

A 0.2 μm thick copper base layer was evaporated onto the substrate prior to plating. Two films were deposited from each solution and their surface resistance and surface finish measured. The dc conductivity of one of the films was then measured and the other film was heat treated at 250°C for two hours in vacuo (below 10^{-4} Torr). The surface resistance and conductivity of the annealed film were then measured. The results are given in Table 9-8. Also listed are the results obtained for evaporated samples of copper and gold.

The recommended conditions for use of these mixtures together with the actual conditions of use are given in Table 9-7. For the bright acid solution, the cell voltage was found to have a greater effect on the brightness than the current density, a cell voltage of 1 to 2 volts yielding a bright deposit. It was also found that at room temperature the solution gave a brighter film than that obtained from a heated solution. The concentrations of copper sulphate and sulphuric acid were the same as for solution C_2 given in section 9-3-2. The conditions for the pyrophosphate solution are extremely critical [76] the pH of the solution having to be continually monitored and controlled. Initial films deposited from this solution had good brightness and conductivity but the solution was soon found to deteriorate. Moderate air agitation provided by a peristaltic pump was used for all solutions except silver where re-circulation was used because air agitation caused vigorous frothing.

A 0.2 μm thick copper base layer was evaporated onto the substrate prior to plating. Two films were deposited from each solution and their surface resistance and surface finish measured. The dc conductivity of one of the films was then measured and the other film was heat treated at 250°C for two hours in vacuo (below 10^{-4} Torr). The surface resistance and conductivity of the annealed film were then measured. The results are given in Table 9-8. Also listed are the results obtained for evaporated samples of copper and gold.

TABLE 9-7 : CONDITIONS FOR USE OF COMMERCIAL PLATING SOLUTIONS

Solution	Deposition Parameter	Recommended Operating Conditions	Operating Conditions Used	Deposition Rate μm/min.
Acid Copper	Current Density (mA/cm^2)	20 - 100	20	0.35
	Temperature ^{o}C	21 - 48	18	
	Agitation	Air or Cathode	Air	
	Anode	High Purity Copper	High Purity Copper	
Bright Acid Copper	Current Density (mA/cm^2)	21 - 109	50	0.40
	Cell Voltage	2 - 4	1.4	
	Temperature ^{o}C	24 - 35	18	
	Agitation	Air	Air	
	Anode	High Purity Copper	High Purity Copper	
Copper Pyrophosphate	Current Density (mA/cm^2)	22	22	0.30
	Temperature ^{o}C	52	52	
	Agitation	Air	Air	
PMD Gold (Cyanide Solution)	Current Density (mA/cm^2)	1 - 5	1.1	0.08
	Temperature ^{o}C	60 - 70	65	
	Agitation	Air or Re-circulation	Air	
	Anode	Stainless Steel, Platinum or Platinised Titanium	Stainless Steel	
PMD Silver (Cyanide Solution)	Current Density (mA/cm^2)	40	5	0.33
	Temperature ^{o}C	20 - 50	30	
	Agitation	Moderate to Vigorous	Re-circulation	
	Anode	Silver	Silver	

TABLE 9-8: Measurements on metal films at d.c. amd 10 GHz

Deposition Method	Thickness (μm)	Surface resistance (ohms)		Microwave Conductivity $(\Omega m)^{-1}$		DC Conductivity $(\Omega m)^{-1}$		CLA (μm)	Theoretical DC Conductivity $(\Omega m)^{-1}$	Measured/Theoretical DC Conductivity (%)		Measured/Theoretical Microwave Conductivity (%)	
			annealed		annealed		annealed				annealed		annealed
		$\times 10^{-2}$	$\times 10^{-2}$	$\times 10^{6}$	$\times 10^{6}$	$\times 10^{6}$	$\times 10^{6}$		$\times 10^{6}$				
P.M.D. gold	5.1	3.38		34.5		36.9		0.07	41.0	90		84.1	
	4.6	3.38	3.28	34.5	36.6		40.4	0.07			98.6	84.1	89.3
Englehardt E56 gold	2.4	3.34		35.2		38.1		0.03	41.0	92.9		86.0	
	2.4	3.33		35.3		37.6		0.03	41.0	91.8		86.2	
Evaporated gold	2.5	3.48		32.5		34.8		0.02	41.0	84.9		79.3	
P.M.D. silver	3.3	3.03		43.3		47.8		0.05	62.9	76.0		68.9	
	3.3	3.00	2.91	43.7	46.5		52.0	0.07			82.6	69.5	73.9
Acid copper	3.5	2.98		44.2		49.7		0.05	58.0	84.6		76.2	
	3.5	2.99	2.96	44.0	44.9		50.5	0.04			87.1	75.9	77.5
Bright acid copper	3.2	2.91		46.6		52.7		0.03	58.0	90.8		80.4	
	3.2	2.90	2.84	46.8	48.8		53.0	0.03			91.3	80.7	84.2
Copper pyrophosphate													
Best result	4.5	2.89		47.1		47.2		0.03	58.0	81.4		81.2	
Worst result	4.8	3.05		42.3		45.4		0.04	58.0	78.4		73.0	
	4.8	3.05	3.03	42.3	42.9		46.0	0.04	58.0		78.3	73.0	73.9
Evaporated copper	3.1	2.86		48.1		52.1		0.01	58.0	89.9		82.9	

Annealing of the samples resulted in a decrease in the surface resistance and an increase in the dc conductivity; this being more noticeable for the silver and gold films deposited from cyanide baths. The effect of the heat treatment on the copper films was generally small.

The best copper film from the pyrophosphate solution showed remarkably good agreement between the rf and dc conductivity measurements. For the other films, the rf conductivities were between 89% and 94% of the measured dc conductivities. This lack of agreement cannot be explained in terms of surface finish because similar discrepancies occurred for the evaporated films which had excellent surface smoothness. The low values of dc conductivity obtained are probably due to impurities in the film drawn out from the solution during the deposition. Raub and Müller [77] state that impurities co-deposited with the metal greatly inhibit the crystal growth in a direction parallel to the substrate surface. This is particularly noticeable with bright solutions. Preferential growth therefore takes place in the direction of current flow (i.e. perpendicular to substrate) yielding a columnar structure. This type of film will therefore exhibit anisotropic conductivity, the conductivity perpendicular to the substrate being higher than in the parallel direction. As both the dc and rf measurements were made with the current flow parallel to the film this could account for the low conductivity values obtained.

Annealing of the samples resulted in a decrease in the surface resistance and an increase in the dc conductivity; this being more noticeable for the silver and gold films deposited from cyanide baths. The effect of the heat treatment on the copper films was generally small.

The best copper film from the pyrophosphate solution showed remarkably good agreement between the rf and dc conductivity measurements. For the other films, the rf conductivities were between 89% and 94% of the measured dc conductivities. This lack of agreement cannot be explained in terms of surface finish because similar discrepancies occurred for the evaporated films which had excellent surface smoothness. The low values of dc conductivity obtained are probably due to impurities in the film drawn out from the solution during the deposition. Raub and Müller [77] state that impurities co-deposited with the metal greatly inhibit the crystal growth in a direction parallel to the substrate surface. This is particularly noticeable with bright solutions. Preferential growth therefore takes place in the direction of current flow (i.e. perpendicular to substrate) yielding a columnar structure. This type of film will therefore exhibit anisotropic conductivity, the conductivity perpendicular to the substrate being higher than in the parallel direction. As both the dc and rf measurements were made with the current flow parallel to the film this could account for the low conductivity values obtained.

All films were examined under a Scanning Electron Microscope (SEM). Figure 9-8 compares the surface obtained from an acid solution with one containing the various brightness and levellers. Clearly the bright acid solution gives a far superior finish. The surface of evaporated and PMD plated gold are shown in figure 9-9. The presence of the "blobs" on the evaporated film is not fully understood but could be possibly due to "spitting" from the electron gun source.

From these results, the following conclusions have been drawn.

a) Owing to the sensitivity of the pyrophosphate solution to the deposition conditions it is concluded that a bright acid solution is preferable because it yields a low surface resistance and is easier to control. Although heat-treatment of the film does improve the surface resistance, for general use it is thought that this extra process is not worthwhile. Copper films must be protected from oxidation by a gold flash. A 150 Å gold flash does not give a detectable change in the surface resistance.

b) Where gold has to be used e.g. for bonding, the Engelhardt E56 solution is preferable to the PMD solution, not because of any real difference in the film properties but merely because it can be used to deposit films at a faster rate. Only the PMD films (both silver and gold) were examined for the effects of heat treatment; this resulted in a conductivity gain of about 7% in each case.

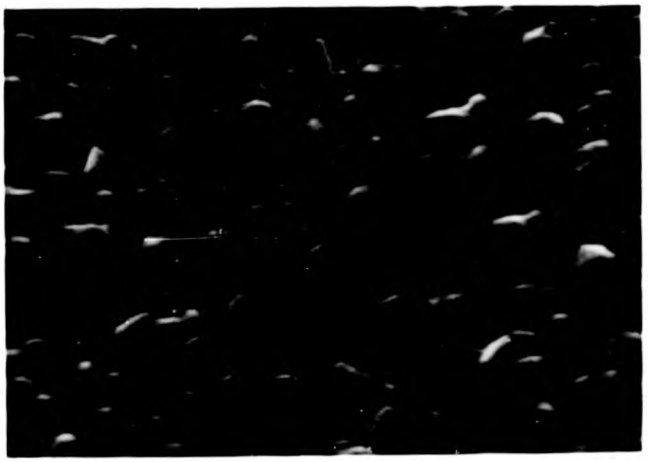

Magnification
x 5,000

2 μm

Deposit from Acid Copper Solution

Magnification
x 5,000

2 μm

Deposit from Bright Acid Copper Solution

FIGURE 9-8 : SEM PHOTOGRAPHS OF PLATED COPPER FILMS

Magnification
X 5,000

2 μm

Evaporated Gold Film

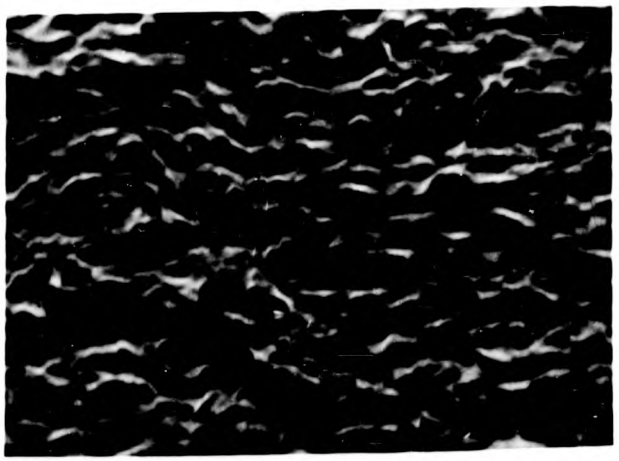

Magnification
X 5,000

2 μm

Deposit from PMD Gold Solution

FIGURE 9-9 : SEM PHOTOGRAPHS OF PLATED AND EVAPORATED GOLD FILMS

9-4 Comments

The cavity has been used successfully to determine surface resistance of both bulk and thin film materials. Factorial design appears to be a very useful technique in determining the best operating conditions for plating baths. It is thought that a similar design applied to the bright acid plating bath could indicate better conditions of operation which would result in improved surface resistance. Time did not allow this to be performed.

Chapter 10

THE EFFECTS OF THE SPUTTERING PARAMETERS ON THE DEPOSITION RATE AND MICROWAVE DIELECTRIC PROPERTIES OF SILICON DIOXIDE FILMS

10-1 Introduction

The effects of the deposition conditions on dielectric film properties at low frequencies have been reported for both sputtered [24] and evaporated [46] films. For evaporated silicon dioxide films, it is now generally accepted that a low deposition rate ($\sim$120Å /min.) is required to produce low loss films. In sputtering, however, there are many different parameters which can influence the deposition rate, as has already been demonstrated (Chapter 3). Vosson [24] measured at 1KHz the dielectric properties of sputtered silicon dioxide prepared using differing deposition rates. He reported an abrupt increase in the dielectric loss and permittivity for deposition rates in excess of 200Å/min. The means of varying the deposition rate was not reported. Such studies are usually performed using the classical experimental approach (Chapter 4) i.e. each parameter to be investigated is varied separately. This technique ignores the existence of any interactions between the parameters. A series of factorially designed experiments has been performed to study the effects of three sputtering parameters on the deposition rate, permittivity and dielectric loss and to observe the effects of interactions between the parameters that might exist.

Much of the work reported in the preceeding chapters has been

directed towards the evaluation of dielectric properties by capacitor measurements. Unforunately, the method of measuring the capacitor properties had not been fully developed by this time. It was therefore decided to return to the cavity technique described in section 5-3. The main disadvantage of this method was the difficulty of obtaining an accurate film thickness measurement; it was found necessary to spend some time in overcoming this problem.

10-2 Accurate Measurement of the Film Thickness Deposited on the Co-Axial Cavity

The original arrangement for masking of the cavity during the deposition is shown in figure 5-2. The failure of this method to provide an accurate thickness measurement was thought to be due to differences in the surface temperatures of the glass slide and the cavity. Further evidence for this was obtained using DC input powers in the region of 500 watts. Under these conditions, the glass slide occasionally cracked and the part of the PTFE sleeve exposed to the discharge became discoloured. A further explanation could be differences in the nucleation and growth rates of the films deposited onto the glass slide and the silver plated cavity surface.

An alternative masking arrangement (figure 10-1) was examined. The glass slide was replaced by a metal disc in such a manner that no PTFE surfaces were exposed to the discharge. The disc was silver plated and highly polished to minimize differences in the nucleation and growth rates.

Intimate contact between the cavity and masking disc was not permissible for fear of damaging the cavity surface during assembly; as a result, the surface temperatures of disc and cavity would not be the same. It followed, therefore, that although measurements of permittivity were more consistent than those found using the original arrangement, the basic problem of surface temperature differences still remained.

It was realised that accurate results could be obtained only if the thickness of the actual film deposited onto the cavity could be measured. This required measurement of the step produced by etching a portion of the deposited film. It was found that a modified P-etch solution worked satisfactorily. The mixture used consisted of:

20 volumes hydrofluoric acid (40%)

10 volumes nitric acid (concentrated)

300 volumes distilled water

Lacomite (a commercially available lacquer which withstands both acids and alkalis) was used to protect the required area of film. Only the minimum amount of silver plating was exposed to the etchant (figure 10-2). This method worked well and caused no measureable attack on the silver plating. An etching time of 20 minutes sufficedfor the complete removal of a film of 2 μm thickness. The use of buffered hydrofluoric acid solutions should be avoided because Mehmet [7] found them to attack silver surfaces.

Values of permittivity and loss tangent calculated using thickness measurements made in the manner described were found to be very repoducible.

Intimate contact between the cavity and masking disc was not permissible for fear of damaging the cavity surface during assembly; as a result, the surface temperatures of disc and cavity would not be the same. It followed, therefore, that although measurements of permittivity were more consistent than those found using the original arrangement, the basic problem of surface temperature differences still remained.

It was realised that accurate results could be obtained only if the thickness of the actual film deposited onto the cavity could be measured. This required measurement of the step produced by etching a portion of the deposited film. It was found that a modified P-etch solution worked satisfactorily. The mixture used consisted of:

20 volumes hydrofluoric acid (40%)

10 volumes nitric acid (concentrated)

300 volumes distilled water

Lacomite (a commercially available lacquer which withstands both acids and alkalis) was used to protect the required area of film. Only the minimum amount of silver plating was exposed to the etchant (figure 10-2). This method worked well and caused no measureable attack on the silver plating. An etching time of 20 minutes sufficedfor the complete removal of a film of 2 μm thickness. The use of buffered hydrofluoric acid solutions should be avoided because Mehmet [7] found them to attack silver surfaces.

Values of permittivity and loss tangent calculated using thickness measurements made in the manner described were found to be very repoducible.

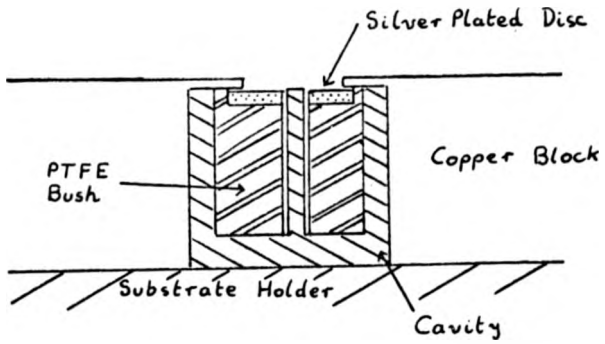

FIGURE 10-1 : ALTERNATIVE MASKING ARRANGEMENT OF THE CAVITY FOR DEPOSITION OF DIELECTRIC FILMS

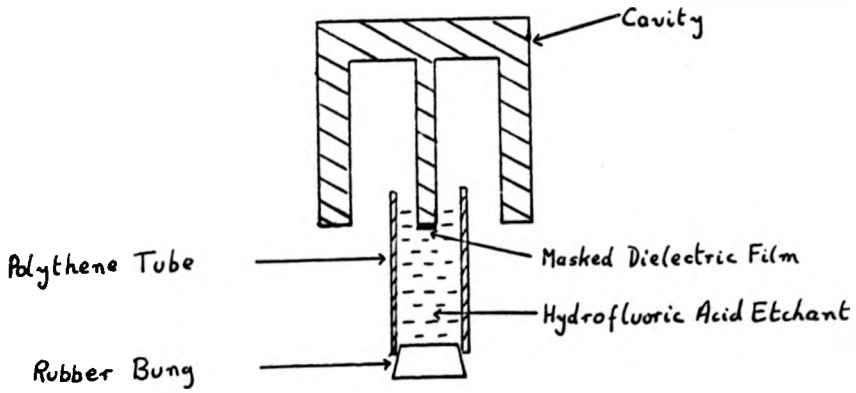

FIGURE 10-2 : ETCHING ARRANGEMENT FOR DIELECTRIC FILM THICKNESS MEASUREMENT

10-3 Design of Experiments

The sputtering parameters thought to be of greatest importance were RF power to the discharge, sputtering pressure and magnetic field strength. However, the sputtering equipment described in Chapter 3 had only facilities built in for the measurement of DC power input to the oscillator and so DC power was monitored as a parameter related to RF power.

Table 10-1 shows the experimental design together with the values of the parameters used. The usual treatment notation is used viz. the presence of a lower case letter indicating the high level of a parameter.

Time did not allow duplication of the treatments to be performed. However, in each treatment, the film was deposited onto two cavities to enable duplicate dielectric measurements to be made. It should therefore be emphasized that only the experimental error of the actual measurement technique will be exhibited in the results. This was thought to be a satisfactory approach, as it was considered that any variations in the dielectric properties arising from treatment duplication would be small because the deposition parameters could be closely controlled. The experimental procedure is listed below.

1) Clean the cavity in Teepol.
2) Rinse in de-ionized water.
3) De-grease in trichloroethylene.
4) Rinse in iso-propyl alcohol and allow to dry.

10-3 Design of Experiments

The sputtering parameters thought to be of greatest importance were RF power to the discharge, sputtering pressure and magnetic field strength. However, the sputtering equipment described in Chapter 3 had only facilities built in for the measurement of DC power input to the oscillator and so DC power was monitored as a parameter related to RF power.

Table 10-1 shows the experimental design together with the values of the parameters used. The usual treatment notation is used viz. the presence of a lower case letter indicating the high level of a parameter.

Time did not allow duplication of the treatments to be performed. However, in each treatment, the film was deposited onto two cavities to enable duplicate dielectric measurements to be made. It should therefore be emphasized that only the experimental error of the actual measurement technique will be exhibited in the results. This was thought to be a satisfactory approach, as it was considered that any variations in the dielectric properties arising from treatment duplication would be small because the deposition parameters could be closely controlled. The experimental procedure is listed below.

1) Clean the cavity in Teepol.
2) Rinse in de-ionized water.
3) De-grease in trichloroethylene.
4) Rinse in iso-propyl alcohol and allow to dry.

TABLE 10-1 : EXPERIMENTAL DESIGN FOR DIELECTRIC INVESTIGATION

	Without Magnetic Field		With Magnetic Field of 1.25 Wb/m^2	
Pressure	DC Input Power			
	400 Watts	550 Watts	400 Watts	550 Watts
10^{-3} Torr	x	w	m	wm
10^{-2} Torr	p	wp	mp	wmp

5) Measure the Q of the cavity and resonant frequency.

6) Deposit dielectric film using the masking arrangement shown in figure 10-1.

7) Measure the Q of the cavity and resonant frequency with the film present.

8) Measure the film thickness on the centre conductor of the cavity using the procedure outlined in section 10-2.

9) Calculate the permittivity and loss tangent using equations 5-1 and 5-2.

For each deposition, the two cavity tops were placed at the same radial distance from the centre of the work table and on a line perpendicular to the target electrode gap. The cavity parameters were measured using the waveguide reflectometer apparatus shown in figures 8-3 and 8-4 . The use of the Gunn diode source yielded a maximum error in ten Q measurements of $\pm$ 0.2% and an error of $\pm$ 0.1 MHz for the resonant frequency, the cavity being dismantled for each measurement.

10-4 Results for Permittivity, Loss Tangent and Deposition Rate

The results obtained for the permittivity, loss tangent and deposition rate measurements are given in tables 10-2, -3, and -4 respectively. Duplication of the measurements allowed the computer programme given in Appendix 2 to be used to assess the significance of the effects and interactions. All depositions were performed with a source/substrate distance of 39mm.

TABLE 10-2 : FACTORIAL ANALYSIS OF PERMITTIVITY MEASUREMENTS

(see Appendix 2 for procedure)

Treatment	Permittivity Sample 1	Permittivity Sample 2	Mean Permittivity	Main Effect	Mean Square	Main Effect and Significance
x	3.57	3.52	3.545	-	-	-
w	3.78	3.58	3.680	+0.1425	8.1225×10^{-2}	W
m	3.24	3.14	3.190	-0.4275	7.31025×10^{-1}	M < 1%
wm	3.67	3.57	3.620	-0.0800	2.56×10^{-2}	WM
p	3.97	3.65	3.860	+0.1325	7.022×10^{-2}	P
wp	4.35	3.89	4.120	-0.1400	7.84×10^{-2}	WP
mp	3.49	3.45	3.470	-0.2200	1.936×10^{-1}	MP ~ 4%
wmp	3.15	3.18	3.165	-0.2275	2.07×10^{-1}	WMP ~ 4%

Note: Mean Square for Significance at 1% level = 2.676×10^{-1}

" " " " " 5% " = 1.260×10^{-1}

" " " " " 10% " = 8.195×10^{-2}

TABLE 10-3 : FACTORIAL ANALYSIS OF LOSS TANGENT MEASUREMENTS

Treatment	Loss Tangent ($\times 10^{-2}$) 1	2	Mean Loss Tangent ($\times 10^{-2}$)	Main Effect	Mean Square	Main Effect and Significance
x	0.39	0.40	0.395	-	-	-
w	1.10	0.95	1.025	$+7.188 \times 10^{-3}$	$.2.066 \times 10^{-4}$	W 4%
m	0.85	0.69	0.770	-1.064×10^{-2}	4.526×10^{-4}	M < 1%
wm	0.49	0.69	0.590	3.750×10^{-5}	5.625×10^{-9}	WM
p	5.30	4.40	4.850	3.506×10^{-2}	4.917×10^{-3}	P < 1%
wp	5.30	6.00	5.650	4.938×10^{-3}	9.752×10^{-5}	WP
mp	2.30	2.38	2.34	-1.034×10^{-2}	4.275×10^{-4}	MP < 1%
wmp	3.07	4.86	3.965	4.088×10^{-3}	6.683×10^{-5}	WMP

Note : Mean Square for Significance at 1% = 3.247×10^{-4}

" " " " " 5% = 1.529×10^{-4}

" " " " " 10% = 9.447×10^{-5}

TABLE 10-4 : FACTORIAL ANALYSIS OF DEPOSITION RATE MEASUREMENTS

Treatment	Deposition Rate (Å/min) Sample 1	Sample 2	Mean Deposition Rate (Å/min)	Main Effect	Mean Square	Main Effect and Significance
x	73	73	73	-	-	-
w	116	106	110	+48	9.216×10^3	W < 1%
m	192	180	186	+80.75	2.608×10^4	M < 1%
wm	220	220	220	+72.5	2.103×10^2	WM ~ 5%
p	87	103	95	-5.5	1.21×10^2	P
wp	139	138	138.5	+12.0	5.76×10^2	WP < 1%
mp	133	125	129	-30.25	3.66×10^3	MP < 1%
wmp	208	203	205.5	+9.95	3.423×10^2	WMP ~ 3%

Note : Mean Square for Significance at 1% level = 4.167×10^2

" " " " " 5% " = 1.961×10^2

" " " " " 10% " = 1.275×10^2

10-4-1 Permittivity Results (Table 10-2)

The majority of the permittivity observations exhibit a dielectric constant lower than the accepted value of 3.8 for bulk silicon dioxide. The only significant effect is that due to the presence of the magnetic field. Applying a magnetic field of 1.25×10^{-2} Wb/m^2 causes a general lowering of the permittivity. The magnetic field and sputtering pressure are also shown to interact. Further calculations show that the application of the magnetic field at 10^{-3} Torr causes a decrease in the permittivity of 6%, while a 16% decrease is observed at a pressure of 10^{-2} Torr. These effects are, however, dependent upon the DC input power as is indicated by the second order interaction WMP. The only general conclusion is that the magnetic field causes a decrease in the permittivity, the actual decrease obtained being governed by the other parameters. This effect may be explained in terms of the argon content of the film. Schwartz and Jones [35] have shown that the argon content of silicon dioxide films is increased by the presence of a magnetic field. In sputtering, the substrate and growing film will receive bombardment by energetic argon ions and electrons. Vossen [39] points out that any surface exposed to an RF discharge will, in most cases, develop a small negative potential relative to the plasma. The increase in argon concentration observed by Schwartz and Jones in the presence of a magnetic field may be attributable to an increase in the negative floating potential of the substrate, resulting in an increase in the argon ion bombardment of the film. It is believed that this effect is the cause of the observed decrease in permittivity when a magnetic field is used.

10-4-2 Loss Tangent Results (Table 10-3)

All three parameters significantly affect the dielectric loss. Increasing the DC input power increases the loss tangent of the film. This may be attributed to the increased deposition rate (Table 10-4) causing an increase in the number of impurities trapped in the film and also trapping of deposited silicon dioxide molecules in non-ideal positions. The application of a magnetic field is again significant, in general causing a decrease in the dielectric loss. This may be explained again in terms of an increase in the negative bias developed on the film surface. Argon ion bombardment of the film will result in some re-sputtering of the film. Impurities and silicon dioxide molecules situated in non-ideal positions will be preferentially sputtered owing to their low binding energy within the film. This will result in improved film quality and lower dielectric loss. P-etch is often used to evaluate the quality of silicon dioxide films [34]. Logan [40] studied the effect of the substrate bias voltage on the P-etch rate of silicon dioxide films and found that a dramatic decrease in the etch rate (corresponding to a high-purity, low-stressed film) occurred for negative bias voltages in the range 10 to 20 volts. Comparison of treatments x and m shows that the loss tangent for the films deposited for treatment m is higher than for those deposited for treatment x. This is due to the increase deposition rate caused by the magnetic field (Table 10-4). As was explained for the effect of DC input power, the increased deposition rate will increase the dielectric loss while the increased bombardment of the film by argon ions caused by the magentic field will tend to counteract this effect. Pressure has a very significant effect on the dielectric loss. An increase in pressure to 10^{-2} Torr can increase

the loss tangent by an order of magnitude. Jones et al [78] have shown that the floating potential of a silicon wafer in an RF discharge is greatly reduced for increasing pressures which reduce the amount of re-sputtering. These workers [79] have also shown that a high re- emission coefficient (i.e. the ratio of the amount of sputtered material re-emitted from the substrate to the amount of incident material) is essential if a high quality film is to be obtained. It is therefore believed that the observed effect of pressure is caused by there being only a small amount of re-sputtering of the film (i.e. a low re-emission coefficient); this results in a high impurity concentration and poorly positioned silicon dioxide molecules. Finally, interaction MP indicates that the effect of the magnetic field is far greater at a pressure of 10^{-2} Torr than at 10^{-3} Torr. This suggests that the amount of re-sputtering caused by the magnetic field at 10^{-2} Torr has a greater effect on the film properties than the accompanying increase in the deposition rate. This is the opposite to that observed for treatments x and m discussed earlier in this section.

10-4-3 Deposition Rate Results (Table 10-4)

As was shown in Chapter 3, an increase in the energy of the ions bombarding the target consequent upon an increase in the power input to the discharge increases the deposition rate. This is indicated by main effect W. The deposition rate is also increased through application of a magnetic field which results in an increase in the ion density and hence increases the sputtering rate.

The magnetic field and input power are also shown to have a significant interaction. For example, disregarding any interactions with pressure, application of a magnetic field of 1.25 $X10^{-2}$ Wb/m^2 causes an 87% increase in the deposition rate for a power input of 400 watts while a 70% increase is obtained for an input of 550 watts. It was reported in section 3-10 that a saturation level in the deposition rate corresponding to a saturation in the ion density appeared to occur for high magnetic field strengths. Increasing the power input to the discharge is also likely to increase the ion density as well as the kinetic energy of the argon ions. It is therefore likely that for high power operation, the observed saturation level in deposition rate will occur at lower magnetic field strengths. This would explain the observed interaction between the input power and magnetic field. An increase in the amount of re-sputtering of the film for high powers in the presence of the magnetic field may be a further explanation for this interaction. As already stated in section 10-4-2, it is believed that the presence of the magnetic field causes ion bombardment of the film. An increase in the power input to the discharge will also increase the energy of the impinging ions on the substrate, causing more material to be re-sputtered from the film and thereby decreasing the effect of the magnetic field on the deposition rate for high power operation. The latter explanation would also account for the lower dielectric loss measured for films deposited for treatment wm than for treatment m (Table 10-3), although interaction WM was not found to be significant for the loss tangent measurements.

Interaction WP shows that increasing the power from 400 watts to

550 watts results in a much larger increase in the deposition rate at 10^{-2} Torr than at a pressure of 10^{-3} Torr, disregarding the interaction with magnetic field. Again interaction MP is significant, indicating that the magnetic field has a far greater influence at 10^{-3} Torr than at 10^{-2} Torr. It will be noticed that the effect of pressure does not appear to be significant with regard to deposition rate. This contradicts the results illustrated by the graph in figure 3-15 where it was shown that increasing the pressure to 10^{-2} Torr decreased the deposition rate. This discrepancy is explained by interaction MP. It will be observed from Table 10-4 that without a magnetic field, increasing the pressure increases the deposition rate. At higher pressures an increased ion density is obtained which will result in higher deposition rates. However, this effect is accompanied by a decrease in the mean free path of the sputtered material opposing the increase in deposition rate. At the investigated pressure of 10^{-2} Torr, the effect of the increased ion density pre-dominates over the mean free path consideration. Comparision of the results obtain in the presence of a magnetic field shows that for a pressure of 10^{-2} Torr a lower deposition rate is obtained, as was shown in figure 3-15. It will be seen, therefore, that the discrepancy is only apparent and the observed differences are completely explained by the occurrence of re-sputtering of the film in the presence of a magnetic field. The effect of pressure on the deposition rate has been reported by other workers. For example, Pratt (80) using a source/substrate distance of 63 mm. (2.5 in.) obtained a linear decrease in the deposition rate of silicon dioxide with increasing pressure from 2×10^{-3} to 2×10^{-2} Torr without a magnetic field. With a magnetic field of 0.34×10^{-2} Wb/m^2 he still observed a

decrease in the deposition rate over this range, but found that the deposition rate at 2 x 10^{-3} Torr had increase by about 100% while at 10^{-2} Torr this increase was only 25%. Vossen [24], on the other hand, found a constant deposition rate from 2 x 10^{-3} Torr to 1.5 x 10^{-2} Torr, above which pressure a decrease occurred. There would, therefore, appear to be some agreement between the present author's results and those quoted above. It is almost certain that other sputtering parameters would explain the discrepancies in these observations. The source/substrate distance is particularly important because this determines the relative effects of the decrease in mean free path of the sputtered material with increasing pressure and the accompanying increase in ion density. Finally, interaction WMP shows that the effect of one parameter depends upon the levels of the other two.

10-5 Deposition of Alumina by RF Sputtering

As a final experiment, an alumina film was deposited by RF sputtering of a 99.5% alumina target. The deposition conditions and the results obtained for the deposition rate and permittivity and loss tangent measurements are listed below.

Magnetic Field	1.25 X 10^{-2} Wb/m^2
DC Input Power	550 Watts
Pressure	10^{-3} Torr
Source/substrate Distance	39 mm
Deposition Rate	118 Å/min
Permittivity at 10 GHz	9.50
Loss tangent at 10 GHz	2.5 x 10^{-3}

From this one measurement, it would appear that alumina may well be a superior alternative to silicon dioxide, yielding a low loss film with a permittivity comparable to the bulk material. Further, the deposition rate attainable, while still retaining good film properties, would be acceptable for a commercial process.

10-6 Comparison of Results

It is generally accepted that RF sputtering yields films of a quality superior to that obtained by evaporation. Mehmet [7] measured the properties of evaporated silicon dioxide at 10 GHz. He obtained permittivities of 3.9 to 4.4 and loss tangents of 0.1 to 0.01. The results given in this chapter show that superior film quality from RF sputtering is only obtained provided that the correct deposition conditions are chosen. The best RF sputtered silicon dioxide film reported here had a permittivity of 3.55 and loss tangent of 4×10^{-3}.

Since this work was performed, Michie [8,81] has measured the quality factor of 1pF planar capacitors at 10 GHz. The electrode loss of the capacitors was calculated from the surface resistance measurements given in chapter 9, thus allowing the dielectric Q, Q_d ($= 1/\tan\delta$) to be evaluated. For a dielectric of RF sputtered silicon dioxide deposited for treatment wm in Table 10-3, Michie has measured dielectric Q's of 130 to 145. The results given in Table 10-3 predict a dielectric Q of 166 for this treatment. Michie has also measured a dielectric Q of 178 for RF sputtered alumina.

The dielectric Q for the alumina film given in section 10-5 is 400. The disagreement between these measured values may be due to different deposition conditions. However, it appears that alumina films are of superior quality to silicon dioxide films.

10-7 Comments

From the analysis of the results given in section 10-4, lower loss silicon dioxide films may be produced if much lower input powers are used, at a pressure of 10^{-3} Torr and in the presence of a magnetic field. If the DC input power is chosen such that the deposition rate is low, say 80Å/min., then the film impurity concentration and the trapping of silicon dioxide molecules in non-ideal positions should be reduced. The magnetic field will cause a certain amount of re-sputtering which should again reduce film contamination. It is unfortunate that the magnetic field reduces the permittivity as well as the dielectric loss. If a low permittivity is unacceptable, a compromise between permittivity and loss tangent may well be obtained by using lower magnetic field strengths.

The dielectric Q for the alumina film given in section 10-5 is 400. The disagreement between these measured values may be due to different deposition conditions. However, it appears that alumina films are of superior quality to silicon dioxide films.

10-7 Comments

From the analysis of the results given in section 10-4, lower loss silicon dioxide films may be produced if much lower input powers are used, at a pressure of 10^{-3} Torr and in the presence of a magnetic field. If the DC input power is chosen such that the deposition rate is low, say 80Å/min., then the film impurity concentration and the trapping of silicon dioxide molecules in non-ideal positions should be reduced. The magnetic field will cause a certain amount of re-sputtering which should again reduce film contamination. It is unfortunate that the magnetic field reduces the permittivity as well as the dielectric loss. If a low permittivity is unacceptable, a compromise between permittivity and loss tangent may well be obtained by using lower magnetic field strengths.

Chapter 11

CONCLUSIONS

11-1 General

Much of the experimental work reported here has involved the use of factorial design. It has been shown that from relatively few experiments, this technique yields a wealth of information that would have been missed if the classical experimental approach had been followed. The use of factorial design should prove invaluable in further work for optimizing processing conditions. Indeed, it is surprising that, after the initial successes of factorial design in agricultural applications, scientific workers have been slow to recognise its advantages.

A process has been developed and patented for the use of relief mask techniques for the deposition of thin film material onto selected areas. The method overcomes the disadvantages of conventional relief mask technology and for this reason is thought to be a significant contribution to the thin film integrated circuit field generally.

In the following sections, the conclusions and suggestions for further work for each of the topics investigated will be outlined.

11-1-1 Evaluation of Substrate Surface Finish

At the present time, the only substrates acceptable for lumped element MICs are quartz and sapphire. It does appear that

manufacturers are now able to reduce the surface roughness of alumina substrates and for this reason, surface finish evaluation of substrates should be performed periodically.

11-1-2 Surface Resistance of Bulk and Thin Film Conductors

A cavity technique has been developed for surface resistance measurements on both bulk and thin film conducting samples. Measurements can be made with an accuracy of $\pm$ 0.0013 Ω. The simplicity of application of the method is a significant advance on former methods. It has been shown that high surface resistance values of bulk conductors is mainly due to work hardening of the surface layers. Much of the work hardening can be removed by prolonged electropolishing and/or annealing, which result in a 12% to 15% decrease in the surface resistance of a machined sample, to a value approaching the accepted dc value.

The measured surface resistance at 10 GHz of evaporated copper films of thicknesses 0.3 μm to 3 μm has been shown to be in good agreement with the theoretical values. This information is of particular use in evaluating the electrode loss of capacitors where a thin bottom electrode is usually required.

The surface resistance of metal conductors formed by electroplating is dependent upon the current density, stirring rate, temperature and chemical composition of the solution. The surface roughness of the deposited films is particularly susceptible to

changes in the plating parameters. Of all the solutions tested, bright acid copper solution was easy to use and gave films having a low surface resistance ($R_s = 0.029\Omega$). For this solution, cell voltage was found to affect the brightness of the film. A further investigation of this solution should be performed using factorially designed experiments, paying particular attention to cell voltage as a variable parameter. The lowest surface resistance of gold films was obtained from Engelhardt E56 solution. Although the difference between the surface resistance of these films and those obtained from the PMD gold solution was small, the latter solution had the added disadvantage of slow deposition rates. The results also showed that there is little to be gained by using silver plated films for MICs. If gold or silver-plated films have to be used, they should be heat-treated because this results in a significant reduction in the surface resistance. Improvement of the copper films by heat treatment was, however, generally small.

11-1-3 The Properties of Dielectric Films

It has been shown that the permittivity and loss tangent at 10 GHz of RF sputtered silicon dioxide films are affected by the magnetic field strength, sputtering pressure and DC input power to the oscillator. A low sputtering pressure and a low deposition rate are required if low loss films are to be produced. The most outstanding effect is that of the magnetic field. The correct application of a magnetic field reduces the permittivity and the loss tangent of the film. As has been explained in sections 10-4-1

and 10-4-2, these effects are due to increased argon concentration in the film and to increased re-sputtering of the film during deposition. The lowest loss tangent recorded here for silicon dioxide films was 0.004 with a permittivity of 3.55. It is thought that the film quality may be improved if the films are deposited at a pressure of 10^{-3} Torr with a magnetic field of 1.25×10^{-2} Wb/m^2 and with a low DC input power so that the deposition rate is of the order of 80Å/min.

This work is by no means complete. Further investigations should include a study of the effects of the source/substrate distance, substrate temperature and purity of the sputtering gas. It has been reported (40) that bias sputtering i.e. external application of a negative potential to the substrate, improves the film quality in terms of the P-etch rate. The effects of this technique should be investigated, although the present findings indicate that this method might reduce the permittivity to an unacceptable level.

The permittivity and loss tangent at 10 GHz of an RF sputtered alumina film were measured to be 9.50 and 2.5×10^{-3} respectively. This result suggests that further work should be directed towards a study of RF sputtered alumina films for use in MICs.

11-2 Comments

The surface resistance measurement technique and the results

obtained are of general importance to the MIC field, allowing better design and construction of both distributed and lumped element circuits. Although more work is still required to optimize the sputtering process for the deposition of dielectric films, the knowledge gained about the effects of the three processing parameters studied here is essential if good quality dielectrics are to be obtained.

References

1) H. Sobol: Applications of integrated circuit technology to microwave frequencies, Proc. IEEE, 59, No. 8, (1971).

2) M.V. Schneider, B. Glance, W.F. Bodtmann: Microwave and millimeter wave hybrid integrated circuits for radio systems, Bell. Syst. Tech. J., p. 1703, (1969).

3) D.A. Daly et al: Lumped elements in microwave integrated circuits, IEEE Trans. MTT., MTT-15, No. 12, p. 713, (1967).

4) M. Caulton: The lumped element approach to microwave integrated circuits, Microwave J., 13, p. 51, (1970).

5) R. De Brecht, M. Caulton: Lumped elements in microwave integrated circuits in the 1-12 GHz range, GMTT - Intl. Microwave Symposium, California, May 1970.

6) R. Glang, L.V. Gregor: Handbook of thin film technology, Eds. L.I. Maissel, R. Glang, McGraw Hill, 1970, Chapter 7.

7) K. Mehmet: Microwave integrated circuits - Preparation and measurement techniques for materials and components, PhD. Thesis, University of Warwick, (1970).

8) D. Michie: Thesis to be submitted to the University of Warwick on the subject of microwave integrated circuits.

9) E.F. Da Silva: Inductors as lumped elements in microwave integrated circuits, MSc. Thesis, University of Warwick, (1972).

10) L. Holland: Vacuum deposition of thin films, Chapmann and Hall (London), 1956.

11) C.S. Aitchison: Lumped components for microwave frequencies, Philips tech. Rev., 32, p. 305, (1971).

12) F. Argoll, A.K. Jonscher: Dielectric properties of thin films of alumimium oxide and silicon oxide, Thin Solid Films, 2, p. 158, (1968).

13) K. Mehmet, M.K. McPhun: A microwave relaxation phenomenon in electron-beam-evaporated films of SiO, J. Phys. D: Appl. Phys., 5, p. 1349, (1972).

14) H. Hirosa, V. Wada: Dielectric properties and DC conductivity of vacuum deposited SiO films, Jap. J. Appl. Phys., 3, p. 179, (1964).

15) M. Caulton: Microwave integrated circuit technology - a summary, IEEE, J. of Solid State Circuits, p. 292, (1970).

16) N. Schwartz, R.W. Berry: Thin film components and circuits, Physics of Thin Films, 2, p. 363, (1964).

17) W. Schilling: The real world of micromin substrates, Microwaves, 7, p. 52, (1968).

18) J.R. Bosnell: The effect of the physical properties of alumina substrates on their use in microwave hybrid circuits, Microelectronics, 3, No. 10, p. 33, (1971).

19) N. Schwartz, R. Brown: A stylus method for evaluating the thickness on thin films and substrate surface roughness, Trans. 8th. Nat. Vacuum Symposium, p. 836, (1961)

20) An introduction to surface texture, issued by The Rank Taylor Hobson Organisation.

21) G.K. Wehner: Sputtering by ion bombardment, Advances in Electronics and Electron Physics, VII, p. 239, Acad. Press, N.Y., 1955.

22) T.I. Putner, G.N. Jackson: Sputtering: its technology and applications, Electronic Equipment News, April, May, June 1968.

23) B. Chapman: The basics of sputtering, Trans. of Conf. and School on the Elements, Techniques and applications of Sputtering, October 1969, Brighton, England.

24) J.L. Vossen, J.J. O'Neil: R.F. sputtering processes, RCA Review June 1968, p. 149.

25) G.K. Wehner, G.S. Anderson: The nature of physical sputtering, Handbook of Thin Film Technology, Eds. Maissel and Glang, McGraw Hill, 1970, Chapter 3.

26) L.I. Maissel: Application of sputtering to the deposition of films, Handbook of Thin Film Technology, Eds. Maissel and Glang, McGraw Hill, 1970, Chapter 4.

27) J. Beynon: Thin film circuits benefit from RF sputtering, Electronic Engineering, 42, No. 513, p. 43, (1970).

28) G.N. Jackson: RF Sputtering, Thin Solid Films, 5, p. 209, (1970). Also: A review of published work on RF sputtering, ERA Rept., No. 70 - 4.

29) G.S. Anderson, W.N. Mayer, G.K. Wehner: Sputtering of dielectrics by high frequency fields, J. Appl. Phys., 33, p. 2991, (1962).

30) P.D. Davidse, L.I. Maissel: Dielectric thin films through RF sputtering, J. Appl. Phys., 37, No. 2, p. 574, (1966).

31) P.D. Davidse: Theory and practice of RF sputtering, Symposium on the Deposition of Thin Films by Sputtering, Rochester N.Y., 1966.

32) A.R. Janus, G.A. Shirm: Preparation and properties of reactively sputtered silicon nitride, Symposium on the Deposition of Thin Films by Sputtering, Rochester N.Y., 1966.

33) D.H. Grantham, L.E. Paradis, D.J. Quinn: High rate RF sputtering system, J. Vac. Sci. Technol., 7, p. 343, (1970).

34) W.A. Pliskin: Comparative evaluation of thin glass films, Electrochem. Soc., 1967, p. 280.

35) G.C. Schwartz, R.E. Jones: Argon content of SiO_2 films deposited by RF sputtering, IBM J. Res. Developm., 14, p. 52, (1970).

36) C.R.D. Priestland: Experiences with an RF sputtering system of the non-grounded double electrode configuration, Vacuum, 19, No. 11, p. 487, (1969).

37) G.T. Murray, G. Hughes: The selection, fabrication and mounting of sputtering sources, Trans. of the Conf. and School on the Elements, Techniques and Applications of Sputtering, Brighton, England, October 1969.

38) B.A. Probyn: Sputtering of insulators in an RF discharge, Vacuum, 18, p. 253, (1968).

39) J.L. Vossen: Control of film properties by RF sputtering techniques, J. Vac. Sci. Technol., 8, No. 5, p. 512, (1971).

40) J.S. Logan: Control of RF sputtered film properties through substrate tuning, Solid State Technol., Dec. 1970, p. 46.

41) O.L. Davies: Design and analysis of industrial experiments, Oliver and Boyd, (1954).

42) W.E. Duckworth:Statistical techniques in technological research, Methuen and Co. Ltd., 1968.

43) O.L. Davies: Statistical methods and production, Oliver and Boyd, 1961.

44) R.S. Butlin: Factorial design and analysis, Engineering Science Report No. 66, University of Warwick, March 1971, (see Appendix 2).

45) B.J. Franklin: RF sputtered quartz dielectric capacitors, Signals Research and Development Establishment, Min. Tech. Report No. 69020, April 1969.

46) G. Siddal: Vacuum deposition of dielectric films for capacitors, Vacuum, 9, p274, (1959).

47) P.J. Harrop, D.S. Campbell: Selection of thin film capacitor dielectrics, Thin Solid Films, 2, p. 273, (1968).

48) A.K. Jonsher, P.A. Walley: Electrical conduction in non-metallic amorphous films, J. Vac. Sci. Technol., 6, p. 662, (1969).

49) A.C. Lynch: Relationships between loss tangent and permittivity, Proc. IEE, 118, p. 244, (1971).

50) M.K.J. Stelter: Chrome masks - The ideal master for photoprocessing, SCP and Solid State Technology, 9, p. 60, (1966).

51) R.S. Butlin, D. Michie: Method for depositing materials on selected areas of a surface, UK Patent Application No. 5342/72.

52) S. Ramo, J.R. Whinnery, T. Van Duzer: Fields and waves in communication electronics, Wiley, 1965, section 5-20.

53) A.B. Pippard: The surface impedance of superconductors and normal metals at high frequencies - II, Proc. Roy. Soc., A191, p. 385, (1947).

54) A.C. Beck, R.W. Dawson: Conductivity measurements at microwave frequencies, Proc. IRE., 38, p. 1181, (1950).

55) R.L. Ramey, T.S. Lewis: Properties of thin metal films at microwave frequencies, J. Appl. Phys., 39, No. 3, p. 1747, (1968).

56) L. Spiers: Surface resistance of metal films at a frequency of 24,000 Mc/s, Nature, 161, p. 601, (1948).

57) H.E. Bussey: Standards and measurements of microwave surface impedance, skin depth, conductivity and Q, IRE Trans. on Instrumentation I-9, p. 171, (1960).

58) E. Maxwell: Conductivity of metallic surfaces at microwave frequencies, J. Appl. Phys., 18, p. 629, (1947).

59) M.E. Brodwin, Pao-Sun Lu: A precise cavity technique for measuring low resistivity semiconductors, Proc. IEEE, 53, p. 1742, (1965).

60) C.G. Montgomery: Techniques of microwave measuremnts, McGraw Hill, 1947, section 5-5.

61) C.G. Montgomery, R.H. Purcell, E.M. Dickie: Principles of microwave circuits, McGraw Hill, 1948, section 2-17.

62) S.E. Miller: Waveguides as a communication medium, Bell Syst. Tech. J., 33, p. 1209, (1954).

63) G.D. Sims: The influence of bends and ellipticity on the attenuation and propagation characteristics of the H_{01} circular waveguide mode, Proc. IEE, 100, pt. IV, p. 25, (1953).

64) C.G. Montgomery, R.H. Purcell, E.M. Dickie: Principles of microwave circuits, McGraw Hill, 1948, Chapter 7.

65) Dr. S.N. Novak: University of Warwick, private communication.

66) D.C. Baird: Experimentation, Prentice Hall, 1965.

67) S.P. Morgan: Effect of surface roughness on eddy current losses at microwave frequencies, J. Appl. Phys., 20, p. 352, (1948).

68) J. Allison, F.A. Benson: Surface roughness and attenuation of precision drawn, chemically polished, electropolished, electroplated, and electroformed waveguides, Proc. IEE, 102, pt. B, p. 251, (1955).

69) R.F. Smallman: Modern physical metallurgy, Butterworths, 1963.

70) R.F. Reed-Hill: Physical metallurgy principles, D. Van Nostrand Co. Inc., 1968.

71) W.C. Elmore: Electrolytic polishing, J. Appl. Phys., 10, p. 724, (1939).

72) W.C. Elmore: Electrolytic polishing II, J. Appl. Phys., 11, p. 797, (1940).

73) Tegart: The electrolytic and chemical polishing of metals, Pergamon Press, 1959.

74) H.A. Wheeler: Formulas for the skin effect, Proc. IRE, 30, p. 412, (1942).

75) A.K. Graham: Electroplating engineering handbook, second edition, Reinhold Book Corp., 1968.

76) Mr. Andrews: GEC, Stoke Works, Coventry, private communication.

77) E. Raub, K. Muller: Fundamentals of metal deposition, Elsevier, 1967.

78) R.E. Jones, C.L. Standley, L.I. Maissel: Re-emission coefficients of Si and SiO_2 films deposited through rf and dc sputtering, J. Appl. Phys., 38, p. 4656 (1967).

79) R.E. Jones, C.L. Standley, L.I. Maissel: Re-emmission of sputtered SiO_2 during growth and its relation to film quality, IBM J. Res. Developm., 14, p. 176, (1970).

80) I.H. Pratt: Processing and evaluation of RF sputtered quartz, Trans. Metallurgical Soc., AIME, 242, p. 526, (1968).

81) R.S. Butlin, D.F. Michie, M.K. McPhun: Measurement of overlay capacitors at x-band with independent assessment of thin-film conductor losses, European Microwave Conference, Brussels, September 1973.

82) Handbook of chemistry and physics, 46th. Ed., 1965 - 1966, The Chemical Rubber Co.

Appendix 1

MAL-FUNCTION OF THE SPUTTERING UNIT

Two faults existed on the sputtering unit. These were poor earthing of the vacuum chamber top plate on which the oscillator was built and incorrect operation of the Penning guage used for monitoring the sputtering pressure. Initially, earthing of the top plate assembly was provided by the earthed screen of the HT cable which was connected to the grounded base plate and to the chassis of the power supply. It was found accidentally that the addition of a second earth lead from the top plate to the base plate extinguished the glow at the indicated operating pressure of 10^{-3} Torr. It was then found that a discharge could only be obtained at very high pressures ($\sim 2.5 \times 10^{-2}$ Torr) as indicated by the gauge. For this reason the gauge was checked against an Edwards Pirani gauge and found to give completely false readings. For example, at a Penning reading of 0.025 Torr, the Pirani indicated less than 10^{-3} Torr. The accuracy of the Pirani is quoted as $\pm$ 3% and was found to be in good agreement with equivalent measurements using a mercury "Vacustat" gauge. The author has since been informed that a kink in the ionization profile of the Penning gauge occurs around 10^{-3} Torr and therefore it cannot be relied on at higher pressures. The results given in Chapter 5 are for films deposited at 10^{-3} Torr as indicated by the Penning gauge. It is believed that the actual deposition pressure was about 5×10^{-4} Torr or less. The fact that it was possible for sputtering to occur at such low pressures by reason of the co-existing defective earth connection has not been investigated.

Appendix 1

MAL-FUNCTION OF THE SPUTTERING UNIT

Two faults existed on the sputtering unit. These were poor earthing of the vacuum chamber top plate on which the oscillator was built and incorrect operation of the Penning guage used for monitoring the sputtering pressure. Initially, earthing of the top plate assembly was provided by the earthed screen of the HT cable which was connected to the grounded base plate and to the chassis of the power supply. It was found accidentally that the addition of a second earth lead from the top plate to the base plate extinguished the glow at the indicated operating pressure of 10^{-3} Torr. It was then found that a discharge could only be obtained at very high pressures ($\sim 2.5 \times 10^{-2}$ Torr) as indicated by the gauge. For this reason the gauge was checked against an Edwards Pirani gauge and found to give completely false readings. For example, at a Penning reading of 0.025 Torr, the Pirani indicated less than 10^{-3} Torr. The accuracy of the Pirani is quoted as $\pm$ 3% and was found to be in good agreement with equivalent measurements using a mercury "Vacustat" gauge. The author has since been informed that a kink in the ionization profile of the Penning gauge occurs around 10^{-3} Torr and therefore it cannot be relied on at higher pressures. The results given in Chapter 5 are for films deposited at 10^{-3} Torr as indicated by the Penning gauge. It is believed that the actual deposition pressure was about 5×10^{-4} Torr or less. The fact that it was possible for sputtering to occur at such low pressures by reason of the co-existing defective earth connection has not been investigated.

Appendix 1

MAL-FUNCTION OF THE SPUTTERING UNIT

Two faults existed on the sputtering unit. These were poor earthing of the vacuum chamber top plate on which the oscillator was built and incorrect operation of the Penning guage used for monitoring the sputtering pressure. Initially, earthing of the top plate assembly was provided by the earthed screen of the HT cable which was connected to the grounded base plate and to the chassis of the power supply. It was found accidentally that the addition of a second earth lead from the top plate to the base plate extinguished the glow at the indicated operating pressure of 10^{-3} Torr. It was then found that a discharge could only be obtained at very high pressures ($\sim 2.5 \times 10^{-2}$ Torr) as indicated by the gauge. For this reason the gauge was checked against an Edwards Pirani gauge and found to give completely false readings. For example, at a Penning reading of 0.025 Torr, the Pirani indicated less than 10^{-3} Torr. The accuracy of the Pirani is quoted as $\pm$ 3% and was found to be in good agreement with equivalent measurements using a mercury "Vacustat" gauge. The author has since been informed that a kink in the ionization profile of the Penning gauge occurs around 10^{-3} Torr and therefore it cannot be relied on at higher pressures. The results given in Chapter 5 are for films deposited at 10^{-3} Torr as indicated by the Penning gauge. It is believed that the actual deposition pressure was about 5×10^{-4} Torr or less. The fact that it was possible for sputtering to occur at such low pressures by reason of the co-existing defective earth connection has not been investigated.

APPENDIX 2

FACTORIAL DESIGN AND ANALYSIS

by

R. S. Butlin

Engineering Science Report No. 66

March 1971

Introduction

It was proposed to use factorial design in an investigation of the effects of the deposition parameters upon the properties of thin silicon dioxide films prepared by RF sputtering. The quality of the films was to be tested by measuring the loss tangents and dielectric constants at 10 GHz. The aim of this report is to explain the design of the experiments and the statistical analysis involved. The advantage of this technique over the classical method is also explained.

Terminology

It is first necessary to define various terms in common use in factorial design.

(1) Factor

This term is used to denote any parameter of an experiment which may be deliberately varied from experiment to experiment e.g. the temperature or pressure at which a chemical reaction is performed.

(2) Level of a Factor

This is the value of a factor examined in a particular experiment.

(3) Treatment

The set of levels of all factors employed in a given trial is called the Treatment or Treatment Combination.

(4) Response

This is the numerical result of a trial for a given treatment.

(5) Effect of a Factor

The effect of a factor is the change in response produced by a change in the level of a factor.

(6) Main Effect (Mean Difference) and Interaction

The main effect or mean difference of a factor is defined as the effect of a factor averaged over all levels of the other factors. If the effect of one factor is different over different levels of another then the two factors are said to interact.

Advantages of Factorial Design

Consider an experiment designed to study the effects of three factors A, B and C. The classical approach is to hold two factors constant and to vary the third, e.g. B and C held constant and A varied. From this, the level of A giving the best result would then be used, C kept constant and B varied. The best value of B would then be used and C varied. In this way, the variation of a factor may be studied. However, the effect of one factor on another is unknown; that is to say, the interaction of factors is ignored. Factorial design, however, overcomes this by considering the combinations of all levels of all factors. For example, if each factor is to be tested at two levels i.e. a low value and a high value, then the total number of experiments to be performed for a three-factor design is $2^3 = 8$, in order to examine all combinations of all levels. In general, for an n-factor two-level experiment, the total number of trials is 2^n. From the eight experiments of the three-factor two-level case, it is possible to study the main effects of the factors A, B and C and also the interactions between the levels.

Design of Experiments

Each trial is given a treatment coding. For example, in a three-factor experiment, if factor A is at its high level and B and C are at their low levels, then the treatment coding is "a" i.e. if the factor is at its high level then the treatment is represented by the lower case letter. If B and C are at their high levels and A is at its low level then the treatment is "bc". The treatment codings for the eight experiments are written in a standard order as shown below:

(1), (a), (b), (ab), (c), (ac), (bc), (abc).

The coding (1) indicates that all the factors are at their low levels. Using this coding system, the design may now be shown in tabular form (see Table 1).

Table 1 : A 2^3 Factorial Design

	C_{low}		C_{high}	
	A_{low}	A_{high}	A_{low}	A_{high}
B_{low}	(1)	(a)	(c)	(ac)
B_{high}	(b)	(ab)	(bc)	(abc)

The treatment coding may be taken to represent the response of the trial for a given treatment.

Calculation of the Main Effects and Interactions

To study the effect of changing a factor from one level to

another, one must calculate the "main effects", i.e. the effect of a factor averaged over all levels of the other factors. For example,

Effect of A for B_{low}, C_{low} = (a) - (1)

" " " " B_{low}, C_{high} = (ac) - (c)

" " " " B_{high}, C_{low} = (ab) - (b)

" " " " B_{high}, C_{high} = (abc) - (bc)

$$\text{Main Effect, A, } = \frac{(a) - (1) + (ac) - (c) + (ab) - (b) + (abc) - (bc)}{4}$$

$$= \frac{(a + ab + ac + abc)}{4} - \frac{(1 + b + c + bc)}{4} \quad \ldots\ldots \text{ eqn (1)}$$

It can be seen from equation (1) why the main effect is sometimes referred to as the Mean Difference as it is the difference between the mean of the responses with the factor at its high level and the mean of the responses with the factor at its low level.

Similarly,

$$\text{Main Effect, B, } = \frac{(b + ab + bc + abc)}{4} - \frac{(1 + a + c + ac)}{4} \quad \ldots\ldots \text{ eqn (2)}$$

The presence of interactions is detected by comparing the effects of one factor over the levels of the other. If no interaction exists, then the effect of factor A, say, will be the same over the different levels of B. Interaction AB is then zero. The main effect of an interaction is defined as the mean difference in effects of one of the factors over the levels of the other. In a 2^2 experiment this can be clearly seen (see Table 2).

Table 2 : A 2^2 Experimental Design

	A_{low}	A_{high}
B_{low}	(1)	(a)
B_{high}	(b)	(ab)

The Main Effect of interaction AB = $\frac{(ab - b) - (a - 1)}{2}$ ..... eqn (3)

This is known as a first order interaction, where

(ab - b) is the effect of A at the high level of B

and (a - 1) is the effect of A at the low level of B

For three-factor experiments, the interaction is calculated as an average over all levels of the third factor. For example, in calculating interaction AB for a three-factor experiment, Table 1 may be reduced to Table 3 by averaging all the results over all levels of C. The interaction AB is then calculated as for a two-factor experiment.

Table 3 : Responses of Table 1 Averaged over all Levels of C

	A_{low}	A_{high}
B_{low}	$\frac{(1 + c)}{2}$	$\frac{(a + ac)}{2}$
B_{high}	$\frac{(b + bc)}{2}$	$\frac{(ab + abc)}{2}$

Main Effect of AB = $\frac{\frac{(ab + abc)}{2} - \frac{(b + bc)}{2} - \frac{(a + ac)}{2} - \frac{(1 + c)}{2}}{2}$

$$= \frac{(ab + abc) - (b + bc)}{4} - \frac{(a + ac) - (1 + c)}{4}$$

..... eqn (4)

Equations (3) and (4) have been calculated by observing the effects of A over the levels of B. The results are exactly the same as if the effects of B over the levels of A had been taken. The second order interaction ABC is defined as the difference in interactions of AB with C at its high level and C at its low level. Table 1 thus reduces to Table 4 and the interaction ABC is calculated as for equation (4).

$$\text{Main Effect of ABC} = \frac{\frac{(abc - bc)}{2} - \frac{(ac - c)}{2} - \frac{(ab - b)}{2} - \frac{(a - 1)}{2}}{2}$$

$$\therefore \text{ Main Effect ABC} = \frac{(abc - bc) - (ac - c)}{4} - \frac{(ab - b) - (a - 1)}{4}$$

..... eqn (5)

Table 4 : Calculation of Second Order Interaction ABC

	AB_{low}	AB_{high}
C_{low}	$\frac{(a - 1)}{2}$	$\frac{(ab - b)}{2}$
C_{high}	$\frac{(ac - c)}{2}$	$\frac{(abc - bc)}{2}$

Expanding equations 1, 2, 4 and 5

$$4A = -(1) + (a) - (b) + (ab) - (c) + (ac) - (bc) + (abc)$$

$$4B = -(1) - (a) + (b) + (ab) - (c) - (ac) + (bc) + (abc)$$

$$4AB = +(1) - (a) - (b) + (ab) + (c) - (ac) - (bc) + (abc)$$

$$4ABC = -(1) + (a) + (b) - (ab) + (c) - (ac) - (bc) + (abc)$$

Although the derivation of the above equations is laborious a very simple method of remembering or re-calculating exists. As previously mentioned, the standard order of treatments is

(1), (a), (b), (ab), (c), (ac), (bc), (abc).

The above equations may be written down immediately by remembering, for example, that for the main effect A all the treatment combinations containing "a" have a plus sign and all those not containing "a" a minus sign. The signs allocated to the treatment combinations for the interactions are obtained by multiplying the signs for the main effects of the factors involved in the interaction.

e.g. $4C = -(1) - (a) - (b) - (ab) + (c) + (ac) + (bc) + (abc)$

$4A = -(1) + (a) - (b) + (ab) - (c) + (ac) - (bc) + (abc)$

$\therefore 4AC = +(1) - (a) + (b) - (ab) - (c) + (ac) - (bc) + (abc)$

The signs required for calculating the main effects for a three-factor experiment are given in Table 5.

Table 5 : Sign Matrix for Three-Factor Design

	Total	4A	4B	4AB	4C	4AC	4BC	4ABC
(1)	+	−	−	+	−	+	+	−
(a)	+	+	−	−	−	−	+	+
(b)	+	−	+	−	−	+	−	+
(ab)	+	+	+	+	−	−	−	+
(c)	+	−	−	+	+	−	−	+
(ac)	+	+	−	−	+	+	−	−
(bc)	+	−	+	−	+	−	+	−
(abc)	+	+	+	+	+	+	+	+

Statistical Significance of Results

Calculation of the main effects enables one to determine the change in response for a change in the level of a factor. The determination of the significance of the main effects requires further statistical analysis. Two significance tests may be used and these are explained in detail in the following sections.

The t-Test

As previously mentioned, the main effect is the difference of two means. The t-test gives the probability that the two means are just samples drawn from the same distribution by comparing the main effect with a standard error. Replication of each treatment allows the standard error to be calculated.

Consider the fully replicated experiment shown in Table 6.

Table 6 : Results for Replicated Three-Factor Experiment

Treatment	Response 1	Response 2	Mean	Main Effect
(1)	151	151	151	304.125
(a)	147	136	141.5	-19.625
(b)	147	139	143	-13.325
(ab)	101	108	104.5	- 7.125
(c)	182	176	179	34.125
(ac)	159	168	163.5	4.325
(bc)	173	176	174.5	9.125
(abc)	158	161	159.5	7.125

To calculate the main effects, the mean of each pair of results is taken and the main effects calculated as before. The different results obtained for a given treatment are due to experimental error. Assuming these results to be normally distributed, then the results for a given treatment are samples drawn from a Gaussian distribution having a mean u and standard deviation σ. The standard deviation for such a distribution is given by

$$\sigma = \sqrt{\frac{(x_i - u)^2}{N}} \qquad \text{..... eqn (6)}$$

where x_i is the i^{th} result

u is the mean of the Normal Population

N is the number of results for a given treatment.

However, u is unknown. The mean, $\bar{x}$, of the sample of the universe is not equivalent to u unless the number of samples is large (>30). It can be shown that if the number of samples is small then the best estimate of the standard deviation is given by

$$s = \sqrt{\frac{(x_i - \bar{x})^2}{(N - 1)}} \qquad \text{..... eqn (7)}$$

where s is the estimated standard deviation

$\bar{x}$ is the sample mean

(N-1) is the weighting factor.

Variance, by definition, is the square of the standard deviation. The estimate variance is therefore given by

$$s^2 = \frac{(x_i - \bar{x})^2}{(N - 1)} \qquad \text{..... eqn (8)}$$

For a replicated experiment, it is therefore possible to caculate the variance of a single result for each treatment combination. The responses for each treatment will have different means, but the variances will only differ because of sampling fluctuations. Thus all samples for all treatments are assumed to have different means but the same variance. It is therefore possible to use the variance of all treatments to give a reliable estimate of the variance of a single result. Owing to the additive property of variances, this can be done by summing the individual variances and taking the mean. Using equation (8) to calculate the variances of each treatment is laborious and can be simplified by the use of the following mathematical manipulation of the equation.

Consider two results x_1 and x_2 for a given treatment. The variance is therefore

$$s^2 = \sum_{i=1}^{2} \frac{(x_i - \frac{x_1 + x_2}{2})^2}{(2 - 1)}$$

$$= \frac{\left[x_1 - \frac{(x_1 + x_2)}{2}\right]^2 + \left[x_2 - \frac{(x_1 + x_2)}{2}\right]^2}{(2 - 1)}$$

$$\therefore s^2 = x_1^2 + \left(\frac{x_1 + x_2}{2}\right)^2 - 2x_1 \frac{(x_1 + x_2)}{2} + x_2^2 + \left(\frac{x_1 + x_2}{2}\right)^2 - 2x_2 \frac{(x_1 + x_2)}{2}$$

$$= x_1^2 + x_2^2 + 2\frac{(x_1 + x_2)^2}{4} - 2\frac{(x_1 + x_2).(x_1 + x_2)}{2}$$

$$= x_1^2 + x_2^2 - (x_1 + x_2)^2 + \frac{(x_1 + x_2)^2}{2}$$

$$= \frac{2x_1^2 + 2x_2^2 - x_1^2 - x_2^2 - 2x_1x_2}{2}$$

$$= \frac{x_1^2 + x_2^2 - 2x_1x_2}{2}$$

$$\therefore s^2 = \frac{(x_1 - x_2)^2}{2} \qquad \text{..... eqn (9)}$$

The sum of the variances, V, for n treatments is therefore

$$V = \sum_{i=1}^{n} \frac{(x_{i1} - x_{i2})^2}{2} \qquad \text{..... eqn (10)}$$

The variance of a single result, V(x), $= \frac{V}{n}$

$$\therefore V(x) = \sum_{i=1}^{n} \frac{(x_{i1} - x_{i2})^2}{2n} \qquad \text{..... eqn (11)}$$

Returning to equation (1), the main effect of A for a 2^3 experiment is

$$A = \frac{(a + ab + ac + abc)}{4} - \frac{(1 + b + c + bc)}{4}$$

For a replicated experiment this becomes

$$A = \frac{\left[\frac{(a_1 + a_2)}{2} + \frac{(ab_1 + ab_2)}{2} + \frac{(ac_1 + ac_2)}{2} + \frac{(abc_1 + abc_2)}{2}\right]}{4}$$

$$- \frac{\left[\frac{(1_1 + 1_2)}{2} + \frac{(b_1 + b_2)}{2} + \frac{(c_1 + c_2)}{2} + \frac{(bc_1 + bc_2)}{2}\right]}{4}$$

$$\therefore A = \frac{(a_1 + a_2 + ab_1 + ab_2 + ac_1 + ac_2 + abc_1 + abc_2)}{8}$$

$$- \frac{(1_1 + 1_2 + b_1 + b_2 + c_1 + c_2 + bc_1 + bc_2)}{8} \qquad \text{..... eqn (12)}$$

Let equation (12) be represented by

$$A = P - Q \qquad \text{..... eqn (13)}$$

The error variance of A is the sum of the variances of P and Q as all variables vary independently (see Appendix i). The error variances

of P and Q are obtained in the following way. Consider the linear function

$$X = a_1x_1 \pm a_2x_2 \pm a_3x_3 \pm a_4x_4 \pm \ldots\ldots\ldots \pm a_nx_n$$

where the quantities x_1, x_2, ... x_n vary independently. The error variance V(X) of X is

$$V(X) = a_1{}^2V(x_1) + a_2{}^2V(x_2) + a_3{}^2V(x_3) \ldots\ldots + a_n{}^2V(x_n)$$

i.e. V(X) is the sum of the variances of x_1 etc. (with the appropriate multipliers) whether the coefficients in the expression are positive or negative. If X is equal to the mean of a random sample $x_1 \ldots . x_n$ drawn from a universe of variance σ^2 then

$$X = (x_1 + x_2 + x_3 + \ldots\ldots\ldots + x_n) \ / \ n$$

This equation is similar to that for P and Q in equation (13). As the variance of single result is the same for all observations then

$$V(x) = V(x_1) = V(x_2) = V(x_3) = \ldots\ldots\ldots\ldots = V(x_n)$$

$$\therefore \quad V(X) = \left(\frac{1}{n}\right)^2V(x_1) + \left(\frac{1}{n}\right)^2V(x_2) + \ldots\ldots\ldots\ldots + \left(\frac{1}{n}\right)^2V(x_n)$$

$$= n.\left(\frac{1}{n}\right)^2V(x)$$

$$= V(x) \ / n \qquad \ldots\ldots \text{ eqn (14)}$$

The error variances of P and Q in equation (13) are therefore

$$V(p) = V(x) \ / n$$

$$V(q) = V(x) \ / n$$

The error variance of A is therefore given by

$$V(A) = \frac{V(x)}{n} + \frac{V(x)}{n}$$

$$\text{The standard error} = \sqrt{V(A)}$$

$$= \sqrt{\frac{V(x)}{n} + \frac{V(x)}{n}}$$

$$= s\sqrt{\frac{1}{n} + \frac{1}{n}}$$

of P and Q are obtained in the following way. Consider the linear function

$$X = a_1x_1 \pm a_2x_2 \pm a_3x_3 \pm a_4x_4 \pm \ldots\ldots\ldots \pm a_nx_n$$

where the quantities x_1, x_2, ... x_n vary independently. The error variance V(X) of X is

$$V(X) = a_1{}^2V(x_1) + a_2{}^2V(x_2) + a_3{}^2V(x_3) \ldots\ldots + a_n{}^2V(x_n)$$

i.e. V(X) is the sum of the variances of x_1 etc. (with the appropriate multipliers) whether the coefficients in the expression are positive or negative. If X is equal to the mean of a random sample $x_1 \ldots . x_n$ drawn from a universe of variance σ^2 then

$$X = (x_1 + x_2 + x_3 + \ldots\ldots\ldots + x_n) \ / \ n$$

This equation is similar to that for P and Q in equation (13). As the variance of single result is the same for all observations then

$$V(x) = V(x_1) = V(x_2) = V(x_3) = \ldots\ldots\ldots\ldots = V(x_n)$$

$$\therefore \quad V(X) = \left(\frac{1}{n}\right)^2V(x_1) + \left(\frac{1}{n}\right)^2V(x_2) + \ldots\ldots\ldots\ldots + \left(\frac{1}{n}\right)^2V(x_n)$$

$$= n. \left(\frac{1}{n}\right)^2V(x)$$

$$= V(x) \ / n \qquad \ldots\ldots \text{ eqn (14)}$$

The error variances of P and Q in equation (13) are therefore

$$V(p) = V(x) \ / n$$

$$V(q) = V(x) \ / n$$

The error variance of A is therefore given by

$$V(A) = \frac{V(x)}{n} + \frac{V(x)}{n}$$

$$\text{The standard error} = \sqrt{V(A)}$$

$$= \sqrt{\frac{V(x)}{n} + \frac{V(x)}{n}}$$

$$= s\sqrt{\frac{1}{n} + \frac{1}{n}}$$

where s is the standard deviation of a single result.

The probability that the two means P and Q are merely samples drawn from the same distribution is given by the ratio

$$t = \frac{P - Q}{s\sqrt{1/n + 1/n}}$$

$$= \frac{\text{Main Effect}}{\text{Standard Error}}$$

for a given number of degrees of freedom ϕ, i.e. for the number of degrees of freedom for which the standard error was calculated. In a fully replicated design, the standard error is calculated using n duplicated results, each duplicate having (2 - 1) degrees of freedom. The degrees of freedom, ϕ, for the standard error is

$$\phi = N(2 - 1)$$

where N is the number of treatments.

Percentage points of the t-distribution for various degrees of freedom are given in Table 7.

As an example of the t-test, a full analysis of the results of Table 6 is given in Table 8.

The percentage points given in Table 8 are calculated as follows:-

The variance of a single result, V(x), $= \sum_{i=1}^{n} \frac{(x_{i1} - x_{i2})^2}{2n}$

$= 369/16$

$= 23$

Standard error of main effects $= \sqrt{\frac{V(x)}{n} + \frac{V(x)}{n}}$

$= \sqrt{\frac{23}{8} + \frac{23}{8}}$

$= 2.4$

Table 7

Percentage Points of the t-Distribution

ϕ									
1	1·00	2·41	6·31	12·7	25·5	63·7	127	637	1
2	0·816	1·60	2·92	4·30	6·21	9·92	14·1	31·6	2
3	0·765	1·42	2·35	3·18	4·54	5·84	7·45	12·9	3
4	0·741	1·34	2·13	2·78	3·75	4·60	5·60	8·61	4
5	0·727	1·30	2·01	2·57	3·36	4·03	4·77	6·86	5
6	0·718	1·27	1·94	2·45	3·14	3·71	4·32	5·96	6
7	0·711	1·25	1·89	2·36	3·00	3·50	4·03	5·40	7
8	0·706	1·24	1·86	2·31	2·90	3·36	3·83	5·04	8
9	0·703	1·23	1·83	2·26	2·82	3·25	3·69	4·78	9
10	0·700	1·22	1·81	2·23	2·76	3·17	3·58	4·59	10
11	0·697	1·21	1·80	2·20	2·72	3·11	3·50	4·44	11
12	0·695	1·21	1·78	2·18	2·68	3·06	3·43	4·32	12
13	0·694	1·20	1·77	2·16	2·65	3·01	3·37	4·22	13
14	0·692	1·20	1·76	2·14	2·62	2·98	3·33	4·14	14
15	0·691	1·20	1·75	2·13	2·60	2·95	3·29	4·07	15
16	0·690	1·19	1·75	2·12	2·58	2·92	3·25	4·01	16
17	0·689	1·19	1·74	2·11	2·57	2·90	3·22	3·96	17
18	0·688	1·19	1·73	2·10	2·55	2·88	3·20	3·92	18
19	0·688	1·19	1·73	2·09	2·54	2·86	3·17	3·88	19
20	0·687	1·18	1·72	2·09	2·53	2·85	3·15	3·85	20
21	0·686	1·18	1·72	2·08	2·52	2·83	3·14	3·82	21
22	0·686	1·18	1·72	2·07	2·51	2·82	3·12	3·79	22
23	0·685	1·18	1·71	2·07	2·50	2·81	3·10	3·77	23
24	0·685	1·18	1·71	2·06	2·49	2·80	3·09	3·74	24
25	0·684	1·18	1·71	2·06	2·49	2·79	3·08	3·72	25
26	0·684	1·18	1·71	2·06	2·48	2·78	3·07	3·71	26
27	0·684	1·18	1·70	2·05	2·47	2·77	3·06	3·69	27
28	0·683	1·17	1·70	2·05	2·47	2·76	3·05	3·67	28
29	0·683	1·17	1·70	2·05	2·46	2·76	3·04	3·66	29
30	0·683	1·17	1·70	2·04	2·46	2·75	3·03	3·65	30
40	0·681	1·17	1·68	2·02	2·42	2·70	2·97	3·55	40
60	0·679	1·16	1·67	2·00	2·39	2·66	2·91	3·46	60
120	0·677	1·16	1·66	1·98	2·36	2·62	2·86	3·37	120
∞	0·674	1·15	1·64	1·96	2·24	2·58	2·81	3·29	∞

ϕ is the number of degrees of freedom.

The standard error divided into the main effects gives t with 8 degrees of freedom. Using Table 7, the percentage probability points are obtained. A minimum significance level of 5% is usually used.

Table 8 : Typical t-test Analysis

Treatment	Responses x_1	x_2	$(x_1-x_2)^2$	Main Effect	t	Probab-ility %	Effect
(1)	151	151	0	304.125			Mean Total
(a)	147	136	121	-19.625	8.2	0.1	A
(b)	147	139	64	-13.375	5.6	0.1	B
(ab)	101	108	49	- 7.125	3.0	1.5	AB
(c)	182	176	36	34.125	14.3	0.1	C
(ac)	159	168	81	4.375	1.8	10.0	AC
(bc)	173	176	9	9.125	3.8	0.5	BC
(abc)	158	161	9	7.375	3.0	1.5	ABC
Totals	2433		369				

F-test

In a two-level experiment, the main effects are uniquely defined. In three-(or more) level experiments, the main effects are represented by differences or comparisons between the means corresponding to different levels of the factors, and can be expressed in several ways. In such a situation the t-test cannot be used but is replaced by the F-test or Variance Ratio test.

The standard error divided into the main effects gives t with 8 degrees of freedom. Using Table 7, the percentage probability points are obtained. A minimum significance level of 5% is usually used.

Table 8 : Typical t-test Analysis

Treatment	Responses x_1	x_2	$(x_1-x_2)^2$	Main Effect	t	Probab -ility	Effect
(1)	151	151	0	304.125			Mean Total
(a)	147	136	121	-19.625	8.2	0.1	A
(b)	147	139	64	-13.375	5.6	0.1	B
(ab)	101	108	49	- 7.125	3.0	1.5	AB
(c)	182	176	36	34.125	14.3	0.1	C
(ac)	159	168	81	4.375	1.8	10.0	AC
(bc)	173	176	9	9.125	3.8	0.5	BC
(abc)	158	161	9	7.375	3.0	1.5	ABC
Totals	2433		369				

F-test

In a two-level experiment, the main effects are uniquely defined. In three-(or more) level experiments, the main effects are represented by differences or comparisons between the means corresponding to different levels of the factors, and can be expressed in several ways. In such a situation the t-test cannot be used but is replaced by the F-test or Variance Ratio test.

The distribution of the ratio of two estimates of variance obtained from two independent samples drawn from a normal universe is called the F-distribution. It depends only on ϕ_1 and ϕ_2, the number of degrees of freedom associated with the two estimates of variance.

The F-distribution is used to decide whether two independent estimates of variance can reasonably be accepted as being two estimatesof the variance of a single Normal distribution. The probability that two such independent estimates can have a particular ratio can be calculated and are tabulated in Table 9. The F-test can, however, be used for t-test situations, for example, in two-level experiments where it can be shown that $F = t^2$. The use of the F-test for two-level experiments only will be described, as multi-level designs are outside the scope of this report.

Returning to the definition of the main effect, it can be seen that the main effect is the difference between two treatments. In general for a 2^N experiment

Main Effect, A, $= \frac{1}{n}$ (sum of treatments with A high) − (sum of treatments with A low)

Let this be written as $A = \frac{1}{n} (X_1 - X_2)$

where n is equal to the number of observations contributing to X_1 and X_2.

The variance of $A = \frac{1}{n}$. Variance of $(X_1 - X_2)$

$$S_X^2 = \sum_{i=1}^{2} \frac{(X_i - \overline{X})^2}{(2 - 1)}$$

where $\overline{X}$ is the mean of treatment totals X_1 and X_2 and $(2 - 1)$ is the number of degrees of freedom.

Table 9

PROBABILITY POINTS OF THE VARIANCE RATIO (*F*-DISTRIBUTION)

Probability point	ϕ_2	ϕ_1 (corresponding to greater mean square)																	
		1	2	3	4	5	6	7	8	9	10	12	15	20	24	30	40	60	120	∞
0·1	1	39·9	49·5	53·6	55·8	57·2	58·2	58·9	59·4	59·9	60·2	60·7	61·2	61·7	62·0	62·3	62·5	62·8	63·1	63·3
0·05		161	199	216	225	230	234	237	239	241	242	244	246	248	249	250	251	252	253	254
0·01		4052	4999	5403	5625	5764	5859	5928	5982	6022	6056	6106	6157	6209	6235	6261	6287	6313	6339	6366
0·1	2	8·53	9·00	9·16	9·24	9·29	9·33	9·35	9·37	9·38	9·39	9·41	9·42	9·44	9·45	9·46	9·47	9·47	9·48	9·49
0·05		18·5	19·0	19·2	19·2	19·3	19·3	19·4	19·4	19·4	19·4	19·4	19·4	19·4	19·5	19·5	19·5	19·5	19·5	19·5
0·01		98·5	99·0	99·2	99·2	99·3	99·3	99·4	99·4	99·4	99·4	99·4	99·4	99·4	99·5	99·5	99·5	99·5	99·5	99·5
0·1	3	5·54	5·46	5·39	5·34	5·31	5·28	5·27	5·25	5·24	5·23	5·22	5·20	5·18	5·18	5·17	5·16	5·15	5·14	5·13
0·05		10·1	9·55	9·28	9·12	9·01	8·94	8·89	8·85	8·81	8·79	8·74	8·70	8·66	8·64	8·62	8·59	8·57	8·55	8·53
0·01		34·1	30·8	29·5	28·7	28·2	27·9	27·7	27·5	27·3	27·2	27·1	26·9	26·7	26·6	26·5	26·4	26·3	26·2	26·1
0·1	4	4·54	4·32	4·19	4·11	4·05	4·01	3·98	3·95	3·94	3·92	3·90	3·87	3·84	3·83	3·82	3·80	3·79	3·78	3·76
0·05		7·71	6·94	6·59	6·39	6·26	6·16	6·09	6·04	6·00	5·96	5·91	5·86	5·80	5·77	5·75	5·72	5·69	5·66	5·63
0·01		21·2	18·0	16·7	16·0	15·5	15·2	15·0	14·8	14·7	14·5	14·4	14·2	14·0	13·9	13·8	13·7	13·7	13·6	13·5
0·1	5	4·06	3·78	3·62	3·52	3·45	3·40	3·37	3·34	3·32	3·30	3·27	3·24	3·21	3·19	3·17	3·16	3·14	3·12	3·10
0·05		6·61	5·79	5·41	5·19	5·05	4·95	4·88	4·82	4·77	4·74	4·68	4·62	4·56	4·53	4·50	4·46	4·43	4·40	4·36
0·01		16·3	13·3	12·1	11·4	11·0	10·7	10·5	10·3	10·2	10·1	9·89	9·72	9·55	9·47	9·38	9·29	9·20	9·11	9·02
0·1	6	3·78	3·46	3·29	3·18	3·11	3·05	3·01	2·98	2·96	2·94	2·90	2·87	2·84	2·82	2·80	2·78	2·76	2·74	2·72
0·05		5·99	5·14	4·76	4·53	4·39	4·28	4·21	4·15	4·10	4·06	4·00	3·94	3·87	3·84	3·81	3·77	3·74	3·70	3·67
0·01		13·7	10·9	9·78	9·15	8·75	8·47	8·26	8·10	7·98	7·87	7·72	7·56	7·40	7·31	7·23	7·14	7·06	6·97	6·88
0·1	7	3·59	3·26	3·07	2·96	2·88	2·83	2·78	2·75	2·72	2·70	2·67	2·63	2·59	2·58	2·56	2·54	2·51	2·49	2·47
0·05		5·59	4·74	4·35	4·12	3·97	3·87	3·79	3·73	3·68	3·64	3·57	3·51	3·44	3·41	3·38	3·34	3·30	3·27	3·23
0·01		12·2	9·55	8·45	7·85	7·46	7·19	6·99	6·84	6·72	6·62	6·47	6·31	6·16	6·07	5·99	5·91	5·82	5·74	5·65
0·1	8	3·46	3·11	2·92	2·81	2·73	2·67	2·62	2·59	2·56	2·54	2·50	2·46	2·42	2·40	2·38	2·36	2·34	2·32	2·29
0·05		5·32	4·46	4·07	3·84	3·69	3·58	3·50	3·44	3·39	3·35	3·28	3·22	3·15	3·12	3·08	3·04	3·01	2·97	2·93
0·01		11·3	8·65	7·59	7·01	6·63	6·37	6·18	6·03	5·91	5·81	5·67	5·52	5·36	5·28	5·20	5·12	5·03	4·95	4·86
0·1	9	3·36	3·01	2·81	2·69	2·61	2·55	2·51	2·47	2·44	2·42	2·38	2·34	2·30	2·28	2·25	2·23	2·21	2·18	2·16
0·05		5·12	4·26	3·86	3·63	3·48	3·37	3·29	3·23	3·18	3·14	3·07	3·01	2·94	2·90	2·86	2·83	2·79	2·75	2·71
0·01		10·6	8·02	6·99	6·42	6·06	5·80	5·61	5·47	5·35	5·26	5·11	4·96	4·81	4·73	4·65	4·57	4·48	4·40	4·31
0·1	10	3·28	2·92	2·73	2·61	2·52	2·46	2·41	2·38	2·35	2·32	2·28	2·24	2·20	2·18	2·16	2·13	2·11	2·08	2·06
0·05		4·96	4·10	3·71	3·48	3·33	3·22	3·14	3·07	3·02	2·98	2·91	2·84	2·77	2·74	2·70	2·66	2·62	2·58	2·54
0·01		10·0	7·56	6·55	5·99	5·64	5·39	5·20	5·06	4·94	4·85	4·71	4·56	4·41	4·33	4·25	4·17	4·08	4·00	3·91
0·1	11	3·23	2·86	2·66	2·54	2·45	2·39	2·34	2·30	2·27	2·25	2·21	2·17	2·12	2·10	2·08	2·05	2·03	2·00	1·97
0·05		4·84	3·98	3·59	3·36	3·20	3·09	3·01	2·95	2·90	2·85	2·79	2·72	2·65	2·61	2·57	2·53	2·49	2·45	2·40
0·01		9·65	7·21	6·22	5·67	5·32	5·07	4·89	4·74	4·63	4·54	4·40	4·25	4·10	4·02	3·94	3·86	3·78	3·69	3·60
0·1	12	3·18	2·81	2·61	2·48	2·39	2·33	2·28	2·24	2·21	2·19	2·15	2·10	2·06	2·04	2·01	1·99	1·96	1·93	1·90
0·05		4·75	3·89	3·49	3·26	3·11	3·00	2·91	2·85	2·80	2·75	2·69	2·62	2·54	2·51	2·47	2·43	2·38	2·34	2·30
0·01		9·33	6·93	5·95	5·41	5·06	4·82	4·64	4·50	4·39	4·30	4·16	4·01	3·86	3·78	3·70	3·62	3·54	3·45	3·36
0·1	13	3·14	2·76	2·56	2·43	2·35	2·28	2·23	2·20	2·16	2·14	2·10	2·05	2·01	1·98	1·96	1·93	1·90	1·88	1·85
0·05		4·67	3·81	3·41	3·18	3·03	2·92	2·83	2·77	2·71	2·67	2·60	2·53	2·46	2·42	2·38	2·34	2·30	2·25	2·21
0·01		9·07	6·70	5·74	5·21	4·86	4·62	4·44	4·30	4·19	4·10	3·96	3·82	3·66	3·59	3·51	3·43	3·34	3·25	3·17
0·1	14	3·10	2·73	2·52	2·39	2·31	2·24	2·19	2·15	2·12	2·10	2·05	2·01	1·96	1·94	1·91	1·89	1·86	1·83	1·80
0·05		4·60	3·74	3·34	3·11	2·96	2·85	2·76	2·70	2·65	2·60	2·53	2·46	2·39	2·35	2·31	2·27	2·22	2·18	2·13
0·01		8·86	6·51	5·56	5·04	4·69	4·46	4·28	4·14	4·03	3·94	3·80	3·66	3·51	3·43	3·35	3·27	3·18	3·09	3·00
0·1	15	3·07	2·70	2·49	2·36	2·27	2·21	2·16	2·12	2·09	2·06	2·02	1·97	1·92	1·90	1·87	1·85	1·82	1·79	1·76
0·05		4·54	3·68	3·29	3·06	2·90	2·79	2·71	2·64	2·59	2·54	2·48	2·40	2·33	2·29	2·25	2·20	2·16	2·11	2·07
0·01		8·68	6·36	5·42	4·89	4·56	4·32	4·14	4·00	3·89	3·80	3·67	3·52	3·37	3·29	3·21	3·13	3·05	2·96	2·87
0·1	16	3·05	2·67	2·46	2·33	2·24	2·18	2·13	2·09	2·06	2·03	1·99	1·94	1·89	1·87	1·84	1·81	1·78	1·75	1·72
0·05		4·49	3·63	3·24	3·01	2·85	2·74	2·66	2·59	2·54	2·49	2·42	2·35	2·28	2·24	2·19	2·15	2·11	2·06	2·01
0·01		8·53	6·23	5·29	4·77	4·44	4·20	4·03	3·89	3·78	3·69	3·55	3·41	3·26	3·18	3·10	3·02	2·93	2·84	2·75
0·1	17	3·03	2·64	2·44	2·31	2·22	2·15	2·10	2·06	2·03	2·00	1·96	1·91	1·86	1·84	1·81	1·78	1·75	1·72	1·69
0·05		4·45	3·59	3·20	2·96	2·81	2·70	2·61	2·55	2·49	2·45	2·38	2·31	2·23	2·19	2·15	2·10	2·06	2·01	1·96
0·01		8·40	6·11	5·18	4·67	4·34	4·10	3·93	3·79	3·68	3·59	3·46	3·31	3·16	3·08	3·00	2·92	2·83	2·75	2·65
0·1	18	3·01	2·62	2·42	2·29	2·20	2·13	2·08	2·04	2·00	1·98	1·93	1·89	1·84	1·81	1·78	1·75	1·72	1·69	1·66
0·05		4·41	3·55	3·16	2·93	2·77	2·66	2·58	2·51	2·46	2·41	2·34	2·27	2·19	2·15	2·11	2·06	2·02	1·97	1·92
0·01		8·29	6·01	5·09	4·58	4·25	4·01	3·84	3·71	3·60	3·51	3·37	3·23	3·08	3·00	2·92	2·84	2·75	2·66	2·57

$$\therefore \quad S_A^2 = \sum_{i=1}^{2} \frac{(X_i - \bar{X})^2}{n(2-1)}$$

where n is the number of observations contributing to the treatment totals.

The term $\sum_{i=1}^{2} \frac{(X_i - \bar{X})^2}{n}$ is usually referred to as the sum of the squares.

The sum of the squares for each effect is calculated and the total sum of the squares (TSS) obtained. This is then compared with the corrected total of the sum of the squares (CTSS) i.e. the squared deviation of each response about their common mean. It is shown in Appendix ii that for a non-replicated experiment, the TSS should equal the CTSS and this is a useful check on the mathematics. In a replicated experiment, however, the TSS and CTSS will differ as the TSS will be calculated from the mean response for each treatment whereas the CTSS is calculated from each response. The difference between the TSS and CTSS in this case gives rise to an "error sum of the squares." The CTSS may be expressed mathematically by

$$\text{CTSS} = \sum_{i=1}^{N} (x_i - \bar{x})^2$$

where $\bar{x}$ is the mean of all responses

x_i is the i^{th} response

N is the number of responses

$$\text{CTSS} = \sum_{i=1}^{N} x_i^2 + \bar{x}^2 - 2x_i\bar{x}$$

$$= \sum x_i^2 - 2\sum x_i\bar{x} + N\bar{x}^2$$

$$= \sum x_i^2 - 2\sum x_i \sum \frac{x_i}{N} + N\left(\sum \frac{x_i}{N}\right)^2$$

$$= \sum x_i^2 - \frac{2(\sum x_i)^2}{N} + \frac{(\sum x_i)^2}{N}$$

$$= \sum x_i^2 - \frac{(\sum x_i)^2}{N} \qquad \ldots\ldots\ldots \text{ eqn (15)}$$

$$\therefore \quad S_A^2 = \sum_{i=1}^{2} \frac{(X_i - \bar{X})^2}{n(2-1)}$$

where n is the number of observations contributing to the treatment totals.

The term $\sum_{i=1}^{2} \frac{(X_i - \bar{X})^2}{n}$ is usually referred to as the sum of the squares.

The sum of the squares for each effect is calculated and the total sum of the squares (TSS) obtained. This is then compared with the corrected total of the sum of the squares (CTSS) i.e. the squared deviation of each response about their common mean. It is shown in Appendix ii that for a non-replicated experiment, the TSS should equal the CTSS and this is a useful check on the mathematics. In a replicated experiment, however, the TSS and CTSS will differ as the TSS will be calculated from the mean response for each treatment whereas the CTSS is calculated from each response. The difference between the TSS and CTSS in this case gives rise to an "error sum of the squares." The CTSS may be expressed mathematically by

$$\text{CTSS} = \sum_{i=1}^{N} (x_i - \bar{x})^2$$

where $\bar{x}$ is the mean of all responses

x_i is the i^{th} response

N is the number of responses

$$\text{CTSS} = \sum_{i=1}^{N} x_i^2 + \bar{x}^2 - 2x_i\bar{x}$$

$$= \sum x_i^2 - 2\sum x_i\bar{x} + N\bar{x}^2$$

$$= \sum x_i^2 - 2\sum x_i \sum \frac{x_i}{N} + N\left(\sum \frac{x_i}{N}\right)^2$$

$$= \sum x_i^2 - \frac{2(\sum x_i)^2}{N} + \frac{(\sum x_i)^2}{N}$$

$$= \sum x_i^2 - \frac{(\sum x_i)^2}{N} \qquad \ldots\ldots\ldots \text{ eqn (15)}$$

i.e. CTSS is equal to the sum of the squares of the observations minus the sum of all the observations squared, divided by the number of observations. Use of equation (15) enables the CTSS to be calculated quickly.

Having calculated the sum of the squares and error sum of the squares the mean squares or variances of each effect are obtained by dividing the sum of the squares by the number of degrees of freedom. In two-level experiments each effect has (2-1) degrees of freedom and therefore the sum of the squares is equal to the mean square. The number of degrees of freedom of the error mean square is the difference between the degrees of freedom of the CTSS and TSS. The CTSS has (N-1) degrees of freedom where N is the total number of observations e.g. 16 in a fully replicated 2^3 design. The degrees of freedom of the TSS is the sum of the degrees of freedom of each effect e.g. in 2^3 design there are (2^3 - 1) effects each having (2-1) degrees of freedom. The TSS in this case would thus have seven degrees of freedom. The number of degrees of freedom of the error variance is therefore (16 - 1) - 7 = 8.

Finally, the variance, s^2, of the effects is compared with the error variance, s_E^2, by the F-test. As mentioned earlier, this gives the probability that the two variances are independent estimates of the variance, σ^2, of the effects. The F values are given in Table 9. For example, for effect A having estimated variance (mean square) s_A^2, the F value would be

$$F = \frac{s_A^2 \text{ for } \phi_n \text{ degrees of freedom}}{s_E^2 \text{ for } \phi_d \text{ degrees of freedom}}$$

From Table 9, the F values for ϕ_n and ϕ_d degrees of freedom are compared with that obtained and the percentage probability points obtained. Table 10 shows the results of Table 6 analysed using the F-test. To avoid calculation of the F values of each effect, the mean squares corresponding to the 1%, 5% and 10% significance levels may be found by multiplying the appropriate F values for ϕ_n and ϕ_d degrees of freedom by the error variance s_E^2. The mean squares of the effects may then be compared with the mean squares for the 1%, 5% and 10% probability points.

Table 10 : F-test Analysis

Treatment	Responses		Main Effect	Degrees of Freedom	Sum of Squares = Mean Square
(1)	151	151	304.125		
(a)	147	136	-19.625	1	1,540.5
(b)	147	139	-13.375	1	715.5
(ab)	101	108	- 7.125	1	203.0
(c)	182	176	34.125	1	4,658.0
(ac)	159	168	4.375	1	76.5
(bc)	173	176	9.125	1	333.0
(abc)	158	161	7.375	1	217.5
Totals	2433				7,744.0

Corrected Total of the Sum of the Squares = 7,928.9

Error variance = (7928.9 - 7744.0)/8

= 23.0625

Using Table 9

1% significance level = Error variance x 11.3

= 260.6

5% significance level = Error variance x 5.32

= 122.6

10% significance level = Error variance x 3.46

= 79.7

Comparison of these significance levels with the mean squares of the effects shown in Table 10, shows that effects A, B, C, BC, are highly significant at less than the 1% level. The significance levels of effects AB, and ABC are between 1% and 5%. The probability point of AC is 10%. It can be seen that these results are in line with those given in Table 8.

Estimation of Error Variance from Interactions

If only one response for each treatment is obtained then as mentioned previously the TSS and CTSS are equal and cannot therefore be used to give one estimation of the error. However, if the designer has some previous knowledge of the experiments then it may be possible to eliminate the likelihood of some of the interactions being present. If this is the case, then these interactions may be used to give an estimate of the error mean square. This is done in the following way.

Consider a 2^3 design where all interactions are assumed not to be present. The sum of the squares for all treatments is found in the usual way. The sum of the interaction sum of the squares is then obtained and divided by their total degrees of freedom. The result may be used as the error mean square.

e.g. $\frac{\text{Sum of Squares (AB, AC, BC, ABC)}}{\text{4 degrees of freedom}}$ = Error Mean Square

Care must be taken when using this method, as the error mean square is sensitive to the number of interactions used in the calculations. Obviously, the more interactions used, the more reliable is the error estimate.

Computer Programme for Two-level Designs

A flow chart and the programme are given in Appendix iii. The programme can handle 2-level, 2, 3- or 4-factor experiments. Significance testing is done by use of the F-test and for fully replicated experiments, the 1%, 5% and 10% significance levels are given.

The procedure of the programme is similar to that which would be used if all calculations were being performed manually. Main effects are obtained by use of the sign matrix (see Table 5) discussed earlier. The mean squares, equal to the sum of the squares for two-level experiments, are however, obtained by the following relationship. It can be shown that for two-level designs

$$\text{Mean Square} = M \times 2^{n-1} (\text{Effect})^2$$

where n is the number of factors

and M is the number of replications.

The results of Table 6 have been analysed using the programme and are given in Table 3 (i).

If a computer or desk calculator are not available for computation of the main effects and variances, then a useful tabular method designed by Yates can be used. The reader is referred to the bibliography for further information on the method.

If a computer or desk calculator are not available for computation of the main effects and variances, then a useful tabular method designed by Yates can be used. The reader is referred to the bibliography for further information on the method.

Bibliography

(1) O.L. Davies, "Design and Analysis of Industrial Experiments", Oliver and Boyd, 1954.

(2) N.E. Duckworth, "Statistical Techniques in Technological Research" Methuen and Co. Ltd., 1968.

(3) O.L. Davies, "Statistical Methods in Research and Production", Oliver and Boyd, 1961.

Results used for Tables 6, 8 and 10 are taken from reference 2 given above.

Appendix i

Variance and Covariance

Consider that two quantities x_1 and x_2 are measured, and a third quantity X is given by

$$X = ax_1 \pm bx_2$$

Suppose that a number of observations of x_1 and x_2, and hence of X, are made and the means taken.

$$u = au_1 \pm bu_2$$

where u_1 is the mean of observations of x_1

u_2 " " " " " " x_2

and u " " " " " " X.

Let δx be the deviation of an observation from its mean.

$$\delta X = a\delta x_1 \pm b\delta x_2$$

$$(\delta X)^2 = a^2(\delta x_1)^2 + b^2(\delta x_2)^2 \pm 2ab\delta x_1 o x_2$$

The mean of $(\delta x_1)^2$ over all observations is the variance $V(x_1)$.

$$V(X) = a^2V(x_1) + b^2V(x_2) \pm 2ab.\text{cov } \delta x_1\delta x_2$$

The quantity cov $\delta x_1\delta x_2$ is the coveriance and is defined as $\sum \delta x_1\delta x_2/N$ where N is the number of observations. The covariance is the measure of the degree of correlation between the variables x_1 and x_2. If the variables are independent of each other ie. a variation of x_1 has no effect on x_2, then the covariance is Zero. In such a case, the variance V(X) is given by

$$\underline{V(X) = a^2V(x_1) + b^2V(x_2)}$$

Appendix ii

Relation between TSS and CTSS for Non-duplicated Experiments

Consider a 2^2 design with factors A and B.

Sum of the Squares of A = $\frac{[(a + ab) - \bar{X}]^2}{2} + \frac{[(1 + b) - \bar{X}]^2}{2}$

where $\bar{X} = (1 + a + b + ab)/2 = T/2$

Sum of the Squares of A = $\frac{(a + ab)^2 + (1 + b)^2}{2} - \frac{T^2}{4}$

Similarly

Sum of the Squares of B = $\frac{(ab + b)^2 + (1 + a)^2}{2} - \frac{T^2}{4}$

Sum of the Squares of AB = $\frac{(1 + ab)^2 + (a + b)^2}{2} - \frac{T^2}{4}$

$TSS = SS_A + SS_B + SS_{AB}$

$$TSS = \frac{1}{2}\left[3(1^2 + a^2 + b^2 + ab^2) - 2(1a + 1b + aab + bab + 1ab + ab) - \frac{3T^2}{2}\right]$$

Now $T^2 = (1 + a + b + ab)^2$

$$= (1^2 + a^2 + b^2 + ab^2) + 2(1a + 1b + aab + bab + 1ab + ab)$$

$$TSS = \frac{1}{2}\left[2(1^2 + a^2 + b^2 + ab^2) + T^2 - \frac{3T^2}{2}\right]$$

$$TSS = (1^2 + a^2 + b^2 + ab^2) - \frac{T^2}{4} \qquad \ldots\ldots \text{ eqn (a)}$$

From a comparison of equation (a) and equation (15) it can be seen that the TSS is equal to the CTSS for non-replicated experiments.

Appendix (iii)

Flow Chart for Computer Programme

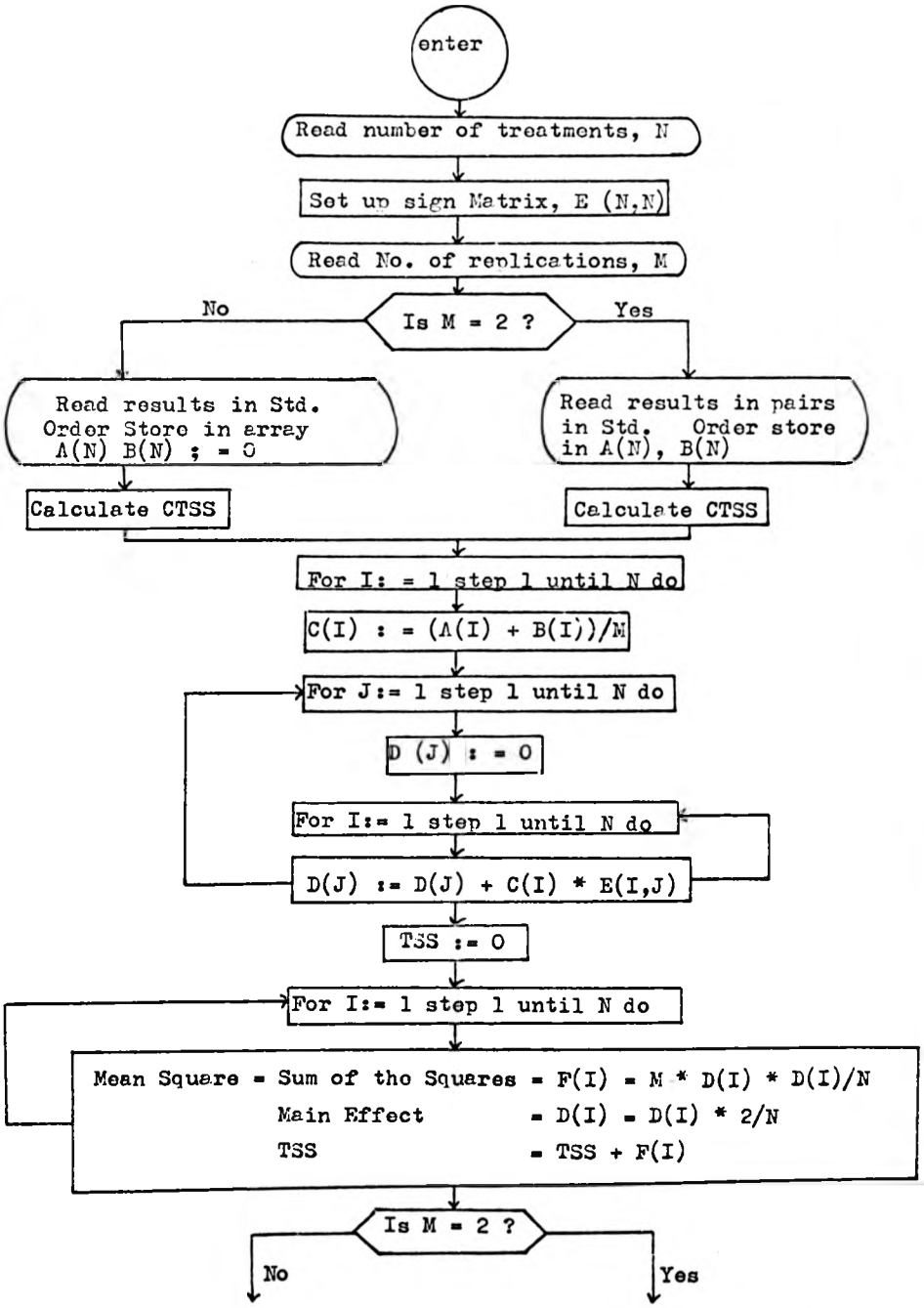

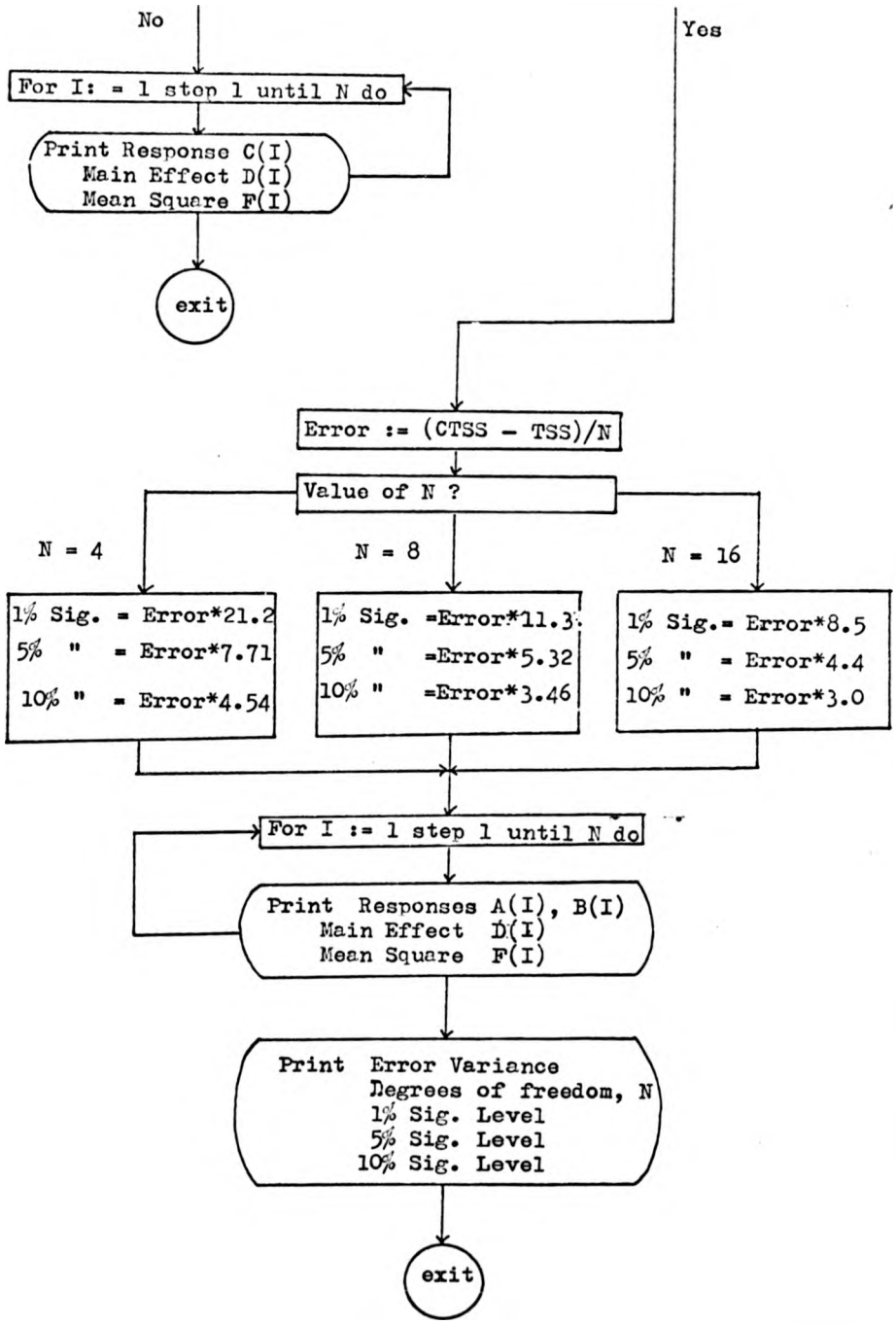
No
Yes
For I: = 1 step 1 until N do
Print Response C(I)
Main Effect D(I)
Mean Square F(I)
exit
Error := (CTSS - TSS)/N
Value of N ?
N = 4
N = 8
N = 16
1% Sig. = Error*21.2
5% " = Error*7.71
10% " = Error*4.54
1% Sig. =Error*11.3
5% " =Error*5.32
10% " =Error*3.46
1% Sig.= Error*8.5
5% " = Error*4.4
10% " = Error*3.0
For I := 1 step 1 until N do
Print Responses A(I), B(I)
Main Effect D(I)
Mean Square F(I)
Print Error Variance
Degrees of freedom, N
1% Sig. Level
5% Sig. Level
10% Sig. Level
exit

Computer Programme for Factorial Analysis

```
&NOS;      ES/A108/AB;

&ALGOL;

&LIST;

STATISTICS;
"BEGIN"
"INTEGER" N,M,J,I;
"REAL" TOTAL,TSS,CTSS,ERROR,SIG1,SIG2,SIG3;
"READ" N,M;
"COMMENT"    N IS NUMBER OF TREATMENT COMBINATIONS
             M IS NUMBER OF REPLICATIONS
             IF M=2 READ IN RESULTS IN PAIRS IN STANDARD
             ORDER
             IF M=1 READ IN RESULTS IN STANDARD ORDER;
"BEGIN"
"ARRAY"A,B,C,D,F[1:N];
"INTEGER" "ARRAY" E[1:N,1:N];
TOTAL:=0;CTSS:=0;
SCALED(6); SAMELINE;
"FOR"I:=1"STEP"1"UNTIL"N"DO"
"BEGIN" "IF" M=2 "THEN"
"READ" A[I];
B[I]:=0;
"END";
"END";
"FOR" I:=1 "STEP" 1 "UNTIL" N "DO"
"BEGIN"
C[I]:= (A[I]+B[I])/M;
TOTAL:= A[I]+B[I]+TOTAL;
CTSS:= CTSS+A[I]*A[I]+B[I]*B[I];
"END";
CTSS:= CTSS-TOTAL*TOTAL/(N*M);
"IF" N "GE" 4 "THEN"
"BEGIN"
"FOR" I:=1 "STEP" 1 "UNTIL" N "DO"
"BEGIN"
E[I,1]:=1;
"END";
E[1,2]:=-1;E[2,2]:=1;E[3,2]:=-1;E[4,2]:=1;
E[1,3]:=-1;E[2,3]:=-1;E[3,3]:=1;E[4,3]:=1;
"FOR"I:=1"STEP"1"UNTIL"4"DO"
"BEGIN"
E[1,4]:=E[I,2]*E[I,3];
"END"
"END" "ELSE""GOTO"FINISH;
"IF"N"GE"8"THEN"
"BEGIN"
E[5,2]:=-1;E[6,2]:=1;E[7,2]:=-1;E[8,2]:=1;
E[5,3]:=-1;E[6,3]:=-1;E[7,3]:=1;E[8,3]:=1;
```

```
C[I,1]:=-1;C[I,2]:=-1;C[I,3]:=-1;C[I,4]:=-1;
C[I,5]:=1;C[I,6]:=1;C[I,7]:=1;C[I,8]:=1;
"FOR"I:=5"STEP"1"UNTIL"8"DO"
"BEGIN"
C[I,4]:=C[I,2]*C[I,3];
"END";
"FOR"I:=1"STEP"1"UNTIL"8"DO"
"BEGIN"
C[I,6]:=C[I,2]*C[I,4];
C[I,7]:=C[I,3]*C[I,5];
C[I,8]:=C[I,2]*C[I,3]*C[I,5];
"END"
"END"
"GLOBAL""GOTO"SWITCH;
"IF"Y=16"THEN"
"BEGIN"
C[9,2]:=-1;C[10,2]:=1;C[11,2]:=-1;C[12,2]:=1;
C[13,2]:=-1;C[14,2]:=1;C[15,2]:=-1;C[16,2]:=1;
C[9,3]:=-1;C[10,3]:=-1;C[11,3]:=1;C[12,3]:=1;
C[13,3]:=-1;C[14,3]:=-1;C[15,3]:=1;C[16,3]:=1;
C[9,5]:=-1;C[10,5]:=-1;C[11,5]:=-1;C[12,5]:=-1;
C[13,5]:=1;C[14,5]:=1;C[15,5]:=1;C[16,5]:=1;
"FOR"I:=9"STEP"1"UNTIL"16"DO"
"BEGIN"
C[I,6]:=C[I,2]*C[I,3];
C[I,7]:=C[I,2]*C[I,5];
C[I,8]:=C[I,3]*C[I,5];
C[I,9]:=C[I,2]*C[I,3]*C[I,5];
C[I,9]:=1;
"END";
"FOR"I:=1"STEP"1"UNTIL"8"DO"
"BEGIN"
C[I,9]:=-1;
"END";
"FOR"I:=1"STEP"1"UNTIL"16"DO"
"BEGIN"
C[I,10]:=C[I,2]*C[I,9];
C[I,11]:=C[I,3]*C[I,9];
C[I,12]:=C[I,4]*C[I,3]*C[I,9];
C[I,13]:=C[I,5]*C[I,9];
C[I,14]:=C[I,2]*C[I,5]*C[I,9];
C[I,15]:=C[I,3]*C[I,5]*C[I,9];
C[I,16]:=C[I,2]*C[I,3]*C[I,5]*C[I,9];
"END"
"END"
"GLOBAL""GOTO"SWITCH;
SWITCH:="PAINT" //565\PAIN EFFECT/520\MEAN SQUARE/LAA;
"FOR"J:=1"STEP"1"UNTIL"N"DO"
"BEGIN"
D[J]:=0;
"FOR"I:=1"STEP"1"UNTIL"M"DO"
"BEGIN"
D[J]:=D[J]+C[I]*E[I,J];
"END"
"END";
TSS:=0;
```

```
"FOR"I:=1"STEP"1"UNTIL"N"DO"
"BEGIN"
F[I]:=F*D[I]*D[I]/N;
D[I]:=D[I]**2/N;
TSS:=TSS+F[I];
"IF" I=N "THEN"
"PRINT" A[I],///320\\,B[I],///320\\,D[I],///320\\,F[I],///L3\\
"ELSE" "PRINT" ///532\\,A[I],///320\\,D[I],///320\\,F[I],///L3\\;
"END";
TSS:= TSS-F[I];
ERROR:=ABS(CTSS-TSS)/N;
"IF"I=2 "THEN"
"BEGIN"
"PRINT"/ERROR MEAN SQUARE= \,ERROR,///L\\,//DEGREES OF
FREEDOM= \,N,///L\\;
"END"
"ELSE""GOTO"FINISH;
"IF" N=4 "THEN"
"BEGIN"
SIG1:=ERROR*21.2;
SIG2:=ERROR*7.71;
SIG3:=ERROR*4.54;
"END"
"ELSE"
"IF" N=8 "THEN"
"BEGIN"
SIG1:=ERROR*11.3;
SIG2:=ERROR*5.32;
SIG3:=ERROR*3.46;
"END"
"ELSE"
"IF" N=10 "THEN"
"BEGIN"
SIG1:=ERROR*8.53;
SIG2:=ERROR*4.49;
SIG3:=ERROR*3.09;
"END";
"PRINT"/SIGNIFICANCE LEVEL AT 1 PER CENT= \,SIG1,///L\\,
       /SIGNIFICANCE LEVEL AT 5 PER CENT= \,SIG2,///L\\,
       /SIGNIFICANCE LEVEL AT 10PER CENT= \,SIG3,///L\\;
"PRINT" CTSS,///L\\,TSS,///L\\;
FINISH:"END";
"END";
```

Table 3(i): Computer Analysis of the results given in Table 6

		MAIN EFFECT	MEAN SQUARE
$1.51000_{10}+02$	$1.51000_{10}+02$	$3.04125_{10}+02$	$3,69968_{10}+05$
$1.47000_{10}+02$	$1.36000_{10}+02$	$-1.96250_{10}+01$	$1,54056_{10}+03$
$1.47000_{10}+02$	$1.39000_{10}+02$	$-1.33750_{10}+01$	$7,15562_{10}+02$
$1.01000_{10}+02$	$1.08000_{10}+02$	$-7.12500_{10}+00$	$2,03062_{10}+02$
$1.82000_{10}+02$	$1.76000_{10}+02$	$3.41250_{10}+01$	$4,65806_{10}+03$
$1.59000_{10}+02$	$1.68000_{10}+02$	$4.37500_{10}+00$	$7,65625_{10}+01$
$1.73000_{10}+02$	$1.76000_{10}+02$	$9.12500_{10}+00$	$3,33062_{10}+02$
$1.58000_{10}+02$	$1.61000_{10}+02$	$7.37500_{10}+00$	$2,17562_{10}+02$

ERROR MEAN SQUARE= $2.30625_{10}+01$
DEGREES OF FREEDOM= 8
SIGNIFICANCE LEVEL AT 1 PER CENT= $2.60606_{10}+02$
SIGNIFICANCE LEVEL AT 5 PER CENT= $1.22692_{10}+02$
SIGNIFICANCE LEVEL AT 10 PER CENT= $7.97963_{10}+01$
$7.92894_{10}+03$
$7.74444_{10}+03$

PATENTS FORM NO. 3 APPENDIX 3 12608

PATENTS ACT 1949

COMPLETE SPECIFICATION

5342/72
4th February, 1972

METHOD FOR DEPOSITING MATERIAL ON SELECTED AREAS OF A SURFACE

We, NATIONAL RESEARCH DEVELOPMENT CORPORATION, a British Corporation established by Statute, of Kingsgate House, 66 - 74 Victoria Street, London, S.W.1, do hereby declare the invention for which we pray that a patent may be granted to us, and the method by which it is to be performed, to be particularly described in and by the following statement:-

The present invention relates to a method of forming a layer of a material in selected areas on a surface of the same or a different material, and to articles made by the method. The method is particularly but not exclusively useful in the fabrication of lumped components for microwave integrated circuits.

In such circuits components must be small compared to a wavelength, and for this reason a substrate with a low dielectric constant is chosen, for example quartz. The dielectric most commonly used in silicon dioxide SiO_2 because it is a low loss material. Obviously, as the dielectric and substrate are of the same material, etching of the dielectric will result in etching of the substrate thus preventing the dielectric area from being formed using conventional photolithographic techniques.

In low frequency circuit techniques, this problem can be overcome by depositing the dielectric through an out-of-contact metal mask which defines the dielectric area. For microwave integrated circuits, the required dielectric area is too small to be defined by a metal mask, the typical dimensions of a 1pF capacitor being 100 microns (μm) by 300μm. To deposit dielectric over an area of this size use can be made of a negative relief mask; that is a mask which forms a fairly thick covering in a shape which is the complement of the area of the required deposition.

If such a mask is made of photoresist any remaining particles of underdeveloped resist cause pinholes in the dielectric. This is, of course, disastrous in capacitor fabrication as a direct

short between electrodes results. It has also generally been found that the adhesion of films is impaired where photoresist once existed.

Alternatively, if such a mask is made of metal it can be made in two ways.

By depositing a thick layer of metal and then etching the required pattern. This results in severe undercutting of the metal, leading to poorly defined dielectric areas; or by depositing a thin layer of metal, etching the required pattern, and then plating to the required thickness. This virtually eliminates undercutting thus improving the area definition. However, plating up to the metal mask will also involve plating up of the connection to the lower electrode of a capacitor.

For these reasons, it can be seen that both photoresist relief masks and metal relief masks have severe disadvantages.

According to the present invention there is provided a method of depositing material in a selected area on a surface, including depositing a protective layer over, and in contact with, a surface which includes the area on which a material is to be deposited, the material of the protective layer having an etchant which does not attack the material or materials of the surface, depositing a layer of photoresist over the protective layer, exposing and developing the photoresist to provide a mask which is the complement of the said selected area, etching away that part of the protective layer revealed after developing the photoresist, depositing over that part of the said surface revealed after etching the protective

short between electrodes results. It has also generally been found that the adhesion of films is impaired where photoresist once existed.

Alternatively, if such a mask is made of metal it can be made in two ways.

By depositing a thick layer of metal and then etching the required pattern. This results in severe undercutting of the metal, leading to poorly defined dielectric areas; or by depositing a thin layer of metal, etching the required pattern, and then plating to the required thickness. This virtually eliminates undercutting thus improving the area definition. However, plating up to the metal mask will also involve plating up of the connection to the lower electrode of a capacitor.

For these reasons, it can be seen that both photoresist relief masks and metal relief masks have severe disadvantages.

According to the present invention there is provided a method of depositing material in a selected area on a surface, including depositing a protective layer over, and in contact with, a surface which includes the area on which a material is to be deposited, the material of the protective layer having an etchant which does not attack the material or materials of the surface, depositing a layer of photoresist over the protective layer, exposing and developing the photoresist to provide a mask which is the complement of the said selected area, etching away that part of the protective layer revealed after developing the photoresist, depositing over that part of the said surface revealed after etching the protective

layer, a layer of that material, which it is required to deposition the selected area, removing the remaining photoresist, and etching away the remaining part of the protective layer.

The invention also extends to articles such as integrated circuits, thin film components, including thin film capacitors, made using the method of the preceding paragraph.

Since the material deposited on the selected areas is not etched, a material can be deposited in these areas on a surface of the same material, or a material can be deposited for which no suitable etchant exists. Since the photoresist is applied over the protective layer it is entirely removed in the selected areas before the material is deposited and no pinholes can form. Further, undercutting is avoided, as is plating up of the connection to the lower electrode in capacitor fabrication.

The material deposited adheres well to the surface since the photoresist has not been in contact with the surface, and there is no undercutting of the deposited material. In fact by varying the thickness of the protective layer deposit ed and varying the time for etching the parts of the protective layer away in forming the mask, the edge profile of the material deposited can be controlled. The method of achieving such control will be described in more detail later.

Additionally, since an out-of-contact mask is not used, definition is improved.

The protective layer may for example be copper, aluminium, chromium, gold or any material whose etchant does not attack the

photoresist or, in fabricating a capacitor a lower metal electrode which is deposited before the protective layer to form one electrode of the capacitor.

When making microwave capacitors suitable dielectric materials include Silicon Dioxide (SiO_2), Silicon Monoxide, Alumina (Al_2O_3), Yttrium Oxide, Silicon Nitride, and Tantalum Pentoxide (Ta_2O_5). Suitable substrates include Quartz (SiO_2), Alumina, Sapphire, ferrite and glass. The electrodes may for example be copper, gold, aluminium, silver or tantalum.

When the electrodes are gold and the metal mask is copper the etchant for the copper may be Ferric Chloride.

The following photoresists may, for example, be used: Shipley positive types AZ 111, AZ 340, AZ 1350 or AZ 1350H; or Kodark negative types KPR, KRP 2, KPR 3, KMER, KOR and KTFR.

Certain embodiments of the invention will now be described by way of example with reference to the accompanying drawings, in which:-

Figures 1(a) and 1(b) are plan and cross-sectional views of the lower electrode of a thin film capacitor deposited on a substrate,

Figures 2(a) and 2(b) are plan and cross-sectional views after a metal layer has been deposited in making the capacitor using the method of the present invention,

Figures 3(a) and 3(b) are plan and cross-sectional views after photoresist has been applied to the copper layer and has been exposed and developed,

Figures 4(a) and 4(b) are plan and cross-sectional views after the metal layer has been etched away where revealed by the development of the photoresist,

Figures 5(a) and 5(b) are plan and cross-sectional views after a layer of dielectric has been deposited,

Figures 6(a) and 6(b) are plan and cross-sectional views after the remaining photoresist and copper has been removed,

Figures 7(a) and 7(b) are plan and cross-sectional views after the upper electrode of the capacitor has been deposited, and

Figures 8(a), 8(b), 9(a) and 9(b) are cross-sectional views illustrating how material can be deposited using the method according to the present invention to give a desired edge profile to the material deposited.

In the above mentioned figures the vertical scale is enlarged relative to the horizontal scale in order to show detail clearly.

In Figures 1(a) and 1(b) the lower gold electrode 10 of a capacitor to be fabricated has already been deposited on a quartz substrate 11 using a conventional photolithographic technique. Such techniques are described in "An Introduction to Photofabrication using Kodak Photosensitive Resists", Kodak publication No.P-79. The materials used are a chromium seed layer 500Å thick, and gold 0.5μm thick. The etches used are chromium: 50 grams potassium ferrocyanide, 15 grams sodium hydroxide and 200 cc water; and gold: solution of iodine in potassium iodide.

A protective layer 12 of copper one μm thick is then deposited by evaporation at 10^{-6} torr over the whole surface of the substrate 11

and the gold electrode 10, the result being as shown in Figures 2(a) and 2(b).

Next a layer of photoresist 13, typically 20μm thick but varying between 10 and 30μm depending on the thickness of silicon oxide to be deposited, and the area to be covered, is applied over the copper layer 12 by dip coating. After allowing the volatile solvents in the photoresist to evaporate by leaving for ten minutes, the substrate, gold electrode and photoresist are baked at 70°C for twenty minutes. The photoresist is then exposed for ten minutes through an optical mask and developed [see Figures 3(a) and 3(b)] for five minutes in Shipley AZ 303 developer, diluted one part to four parts water. The exposure is such that the part of the photoresist remaining after development is the complement or "negative" of the areas where the dielectric is to be deposited. A suitable photoresist is Shipley positive AZ 111. After development the remaining photoresist is baked at 70°C for thirty minutes. The copper is then etched away at room temperature where revealed through the development of the photoresist. This etch is carried out for ninety seconds and gives the negative relief mask of Figures 4(a) and 4(b). The etchant used is 0.05 gms of ferric chloride per cubic centimetre of water.

A one μm layer of silicon dioxide 14, the dielectric for the capacitor, is now deposited by sputtering at 5×10^{-3} torr in 99.995% pure Argon at 20°C to give the situation shown in Figures 5(a) and 5(b). Then the remaining photoresist is removed by soaking in acetone with gentle agitation, and the remaining copper

is etched away in ferric chloride with the result shown in Figures 6(a) and 6(b). Lastly another gold contact 15, 0.5μm thick, is deposited using a conventional photolithographic technique as mentioned in connection with electrode 10 [see Figures 7(a) and 7(b)]. The contact 15 and the unprotected area of lower electrode 10 are then electroplated to 3μm.

One further advantage of the above method is that some control over the edge profile of the material deposited is possible. For example if the copper layer is say 1μm thick and it is etched, as described above, prior to deposition of the dielectric for a comparatively short time, say 90 seconds, then only a small amount of undercutting occurs (see Figure 8(a)) and the edge profile as shown at 16 in Figure 8(b) is nearly vertical. For a longer etching time, say 120 seconds, then more undercutting occurs Figures 9(a) and 9(b) with the result that the edge profile 17 is inclined to the vertical. A dielectric edge profile as shown in Figure 9(b) substantially avoids the possibility of a discontinuity in the upper electrode at the point where it passes over an abrupt step at the edge of the dielectric layer.

is etched away in ferric chloride with the result shown in Figures 6(a) and 6(b). Lastly another gold contact 15, 0.5μm thick, is deposited using a conventional photolithographic technique as mentioned in connection with electrode 10 [see Figures 7(a) and 7(b)]. The contact 15 and the unprotected area of lower electrode 10 are then electroplated to 3μm.

One further advantage of the above method is that some control over the edge profile of the material deposited is possible. For example if the copper layer is say 1μm thick and it is etched, as described above, prior to deposition of the dielectric for a comparatively short time, say 90 seconds, then only a small amount of undercutting occurs (see Figure 8(a)) and the edge profile as shown at 16 in Figure 8(b) is nearly vertical. For a longer etching time, say 120 seconds, then more undercutting occurs Figures 9(a) and 9(b) with the result that the edge profile 17 is inclined to the vertical. A dielectric edge profile as shown in Figure 9(b) substantially avoids the possibility of a discontinuity in the upper electrode at the point where it passes over an abrupt step at the edge of the dielectric layer.

is etched away in ferric chloride with the result shown in Figures 6(a) and 6(b). Lastly another gold contact 15, 0.5μm thick, is deposited using a conventional photolithographic technique as mentioned in connection with electrode 10 [see Figures 7(a) and 7(b)]. The contact 15 and the unprotected area of lower electrode 10 are then electroplated to 3μm.

One further advantage of the above method is that some control over the edge profile of the material deposited is possible. For example if the copper layer is say 1μm thick and it is etched, as described above, prior to deposition of the dielectric for a comparatively short time, say 90 seconds, then only a small amount of undercutting occurs (see Figure 8(a)) and the edge profile as shown at 16 in Figure 8(b) is nearly vertical. For a longer etching time, say 120 seconds, then more undercutting occurs Figures 9(a) and 9(b) with the result that the edge profile 17 is inclined to the vertical. A dielectric edge profile as shown in Figure 9(b) substantially avoids the possibility of a discontinuity in the upper electrode at the point where it passes over an abrupt step at the edge of the dielectric layer.

WHAT WE CLAIM IS:-

1. A method of depositing material in a selected area on a surface, including depositing a protective layer over, and in contact with, a surface which includes the area on which a material is to be deposited, the material of the protective layer having an etchant which does not attack the material or materials of the surface, depositing a layer of photoresist over the protective layer, exposing and developing the photoresist to provide a mask which is the complement of the said selected area, etching away that part of the protective layer revealed after developing the photoresist, depositing over that part of the said surface revealed after etching the protective layer, a layer of that material, which it is required to deposit on the selected area, removing the remaining photoresist, and etching away the remaining part of the protective layer, the method being such that the material which it is required to deposit is deposited on the surface in the selected area only.

2. A method of depositing material in selected areas on a surface, including depositing a protective layer over a surface of a substrate which includes areas on which a material is to be deposited, the material of the protective layer having an etchant which does not attack the material or materials of the surface, depositing a layer of photoresist over the protective layer, exposing and developing the photoresist to provide a mask which is the complement of the said selected areas, etching away that part of the protective layer revealed after developing the photoresist, depositing, by other

than electrodeposition, over the photoresist mask and the revealed part of the surface, a layer of that material, which it is required to deposit on the selected areas, removing the remaining photoresist and etching away the remaining part of the protective layer, the method being such that the material which it is required to deposit is deposited on the surface in the said selected areas only.

3. A method of depositing electrically non-conducting material in a selected area on a surface, including depositing a protective layer over a surface which includes the area on which the electrically non-conducting material is to be deposited, the material of the protective layer having an etchant which does not attack the material or materials of the surface, depositing a layer of photoresist over the protective layer, exposing and developing the photoresist to provide a mask which is the complement of the said selected area, etching away that part of the protective layer revealed after developing the photoresist, depositing over that part of the said surface revealed after etching the protective layer, a layer of the electrically non-conducting material, removing the remaining photoresist, and etching away the remaining part of the protective layer, the method being such that the electrically non-conducting material is deposited on the surface in the said selected area only.

4. A method of making one or more capacitors according to any preceding claim wherein the material which is deposited on the said selected area or areas is a dielectric material, including forming a first electrode or electrodes by depositing an area or areas of conducting material within, or extending into, the selected area or

areas before the protective layer is deposited, and depositing another area or areas of the said conducting material or another conducting material over the dielectric material after the photoresist and the protective layer have been removed to form a second electrode or electrodes, the said conducting material being a different material from the material of the protective layer and one which is not etched by at least one etchant for the material of the protective layer.

5. A method according to any preceding claim wherein the protective layer includes at least one of the following: copper, aluminium, chromium, nichrome, nickel, and gold.

6. A method according to any preceding claim wherein the material which is deposited on the said selected area or areas includes at least one of the following: silicon dioxide, silicon monoxide, alumina, yttrium oxide, silicon nitride, and tantalum pentoxide.

7. A method according to any preceding claim wherein the material forming the said surface includes quartz or alumina, or sapphire, ferrite or glass.

8. A method according to Claim 5 or 6 or 7 insofar as dependent on Claim 4, wherein the, or one of the, conducting materials is copper, or gold, or aluminium, or silver or tantalum.

9. A method according to any preceding claim wherein the photoresist is of a type which requires hardening before part of the protective layer is etched away, including the step of baking the photoresist for a time and at a temperature sufficient to ensure it

is not wholly or partially removed when the said part of the protective layer is etched away.

10. A method according to any preceding claim wherein the etching away of that part of the protective layer revealed after developing the photoresist is carried out for a time determined by the required edge profile of the material which is to be deposited in the selected area or areas.

11. An article including a layer of material deposited in a selected area, or selected areas, of a surface by a method according to any preceding claim.

12. An integrated circuit including a layer of material deposited in a selected area, or selected areas, of a surface by a method according to any preceding claim.

13. An electrical thin-film component or a capacitor including a layer of material deposited in a selected area, or selected areas, of a surface by a method according to any preceding claim.

14. A method of depositing material in a selected area on a surface substantially as hereinbefore described with reference to Figures 1 to 7 of the accompanying drawings.

15. A method of depositing material in a selected area on a surface substantially as hereinbefore described with reference to Figures 1 to 7 and Figure 8 or Figure 9 of the accompanying drawings.

C. HASLER
Chartered Patent Agent
Agent for the Applicants

FIG. 1a.

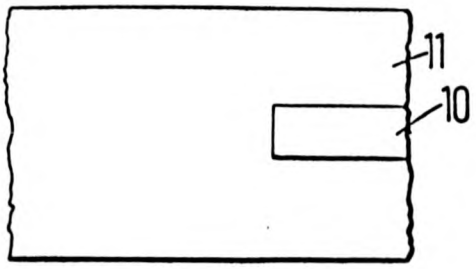

FIG. 1b.

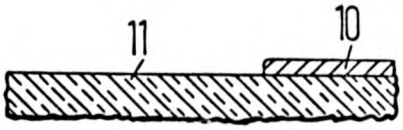

FIG. 2a.

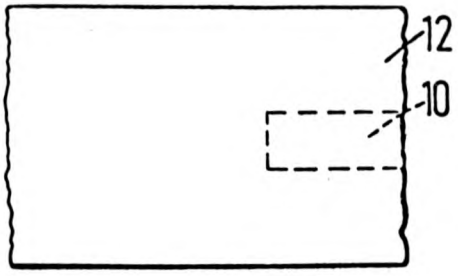

FIG. 2b.

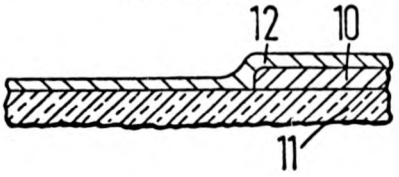

FIG. 3a.

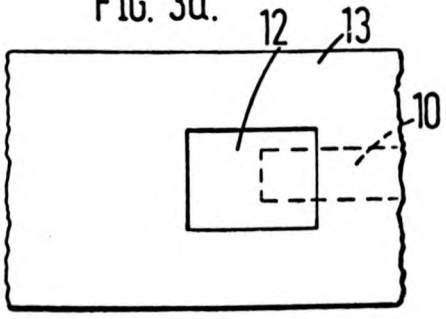

FIG. 3b.

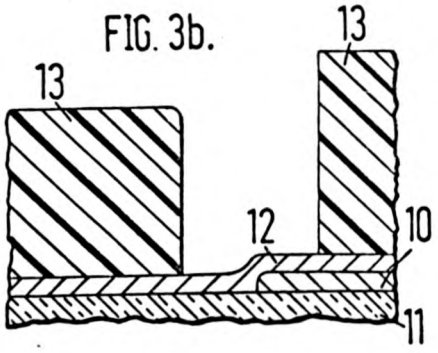

FIG. 4a.

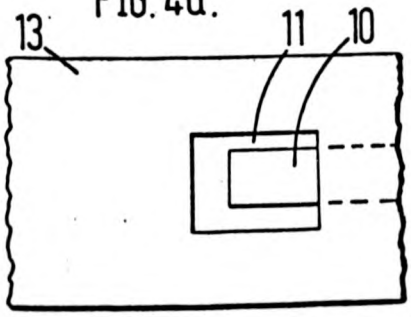

FIG. 4b.

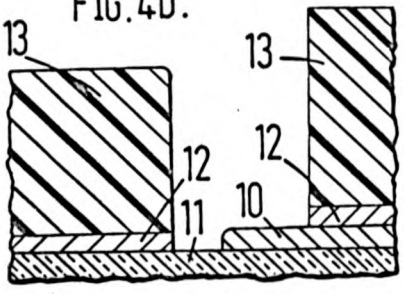

FIG. 5a.

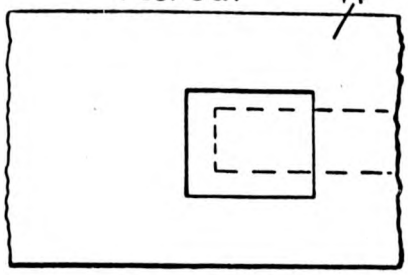

FIG. 5b.

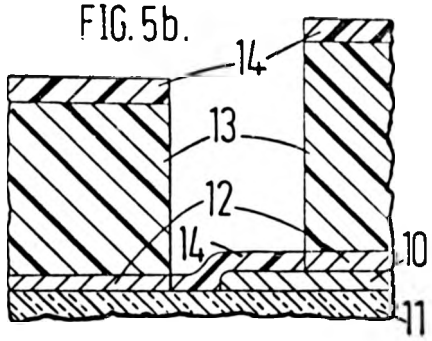

FIG. 6a.

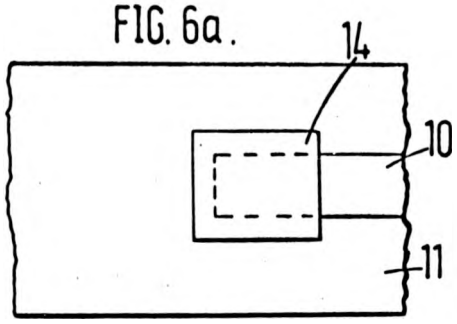

FIG 6b

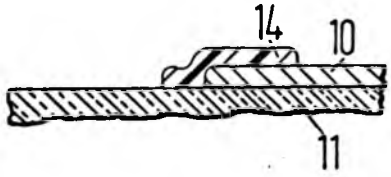

FIG. 7a.

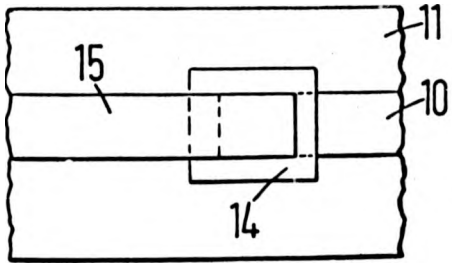

FIG. 7b.

FIG. 8a.

FIG. 8b.

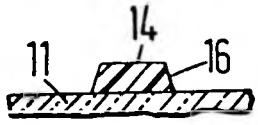

FIG. 9a.

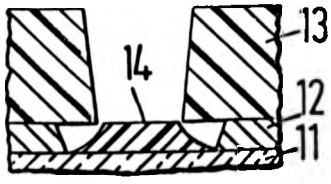

FIG. 9b.

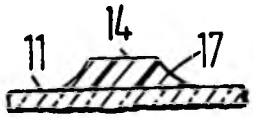

FIG. 5a.

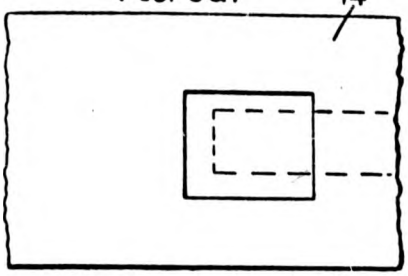

FIG. 5b.

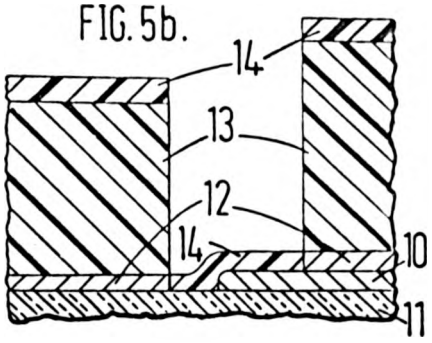

FIG. 6a.

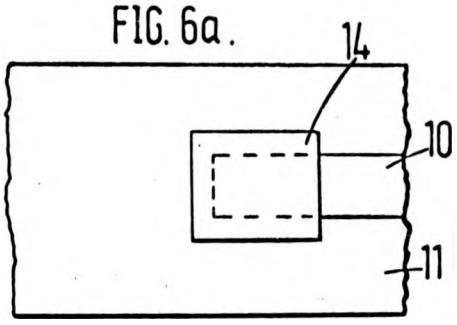

FIG 6b

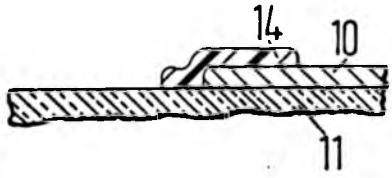

FIG. 7a.

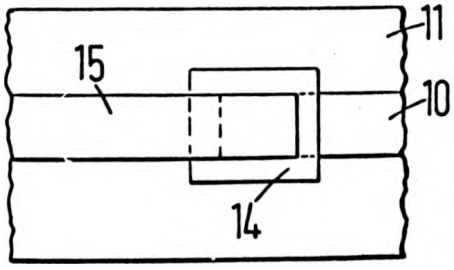

FIG. 7b.

FIG. 8a.

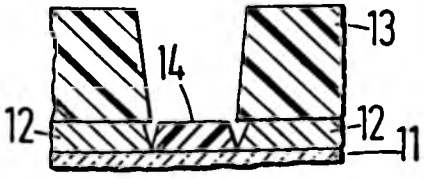

FIG. 8b.

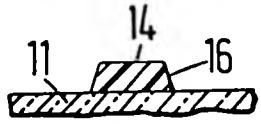

FIG. 9a.

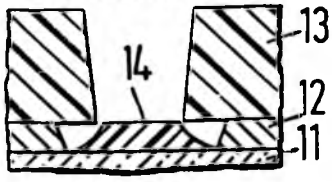

FIG. 9b.

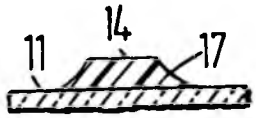

APPENDIX 4

DERIVATION OF THE Q FACTOR FOR AN H_{011} CYLINDRICAL CAVITY

By definition, the Q of a cavity is given by

$$Q = \frac{2 \times \text{total energy stored}}{\text{energy lost per cycle}}$$

$$\frac{1}{Q} = \frac{\text{energy lost per radian } (W')}{\text{total energy stored } (W)}$$

Calculation of the total energy stored

Consider the bore of the cavity shown below.

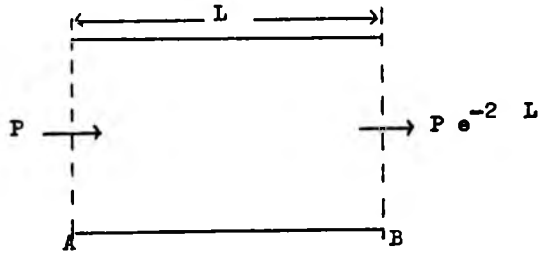

If P is the average power flow in the bore, in a given time t the energy stored is given by

$$\text{energy stored} = Pt$$

The standing wave produced in a cavity may be considered as two waves of equal amplitude travelling in opposite directions. The total energy stored, W, in time t is

$$W = 2Pt \qquad \ldots\ldots \text{A4-1}$$

where $t = L/v_g$

and $v_g = c\lambda/\lambda_g$

where L is the length of the cavity

v_g is the group velocity

λ is the free space resonant wavelength

where λ_g is the guide wavelength

c is the velocity of light

Substituting for t and v_g in equation A4-1 gives

$$W = \frac{2PL\lambda_g}{c\lambda}$$

At resonance for an H_{011} mode

$$L = \lambda_g/2$$

$$\therefore \quad W = \frac{P\lambda_g^2}{c\lambda} \qquad \ldots\ldots \text{A4-2}$$

But $c = \omega\lambda/2\pi$

where ω is the angular resonant frequency

Substituting for c in equation A4-2, the total energy stored is

$$W = \frac{2\pi P}{\omega}\left(\frac{\lambda_g}{\lambda}\right)^2 \qquad \ldots\ldots \text{A4-3}$$

Calculation of energy lostin the cavity

(a) Losses in the bore

Maintaining the principle of two waves flowing in opposite directions, the bore loss is given by

$$\text{Bore Loss} = 2P\left(1 - e^{-2\alpha L}\right)$$

Expanding the exponential series

$$\text{Bore Loss} = 2P\left[1 - \left(1 - 2\alpha L + \frac{4\alpha^2L^2}{2!} - \frac{8\alpha^3L^3}{3!} + \ldots.\right)\right]$$

Provided α is small, the first two terms of the series can be taken as an approximation.

$$\therefore \text{ Bore Loss} = 4\alpha LP$$

The bore loss per radian, W_1, is therefore

$$W_1 = 4\alpha LP/\omega$$

Substituting $L = \lambda_g / 2$ gives

$$W_1 = \frac{2\alpha \lambda_g P}{\omega} \qquad \ldots\ldots \text{A4-4}$$

(b) Losses in the end plates

The magnetic field vectors at the cavity/end plate boundary are shown below.

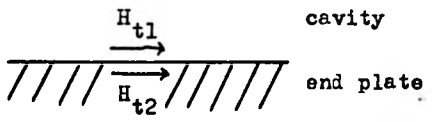

The energy lost in one end plate $= \frac{1}{2} R_s \int_{\text{end plate}} |H_{t2}|^2 \, dA$

where R_s is the surface resistance of the end plate material At each end, however, the magnetic field is twice that for a single travelling wave.

$$\text{energy lost in one end plate} = 2 R_s \int_{\text{end plate}} |H_{t2}|^2 \, dA$$

The energy lost per radian, W_2, in both end plates is therefore given by

$$W_2 = \frac{4R_s}{\omega} \int_{\text{end plate}} |H_{t2}|^2 \, dA \qquad \ldots\ldots \text{A4-5}$$

The incident power flow, P, onto the end plate surface is

$$P = \frac{1}{2} \text{Re} \int_{\text{end plate}} (E_{t1} \times H_{t1}^*) \, dA$$

where E_{t1} and H_{t1} are the tangential electric and magnetic fields incident on the end plate surface.

The wave impedance, Z_w, = E_{t1} / H_{t1}

Substituting for E_{t1} in the power flow equation given above yields

$$P = \frac{1}{2} Z_w \int_{\text{end plate}} |H_{t1}|^2 \, dA$$

$$\int_{\text{end plate}} |H_{t1}|^2 \, dA = \frac{2P}{Z_w} \qquad \ldots\ldots \text{A4-6}$$

For continuity at the cavity/end plate boundary

$$H_{t1} = H_{t2}$$

The integral in equation A4-6 may therefore be substituted in equation A4-5.

$$W_2 = \frac{8R_s P}{Z_w} \qquad \ldots\ldots \text{A4-7}$$

The Q of the cavity is given by

$$\frac{1}{Q} = \frac{W_1 + W_2}{W}$$

Substituting for W, W_1 and W_2 from equations A4-3, -4, and -7

$$\frac{1}{Q} = \frac{\alpha \lambda^2}{\pi \lambda_g} + \frac{4 \lambda^2 R_s}{\pi \lambda_g^2 Z_w} \qquad \ldots\ldots \text{A4-8}$$

Ratio of end plate loss to bore loss (W_2/W_1)

From equations A4-7 and A4-4

$$\frac{W_2}{W_1} = \frac{4R_s}{Z_w \alpha \lambda_g}$$

Let $\alpha = KR_s'$

where R_s' is the surface resistance of the bore material

and K is a function of the free space and cut off wavelengths (see text section 7-2)

The wave impedance, Z_w, = E_{t1} / H_{t1}

Substituting for E_{t1} in the power flow equation given above yields

$$P = \frac{1}{2} Z_w \int_{\text{end plate}} |H_{t1}|^2 \, dA$$

$$\int_{\text{end plate}} |H_{t1}|^2 \, dA = \frac{2P}{Z_w} \qquad \ldots\ldots \text{A4-6}$$

For continuity at the cavity/end plate boundary

$$H_{t1} = H_{t2}$$

The integral in equation A4-6 may therefore be substituted in equation A4-5.

$$W_2 = \frac{8R_s P}{Z_w} \qquad \ldots\ldots \text{A4-7}$$

The Q of the cavity is given by

$$\frac{1}{Q} = \frac{W_1 + W_2}{W}$$

Substituting for W, W_1 and W_2 from equations A4-3, -4, and -7

$$\frac{1}{Q} = \frac{\alpha \lambda^2}{\pi \lambda_g} + \frac{4 \lambda^2 R_s}{\pi \lambda_g^2 Z_w} \qquad \ldots\ldots \text{A4-8}$$

Ratio of end plate loss to bore loss (W_2/W_1)

From equations A4-7 and A4-4

$$\frac{W_2}{W_1} = \frac{4R_s}{Z_w \alpha \lambda_g}$$

Let $\alpha = KR_s'$

where R_s' is the surface resistance of the bore material

and K is a function of the free space and cut off wavelengths (see text section 7-2)

If the bore and end plates are made of the same material

$$R_s' = R_s$$

Under this condition and substituting for α

$$\frac{W_2}{W_1} = \frac{4}{Z_w K \lambda_g}$$

The wave impedance, Z_w, = $\lambda_g \eta / \lambda$

where η is the intrinsic impedance of free space = 377 ohms

$$\frac{W_2}{W_1} = \frac{4\lambda}{K \lambda_g^2 \eta} \qquad \ldots\ldots \text{A4-9}$$

APPENDIX 5

SURFACE RESISTANCE OF A CONDUCTOR OF FINITE THICKNESS

(a) Relationship between the current on the back and front surfaces of a conductor

In a conductor of finite thickness, the current density is complicated by the presence of reflections from the far surface. Consider a wave incident on a conductor as shown below.

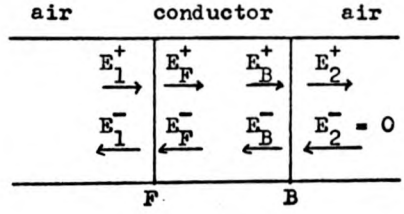

The electric fields,(E), at planes F and B are given by

$$E_F = E_1^+ + E_1^- = E_F^+ + E_F^- \qquad \text{..... A5-1}$$

$$E_B = E_B^+ + E_B^- = E_2^+ \qquad \text{..... A5-2}$$

Again, for continuity across the conductor boundary, the magnetic field,(H), at plane B is given by

$$H_B = H_B^+ + H_B^- = H_2^+ \qquad \text{..... A5-3}$$

The magnetic and electric fields are related by the intrinsic impedance, (η).

i.e. $\eta = E/H$

$$\therefore \quad E_B^+ = \eta H_B^+ \quad , \quad E_B^- = -\eta H_B^- \quad , \quad E_2^+ = \eta_o H_2^+$$

where η is the intrinsic impedance in the conductor

η_o is the intrinsic impedance in air

Substituting E for H in equation A5-3 gives

$$\frac{E_B^+}{\eta} - \frac{E_B^-}{\eta} = \frac{E_2^+}{\eta_o} \qquad \text{..... A5-4}$$

From equations A5-2 and A5-4

$$E_B^+ = XE_2^+ \qquad \text{..... A5-5a}$$

$$E_B^- = YE_2^+ \qquad \text{..... A5-5b}$$

where $$X = \frac{(\eta_o + \eta)}{2\eta_o}$$

and $$Y = \frac{(\eta_o - \eta)}{2\eta_o}$$

The electric field at the front surface is related to the electric field at the back surface by

$$E_F^+ = E_B^+ e^{\gamma t} \qquad \text{..... A5-6a}$$

$$E_F^- = E_B^- e^{-\gamma t} \qquad \text{..... A5-6b}$$

where t is the thickness of the conductor

and γ is the propagation constant

Substituting equations A5-5 into equations A5-6

$$E_F^+ = X e^{\gamma t} E_2^+$$

$$E_F^- = Y e^{-\gamma t} E_2^+$$

$$\therefore \quad \frac{E_2^+}{E_F^+ + E_F^-} = \frac{1}{X e^{\gamma t} + Y e^{-\gamma t}} \qquad \text{..... A5-7}$$

i.e. $$\frac{E_B}{E_F} = \frac{1}{X e^{\gamma t} + Y e^{-\gamma t}}$$

$$\frac{E_B^+}{\eta} - \frac{E_B^-}{\eta} = \frac{E_2^+}{\eta_o} \qquad \text{..... A5-4}$$

From equations A5-2 and A5-4

$$E_B^+ = XE_2^+ \qquad \text{..... A5-5a}$$

$$E_B^- = YE_2^+ \qquad \text{..... A5-5b}$$

where $$X = \frac{(\eta_o + \eta)}{2\eta_o}$$

and $$Y = \frac{(\eta_o - \eta)}{2\eta_o}$$

The electric field at the front surface is related to the electric field at the back surface by

$$E_F^+ = E_B^+ e^{\gamma t} \qquad \text{..... A5-6a}$$

$$E_F^- = E_B^- e^{-\gamma t} \qquad \text{..... A5-6b}$$

where t is the thickness of the conductor

and γ is the propagation constant

Substituting equations A5-5 into equations A5-6

$$E_F^+ = X e^{\gamma t} E_2^+$$

$$E_F^- = Y e^{-\gamma t} E_2^+$$

$$\therefore \quad \frac{E_2^+}{E_F^+ + E_F^-} = \frac{1}{X e^{\gamma t} + Y e^{-\gamma t}} \qquad \text{..... A5-7}$$

$$\text{i.e.} \quad \frac{E_B}{E_F} = \frac{1}{X e^{\gamma t} + Y e^{-\gamma t}}$$

The ratio of current densities is also given by the same relationship.

$$\text{i.e.} \quad \frac{I_B}{I_F} = \frac{1}{X\, e^{\gamma t} + Y\, e^{-\gamma t}}$$

For good conductors $\eta \ll \eta_o$

$$\therefore \quad X = Y = \frac{1}{2}$$

also $$\gamma = (1 + j)/\delta$$

$$\therefore \quad \frac{I_B}{I_F} = \frac{2}{e^{(1+j)t/\delta} + e^{-(1+j)t/\delta}} \qquad \text{..... A5-8}$$

(b) Derivation of surface resistance formula

The variation of current density with depth into a conductor is described by the equation(52)

$$I_z = C_1 e^{-\gamma z} + C_2 e^{\gamma z} \qquad \text{..... A5-9}$$

where I_z is the current density at depth z

and C_1 and C_2 are unknown coefficients

Equation A5-8 provides the boundary conditions for equation A5-9.

At z = 0 $$I_z = I_F$$

$$\therefore \quad C_1 + C_2 = I_F \qquad \text{..... A5-10}$$

At z = t $$I_z = I_B$$

$$\therefore \quad \frac{2I_F}{e^{(1+j)t/\delta} + e^{-(1+j)t/\delta}} = C_1 e^{-\gamma t} + C_2 e^{\gamma t} \qquad \text{..... A5-11}$$

From equations A5-10 and A5-11

$$C_1 = \frac{I_F (e^{2\gamma t} - 1)}{(e^{2\gamma t} - e^{-2\gamma t})}$$

and

$$C_2 = \frac{I_F\,(1 - e^{-2\gamma t})}{(e^{2\gamma t} - e^{-2\gamma t})}$$

Substituting for C_1 and C_2 in equation A5-9

$$I_z = \frac{I_F\left[(1 - e^{-2\gamma t})e^{\ z} - (1 - e^{2\gamma t})e^{-\ z}\right]}{(e^{2\gamma t} - e^{-2\gamma t})} \quad \text{.....A5-12}$$

The surface impedance, Z, is defined by

$$Z = \frac{E_F}{J_z}$$

where J_z is the total current density $= \int_0^t I_z\,dz$

Integrating equation A5-12 yields

$$J_z = \frac{I_F\,(e^{2\gamma t} + e^{-2\gamma t} - 2)}{(e^{2\gamma t} - e^{-2\gamma t})}$$

$$= \frac{I_F\,(\tanh \gamma t)}{\gamma}$$

But $E_F = I_F/\sigma$

where σ is the conductivity

$$\therefore \quad Z = \frac{I_F}{\sigma J_z}$$

Substituting for J_z

$$Z = \frac{\gamma\,(\coth \gamma t)}{\sigma}$$

Substituting for γ

$$Z = \frac{(1+j)\left[\coth (1+j)t/\delta\right]}{\delta\sigma}$$

But $1/\delta\sigma = R_s$, the surface resistance of an infinitely thick conductor.

$$\therefore \quad Z = R_s (1+j) \left[\coth (1+j)t/\delta\right]$$

Separating the above equation into its real and imaginary components yields

$$\text{surface reactance} = \frac{R_s (\sinh 2t/\delta - \sin 2t/\delta)}{(\cosh 2t/ - \cos 2t/)}$$

$$\text{surface resistance} = \frac{R_s (\sinh 2t/\delta + \sin 2t/\delta)}{(\cosh 2t/\delta - \cos 2t/\delta)}$$

SURFACE-RESISTANCE MEASUREMENTS OF THIN CONDUCTING FILMS AT 10 GHz

Indexing terms: Calibration, Cavity resonators, Microwave measurements, Resistance measurements, Surface phenomena, Thin films

The letter describes a technique for calibration of an H_{011} cavity for surface-resistance measurements of thin-film and bulk samples at 10 GHz. After calibration and insertion of the sample, it is only necessary to measure the return loss or v.s.w.r. at resonance. The conductivity and surface resistance of the sample may then be read directly from a graph.

The performance of many microwave integrated circuits (m.i.c.s) is critically dependent on the microwave surface resistance of thin metal films, often built up by electroplating. Experience shows that this surface resistance cannot be predicted from direct-current or low-frequency measurements. This letter describes a technique for calibration of a cylindrical H_{011} cavity for surface-resistance measurements of thin-film and bulk samples at 10 GHz.

The thin film is measured after deposition onto its normal substrate. This forms one end plate of the H_{011} cylindrical cavity, as shown in Fig. 1. A dielectric substrate is supported only by its corners, so that it has no conducting backing. The other end plate forms an integral part of the cavity. This is ideally suited for surface-resistance measurements, as for the pure mode there are no current paths between the bore of the cavity and the end plates. Thus contact resistance of a detachable end plate will have no effect on the Q factor of the cavity. However, associated with the H_{011} mode is the degenerate E_{111} mode. Interference from this mode may be eliminated by putting annular grooves in the solid end of the cavity, as shown. Provided that there is negligible field penetration into the grooves, the effect of the grooves on the H_{011} mode may be obtained by considering the grooved end of the cavity to have an effective conductivity σ_2. The Q factor of the cavity is now given by

$$\frac{1}{Q} = \frac{1}{Q \text{ of bore}} + \frac{1}{Q \text{ of grooved end}} + \frac{1}{Q \text{ of sample end}}$$

i.e.

$$\frac{1}{Q_S} = \frac{K\lambda^2}{\pi\lambda_g^2\delta_1\sigma_1} + \frac{2\lambda^2}{\pi\lambda_g^2 Z_w\delta_2\sigma_2} + \frac{2\lambda^2}{\pi\lambda_g^2 Z_w\delta_s\sigma_s} \quad (1)$$

where λ is the free-space wavelength at resonant frequency $\omega_0/2\pi$, λ_g is the guide wavelength at resonant frequency $\omega_0/2\pi$, Z_w is the wave impedance of H_{01} circular waveguide mode, σ_1 is the conductivity of bore material, δ_1 is the skin depth in bore material, σ_s is the conductivity of sample, δ_s is the skin depth in sample, σ_2 is the effective conductivity of grooved end, δ_2 is the effective skin depth in grooved end, Q_s is the Q factor of cavity with sample, K is the $\alpha\delta_1\sigma_1$ and α is the attenuation constant of H_{01} circular waveguide mode.

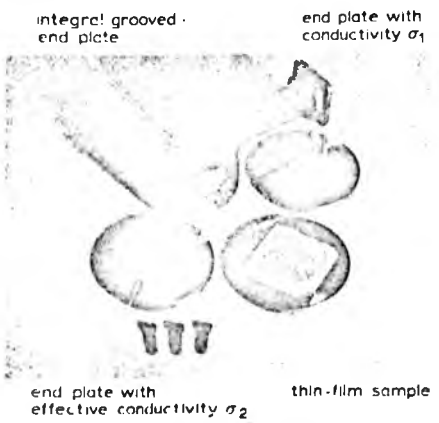

Fig. 1 *Test cavity showing calibration end plates and thin-film sample*

Before the surface resistance of the sample can be found, the surface resistance ($1/\delta\sigma$) of the bore and grooved end plate must be known. This may be found by measuring the cavity Q factor, first with a detachable end plate of conductivity σ_1 and then with an end plate having identical grooves to the opposite end and an effective conductivity σ_2. Thus, three Q factor measurements are required to obtain the surface resistance of the sample. However, these measurements may be greatly simplified, as described below.

Consider the cavity to be represented by a series-tuned circuit with resistance R, coupled via a mutual inductance M[1]. For the cavity, $Q = \omega_0 L/R$, and ω_0 and L may be assumed to remain constant for all conducting samples. Any two Q factor measurements may then be related by

$$\frac{Q_1}{Q_2} = \frac{R_2}{R_1} = \frac{S_2}{S_1}$$

where Q_1 and Q_2 are the cavity Q factors for resistances R_1 and R_2, respectively, giving v.s.w.r.s at resonance of S_1 and S_2. Therefore, Q_1 having been measured, S_1 and S_2, Q_2 may be found. In practice, it has been found more convenient to measure the return loss.

On returning to eqn. 1, we find that Q_s may be written as a function of Q_1 and S_1, the cavity Q factor and the v.s.w.r. for a detachable end plate of conductivity σ_1, and S_s, the v.s.w.r. with the sample end plate. Rearranging the equation gives

$$\frac{1}{\delta_s\sigma_s} = \frac{\pi\lambda_g^2 Zw}{2\lambda^2 Q_1(S_1/S_s)} - \frac{K\lambda_g Zw}{2\delta_1\sigma_1} - \frac{1}{\delta_2\sigma_2}$$

If Q_1, S_1, $\delta_1\sigma_1$ and $\delta_2\sigma_2$ are known, a calibration curve of $1/\delta_s\sigma_s$ against S_s may be drawn. Return-loss measurements have been made on the present cavity to obtain the calibration curve of Fig. 2A, which shows the variation of surface resistance and conductivity of the sample with return loss. Careful analysis of errors yields a maximum error in R_s of $\pm 0{\cdot}0012\,\Omega$. Thus, the cavity having been calibrated, all subsequent surface-resistance measurements may be made by measurement of the return loss at resonance alone.

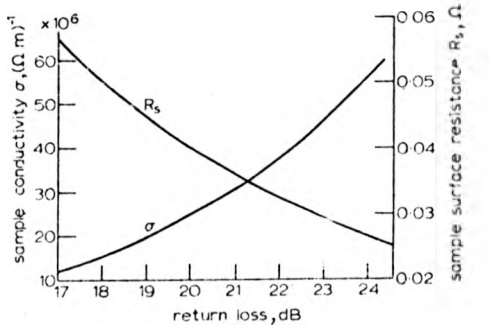

Fig. 2A *Calibration curve showing variation of sample conductivity and surface resistance with return loss*

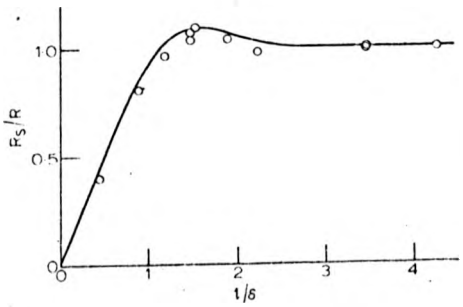

Fig. 2B *Ratio of surface resistances for a thick- and thin-film sample plotted against the ratio thickness/skin depth*

measured values
R_s, R corresponds to an evaporated copper film with $R_s = 0{\cdot}0286\,\Omega$, $\delta = 0{\cdot}72\,\mu m$, $\sigma = 48{\cdot}3 \times 10^6\,(\Omega\,m)^{-1}$

Measurements using this technique yield a conductivity of $57{\cdot}1 \times 10^6\ \Omega^{-1}\ m^{-1}$ for electrolytically polished, vacuum-annealed high-purity bulk copper. This compares favourably with the standard d.c. conductivity for copper of $58{\cdot}0 \times 10^6\ \Omega^{-1}\ m^{-1}$.

Measurements on films with thickness l greater than three skin depths ($l/\delta > 3$) yield the bulk value of surface resistance R_s. For $l/\delta < 3$, the actual microwave surface resistance R for that thickness is given, since the intrinsic impedance of the insulating substrate greatly exceeds that of the film. R is related to R_s by the expression[2]

$$\frac{R_s}{R} = \frac{\cosh(2l/\delta) - \cos(2l/\delta)}{\sinh(2l/\delta) + \sin(2l/\delta)} = (l/\delta \quad \text{for} \quad (l/\delta) < 0{\cdot}4$$

Measurements of R for evaporated copper films are compared with this theory in Fig. 2a, showing good agreement.

Further measurements on films deposited from various plating solutions will be published later.

Acknowledgment: The authors are grateful for support from the UK Science Research Council for this work.

R. S. BUTLIN
M. K. McPHUN

Department of Engineering
University of Warwick
Coventry, War. CV4 7AL, England

30th November 1972

References

1 MONTGOMERY, C. G., DICKE, R. H., and PURCELL, E. M.: 'Principles of microwave circuits' (McGraw-Hill, 1948), section 7.10
2 RAMO, S., WHINNERY, J. R. and VAN DUZER, T.: 'Fields and waves in communication electronics' (Wiley, 1965), section 5.19

Electronics Letters, 8, No. 26, p.637 (1972).

Measurements using this technique yield a conductivity of $57{\cdot}1 \times 10^6\ \Omega^{-1}\,m^{-1}$ for electrolytically polished, vacuum-annealed high-purity bulk copper. This compares favourably with the standard d.c. conductivity for copper of $58{\cdot}0 \times 10^6\ \Omega^{-1}\,m^{-1}$.

Measurements on films with thickness l greater than three skin depths ($l/\delta > 3$) yield the bulk value of surface resistance R_s. For $l/\delta < 3$, the actual microwave surface resistance R for that thickness is given, since the intrinsic impedance of the insulating substrate greatly exceeds that of the film. R is related to R_s by the expression[2]

$$\frac{R_s}{R} = \frac{\cosh(2l/\delta) - \cos(2l/\delta)}{\sinh(2l/\delta) + \sin(2l/\delta)} = (l/\delta \quad \text{for} \quad (l/\delta) < 0{\cdot}4$$

Measurements of R for evaporated copper films are compared with this theory in Fig. 2b, showing good agreement.

Further measurements on films deposited from various plating solutions will be published later.

Acknowledgment: The authors are grateful for support from the UK Science Research Council for this work.

R. S. BUTLIN
M. K. McPHUN

Department of Engineering
University of Warwick
Coventry, War. CV4 7AL, England

30th November 1972

References

1 MONTGOMERY, C. G., DICKE, R. H., and PURCELL, E. M.: 'Principles of microwave circuits' (McGraw-Hill, 1948), section 7.10
2 RAMO, S., WHINNERY, J. R. and VAN DUZER, T.: 'Fields and waves in communication electronics' (Wiley, 1965), section 5.19

Electronics Letters, 8, No. 26, p.637 (1972).

B.14.5.

Proceedings of the European Microwave Conference 1973, Vol.2

MEASUREMENT OF OVERLAY CAPACITORS AT X-BAND WITH INDEPENDENT ASSESSMENT OF THIN-FILM CONDUCTOR LOSSES

R.S. BUTLIN, D.F. MICHIE AND M.K. McPHUN

Department of Engineering,
University of Warwick,
Coventry,
CV4 7AL.
England.

The accurate characterization of thin film microwave overlay capacitors has been impossible in the past, due to transition errors introduced by the enormous difference in size between the components and the measurement system. Most errors, particularly of loss, are due to the use of bond wires.

In this new technique the test capicitator is fabricated as an intrinsic part of an X-band microstrip resonator, eliminating the bond wires, and the capacitor can be measured in the same form as would be used in a practical circuit. Figs. 1 and 2 show the resonator. It is $3\lambda/4$ long with one end short circuited to the ground plane, and the other having a small gap coupling to the measurement system. The test capacitor is in series with the transmission line, positioned at a current maximum.

Conventional thin film techniques are used to construct the resonator. The test capacitor is constructed across a narrow gap in the resonator in two stages. At first it is made without a top electrode, and the resonant frequency and Q of the resonator plus capacitor are measured. Then the top electrode is completed and the measurements are repeated. The capacitor Q factor and capacitance are determined from these measurements and the physical dimensions of the resonator. The capacitance can be measured to within ± 1.2% and the Q factor to within ± 7%, using a resonator with an unloaded Q of 400, deposited on a quartz substrate.

In Fig. 1c is shown a photograph of a completed 1 pF capacitor taken using a scanning electron microscope. Typically the lower electrode consists of 0.75 μm of evaporated copper, the dielectric is 1 μm thick SiO_2 deposited by R.F. sputtering, and the 5 μm thick copper upper electrode is first evaporated and then electroplated. A new photolithographic technique[1] was developed to make these capacitors.

The value of capacitance measured depends on two factors: the true capacitance and the electrode inductance. Similarly the Q factor depends on the electrode loss and the dielectric loss. Short electrodes, i.e. with width/length ratio $W/L > 4$, render the inductance negligible. To separate the contributions to the loss of the capacitor, independent measurements of dielectric loss[2] and electrode conductivity are needed. Here we report our measurements of electrode conductivity.

The Authors wish to thank the U.K. Science Research Council for financial support.

Experience shows that the surface resistance of the films used cannot be predicted from d.c. or l.f. measurements. A new cavity measurement technique[3] is used to measure the surface resistance in X-band. The sample metal film is deposited on a substrate and forms one end plate of an H_{011} cavity. Measurement of the return loss at resonance alone permits the sample surface resistance to be obtained directly from a graph. The maximum error in surface resistance is ± 0.0012 ohms.

Results one evaporated copper films[3] show that the microwave conductivity does not depend on film thickness, and the theoretical relation between film thickness and surface resistance is followed closely in practise. A series of factorially designed experiments[4] was made on films deposited from acid copper electroplating solutions. The effects of plating parameters were related to surface finish, surface resistance, and d.c. conductivity of the films. The composition of the plating solution was shown to be the most important factor.

Table 1 summarizes results obtained at 10 GHz from films deposited using evaporation and electroplating solutions. Two films were deposited from each solution and their microwave surface resistance measured; the d.c. conductivity of one of the films was then measured. The other film was annealed at 250°C for 2 hours in vacuum, and its microwave surface resistance and d.c. conductivity then measured. The copper pyrophoshate solution initially gave the best result, but these solutions deteriorate rapidly, and this result could not be repeated.

We conclude that lowest surface resistance is obtained from acid copper solutions with added brightener, and the effect of annealing on these films is small. Measured microwave conductivities are between 89% and 94% of the measured d.c. values, an effect we attribute to impurities in the film, not surface roughness. Use of silver plating is not advised Annealing of plated gold films is required to achieve low loss.

Some results of measurements on capacitors are shown in table 2.

We conclude that for these dielectrics, the dielectric loss predominates for capacitors with values smaller than 10 pF, the electrode loss becoming significant for C > 10 pF. The electrode loss is dominated by the lower electrode whose thickness is limited by the need for the dielectric to overlap it. Decreasing the lower electrode thickness below 0.75δ (δ=skin depth) gives a rapidly increasing loss. If the upper electrode thickness exceeds 3δ, its contribution to the electrode loss is negligible. The electrode Q factor can be greatly increased by using the configuration of Fig. 3b rather than Fig. 3a. This results in an increase of electrode Q of 75% for W/L = 1.

We expect R.F. sputtered alumina to give much higher dielectric Q factors when the deposition process is optimized.

References

1. R.S. Butlin and D.F. Michie "Method for depositing material on selected areas of a surface" U.K. Patent Application 5342/72.
2. M.K. McPhun and K. Mehmet "Thin film dielectric measurements" chapter of "High frequency dielectric measurements" IPC Science and Technology Press 1973.
3. R.S. Butlin and M.K. McPhun "Surface-resistance measurements of thin conducting films at 10 GHz" Electronics Letters 8, 26, p 637-639, 28th Dec. 1972.
4. O.L. Davis "Design and analysis of industrial experiments" Oliver and Boyd, 1954.

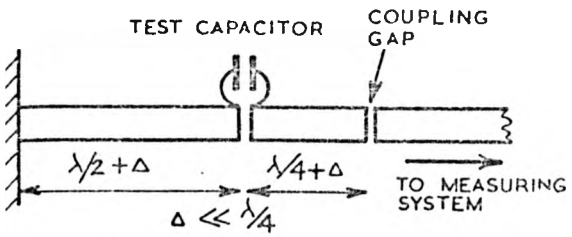

a). SCHEMATIC

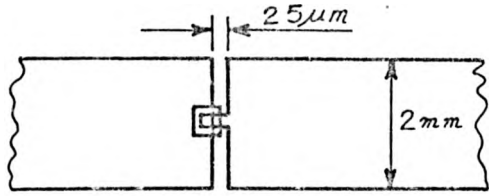

b) CAPACITOR MOUNTED IN GAP

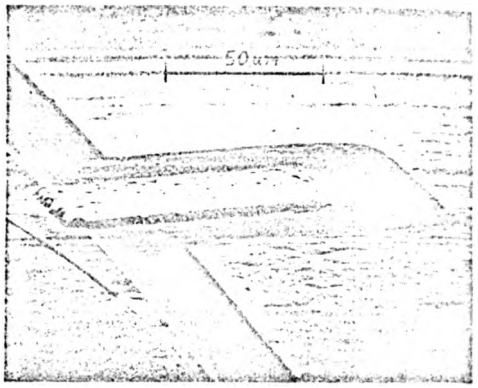

c) DETAIL OF CAPACITOR

FIG. 1. MICROSTRIP RESONATOR WITH OVERLAY CAPACITOR

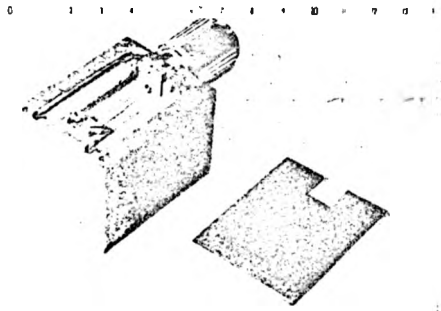

FIG.2. MICROSTRIP RESONATOR MOUNTED IN SHIELDING BOX.

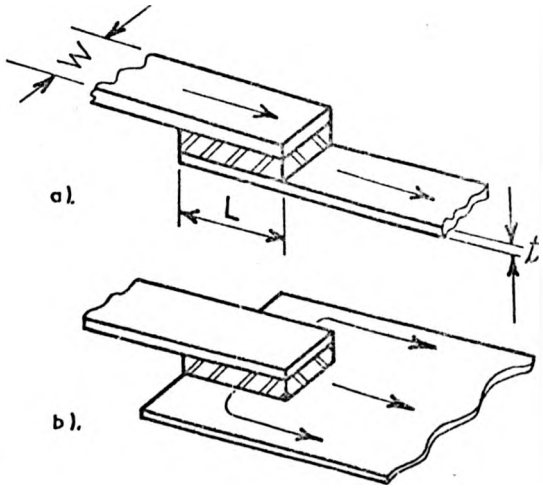

FIG. 3. TWO CAPACITOR CONFIGURATIONS (ARROWS INDICATE DIRECTIONS OF CURRENT FLOW.)

Dielectric	C(pF)	Q	Q electrode	Q dielectric	t(μm)	W/L
SiO_2	1.1	122	1557	133	1.1	1.6
SiO_2	1.0	120	1602	129	0.91	2.01
SiO_2	0,71	137	2349	145	0.72	3.0
Al_2O_3	1.25	164	1803	178	1.1	2.67

TABLE 2 Measurements on Capacitors at 9.5 GHz

TABLE 1 Measurements on metal films at d.c. amd 10 GHz

Deposition Method	Thick-ness (μm)	Surface resistance (ohms)	annealed	Microwave Conductivity $(\Omega m)^{-1}$	annealed	DC Conductivity $(\Omega m)^{-1}$	annealed	CLA (μm)	Theoretical DC Conductivity $(\Omega m)^{-1}$	Measured/Theoretical DC Conductivity (%)	annealed	Microwave Conductivity (%)	annealed
		$\times 10^{-2}$	$\times 10^{-2}$	$\times 10^{6}$	$\times 10^{6}$	$\times 10^{6}$	$\times 10^{6}$		$\times 10^{6}$				
P.M.D. gold	5.1	3.38		34.5		36.9		0.07	41.0	90		84.1	
	4.6	3.38	3.28	34.5	36.6		40.4	0.07			98.6	84.1	89.3
Englehardt E56 gold	2.4	3.34		35.2		38.1		0.03	41.0	92.9		86.0	
	2.4	3.33		35.3		37.6		0.03	41.0	91.8		86.2	
Evaporated gold	2.5	3.48		32.5		34.8		0.02	41.0	84.9		79.3	
P.M.D. silver	3.3	3.03		43.3		47.8		0.05	62.9	76.0		68.9	
	3.3	3.00	2.91	43.7	46.5		52.0	0.07			82.6	69.5	73.9
Acid copper	3.5	2.98		44.2		49.7		0.05	58.0	84.6		76.2	
	3.5	2.99	2.96	44.0	44.9		50.5	0.04			87.1	75.9	77.5
Bright acid copper	3.2	2.91		46.6		52.7		0.03	58.0	90.8		80.4	
	3.2	2.90	2.84	46.8	48.8		53.0	0.03			91.3	80.7	84.2
Copper pyrophosphate													
Best result	4.5	2.89		47.1		47.2		0.03	58.0	81.4		81.2	
Worst result	4.8	3.05		42.3		45.4		0.04	58.0	78.4		73.0	
	4.8	3.05	3.03	42.3	42.9		46.0	0.04	58.0		78.3	73.0	73.9
Evaporated copper	3.1	2.86		48.1		52.1		0.01	58.0	89.9		82.9	

TABLE 1 Measurements on metal films at d.c. amd 10 GHz

Deposition Method	Thick-ness (μm)	Surface resistance (ohms)	annealed	Microwave Conductivity $(\Omega m)^{-1}$	annealed	DC Conductivity $(\Omega m)^{-1}$	annealed	CLA (μm)	Theoretical DC Conductivity $(\Omega m)^{-1}$	Measured/Theoretical DC Conductivity (%)	annealed	Microwave Conductivity (%)	annealed
		$\times 10^{-2}$	$\times 10^{-2}$	$\times 10^{6}$	$\times 10^{6}$	$\times 10^{6}$	$\times 10^{6}$		$\times 10^{6}$				
P.M.D. gold	5.1	3.38		34.5		36.9		0.07	41.0	90		84.1	
	4.6	3.38	3.28	34.5	36.6		40.4	0.07			98.6	84.1	89.3
Englenarat E56 gold	2.4	3.34		35.2		38.1		0.03	41.0	92.9		86.0	
	2.4	3.33		35.3		37.6		0.03	41.0	91.8		86.2	
Evaporated gold	2.5	3.48		32.5		34.8		0.02	41.0	84.9		79.3	
P.M.D. silver	3.3	3.03		43.3		47.8		0.05	62.9	76.0		68.9	
	3.3	3.00	2.91	43.7	46.5		52.0	0.07			82.6	69.5	73.9
Acid copper	3.5	2.98		44.2		49.7		0.05	58.0	84.5		76.2	
	3.5	2.99	2.96	44.0	44.9		50.5	0.04			87.1	75.9	77.5
Bright acid copper	3.2	2.91		46.6		52.7		0.03	58.0	90.8		80.4	
	3.2	2.90	2.84	46.8	48.8		53.0	0.03			91.3	80.7	84.2
Copper pyrophosphate													
Best result	4.5	2.89		47.1		47.2		0.03	58.0	81.4		81.2	
Worst result	4.8	3.05		42.3		45.4		0.04	58.0	78.4		73.0	
	4.8	3.05	3.03	42.3	42.9		46.0	0.04	58.0		78.3	73.0	73.9
Evaporated copper	3.1	2.86		48.1		52.1		0.01	58.0	89.9		82.9	